

THE FORMULATION AND CHARACTERISATION OF CORTICOSTEROID LOADED ETHOSOMES FOR TOPICAL DELIVERY

Björn Franklin Martin (B. PHARM)

A full thesis submitted in the partial fulfilment of the requirements for the degree of

Magister Pharmaceuticae

Faculty of Natural Science, School of Pharmacy,

Discipline of Pharmaceutics

University of the Western Cape, Bellville, South Africa.



UNIVERSITY *of the*
WESTERN CAPE



School of
PHARMACY

Supervisor: Dr. Halima Samsodien

Co-Supervisor: Dr. Naushaad Ebrahim

November 2020

Declaration

I declare that — The formulation and characterisation of corticosteroid loaded ethosomes for topical delivery, is my own work. It has not been submitted before for any degree or examination at this or any other university and all sources used or quoted have been indicated and acknowledged by means of a complete reference.

Björn Franklin Martin

November 2020

Signed: UWC, Bellville.

Dedication

From me to me for me - *“If there’s one thing you can give yourself credit for, it’s for the effort put into producing and understanding the content of this thesis.”*

Publications and presentations

Oral presentations

1. Martin B, Samsodien H, Ebrahim N. Formulation and characterisation of corticosteroid loaded ethosomes for topical delivery. Presented at the 5th University of the Western Cape School of Pharmacy Postgraduate Research Symposium, School of Public Health, University of the Western Cape, Cape Town (9 September 2019)
2. Martin B, Samsodien H, Ebrahim N. Formulation and characterisation of corticosteroid loaded ethosomes for topical delivery. Presented at APSSA annual conference at the Kleinkaa Boutique Hotel in Centurion (9 – 11 October 2019)

Publications

1. Martin B, Wehmeyer A, Upton E. Allergic rhinitis: To sneeze or to wheeze. Pollen is the question, what is the answer? SA Pharm J [Internet]. 2018;85(5):37–42. Available from: <https://www.scopus.com/inward/record.uri?eid=2-s2.0-85056229046&partnerID=40&md5=858f2e9423ef90b642c3e401bab16a03>

Abstract

Background/Introduction: Atopic dermatitis (AD) is one of the most prevalent diseases worldwide. It is a rapidly growing field of study with several research avenues to explore its pathophysiology and to find innovative treatment and management regimens. Clinically, it is classified as a non-contagious, intensely pruritic, inflammatory, chronic skin disorder mediated by abnormalities associated with atopy. Symptoms include inflammation, redness, pain and a negative impact on the patient's overall quality of life. Chronic itching often leads to the formation of lichenified skin, which may increase the thickness of the epidermis and exacerbate the barrier function of the skin. AD is treated with topical corticosteroids which help to decrease inflammation. However, lichenification of the skin may decrease the efficacy of topical dosage forms. Nanomedicine is a rapidly developing field where advances have been made using ethosomes for topical delivery. As such, corticosteroid loaded ethosomal formulations containing hydrocortisone acetate (HCA) and betamethasone valerate (BMV) were developed and characterised to develop novel tools for topical drug delivery.

Aim: This study aimed at developing corticosteroid loaded ethosomes as a pre-formulation component for inclusion in a topical dosage form. To date, no ethosmal formulation with HCA and BMV has been investigated for topical drug delivery.

Method: Ethosomes were synthesised using the hot method and the cold method, a modified version of a double emulsion (o/w/o), solvent evaporation technique, as developed by *Touitou et al, 2007*.¹ Ethosomes were prepared using fixed concentrations of either BMV or HCA (10 mg/ml), ethanol (30% v/v) and purified water (70% v/v) and were comminuted using bath sonication or mini-extrusion. Centrifugation and centrifugal drying were used to purify and isolate the ethosomes for solid state characterisation. The morphology was determined using Scanning electron microscopy (SEM). Ethosomes were characterised using: dynamic light scattering (DLS), Fourier-transform infrared spectroscopy (FTIR), hot stage microscopy (HSM), differential scanning calorimetry (DSC) and thermogravimetric analysis (TGA). The encapsulation efficiency (EE) and drug loading (DL) were determined using validated HPLC methods. Finally, the drug release was determined using Franz diffusion cells and mathematical models were fitted to the % cumulative release data to determine the release kinetics.

Results: Ethosomes were assessed according to the following criteria for topical drug delivery which were determined using dynamic light scattering (DLS): Hydrodynamic diameter (HdD), ~ 200 nm, polydispersity index (PdI) < 0.5 and zeta potential (ζ_p) \pm 30 mV. The optimum formulations contained phosphatidylcholine (PC) 50 mg/ml. Extrusion was found to be the best method for particle reduction based on the reproducibility of the results. The HdD was 163.8 ± 31.99 and 147.7 ± 19.91 for BMV loaded ethosomes and HCA loaded ethosomes respectively and both formulations had an acceptable PdI of 0.049 and 0.111, respectively. SEM analyses indicated that the ethosomes had a spherical shape. Encapsulation of the APIs was verified by the thermoanalyses and possible intermolecular interactions were identified using FTIR. BMV loaded and HCA loaded ethosomes had a respective EE of 74.57 % and 37.30 %, and a DL of 14.91 % and 7.46 %, respectively. The release kinetics best fit the Peppas-Sahlin model indicative of an anomalous non-Fickian diffusion coupled with polymer relaxation and zero order release.

Conclusions: BMV and HCA loaded ethosomes for topical drug delivery were successfully synthesised and characterised. These novel nanoparticles have provided an array of avenues for further investigation and application in the topical delivery of corticosteroids.

Keywords: Hydrocortisone, betamethasone, nanoparticles, topical drug delivery

Acknowledgements

I would like to express my sincere gratitude to the following people:

To Prof Samsodien: Thank you for accepting my research proposal and giving me this research opportunity. Thank you for creating a research environment where I could run with my ideas. Thank you for your willingness to listen. You have helped me manage my enthusiasm and direct my focus, without compromising my ambition. I will always appreciate your unwavering support and guidance throughout this academic adventure.

To Dr Ebrahim: Thank you for input and “open door policy” throughout my research project.

To the pharmaceuticals research group: Jean, Lovette, Zene, Dr Musa, Yves, Rami and Alicia - Thank you for your insight and for critically appraising my work.

To Prof Aucamp: Thank you for training on the HPLC, your positive outlook, and for being present to resolve many queries.

To Prof Coetzee: Thank you for your clinical guidance and encouragement.

To Mr Kippie: Thank you for training on a variety of analytical equipment.

To my family and friends: Thank you for giving me the time and space to complete my Master’s research project.

To Achmat Kamies: Thank you for supporting, inspiring and challenging me throughout my academic years.

Thank you to the pharmaceuticals lecturers – Prof Aucamp, Mr Bapoo, Prof Dube, Dr Ebrahim and Prof Samsodien for developing my pharmaceutical research skills throughout my undergrad years.

Thank you to the UWC Biotechnology, Marine Biodiversity Discovery and Pharmacy Annex labs for allowing to me to use analytical equipment.

Thank you to the National Research Foundation of South Africa for financial assistance.

Thank you to the University of the Western Cape and the UWC School of Pharmacy for providing numerous resources to facilitate the completion of this research project.

List of Abbreviations

AD	atopic dermatitis
API	active pharmaceutical ingredients
ARD	atopic-related diseases
BMV	betamethasone valerate
CLSM	confocal laser scanning microscopy
CNPs	carbon nanoparticles
COX	cyclooxygenase
DLS	dynamic light scattering
DNA	deoxyribonucleic acid
DNCs	dendrimer nano-carriers
DOTAP	1,2- dioleoyl-3-trimethylammonium-propane
DPPG	1,2-dipalmitoyl-sn-glycero-3-phosphatidylglycerol
DSC	differential scanning calorimetry
ECRHS	European community respiratory health survey
EE	encapsulation efficiency
FTIR	Fourier transform infrared spectroscopy
GIT	gastrointestinal tract
H1	histamine 1
HCA	hydrocortisone acetate
HPLC	high performance liquid chromatography
HSM	hot stage microscopy
IgE	immunoglobulin e
IL	interleukin
LBS	lipid based system
MLV	multilamellar vesicles
MNPs	magnetic nanoparticles
PC	phosphatidylcholine
PCS	photon correlation spectroscopy
PE	phosphatidylethanolamine
PI	phosphatidylinositol
PNPs	polymeric nanoparticles

PPG	phosphatidylglycerol
PS	phosphatidylserine
SC	stratum corneum
SEM	scanning electron microscopy
SLNs	solid-lipid nanoparticles
SNPs	silica nanoparticles
TC	topical corticosteroids
TEM	transmission electron microscopy
T _g	glass transition
TGA	thermogravimetric analysis
Th1	T helper 1
Th2	T helper 2
UE	emulsifying ointment
UEA	aqueous cream
UV	ultraviolet
XRD	X-ray diffraction
ζ _p	zeta potential

List of Figures

Figure 2.1.1-1: A diagrammatical representation of a cross-section of human skin showing the different cell layers and appendages.	6
Figure 2.3-1: Normal skin and lichenified skin resulting from chronic scratching.	9
Figure 2.3.1-1: A simplified diagrammatical representation of the pathophysiology of AD, showing an inflammatory cascade that occurs on the onset of an allergen invading the body, triggering genomic and non-genomic responses.....	11
Figure 2.3.3-1: A summary of the standard treatment of atopic dermatitis.....	13
Figure 2.5.2-1: A diagrammatical representation of a cross section of the skin showing the pathways associated with transdermal drug delivery.....	17
Figure 2.7-1: The chemical structure of the perhydro-1,2-cyclopentenophenanthrene skeleton for corticosteroids with carbon numbering and rings.	19
Figure 2.10-1: A diagrammatical representation of the genomic and non-genomic responses associated with the mechanism of action of glucocorticoids acting on the stratum basale	22
Figure 3.1-1: A perspective of the nanoscale.....	25
Figure 3.2-1: Classification of lipid based systems for drug delivery	27
Figure 3.4-1: A schematic showing the different types of ethosomes and their components. All ethosomes contain a phospholipid bilayer and a hydro-ethanolic core which may or may not contain an API. Binary ethosomes contain additional alcohol and transethosomes contain a surfactant.	29
Figure 3.5-1: Chemical structure of phosphatidylcholine.....	31
Figure 3.8-1: Proposed mechanisms of action for lipid based drug delivery systems:.....	35
Figure 4.2.1-1: A schematic representation showing the mechanism in which comminution is achieved by sonication.....	41
Figure 4.2.2-1: A mini extruder and its components.	43
Figure 4.4-1: Phase diagram of water	45
Figure 4.6.2-1: A diagrammatical representation of the electrical double layer of a nanoparticle dispersed within a colloidal suspension.	50
Figure 4.8-1: A simplified FTIR spectrogram showing the different peak sizes.....	54
Figure 4.11-1: A diagrammatical representation of the possible mechanisms of drug release of ethosomes.	59
Figure 5.2.1-1: An overview of the hot and cold method used for ethosome synthesis.....	64
Figure 5.3-1: An overview of the comminution methods utilised in ethosome synthesis.....	66

Figure 5.4-1: An overview of the purification and isolation methods used in this study	67
Figure 5.11-1: A summary of the experimental setup for drug release determination from corticosteroid loaded ethosomes using Franz diffusion cells.	75
Figure 6.1.1-1: Fourier transform infrared spectroscopy (FTIR) spectra of pure betamethasone valerate (BMV) compared to its reference spectrum.	82
Figure 6.1.1-2: The chemical structure of betamethasone valerate annotated with functional groups observed in the Fourier transform infrared spectroscopy (FTIR) spectrum.	83
Figure 6.1.1-3: Fourier transform infrared spectroscopy (FTIR) spectra of pure hydrocortisone acetate compared to its reference spectrum.	84
Figure 6.1.1-4: The chemical structure of hydrocortisone acetate (HCA) annotated with functional groups observed on the Fourier transform infrared spectroscopy (FTIR) spectrum.	85
Figure 6.1.1-5: Fourier transform infrared spectroscopy (FTIR) spectra of pure phosphatidylcholine compared to its reference spectrum.	86
Figure 6.1.1-6: The chemical structure of phosphatidylcholine (PC) annotated with functional groups observed on the Fourier transform infrared spectroscopy (FTIR) spectrum	87
Figure 6.1.1-7: Fourier transform infrared spectroscopy (FTIR) spectra of pure cholesterol compared to its reference spectrum.	88
Figure 6.1.1-8: The chemical structure of cholesterol annotated with functional groups observed on the Fourier transform infrared spectroscopy (FTIR) spectrum	89
Figure 6.1.1-1: Differential scanning calorimetry (DSC) thermograms of hydrocortisone acetate (HCA), betamethasone valerate (BMV), phosphatidylcholine (PC) and cholesterol. .	90
Figure 6.2-1: The size distribution of ethosomes synthesised using the hot and cold method at PC concentrations of 10 mg/ml, 25 mg/ml and 50 mg/ml.	92
Figure 6.2-2: The zeta-potential of crude ethosomes synthesised using the hot and cold methods at phosphatidylcholine (PC) concentrations of 10 mg/ml, 25 mg/ml and 50 mg/ml.	94
Figure 6.3-1: The size distribution of unloaded, sonicated and extruded crude ethosomes synthesised using the hot and cold methods at a PC concentration of 50 mg/ml.	96
Figure 6.3-2: A macroscopic view of the ethosomal colloidal suspensions showing a change in turbidity before and after extrusion. (Extruding from right syringe to left syringe.)	97
Figure 6.3-3: The zeta-potential of unloaded crude ethosomes synthesised using the hot and cold methods at a phosphatidylcholine concentration of 50 mg/ml.	99

Figure 7.1-1: Vials containing ethosomal colloidal suspensions showing the difference in turbidity and sedimentation. Image captured 24 hours after synthesis.....	102
Figure 7.2-1: The size distribution of unloaded, betamethasone valerate (BMV) loaded and hydrocortisone acetate (HCA) loaded crude ethosomes synthesised using the hot and cold method.....	104
Figure 7.2-2: The zeta-potential of unloaded, betamethasone valerate (BMV) loaded and hydrocortisone acetate (HCA) loaded crude ethosomes synthesised using the hot and cold methods.	105
Figure 7.3-1: The size distribution of unloaded, BMV loaded and HCA loaded sonicated ethosomes synthesised using the hot and cold method.....	108
Figure 7.3-2: The ζ_p of unloaded, BMV loaded and HCA loaded sonicated ethosomes synthesised using the hot and cold methods.	110
Figure 7.3-3: The size distribution of unloaded, BMV loaded and HCA loaded extruded ethosomes synthesised using the hot and cold method.....	111
Figure 7.3-4: The zeta-potential of unloaded, BMV loaded and HCA loaded extruded ethosomes synthesised using the hot and cold methods.	113
Figure 7.5-1: Morphology of phosphatidylcholine, betamethasone valerate and Hydrocortisone acetate used in HM and CM ethosome preparation at different magnifications (Mag).....	114
Figure 7.5.1-1: SEM analyses of unloaded extruded ethosomes prepared using the hot and cold methods, at different magnification (Mag)	115
Figure 7.5.1-2: SEM analyses of BMV loaded extruded ethosomes prepared using the hot and cold methods, at different magnification (Mag)	116
Figure 7.5.1-3: SEM analyses of HCA loaded extruded ethosomes prepared using the hot and cold methods, at different magnification (Mag)	117
Figure 7.6-1: FTIR spectrograms showing the interactions between the ethosome components. The arrows indicate the peaks at which chemical shifts in wave number or intensity occurred.....	119
Figure 7.7-1: HSM analyses displaying observed thermal events and the corresponding temperatures for betamethasone valerate (BMV), hydrocortisone acetate (HCA), phosphatidylcholine (PC), unloaded ethosomes, BMV loaded and HCA loaded ethosomes.	122

Figure 7.8-1: DSC analyses of betamethasone valerate (BMV), hydrocortisone acetate (HCA), phosphatidylcholine (PC), unloaded ethosomes, BMV loaded and HCA loaded ethosomes. The arrows correspond to the thermal events that were identified in the samples.	125
Figure 7.9-1: TGA analyses of betamethasone valerate (BMV), hydrocortisone acetate (HCA), phosphatidylcholine (PC), unloaded ethosomes, BMV loaded and HCA loaded ethosomes.....	127
Figure 7.10-1: The HPLC chromatogram of BMV showing the betamethasone valerate (BMV) analyte peak at a retention time of approximately~9.1 min.	130
Figure 7.10.2-1: HPLC chromatogram of hydrocortisone acetate (HCA) showing an HCA analyte peak at a retention time of approximately~3.2 min.	131
Figure 7.10.3-1: Linearity curves of betamethasone valerate (BMV) and hydrocortisone (HCA).	132
Figure 7.10.4-1: Chromatogram of mobile phase (acetonitrile: H ₂ O = 60:40).....	133
Figure 7.10.7-1: Chromatograms of betamethasone valerate (BMV) and hydrocortisone acetate (HCA) showing the effect of change in wavelength on detection of the analyte. The initial wavelength (254 nm) is shown as a red chromatogram; the altered wavelength (240 nm) is shown as a black chromatogram.	136
Figure 7.11-1: The encapsulation efficiency (EE) and drug loading (DL) of crude and extruded ethosomes loaded with betamethasone valerate (BMV) and hydrocortisone acetate (HCA).	138
Figure 8.1-1: The size distribution and zeta potential of unloaded, betamethasone valerate (BMV) loaded and hydrocortisone acetate (HCA) loaded cholesterol (Chol) ethosomes at cholesterol concentrations of 7.5 mg/ml, 10 mg/ml and 15 mg/ml.	144
Figure 8.5-1: SEM analyses of betamethasone valerate (BMV) loaded and hydrocortisone acetate (HCA) loaded ethosomes, with and without cholesterol, taken at magnification (Mag).	148
Figure 8.6-1: FTIR spectrograms of betamethasone valerate (BMV) loaded and hydrocortisone acetate (HCA) loaded ethosomes with and without cholesterol. Arrows indicate peaks shifts in wave number and/or intensity occurred and/or absence/appearance of new peaks.....	150
Figure 8.7-1: HSM analyses displaying observed thermal events and their corresponding temperatures for cholesterol, unloaded, betamethasone valerate (BMV) loaded ethosomes	

with and without cholesterol and hydrocortisone acetate (HCA) loaded ethosomes with and without cholesterol.....	152
Figure 8.8-1: Differential scanning calorimetry (DSC) thermograms of cholesterol (Chol), Chol ethosomes, betamethasone valerate (BMV) loaded and hydrocortisone acetate (HCA) loaded ethosomes with and without cholesterol.	153
Figure 8.9-1: TGA thermograms of cholesterol, Chol ethosomes, BMV loaded and HCA loaded ethosomes with and without cholesterol.	155
Figure 8.9-2: Thermogravimetric analyses thermograms of cholesterol (Chol), Chol ethosomes, betamethasone valerate (BMV) loaded and hydrocortisone acetate (HCA) loaded ethosomes with and without cholesterol.	155
Figure 8.10-1: encapsulation efficiency (EE) and drug loading (DL) of betamethasone valerate (BMV) and hydrocortisone acetate (HCA) loaded Chol ethosomes with and without cholesterol.	157
Figure 8.11-1: The percentage drug release of different ethosomal formulations and the respective standards over a period of 6 hours. Crude = ethosomes without comminution. ..	158
Figure 8.12-1: The release of betamethasone valerate (BMV) and hydrocortisone acetate (HCA) loaded formulations plotted against the Peppas-Sahlin model.	160
Figure A-1: Thermogravimetric analyses 1 st derivative data of pure components and ethosomes, showing thermal events generated using Pyris™ Software	181

List of Tables

Table 2.8-1: Topical preparations containing glucocorticoids	20
Table 2.9-1: Physicochemical properties of hydrocortisone acetate and betamethasone valerate ^{73,74}	21
Table 3.4-1: Ethosomes loaded with active pharmaceutical ingredients (APIs) prepared for transdermal drug delivery	30
Table 4.2-1: The size classification of lipid based drug delivery vesicles.....	40
Table 4.5-1: Parameters which influence ethosomes and the analytical techniques used for analysis.....	47
Table 4.6.3-1: The standard zeta potential values and their related stability behaviour.....	51
Table 4.7-1: An overview of the influence of selected parameters on the quality of HPLC analysis.....	52
Table 4.10.2-1: Characteristics which influence glass transition temperatures of solid state compounds using thermogravimetric analysis.....	57
Table 4.12-1: Mathematical models and their associated release mechanisms	60
Table 5.2.3-1: Ethosome formulations containing BMV and HCA	65
Table 6.1.1-1: The experimental and theoretical Fourier transform infrared spectroscopy (FTIR) spectrum frequencies analysed for betamethasone valerate (BMV) fingerprint region (<1400 cm ⁻¹)	83
Table 6.1.1-2: The experimental and theoretical Fourier transform infrared spectroscopy (FTIR) spectrum frequencies analysed for hydrocortisone acetate (HCA) fingerprint region (<1400 cm ⁻¹)	85
Table 6.1.1-3: The experimental and theoretical Fourier transform infrared spectroscopy (FTIR) spectrum frequencies analysed for phosphatidylcholine (PC) fingerprint region (<1400 cm ⁻¹)	87
Table 6.1.1-4: The experimental and theoretical Fourier transform infrared spectroscopy (FTIR) spectrum frequencies analysed for cholesterol's fingerprint region (< 1400 cm ⁻¹).....	89
Table 6.2-1: The hydrodynamic diameter (HdD), polydispersity index (PdI) and zeta-potential (ζ_p) of unloaded ethosomes prepared using the HM and CM with varying phosphatidylcholine concentrations ($n=3$)	92
Table 6.3-1: The hydrodynamic diameter (HdD), polydispersity index (PdI) and zeta-potential (ζ_p) of crude, sonicated and extruded ethosomes prepared using the hot and cold methods ($n=3$).....	95

Table 7.2-1: The hydrodynamic diameter (HdD), polydispersity index (PdI) and zeta-potential (ζ_p) of unloaded and corticoid loaded ethosomes ($n=3$)	103
Table 7.3-1: The hydrodynamic diameter (HdD), polydispersity index (PdI) and zeta-potential (ζ_p) of sonicated (S) unloaded and corticosteroid loaded ethosomes ($n=3$).....	107
Table 7.3-2: The hydrodynamic diameter (HdD), polydispersity index (PdI) and zeta-potential (ζ_p) of unloaded and corticosteroid loaded extruded (E) ethosomes ($n=3$)	110
Table 7.10.1-1: The chromatographic profile data of betamethasone valerate (BMV) ($n=3$)	131
Table 7.10.2-1: The chromatographic profile data of hydrocortisone acetate (HCA) ($n=3$)	132
Table 7.10.5-1: Repeatability and accuracy of betamethasone valerate (BMV) and hydrocortisone acetate (HCA) at a concentration of 1 mg/ml	134
Table 7.10.6-1: Inter-day precision of betamethasone valerate (BMV) and hydrocortisone acetate (HCA) ($n=3$).....	135
Table 7.10.7-1: Limits of detection and quantification of betamethasone valerate (BMV) and hydrocortisone acetate (HCA) ($n=3$).....	136
Table 7.11-1: The encapsulation efficiency (EE) and drug loading (DL) of betamethasone valerate (BMV) and hydrocortisone acetate (HCA) loaded ethosomes ($n=2$)	137
Table 8.1-1: The size distribution and zeta potential of unloaded, betamethasone valerate (BMV) loaded and hydrocortisone acetate (HCA) loaded cholesterol (Chol) ethosomes at cholesterol concentrations of 7.5 mg/ml, 10 mg/ml and 15 mg/ml.	143
Table 8.4-1: A comparison of the HdD, PdI and ζ_p of unloaded, BMV loaded and HCA loaded ethosomes, with and without cholesterol. ($n=3$).....	146
Table 8.10-1: The encapsulation efficiency (EE) and drug loading (DL) of betamethasone valerate (BMV) and hydrocortisone acetate (HCA) loaded Chol ethosomes ($n=2$)	156
Table 8.12-1: Mathematical modelling of betamethasone valerate (BMV) loaded and hydrocortisone acetate (HCA) loaded ethosomal release kinetics.....	159
Table A-1: FTIR analyses of Chol ethosomes with assigned functional groups.....	181

List of Equations

Equation 1: Relative centrifugal force	45
Equation 2: Stokes- Einstein equation	48
Equation 3: Fundamental vibrational frequency	53
Equation 4: Percentage recovery	72
Equation 5: Limit of detection	73
Equation 6: Limit of quantification.....	73
Equation 7: Percentage yield	74
Equation 8: Drug loading	74
Equation 9: Encapsulation efficiency	75
Equation 10: Standard curve of BMV	133
Equation 11: Standard curve of HCA	133

Table of contents

DECLARATION.....	II
DEDICATION.....	III
PUBLICATIONS AND PRESENTATIONS	IV
ABSTRACT.....	V
ACKNOWLEDGEMENTS	VII
LIST OF ABBREVIATIONS	VIII
LIST OF FIGURES	X
LIST OF TABLES	XV
LIST OF EQUATIONS.....	XVII
TABLE OF CONTENTS	XVIII
Chapter 1: Introduction.....	1
1. Introduction.....	2
1.1. Overview	2
1.2. Aims and objectives	5
Chapter 2: Atopic Dermatitis	1
2. Introduction	5
2.1. Skin.....	5
2.1.1. Histology	5
2.1.2. Physiology.....	6
2.2. Atopic diseases.....	8

2.3. Atopic dermatitis	9
2.3.1. Pathophysiology	10
2.3.2. Symptoms.....	12
2.3.3. Treatment	13
2.4. Topical Dosage forms	15
2.5. Transdermal drug delivery	15
2.5.1. Factors affecting permeation.....	16
2.5.2. Routes of permeation	16
2.6. Steroids.....	18
2.7. Chemical Structure of corticosteroids	18
2.8. Glucocorticoids	19
2.9. Hydrocortisone and betamethasone	21
2.10. Mechanism of action	22
Chapter 3: Nanotechnology and ethosomes	24
3. Introduction	25
3.1. Nanotechnology	25
3.2. Lipid based systems	27
3.3. Nanoparticles and transdermal drug delivery.....	27
3.4. Ethosomes	28
3.5. Phospholipids	31
3.6. Ethanol	32
3.7. Cholesterol	33
3.8. Ethosome mechanism of permeation	34
3.9. Advantages and disadvantages of ethosomes as novel drug delivery systems in transdermal permeation.....	36
Chapter 4: Nanoparticle synthesis	38
4. Introduction	39
4.1. Nanoparticle synthesis.....	39
4.2. Comminution of nanoparticles in suspension	40
4.2.1. Sonication.....	41
4.2.2. Extrusion	43
4.3. Centrifugation.....	44

4.4. Lyophilisation.....	45
4.5. Characterisation of Nanoparticles	46
4.6. Dynamic light scattering	48
4.6.1. Particle size	48
4.6.2. Polydispersity Index.....	49
4.6.3. Zeta potential.....	50
4.7. High performance liquid chromatography	51
4.8. Fourier transform infrared spectroscopy	53
4.9. Scanning electron microscopy	55
4.10. Thermoanalyses.....	55
4.10.1. Hot stage microscopy	56
4.10.2. Differential scanning calorimetry.....	56
4.10.3. Thermogravimetric analysis.....	58
4.11. Drug release.....	58
4.12. Mathematical models of drug release.....	60

Chapter 5 Materials and Methods 62

5. Introduction	63
5.1. Identification of betamethasone valerate, hydrocortisone acetate and cholesterol	63
5.2. Preparation of unloaded ethosomes.....	63
5.2.1. Cold Method.....	63
5.2.2. Hot Method	64
5.2.3. Preparation of corticosteroid loaded ethosomes.....	65
5.3. Comminution of ethosomes	65
5.3.1. Sonication.....	66
5.3.2. Extrusion	66
5.4. Purification	67
5.4.1. Centrifugation.....	68
5.4.2. Centrifugal drying	68
5.5. Analysis and characterisation.....	68
5.5.1. Hydrodynamic Diameter and Polydispersity Index	69
5.5.2. Zeta-potential	69
5.6. High performance liquid chromatography	70

5.6.1. Preparation of the standard solutions for calibration	70
5.6.2. HPLC chromatographic conditions.....	71
5.7. HPLC method validation.....	71
5.7.1. Specificity.....	71
5.7.2. Repeatability.....	72
5.7.3. Linearity	72
5.7.4. Accuracy.....	72
5.7.5. Intermediate Precision.....	73
5.7.6. Limit of detection and limit of quantification	73
5.7.7. Robustness.....	73
5.8. Percentage yield	74
5.9. Determination of drug loading	74
5.10. Determination of encapsulation efficiency	74
5.11. <i>In-vitro</i> drug release of ethosomes	75
5.11.1. Mechanism of release.....	76
5.12. Scanning electron microscopy	76
5.13. Fourier-transform infrared spectroscopy.....	77
5.14. Hot stage microscopy	77
5.15. Thermogravimetric analysis.....	78
5.16. Differential scanning calorimetry.....	78

Chapter 6: Results and Discussion - ethosomal Formulation

Development.....	80
6. Introduction	81
6.1. Analysis of pure components	81
6.1.1. FTIR analysis of pure compounds	82
6.1.2. DSC Analysis of pure components	90
6.2. The effect of PC concentration on ethosomes.....	91
6.3. The effect of sonication and extrusion on unloaded ethosomes.....	95
6.4. Conclusion.....	100

Chapter 7: Results and Discussion - Loaded ethosomal formulation

development.....	101
-------------------------	------------

7. Introduction	102
7.1. The preparation of hydrocortisone acetate and betamethasone valerate loaded ethosomes	102
7.2. The effect of corticosteroids on crude ethosomes	103
7.3. The effect of corticosteroid loading on sonicated and extruded ethosomes.....	106
7.4. Preparation of ethosomes for solid state analyses.....	113
7.5. Scanning electron microscopy	114
7.5.1. The morphology of HM and CM ethosomes	115
7.6. FTIR analysis of BMV loaded and HCA loaded ethosomes	118
7.7. Hot stage microscopy analysis of BMV loaded and HCA loaded ethosomes.....	121
7.8. Differential scanning calorimetry.....	124
7.9. Thermogravimetric analysis	126
7.10. HPLC analyses	130
7.10.1. BMV chromatogram analysis.....	130
7.10.2. HCA Chromatogram	131
7.10.3. Linearity	132
7.10.4. Specificity.....	133
7.10.5. Intraday precision (Repeatability) and accuracy	134
7.10.6. Inter-day precision.....	135
7.10.7. Limit of detection and Limit of quantification.....	135
7.10.8. Robustness.....	136
7.11. Drug loading and Encapsulation efficiency	137
7.12. Conclusion.....	140

Chapter 8: Results and Discussion - Loaded ethosomal formulations with cholesterol141

8. Introduction	142
8.1. The effect of cholesterol on the size distribution and zeta potential of unloaded, BMV loaded and HCA loaded Chol ethosomes.....	143
8.2. The effect of cholesterol on the PDI of ethosomes	145
8.3. The effect of cholesterol on the zeta potential of ethosomes	145

8.4. A comparison of the HdD, PDI and ζ_p of unloaded, BMV loaded and HCA loaded ethosomes, with and without cholesterol.....	146
8.5. SEM analysis of corticosteroid loaded Chol ethosomes	147
8.6. FTIR of analysis of BMV loaded and HCA loaded Chol ethosomes. .	149
8.7. HSM analyses of BMV loaded and HCA loaded ethosomes with and without cholesterol.....	151
8.8. Differential scanning calorimetry analyses of corticosteroid loaded Chol ethosomes.....	153
8.9. Thermogravimetric analysis of unloaded, BMV loaded and HCA loaded Chol ethosomes	154
8.10. Drug loading and encapsulation efficiency	156
8.11. Drug release.....	157
8.12. Release kinetics and mathematical modelling of GC loaded ethosomes 159	
8.13. Conclusion.....	161

Chapter 9: Conclusion and recommendation162

9. Conclusion.....	163
9.1. Recommendation.....	165
9.2. References	167

“Always laugh when you can. It is cheap medicine.”

-Lord Byron, 19th Century English romantic poet



UNIVERSITY *of the*
WESTERN CAPE

CHAPTER 1: INTRODUCTION



School of
PHARMACY

1. Introduction

In this chapter, we introduce the thesis and provide a rationale for the preparation of corticosteroid loaded ethosomes for topical delivery

1.1. Overview

Atopic dermatitis (AD) is one of the most prevalent diseases worldwide. It is a rapidly growing field of study with several research avenues to explore its pathophysiology and to find innovative treatment and management regimens. Clinically, it is classified as a non-contagious, intensely pruritic, inflammatory, chronic skin disorder mediated by abnormalities associated with atopy.² Such abnormalities include abnormal T-lymphocyte function characterized by a predominance of T helper 1 (Th1) and T helper 2 (Th2) related physiological responses.³ This results in a cascading inflammatory reaction resulting in the production of interleukins and immunoglobulins which exacerbate the disease.⁴ Research has shown that there are significant links between AD, stress and autoimmune diseases, with a most significant heredity association between AD and asthma.⁵

The presence of multiple confounding factors associated with AD have created considerable confusion about uniform criteria for the diagnosis and thus, have provided a need for standardized guidelines on diagnosing and managing this condition.⁶ Generally, in practice, the measurement of disease severity and outcome in AD is based on a series of subjective assessments of symptoms. This is influenced by: a thorough patient history, evaluation of clinical manifestations by a physician and the impact on the patient's quality of life.⁷ These clinical manifestations, often characterised by the severity of erythematous skin, are commonly present in the flexural areas of the skin, such as in the nape of the neck, elbow and knee joints.⁸ The result of the assessment determines the extent of the pharmacotherapeutic interventions. To date, there is no absolute therapy for the treatment of AD, owing to a complex pathogenic interplay between the patient's susceptible genes, skin barrier abnormalities and immune dysregulation. Nevertheless, various pharmacological and non-pharmacological approaches have been explored.⁹ Conventional treatment for patients diagnosed with AD includes topical use of corticosteroids, emollients, bath oils, and oral anti-histamines.⁴

Since chronic skin diseases like AD involve long-term glucocorticoid treatment, fear of adverse effects as a result of systemic release may lead to underutilization of drugs,

especially in children. Ineffective therapy as a result of incorrectly prescribed topical dosage forms also influences the willingness of the patient to continue pharmacotherapy. Patient adherence is, therefore, crucial for successful clinical outcomes.¹⁰

Currently, corticosteroids are the most widely used class of anti-inflammatory drugs.⁵ The introduction of topical hydrocortisone in the early 1950s provided significant advantages over previously available therapies and initiated a new era for dermatological therapy. Their clinical effectiveness in the treatment of dermatological disorders is related to their vasoconstrictive, anti-inflammatory, immunosuppressive and anti-proliferative effects.¹¹ Fortunately, systemic side effects of topical corticosteroids (TC) are rare, but may occur in infants and elderly patients.¹² Possible systemic side effects are related directly to factors such as: the application site, duration of application, potency, and occlusion of the medication.¹¹ The application of high-potency corticosteroids should be limited, when possible, to a twice-a-day basis for three to four weeks.¹³ The management of inflammatory diseases with corticosteroids should be tailored to the specific patient's benefit in TC therapy due to the associated number of possible side-effects that limit their use. Such side-effects include osteoporosis, hyperglycaemia and atrophy.¹⁴ Atrophy, at a biological level, refers to a decrease in dermal connective tissue and is characterized by the loss of elasticity and the thinning of the dermis.¹² One of the founding factors for this adverse effect is noted by a histological reduction in the size of corneocytes in the epidermis resulting from high doses of topically applied steroidal medicines.

Betamethasone valerate (BMV) and hydrocortisone acetate (HCA) are commonly used glucocorticoids (GCs) for moderate to severe and mild to moderate inflammatory conditions, respectively. Their use is limited due to an array of side effects which may occur as a result of limited stratum corneum (SC) penetration. Regardless, these active pharmaceutical ingredient (APIs) are utilised in a variety of topical formulations such as ointments, creams, gels and lotions. Although these formulations have their advantages when applied to the skin, they are not specific to AD. The lichenified property of AD results in a thicker epidermal layer, making transdermal permeation more challenging.

Dermal drug delivery involves the topical application of APIs to the skin in the treatment of skin diseases, wherein high concentrations of APIs can be localised at the site of action.¹⁵ Due to the large surface area of the skin utilised for transdermal drug delivery, the skin provides an alternative desirable route of administration over the oral route. This route of

administration bypasses the liver and subsequently avoids the first pass metabolism inactivation effect. Avoiding first pass metabolism may also significantly increase the bioavailability of the drug. A controlled delivery of drugs through the skin can induce steady-state plasma-drug concentrations and reduce the drug spike concentrations observed from orally administered drugs.¹⁶

One of the main functions of the skin is to protect the body from extraneous factors as it, essentially, keeps in what is required and keeps out what is not required. Transdermal drug delivery is challenging because the skin, as a natural barrier, inhibits the absorption of foreign materials. i.e. materials not endogenous to the human body.¹⁷ Although APIs are utilised for their benefits, the body may recognise them as foreign materials and inhibit transdermal permeation. Factors limiting the success of transdermal dosage forms may arise from adverse reactions associated with specific APIs and/or the excipients utilised within the topical formulation e.g. cream, lotion, ointment, and gel. Transdermal drug delivery studies have shown that the formulation limitations may include: a lag time associated with the delivery of the drug across the skin resulting in a delay in onset of action, variation of absorption rate based on the site of application, skin disease (absorption may be delayed, especially in the case of water-soluble compounds), and variation in adhesive effectiveness in different individuals.¹⁶ For this reason, APIs tend to have a very low permeation rate. Therefore, several methods (e.g. iontophoresis, needless jet injectors, sonophoresis, electroporation) have been assessed to improve topical drug delivery systems.¹⁶ One approach under investigation is the use of nanoparticle formulations.¹⁵

The emergence of nanotechnology has allowed for an influx in novel drug delivery systems intended for pharmacotherapeutic application. This has broadened the manner in which pharmaceutical dosage forms may be optimised to deliver APIs to their intended systemic sites of action in the human body. Since the advent of nanotechnology, a variety of nanoparticles (particles sized 1-200 nm), such as nano-emulsions, niosomes, liposomes, dendrimers and ethosomes have been designed to overcome the specific obstacles associated with the delivery of its respective APIs.¹⁸ These challenges may include complications regarding palatability, poor dissolution rates, poor gastrointestinal tract (GIT) drug absorption, overcoming first pass metabolism, targeted cell delivery and transdermal permeation.¹⁹

Liposomes, often used for dermatological application, are nano-sized drug carriers developed during pre-formulation for the optimisation of transdermal drug delivery.²⁰ Although they are considered promising nano-vesicular systems, liposomes have limitations regarding vesicle flexibility - an influential characteristic for transdermal permeation, and limited stability.²¹ As such, liposomes have been optimised by the addition of surfactants and other excipients to increase their physical and chemical stability and resultant permeation characteristics. Ethosomes, a slight modification on well-established liposomes, are novel nano-carrier systems used for the delivery of APIs having low penetration through the skin. These nano carriers are suited for the encapsulation of both hydrophilic and lipophilic APIs. These lipid vesicles containing phospholipids, alcohol (ethanol and isopropyl alcohol) and water, permeate through the skin layers more rapidly and possess significantly higher transdermal flux in comparison to conventional liposomes.²² Additionally, the incorporation of biocompatible materials make these nano-drug delivery systems decrease the likelihood of immune system rejection of the encapsulated API. Coupled with numerous other advantages, ethosomes are potential API vectors for transdermal drug delivery.²³ Therefore, ethosomes encapsulated with either BMV or HCA provided an avenue for research investigation to overcome the challenges associated with topical drug delivery systems used in the management of AD.

1.2. Aims and objectives

- A.** To conduct a literature search regarding the pathophysiology and treatment of atopic dermatitis and the obstacles surrounding transdermal drug delivery
- B.** To review the different types of nanoparticles and select the most appropriate for the purpose of this study
- C.** To formulate the most appropriate nanoparticle using hot and cold methods
- D.** To characterise the nanoparticle according to its physical and chemical stability
- E.** To compare the results of the hot and cold methods based on the particle size, polydispersity index, zeta-potential, encapsulation efficiency and drug loading
- F.** To select the most appropriate formulation method and optimise the nanoparticle formulation according to the same parameters.
- G.** To determine the drug release rate and mechanism of drug release from the nanoparticle using mathematical models.



UNIVERSITY *of the*
WESTERN CAPE

CHAPTER 2: ATOPIC DERMATITIS



School of
PHARMACY

2. Introduction

In this chapter, **objective A** will be discussed where the skin disease - atopic dermatitis, the treatment route, transdermal permeation and the obstacles surrounding transdermal drug delivery are reviewed.

2.1. Skin

Covering a total surface area of approximately 1.8 m^2 , the skin is the largest human organ.²⁴ Apart from providing contact between the human body and the external environment, the skin has many physiological functions which help to regulate homeostasis within the human body. These functions include: mechanical support, chemical barrier, radiation barrier, osmoregulation and thermoregulation.²⁵ The skin functions as a two way barrier. It controls the loss of water, electrolytes and other body constituents, while simultaneously preventing entry of unwanted solutes from the environment. As a rate limiting step of transdermal flux, it serves as a permeability barrier, however the large surface area and easy accessibility renders it as an attractive route for drug delivery.¹

2.1.1. Histology

The human skin is composed of a series of layers: the epidermis, dermis and hypodermis (**Figure 2.1.1-1**). Each layer has a distinct composition and function - the respective function of which is influenced by the composition of cells and tissue within it. The outermost layer, the epidermis, is composed of keratinocytes with five different strata: *stratum basale*, *stratum spinosum*, *stratum granulosum*, *stratum lucidum* and *stratum corneum* (SC).¹¹ However, the *stratum lucidum* is only present in the palms of the hands and the soles of the feet. SC, also referred to as the horny layer, is the external barrier layer of the skin is located in the outermost layer of the epidermis.¹¹ This layer of keratinocytes is in contact with the external environment.

The stratum corneum (outer most layer of the epidermis) consists of corneocytes and is the rate limiting barrier for anything entering or exiting the human body. The dermis is the “middle layer” which is predominantly innervated by blood vessels and sensory receptors. Subcutaneous tissue (hypodermis) is comprised of adipocytes which provide insulation and influence thermoregulation. The skin appendages consist of eccrine (sweat) glands, hair follicles and sebaceous glands which influence homeostasis.

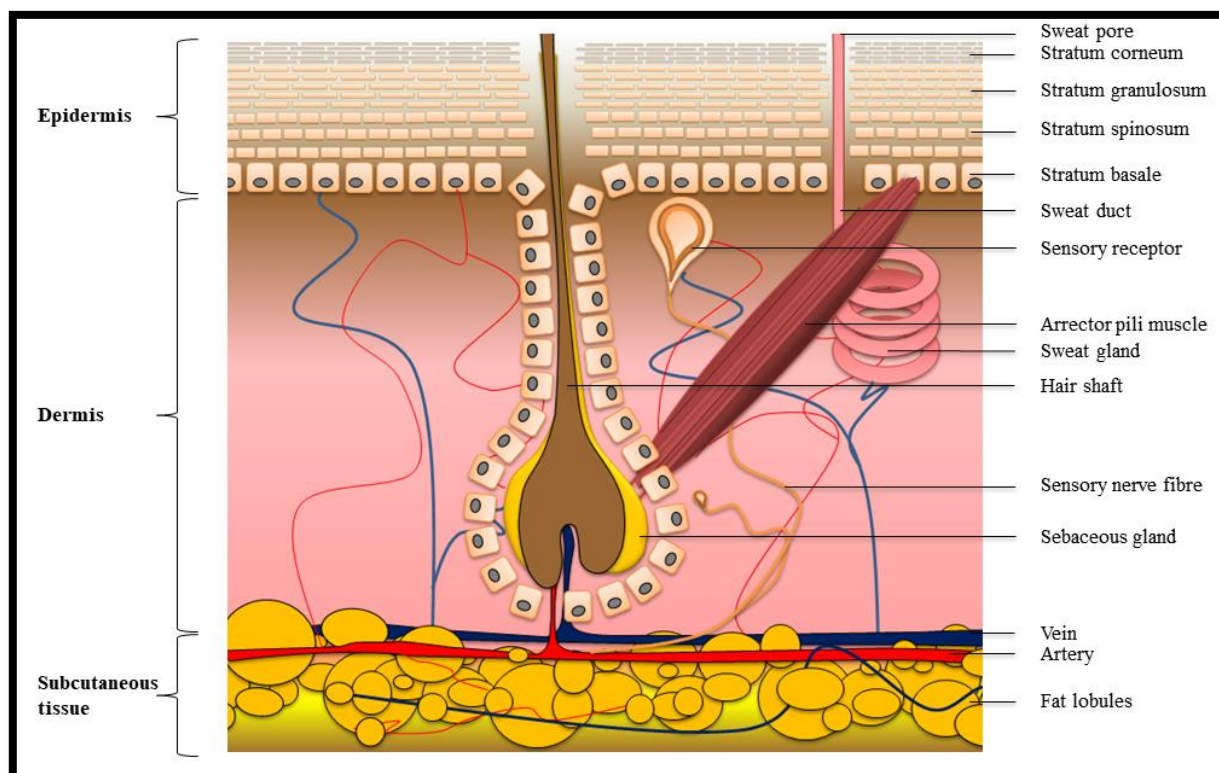
Adapted from ¹⁷

Figure 2.1.1-1: A diagrammatical representation of a cross-section of human skin showing the different cell layers and appendages.

The major fractions of healthy SC are neutral lipids (78%) and sphingolipids (18%) together with a small amount of polar lipids.¹⁷ Both saturated and unsaturated fatty chains exist in all neutral lipid species, with unsaturated chains predominating except for the free fatty acids fraction.¹⁷ The ceramide (sphingolipid) fraction primarily consists of saturated fatty acid chains. Thus, many lipid species exist in the horny layer, differing both in type and chain length, forming a bilayer structure with a complex lipid mixture. The cells found in the SC are called corneocytes. These cells are dead cells (i.e the cell nucleus is absent). The epidermis without the SC is usually termed the viable epidermis and is usually the API target for pharmacotherapeutic activity. As most APIs applied onto the skin permeate along the lipid domains, the organization and composition of the lipid component is considered to be very important for the skin barrier function.²⁶

2.1.2. Physiology

Primarily serving as a barrier between the external environment and the complex internal anatomy of the human body, the skin has a variety of functions. These functions, mediated by its different layers, may be classified into 2 main groups: protective and mechanical.

Protective properties

The main function of the skin is to serve a protective purpose. Located at the frontier of the body's perimeter defence system, the skin is the barrier that regulates the movement of endogenous and exogenous material in the human body. Although the SC constitutes only 10% of the entire skin, it contributes to over 80% of the cutaneous barrier function.²⁷

The skin, also acts as a chemical barrier. This function regulates the movement of molecules or compounds across the skin. Packed with corneocytes, the SC also acts as a microbiological barrier. These dead skin cells are shed daily and are constantly replaced. The arrangement of these cells serves as a barrier that protects against foreign organisms attempting to penetrate the epidermal layer of the skin to access the viable dermal tissue. On its surface, the skin is also covered with microorganisms which, similar to gut flora, have a symbiotic relationship with the host.⁷ In this instance, the microorganisms assist in the natural defence system of the skin. If the epidermal layer of corneocytes is compromised, microorganisms may enter the skin through the superficial cracks, replicate and cause infection in the dermis. These cracks may be the consequence of pruritus, inflammation, key enzymatic reactions, bacterial flora, immune signalling compounds or a failure to preserve the acidic pH.²⁷ Furthermore, the SC is a biosensor that regulates the response of the epidermis by sensing the level of cytokines and growth factors which bind to cellular receptors to stimulate proliferation and differentiation of cells. This promotes strong healthy skin and stimulates collagen and elastin that are key inflammatory reaction indicators.¹⁷

The skin also acts as a radiation barrier by minimizing the effects of ultraviolet (UV) and infrared (IR) radiation.²⁸ These potentially harmful rays are absorbed and the associated heat is dissipated through the regulation of blood flux and/or perspiration. This is achieved due to the anatomy of the dermis which has an adequate supply of vasculature to facilitate these processes.

As a heat barrier, the skin is influential in thermoregulation. Due to varying thicknesses in the SC across the body, it does not effectively protect the underlying living tissues from extreme temperatures. However, assisted by adipose tissue, it is the primary organ responsible for preserving the core body temperature at 37 °C. To conserve heat, the peripheral circulation shuts down to minimize surface heat loss; shivering generates energy when chilling is severe.

To lose heat, blood vessels dilate, eccrine sweat glands pour out their dilute saline secretion, water evaporates, and removal of the heat of vaporization cools the body.²⁵

The SC is a highly lipophilic layer which is almost impermeable to water and its structure contributes to osmoregulation which prevents the loss of water from the epidermis.²⁹ As the main function of the skin is to protect the underlying tissues and organs, skin hydration protects humans against the dry environment. The SC maintenance of the body's hydration is critical in aiding skin flexibility.³⁰ Considering the large volume of water within the body, the skin plays an influential role in osmoregulation in order to facilitate the movement of water out of the body via eccrine glands.

When the skin undergoes trauma, it may bruise, blister or rupture. During the healing process, facilitated by the capillary anastomoses in the dermis, the skin will repair. Overcompensation may result in lichenification (a thickening of the epidermis, sometimes producing callouses and corns).^{14,31} This adaptation may also serve as a protective function to maintain the barrier function of the skin.

Mechanical properties

Relative to the epidermis, the dermis provides a supportive mechanical property to the skin. The elasticity of the skin is a mechanical function maintained by the dermis. With age, the skin wrinkles and becomes more rigid. The thin horny layer is quite strong and is dependent on its pliability by the correct balance of lipids, water-soluble hygroscopic substances i.e. the natural moisturising factor and water. Research has shown that skin accounts for 8 % total body water and is comprised of 65 % water.³² The tissue requires 10-20% of moisture to act as a plasticizer and to maintain its suppleness. The skin, therefore, plays an important part in regulating protective functions against external, mechanical, chemical, microbial and physical influences.

2.2. Atopic diseases

Atopy (Greek: *atopia*, out of place) denotes an inherited, genetic predisposition or familial response resulting in the elevated expression of immunoglobulin E (IgE) antibodies in response to an allergen.³³ This type I hypersensitivity reaction is the result of an immune response triggered by a relatively minute amount of common environmental proteins such as pollen, house dust mites, and food allergens.³⁴

Atopic diseases, particularly in childhood, are detrimental to public health. According to the WHO, every third person in the world suffers from at least one atopic disease and most cases manifest in childhood.³⁵ The incidence of atopic diseases such as atopic dermatitis (AD), allergic rhinitis and asthma has increased in both children and adults.^{36,37} However, there is a marked worldwide variation in the prevalence of both symptoms and diagnoses among children, ranging from 1.6% to 36.7% for asthma symptoms, 1.4% to 39.8% for rhinoconjunctivitis symptoms, and 0.3% to 20.5 % for atopic eczema symptoms.³⁴

Although atopic diseases are usually characterised by their associated clinical manifestations, it can be present in the form of asymptomatic sensitization where an individual, with confirmed allergic sensitization to one or more allergens, does not exhibit clinical allergy.² However, although there is an overwhelming amount of evidence to support the claim that atopic diseases stem from atopy, an atopic disease can be present in a non-sensitized individual (e.g. in non-atopic asthma).^{34,38} Supported by the advent of the *Atopic March*, research has been directed at better understanding the aetiology and pathophysiology associated with branches of disease stemming from atopy.^{34,39}

2.3. Atopic dermatitis

Atopic dermatitis (AD) is the most common skin allergic disease, affecting 1% to 20% of the population and has an onset in 80% of cases in children younger than 2 years of age. Although there is no significant difference between genders in the first years of life, it is more frequent in women (60%) than in men (40%) after 6 years. AD usually reverts to remission symptoms before 5 years in 40% to 80% of patients and in 60% to 90% at 15 years of age.



AD – “Normal” Skin



AD - Lichenified Skin

Figure 2.3-1: Normal skin and lichenified skin resulting from chronic scratching.

During this remission period, the symptoms of AD are less severe or absent.⁴⁰

The history of AD has been complicated by the lack of recognition of the full clinical and pathogenic spectrum of this disease. A review of the many names given to this disease reveals the intent of the early physicians to characterise this disease by implicating one of the many features (e.g., infantile eczema, "allergic" eczema, eczema flexorum, "neurodermatitis").⁴¹ It was not until 1933 that Dr Wise and Dr Sulzberger coined the phrase atopic eczema when they noted the high incidence of "atopy".⁴¹ For this reason, AD and eczema are often used synonymously as they both refer to a chronic skin disease with origins of atopy. The acute phase of AD, as seen in infantile form, shows features of acute or subacute eczema with spongiosis, acanthosis, oedema and infiltration of the dermis with lymphocytes, histocytes, plasma cells and eosinophils.^{42,43} When lichenification (**Figure 2.3-1**) occurs in older age groups, the picture resembles that of chronic eczema, with an increasing number of Langerhans cells.^{44,45} These dendritic cells are antigen-presenting immune cells which are prominent in all layers of the epidermis and are most prominent in the *stratum spinosum*.

2.3.1. Pathophysiology

AD is a complex and multifactorial disease. It is strongly linked to genetic pre-dispositioning factors, and usually results in skin barrier dysfunction, which then establishes the basis for inflammatory responses, leading to dermatitis.⁴⁶ Research has shown that AD occurs as a result of both genomic and non-genomic responses (**Figure 2.3.1-1**).⁴⁷ It is currently known that the pathophysiology of AD is mediated, in part, by abnormal T-lymphocyte function. This dysregulation of T-cell function is characterized by a predominance of T helper 2 (Th2)-related cytokine production over T helper 1 (Th1) responses.³

The main cytokines involved in the pathogenesis are the Th2 immune mediators, IL-4 and IL-13.^{43,48} These cytokines have demonstrated genetic mutations resulting in polymorphisms linking AD to a familial predisposition. Multiple genes and associated genetic mutations may be involved in the pathology of AD. Studies have shown that IL-4 decreases expression of multiple genes in the epidermal differentiation complex that regulates epidermal barrier function.⁴³ Keratinocytes differentiated in the presence of IL-4 and IL-13 exhibited significantly reduced filaggrin (FLG) gene expression, even in patients without FLG mutations, contributing to a defective skin barrier in patients with AD.⁴² This imbalance in

immunologic cells favours an autoimmune diagnosis and shifts the focus pathogenesis from environmental factors to a genetic predisposition. These cells are involved in IgE-mediated

Adapted from 6,40–42,174,175

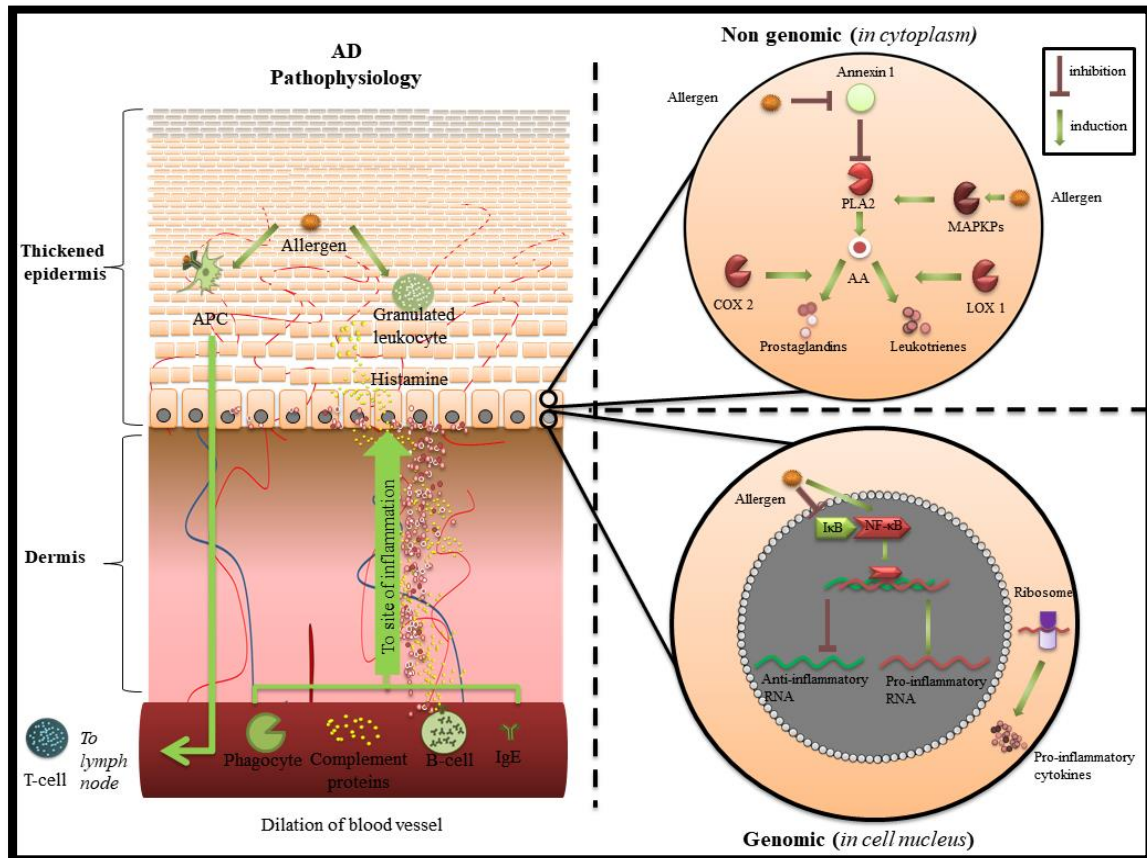


Figure 2.3.1-1: A simplified diagrammatical representation of the pathophysiology of AD, showing an inflammatory cascade that occurs on the onset of an allergen invading the body, triggering genomic and non-genomic responses.

hypersensitivity as well as an autoimmune response. The filaggrin gene, which codes for a protein (profilargin) and is responsible for epidermal structure is another role player in the pathogenesis of AD. Studies have shown that patients suffering from AD have a significant reduction (up to 50 %) in profilargin conferring risk when compared to healthy patients.³¹ Other genes from the immune system involved include: STAT-6, RANTES and TGF-beta).⁴⁰

The skin is innervated by immune cells which defend the body against foreign materials such as viruses, allergens and bacteria. Once foreign material enters the skin via a lesion, the innate immunity activates immune cells to suppress it. Granulated cells, such as mast cells, detect the antigen of the foreign body and are triggered to release histamine. The release of

histamine results in vasodilation and an inflammatory cascade which results in the migration of immune cells in the plasma (monocytes) to infiltrate the infected tissue (macrophages). Leukocytes, such as neutrophils (first responders), infiltrate the tissue via diapedesis and engulf the pathogen. Once the pathogen is engulfed via phagocytosis, it is destroyed and its remnants (amino acid chains) are presented on the cell's surface on a major histocompatibility type I (MHC-I) receptor. The expression of the antigen on the membrane bound protein MHC-I results in the release of interleukins and other cytokines to induce leucocytosis and the release of complement proteins to be secreted by the liver. Complement proteins assist in the detection of the invading organism and destroy it via opsonisation, agglutination and lysis. This increases the ability of the immune system to detect the foreign body. Antigen presenting cells, such as the Langerhans cell, engulf the pathogen and present it on the cell surface on a major histocompatibility type II (MHC-II) receptor. The expression of the antigen on the MHC-II receptor results in the activation of the adaptive immune system where T cells and B cells are then activated. The activation of T cells and B cells results in their maturation, proliferation and differentiation in the lymph nodes resulting in the expression of immunoglobulins such as immunoglobulin E (IgE). In the non-genomic pathway, the MHC-I expression on infected viable epidermal cells results in apoptosis by the natural killer cells (NKs).

The structural integrity of the epidermal cells becomes compromised resulting in the phospholipid bilayer's breakdown and the metabolism of phospholipids to inflammatory mediators such as arachidonic acid (AA), leukotrienes and prostaglandins. In the genomic pathway, the antigen triggers nuclear factor κ B to initiate gene transcription where RNA migrates from the cell nucleus to the ribosomes resulting in the synthesis of pro-inflammatory cytokines.

2.3.2. Symptoms

AD may be characterised by the classical symptoms associated with inflammation. These symptoms include redness (*rubor*), pain (*dolor*), heat (*calor*) and swelling (*tumor*). Other less clinical symptoms may include interrupted sleep, low self-esteem, anxiety and hyper self-awareness. Pruritus, the most common resultant symptom, may be described as an unpleasant sensation in the skin, provoking a motor response to scratch.

Immunologic factors and the central nervous system are integral components in understanding the pathophysiology of an itch. This mechanism is poorly understood but has been linked to increased histamine 1 (H₁) levels in the bloodstream.⁴⁹ Unfortunately, in an attempt to alleviate the symptoms by scratching, further irritation of the skin often occurs resulting in subsequent exacerbation where the reflex response is to scratch again. AD is a typical example of a pruritic associated disease, where chronic skin lesions result from the

Adapted from ⁶

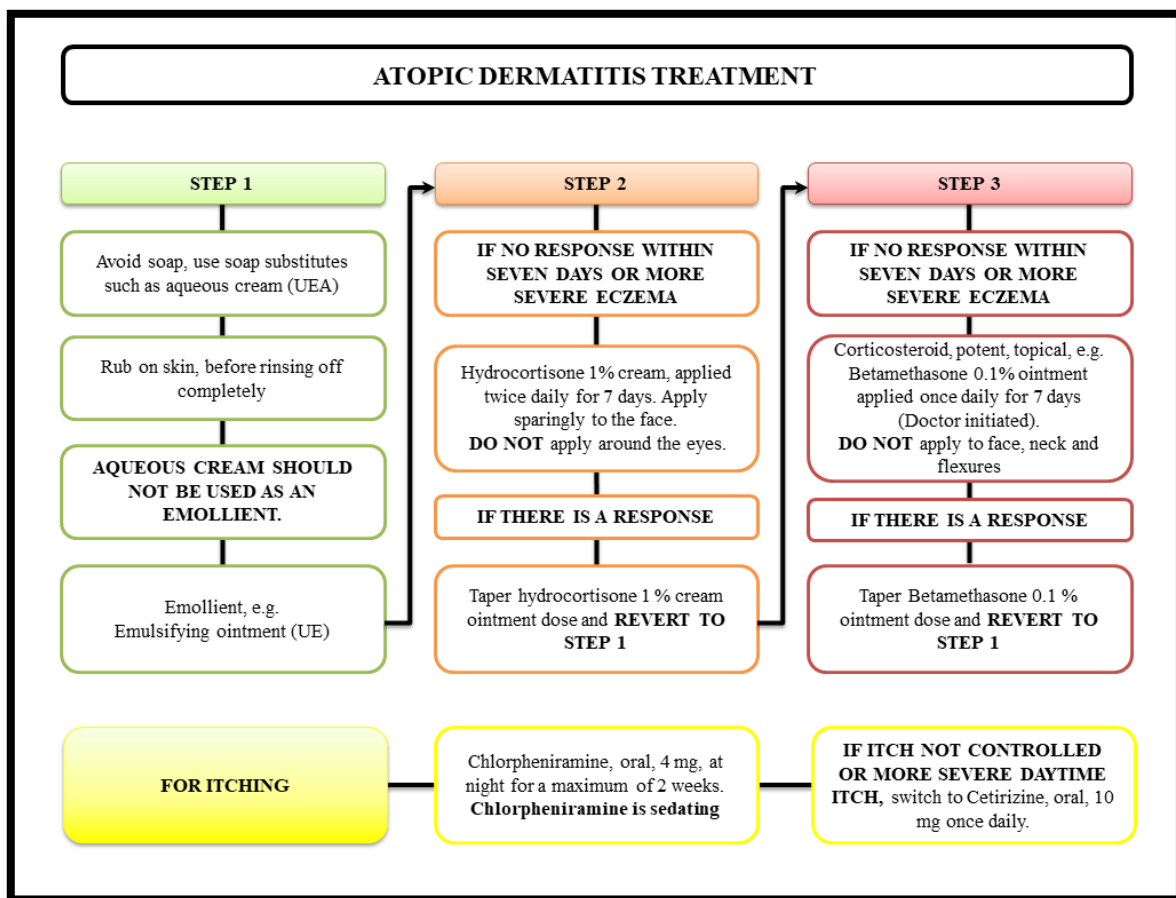


Figure 2.3.3-1: A summary of the standard treatment of atopic dermatitis patient’s intensive scratching or rubbing of the itchy areas.⁴¹

2.3.3. Treatment

AD is usually a chronic condition and requires long term care. Sufferers of AD are particularly susceptible to opportunistic co-infections which are managed accordingly. Symptoms are usually characterised according to the severity of the inflammation and clinical manifestations of the skin. AD has no known cure and the symptoms are managed with pharmacological and non-pharmacological measures.

In general, non-pharmacological measures may be implemented to reduce the exacerbation of the disease. These measures include: patients being aware of any material (e.g. apparel, bedding) which makes direct contact with the skin and causes skin irritation, then making a conscious effort to avoid such items, trimming finger nails to a short length to reduce the effect on the skin when scratching, inevitable scratching should be avoided or managed to avoid causing harm and triggering inflammatory mediators, good personal hygiene with regular washing to remove crusts and accretions.⁴⁰ Patients should be encouraged to reduce the frequency of sweating and to keep cool. Implementing these measures reduces the risk of secondary infection. Although patient diet role may have no role in AD treatment, it is still beneficial to monitor the effect of any consumed items. It may be of significance that histidine is an essential amino acid which is converted into histamine – an inflammatory mediator associated with pruritus. Linoleic acid (omega-6) and alpha linolenic acid (omega-3) are essential fatty acids obtained from a patient's diet. These essential fatty acids may act as a substrate for inflammatory by-products such as arachadonic acid in an AD sensitised patient.

Due to exacerbation of the inflammation with fragranced soaps, patients are encouraged to wash using aqueous cream (UEA). UEA should be applied to the skin before it is rinsed off completely and the skin should be air-dried. However, UEA contains sodium lauryl sulphate (SLS) – a surfactant with a variety of pharmaceutical applications including: penetration enhancer, solubilising agent and emulsifying agent. The epidermal water barrier can be disrupted by SLS which may facilitate the permeation of foreign materials through skin. An investigation has shown that concomitant topical application of aeroallergens and irritants on the skin of sensitized atopic subjects leads to more severe barrier disruption.⁵⁰ Therefore, it is advised that UEA should not be used as a moisturising agent. Pharmacological interventions (**Figure 2.3.3-1**) are usually implemented if there is no non-pharmacological response within seven days; or in instances where the AD is severe.

In even more severe cases, a more potent topical corticosteroid (e.g. clobetasol propionate 0.05 % ointment) is applied.⁵¹ Antihistamines (e.g. cetirizine, oral, 10 mg, once daily) may supplement this treatment to manage associated pruritus which, when resolved by scratching, may aggravate the already present inflammatory symptoms.⁴⁹ Therapeutically, the most consistent antipruritic agents remain the systemic and topical immunomodulators i.e. corticosteroids.⁴¹

2.4. Topical Dosage forms

Since corticosteroids are associated with an array of adverse effects, it is necessary to limit systemic circulation and promote a localised pharmacological action. To facilitate this rationale, topical drug delivery is the most suitable drug delivery system for the symptomatic management of AD.^{2,52,53} These preparations allow localized administration of the drug via a surface membrane through ophthalmic, vaginal, dermal and rectal routes.¹⁸ Topical dosage forms include a variety of formulations intended for cosmetic or dermatological application to healthy as well as diseased skin.²⁶ These formulations, varying in physicochemical nature and rheological properties may have phase variations which range from solid through to semisolid to liquid. For medicinal purposes, APIs are rarely administered alone, but rather as part of a formulation, in combination with one or more excipients that increase stability of the formulation and shelf-life, increase solubility and subsequent bioavailability, and ultimately optimise drug delivery.⁵⁴

2.5. Transdermal drug delivery

Dermal drug delivery is the topical application of drugs to the skin, wherein high concentrations of drugs can be localised at the site of action, thereby reducing the systemic drug levels and side effects.⁵⁵ Among the different non-invasive routes available to the patient, the transdermal route has become increasingly popular and accounts for about 12% of the global drug delivery market. It provides a viable administration route for potent, low molecular weight APIs which cannot withstand the hostile environment of the GIT and bypasses first pass metabolism by the liver. Due to ease of administration of topical medicines and other advantages over corresponding oral, injectable and inhaler systems, transdermal drug delivery systems are experiencing a high growth rate.⁵⁶

Despite the many advantages of the skin as a site of drug delivery, only few a drugs are currently on the market as transdermal delivery systems.²³ The primary reason for this is the low permeability of drugs through the SC, which, as the primary interface of the epidermal barrier, acts as the rate limiting step of transdermal permeation.^{57,58} Various strategies to overcome these barrier properties are constantly being explored. Many techniques have been aimed to disrupt and weaken the highly organized intercellular lipids in an attempt to enhance drug transport across the intact skin or to increase the driving force for permeation of drugs across this skin barrier.^{57,61,62} Ideally, these investigations should employ human skin.

However, samples of human skin of sufficient size and quality for permeation experiments are not readily accessible to most investigators and are only available in limited amounts. Thus, many biological (e.g porcine skin, rat skin) and synthetic models (e.g. nitrocellulose, cellophane) have been explored to replace human skin.^{27,61} Transdermal drug delivery is an effective administration route for the management of a variety of skin diseases.^{2,45,46} Since AD presents as an abnormal clinical manifestation of the skin most commonly associated with varying degrees of inflammation, topical pharmacotherapeutic formulations are most commonly used in its management.

2.5.1. Factors affecting permeation

The factors that affect the permeation of topically applied agents through the SC are: size, shape, superficial charges, lipophilicity, presence of penetration enhancers, type of formulation, molecular weight, aqueous solubility, and physical state of the stratum corneum.⁶⁴ These precipitating factors are mediated by a series of defensive homeostatic processes such as, the low pH (5.5-6.5), of the skin, the presence of metabolic enzymes in the skin, and the transcutaneous concentration gradient that regulate the movement of substances into and out of the epidermis.^{16,54,65}

2.5.2. Routes of permeation

The SC is considered as the rate limiting barrier in transdermal permeation of most molecules.¹⁷ For many molecules applied to the skin, two main routes of skin permeation have been defined: the trans-epidermal and trans-appendageal pathways.⁵⁵

The skin has many interfacial boundaries which influence transdermal permeation (**Figure 2.5.2-1**). These interfacial boundaries include: the skin surface, the stratum corneum, the appendages (eccrine glands and hair follicle), the viable epidermis (nucleated skin cells), the dermis, and blood vessels. Diffusion is the common mechanism by which APIs move through the interfacial boundaries.

Transdermal permeation of molecules/compounds via the trans-epidermal pathway involves the transport of compounds across the intact SC. This pathway can be further subdivided into two micro pathways i.e. the intercellular route and the transcellular route. The intercellular route is the primary route of permeation which is a continuous convoluted pathway through adjacent intercellular lipid spaces. The transcellular route is the secondary route of

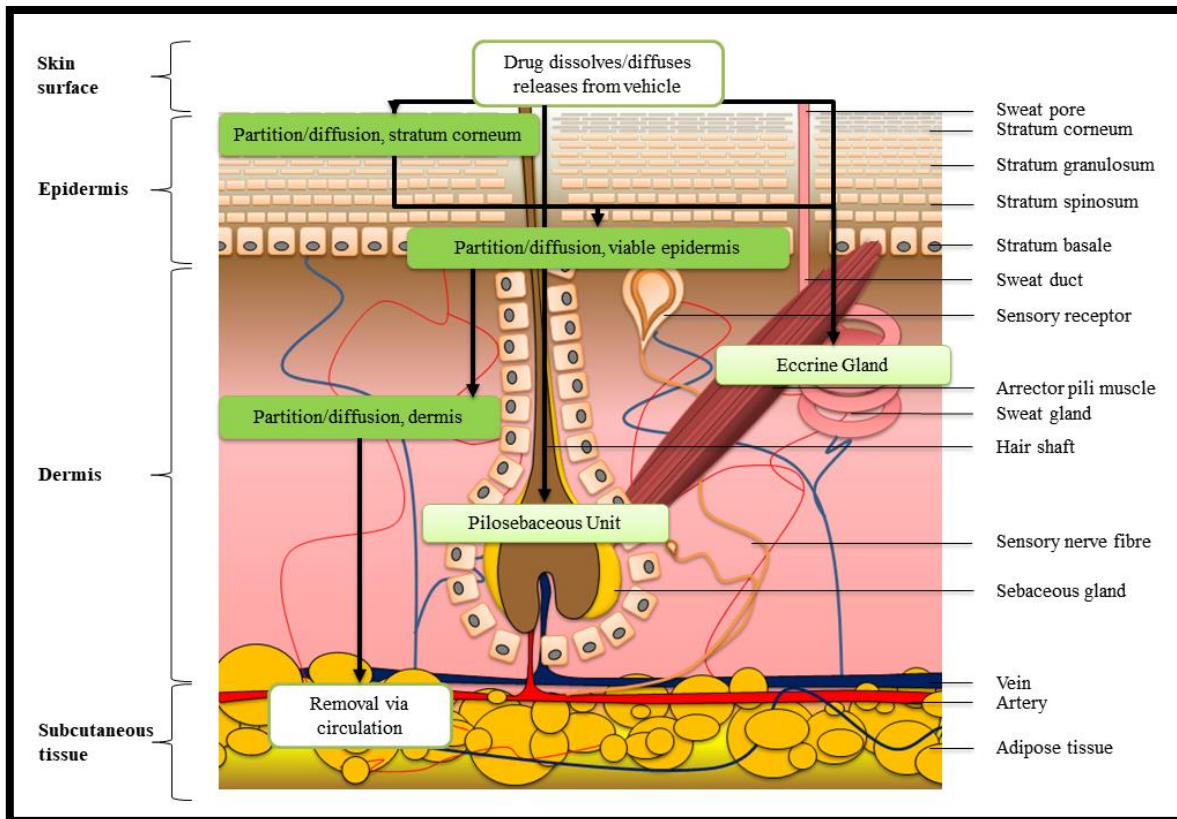
Adapted from ^{17,25,29}

Figure 2.5.2-1: A diagrammatical representation of a cross section of the skin showing the pathways associated with transdermal drug delivery.

permeation where molecules transverse the external membrane of keratinocytes at the epidermis and then across the intercellular lipids.¹⁷ Most drug absorption is transcellular and it is unlikely that noticeable absorption occurs between cells. It is a passive diffusion process, where the magnitude of permeation will not only depend on the integrity and efficacy of the epidermal barrier, but which will be influenced by the drug itself as well as its carrier.⁵⁸

Although most permeation transpires transcellularly, the sweat glands and hair follicles with their associated sebaceous glands also provide an avenue for transdermal permeation. These transappendageal routes, also referred to as the shunt routes, are less common due to the relative skin surface occupied by skin appendages.¹⁸ Even though less significant in terms of a target for drug delivery (hair follicles occupy approximately 0.1% of the surface area of human skin), follicular number, opening diameter and follicular volume are important considerations in drug delivery through these appendages.¹⁷

Regardless of the route, there are junctions composed of both lipophilic and hydrophilic regions which affect the rate of permeation. Research has shown that drugs with low molecular weight (below 800 Daltons) and highly hydrophilic and highly lipid soluble show the greatest penetration.⁵⁸ The formulation vehicle that contains the applied drug and the degree of hydration of the skin are important factors which influence drug flux. Occluding the epidermis increases its water content, enhancing drug absorption.

It is also important to note that the dermis has a rich supply of blood and macrophages, lymph vessels, dendritic cells, and nerve endings. Immunological components influence the transdermal route because therapeutic agents have to bypass these endogenous defence systems. Potential recognition of such agents can result in degradation and a subsequent decreased bioavailability.

2.6. Steroids

Steroids are a group of cholesterol derived lipophilic, low-molecular weight compounds which, apart from being chemically synthesised, are obtained from a variety of different marine, terrestrial, and synthetic sources. The steroid family includes the sterols, a number of hormones (both gonadal and adrenal cortex hormones) and some hydrocarbons.⁶⁶ Steroid hormones are the chemical messengers responsible for specific biological functions. Depending upon the function performed and the site of action, the steroid hormones are categorized as: sex steroids, corticosteroids, anabolic steroids and vitamin D.^{67,68} Topical corticosteroids represent a significant milestone in dermatologic therapy. Topical hydrocortisone was the first corticosteroid to be successfully employed in the treatment of selected dermatoses.⁸

2.7. Chemical Structure of corticosteroids

All steroids are derived from cholesterol.⁶⁸ This forms the steroidal nucleus which is numbered and, therefore, different classes of steroids resemble closely since all of them have the same basic perhydro-1,2-cyclopentenophenanthrene skeleton (A, B, C, D rings in **Figure 2.7-1**). A slight variation in this skeleton or the introduction of functional groups results in various classes of steroids.⁶⁹

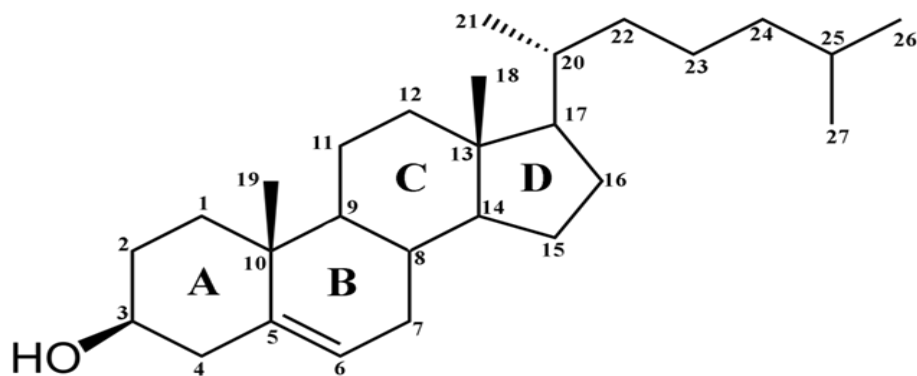


Figure 2.7-1: The chemical structure of the perhydro-1,2-cyclopentenophenanthrene skeleton for corticosteroids with carbon numbering and rings.

Steroids are involved in a wide range of physiologic systems such as: stress response, immune response, regulation of inflammation, carbohydrate metabolism and protein catabolism. Electrolyte balance in the blood stream and subsequent effects on osmotic pressure are a result of the promotion of sodium retention in the kidneys.⁵¹ Examples of endogenous corticosteroids include cortisol (a glucocorticoid) and aldosterone (a mineralocorticoid). Aldosterone is structurally very similar to cortisol, except that it lacks the 17 α -hydroxyl group, and has an aldehyde at the 18-methyl. The 18-aldehyde is critical for mineralocorticoid activity; the sole difference between cortisol and aldosterone is the 18-aldehyde, but aldosterone has 200 times higher mineralocorticoid activity than corticosterone.^{47, 68}

2.8. Glucocorticoids

Glucocorticoids (GCs), such as cortisol, are steroid hormones that affect energy metabolism (among a large variety of other actions). Hydrocortisone is the most potent glucocorticoid secreted by the adrenal gland. Naturally occurring GCs and related semisynthetic analogues can be evaluated in terms of their ability to sustain life, to stimulate an increase in blood glucose concentrations and a deposition of liver glycogen, to decrease circulating eosinophils, to affect immune system functions, inflammatory responses, and cell growth.⁷⁰ These steroids are available as medicines in a variety of dosage forms in varying concentrations depending on the GC potency (**Table 2.8-1**).

Table 2.8-1: Topical preparations containing glucocorticoids

CLASSIFICATION	GLUCOCORTICOID	CONC. (% w/w)	TOPICAL DOSAGE FORM
Weak	Dexamethasone	0.001	Cream
	Methylprednisolone	0.01	Cream
Weak-mild	Alclometasone dipropionate	0.05	Ointment, cream
	Prednicarbate	0.1	Cream
	Hydrocortisone valerate	0.1	Cream
Mild	Triamcinolone acetonide	0.1	Lotion
	Fluocinolone acetonide	0.1	Cream
Mild- moderate	Betamethasone valerate	0.01	Lotion
	Amcinonide	0.1	Lotion
Moderate	Betamethasone valerate	0.01	Ointment
	Fluocinonide	0.05	Ointment, cream, gel
Potent	Mometasone furoate	0.1	Ointment
	Clobetasol propionate	0.05	Ointment, cream, foam, spray, gel
Very potent	Halobetasol propionate	0.05	Ointment, cream

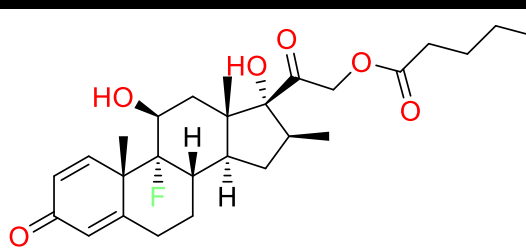
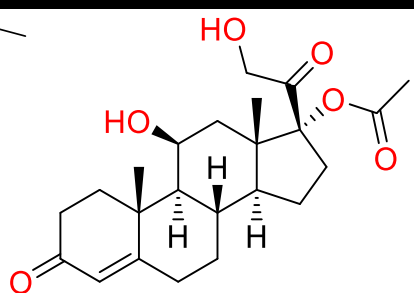
The major pharmacotherapeutic uses of GCs include the treatment of rheumatoid diseases, symptomatic relief from asthma, allergic conditions, topical application for various dermatologic disorders and cancer therapy.^{20,71}

GCs are generally classified according to their activity profile. This classification is only of limited value, because activity is not only determined by intrinsic characteristics of the various steroids, but also by the level of penetration upon application. Penetration in turn depends on many factors such as the formulation and the skin condition.⁷² Occlusion has shown to have positive implications on corticosteroid activity.⁵³ Knowledge of the numerous steroid products, structure-activity relationships, and available dosage forms will result in significant benefits for patients with minimal troublesome toxicities and more effective treatment options.

2.9. Hydrocortisone and betamethasone

Hydrocortisone and Betamethasone are corticosteroids with predominant glucocorticoid and to a lesser extent mineralocorticoid activities. However, betamethasone exerts less mineralocorticoid activities than hydrocortisone.

Table 2.9-1: Physicochemical properties of hydrocortisone acetate and betamethasone valerate^{73,74}

COMPOUND	BETAMETHASONE VALERATE	HYDROCORTISONE ACETATE
Molecular structure		
Chemical formula	C ₂₇ H ₃₇ FO ₆	C ₂₃ H ₃₂ O ₆
Molecular weight	476.585 g/mol	404.497 g/mol
Solubility	0.0067 mg/mL (theoretical) Very slightly soluble in water (1 000 - 10 000 ml/g) and soluble in alcohol (10 - 30 ml/g)	0.0582 mg/mL (theoretical)- Practically insoluble in water (>10 000 ml/g) and sparingly soluble in alcohol (30 - 100 ml/g).
Melting Point	~196 °C	~224 °C
pKa	Strongest Acidic (13.4) Strongest Basic (-3.3)	Strongest Acidic (12.61) Strongest Basic (-2.8)
LogP	3.76	1.72
Uses	Symptomatic relief of mild to moderate inflammatory diseases.	Symptomatic relief of moderate to severe inflammatory diseases.
Half-Life	5.6 hours	6-8 hours
Adverse effects	The long-term use of glucocorticoids is associated with severe adverse effects including osteoporosis, hyperglycaemia, muscle wasting, hypertension, and impaired wound healing.	

Although these compounds are from the same drug class, their physicochemical characteristics, pharmacokinetic and pharmacodynamics properties vary (Table 2.9-1).⁷⁵

2.10. Mechanism of action

GCs exhibit their powerful anti-inflammatory effects via 2 distinct mechanisms: the genomic and non-genomic pathways (Figure 2.10-1).⁴⁷

Adapted from^{47,70,76,17,25,29}

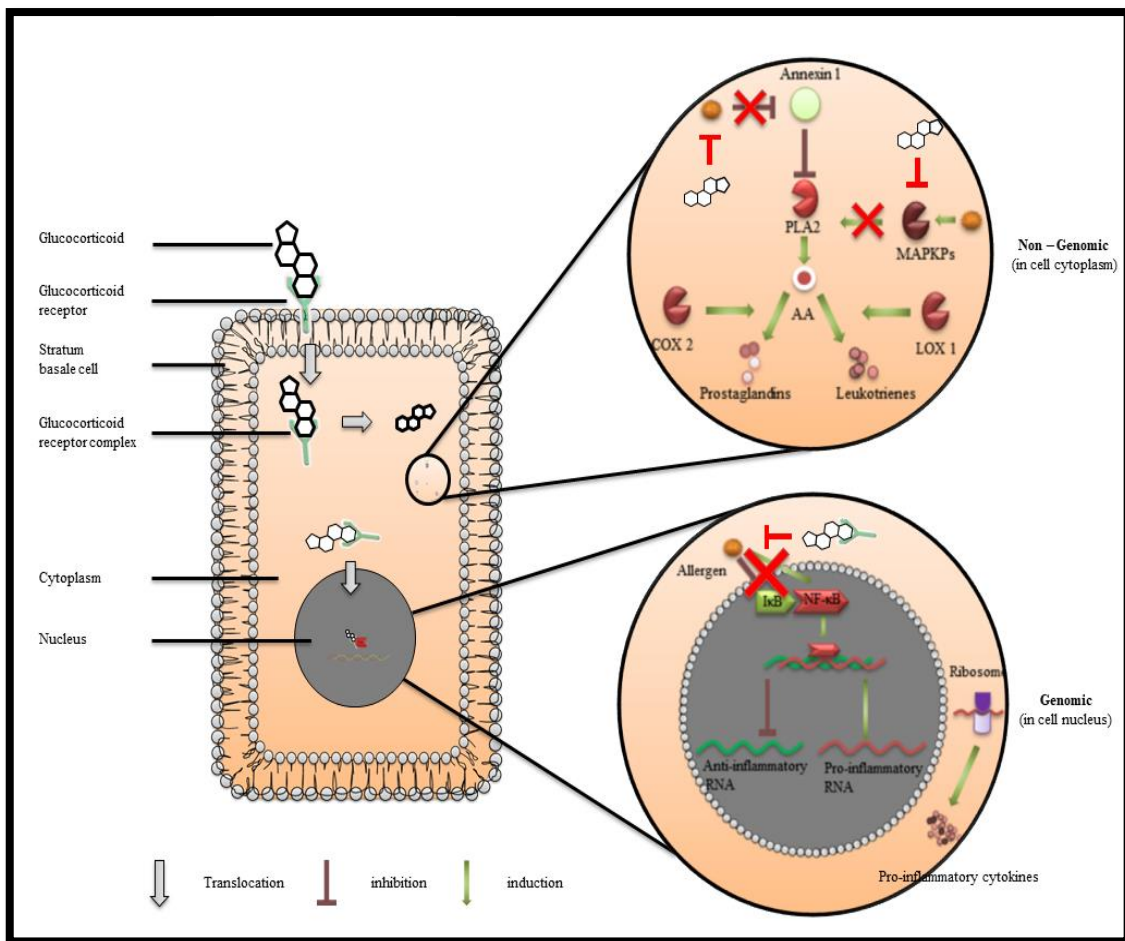


Figure 2.10-1: A diagrammatical representation of the genomic and non-genomic responses associated with the mechanism of action of glucocorticoids acting on the stratum basale

GCs bind to a glucocorticoid receptor – a membrane bound protein expressed on the surface of all nucleated cells. The binding of the glucocorticoid to the receptor results in the formation of a glucocorticoid-receptor complex which translocates to the cell cytoplasm.

Once GCs enter the cell, they bind to the cytosolic receptor, which is expressed on all nucleated cells, to form a GCS receptor complex. After binding to the receptor the newly formed glucocorticoid receptor - ligand complex translocates into the cell nucleus, where it binds to many glucocorticoid response elements (GRE) in the promoter region of the target genes. The DNA bound receptor then interacts with basic transcription factors, causing the increase in expression of specific target genes. The anti-inflammatory actions of corticosteroids are thought to involve lipocortins, phospholipase A2 inhibitory proteins which, through inhibition arachidonic acid, control the biosynthesis of prostaglandins and leukotrienes. Specifically glucocorticoids induce lipocortin-1 (annexin-1) synthesis, which then binds to cell membranes preventing the phospholipase A2 from coming into contact with its substrate arachidonic acid. This leads to diminished eicosanoid production. The cyclooxygenase (both COX-1 and COX-2) expression is also suppressed, potentiating the effect. Glucocorticoids also stimulate the lipocortin-1 escaping to the extracellular space, where it binds to the leukocyte membrane receptors and inhibits various inflammatory events: epithelial adhesion, emigration, chemotaxis, phagocytosis, respiratory burst and the release of various inflammatory mediators (lysosomal enzymes, cytokines, tissue plasminogen activator, chemokines etc.) from neutrophils, macrophages and mast cells. Additionally, the immune system is suppressed by corticosteroids due to a decrease in the function of the lymphatic system, a reduction in immunoglobulin and complement protein concentrations.⁷⁰

Corticosteroids are useful pharmacotherapeutic agents but their use is limited by adverse effects arising from non-localised drug delivery. Therefore, intense research dedicated to the optimisation of transdermal drug delivery systems will potentially provide safer and more effective medicines for topical administration. This is very significant considering the abundance of chronic skin diseases, such as AD, managed with long-term corticosteroid therapy.⁷⁷



UNIVERSITY *of the*
WESTERN CAPE

CHAPTER 3: NANOTECHNOLOGY AND ETHOSOMES



School of
PHARMACY

3. Introduction

In this chapter, we review nanoparticles, their synthesis and their applications in medicine. We specifically review ethosomes, the function of the ethosomal excipients and their pharmaceutical applications as novel tools for topical drug delivery.

3.1. Nanotechnology

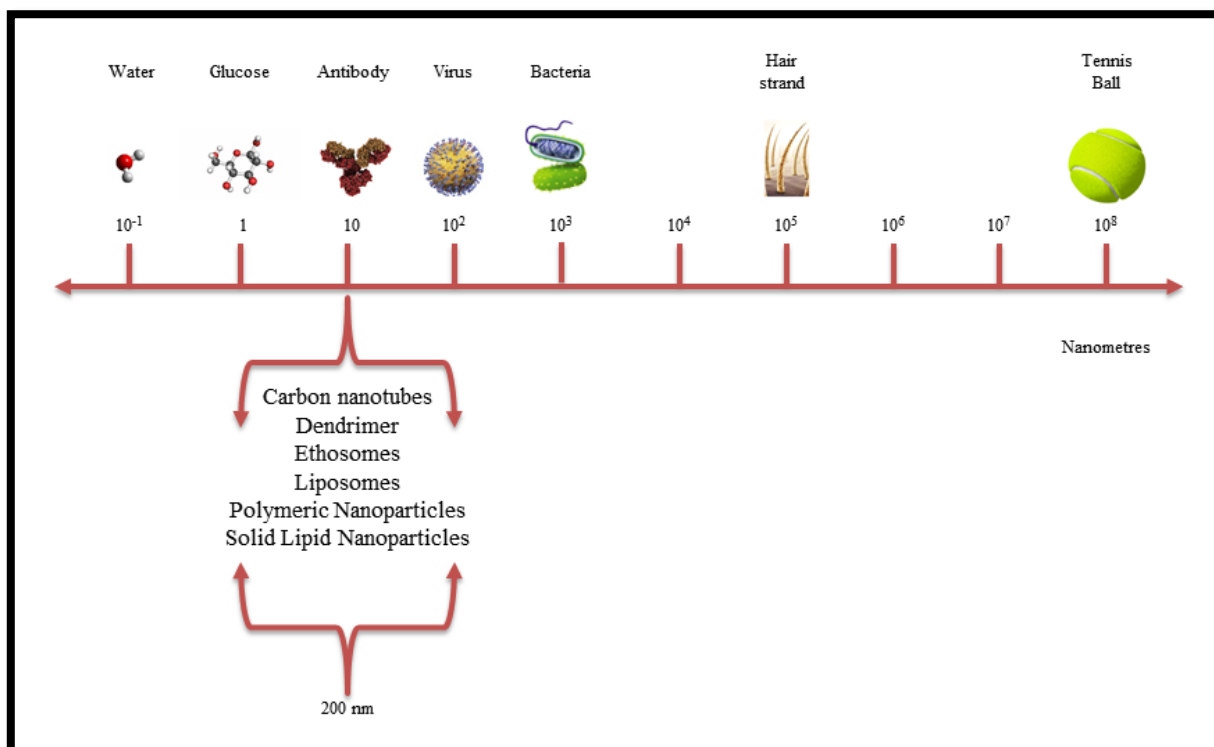


Figure 3-1: A perspective of the nanoscale

The term “nanotechnology” is derived from the Greek word ‘*nano*’, which means dwarf, and from the Greek word *tekhнологia*, which refers to ‘systematic treatment’.⁷⁸ Nanotechnology is the science of manipulating matter to create, characterise, analyse, utilise and optimise materials within the nano-range (1 - 999 nm).²⁰ To help conceptualise the size of the aforementioned materials, a perspective of the nanoscale is provided in **Figure 3.1-1**. Pharmaceutical nanotechnology is divided in two basic types of nano tools: nano-devices and nano-materials. These materials can be sub-classified into nano-crystalline and nano structured materials. Nano-structures consists of nanoparticles such as: solid-lipid nanoparticles (SLNs), polymeric nanoparticles (PNPs), dendrimer nano-carriers (DNCs), silica nanoparticles (SNPs), carbon nanoparticles (CNPs), magnetic nanoparticles (MNPs).⁷⁹

The extent of the diversity of these tools has allowed for its application to a variety of research fields such as chemistry, biology, physics, materials science, and engineering. Research has shown that the integration of nanotechnology within the medical sector has conferred health benefits, which has led to advances in nano-medicine.⁸⁰ Subsequently, it has been applied in the context of medicine and pharmaceutical sciences for: diagnostic purposes, treatment and prevention of a wide range of diseases.¹⁵

Nanostructures, such as polymeric nanoparticles, have provided an avenue for treatments tailored for specific interactions with the skin. The incorporation of nanoparticles within transdermal drug delivery systems has facilitated movement of APIs through the epidermis.^{17,76,77} The utilisation of nanostructures allows for several avenues to mitigate the effect of inflammation on cutaneous physiology, barrier function and aesthetics.²⁶

Nanoparticles exist in a variety of forms and their subsequent application serves a variety of functions in the development of innovative pharmaceutical dosage forms. Utilised in the pre-formulation of pharmacotherapeutic agents, nanoparticles are employed as: nano-capsules for drug delivery, cell surface receptors enabling targeted drug delivery and pathogen detection, nanoparticle tubes enabling targeted drug release, polymer “carrier” molecules enabling cancer therapies and, “nano-factories” enabling nano-based drug synthesis.⁸³

One of the main advantages of nanoparticles is directly associated with the particle size. A smaller particle size imparts numerous desirable properties when used in topical applications, as it allows for penetration through most physiological barriers.⁷⁹ This is critical considering the protective physiological function of the epidermis. The small size of nanoparticles also allows for a higher surface area to volume ratio, allowing for greater exposure of active molecules per dose administered. This may influence the efficiency of topical dosage forms, resulting in a greater predisposition for a localised pharmacotherapeutic activity.

Nano-encapsulation provides a new method for sustained release and for delivering unstable or insoluble compounds. This pre-formulation component of dosage formulation development is able to be optimised to suit the physicochemical properties of the API used, as well as the dosage formulation for which it is intended. The susceptibility to modification allows for a variety of topical parameters, such as particle size, stability, API associated adverse effects and solubility, to be tailored for distinct uses.⁸⁴ Nanoparticles may be a solution to overcoming many associated parameters.⁵⁷

3.2. Lipid based systems

When considering the pre-formulation of nanoparticles for enhanced drug delivery, lipid based systems (LBS) are popular amongst researchers. These systems have the potential to influence the pharmacokinetic and physicochemical properties of drugs. Each system consists of a unique mechanism of drug delivery which is influenced by the type of lipid and the way in which it interacts with other components within the system. This variety has resulted in the classification of these LBS into 3 sub categories i.e. lipid particulate based, emulsion based and vesicular based and lipid systems (**Figure 3.2-1**).⁶⁴

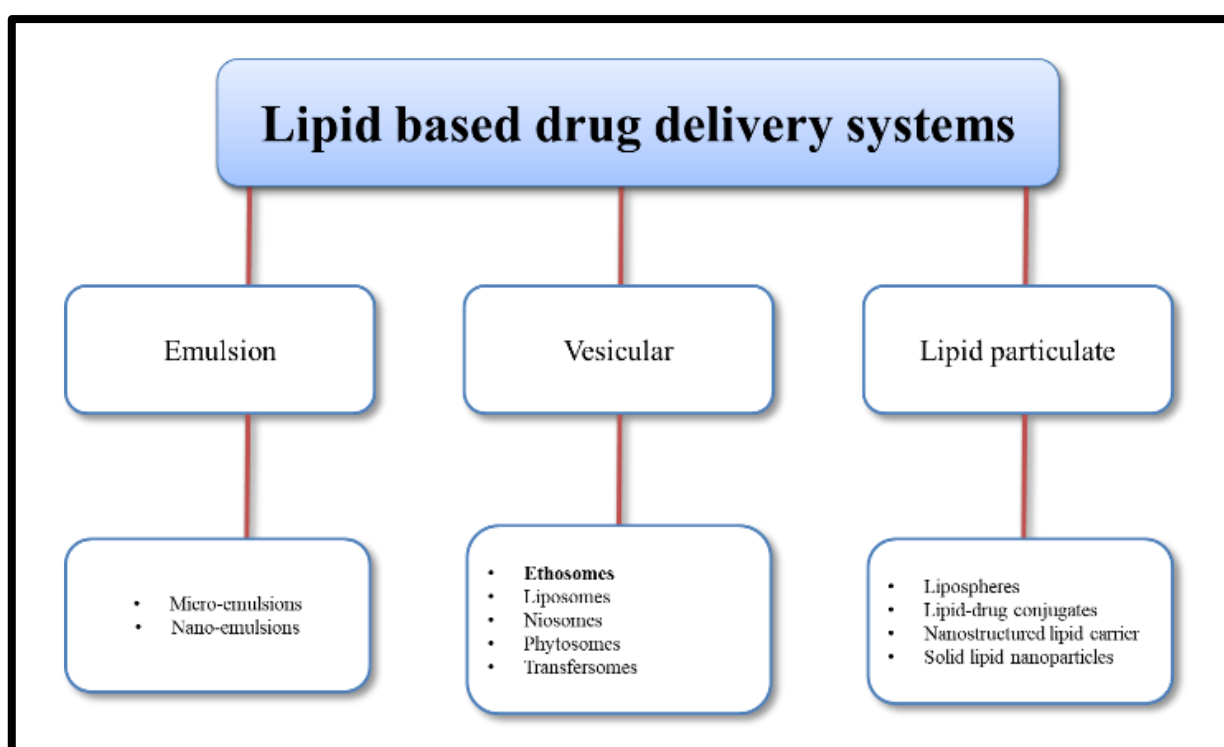


Figure 3.2-1: Classification of lipid based systems for drug delivery

3.3. Nanoparticles and transdermal drug delivery

Considering the protective barrier function of the skin, healthy skin is relatively impervious to penetration. However, numerous *in vitro* studies regarding transdermal permeation have shown that nanoparticles facilitate drug penetration through the SC.^{1,52,85} Additionally, transdermal studies have shown varying conclusions regarding routes of permeation. As previously mentioned, transdermal penetration occurs via the transcellular, follicular and intercellular pathways.⁸⁶ Cell culture experiments with human epidermal keratinocytes have

shown that nanoparticles were observed in cytoplasmic vacuoles, indicating that transcellular permeation was achieved.¹⁸ However, if the particle sizes of nanoparticles remain below 100 nm, they can access any cell of the body by endocytosis/pinocytosis, and therefore pose a higher risk potential.⁹ With permeability to particles 200 - 300 μm , the transappendageal route, particularly hair follicles, may provide the most favourable route for the delivery of nanoparticles.²⁶ Hair follicles only make up a small surface area (0.1%) but are able to act as reservoirs for topically applied medicines.⁸⁷ Nanoparticles with elastic deformation characteristics have been observed to penetrate the skin when it is flexed.⁸⁸⁻⁹⁰ Apart from an elastic deformation property attributed to the nanoparticle, mechanical deformation of the skin is influential in the efficiency and effectiveness of transdermal drug delivery. Deformation of the SC lipid domains facilitates the permeation of APIs through tortuous intercellular pathways. Owing to research regarding the effect on mechanical deformation of the skin and vesicle flexibility, ethosomes were investigated as potential nano candidates for topical drug delivery.^{1,23}

3.4. Ethosomes

Ethosomes (**Figure 3.4-1**), composed of ethanol, phospholipid, and water, were developed by *Touitou et al, 2007* as additional novel lipid carriers and have been reported to improve transdermal permeation of various drugs.¹

Ethosomes are soft, malleable vesicles which, in comparison to conventional liposomes, permeate the skin more rapidly and have a significantly higher transdermal flux.^{1,15,57,91} The increase in permeation into the deeper dermal layers is due to the relatively higher ethanol concentration which results in a reduced vesicle size. It has also been suggested that there is a synergistic effect resulting from the combination of phospholipids and high ethanol concentration. Phospholipids facilitate the movement of drugs across biological membranes due to their biocompatible lipophilic nature, whereas ethanol acts as a permeation enhancer by disrupting the membrane to increase permeability and allow the drug to pass through. Human skin has a selective permeability for drugs. Ethosomes are able to encapsulate a variety of APIs with various physicochemical characteristics e.g. hydrophilic, amphiphilic, lipophilic.

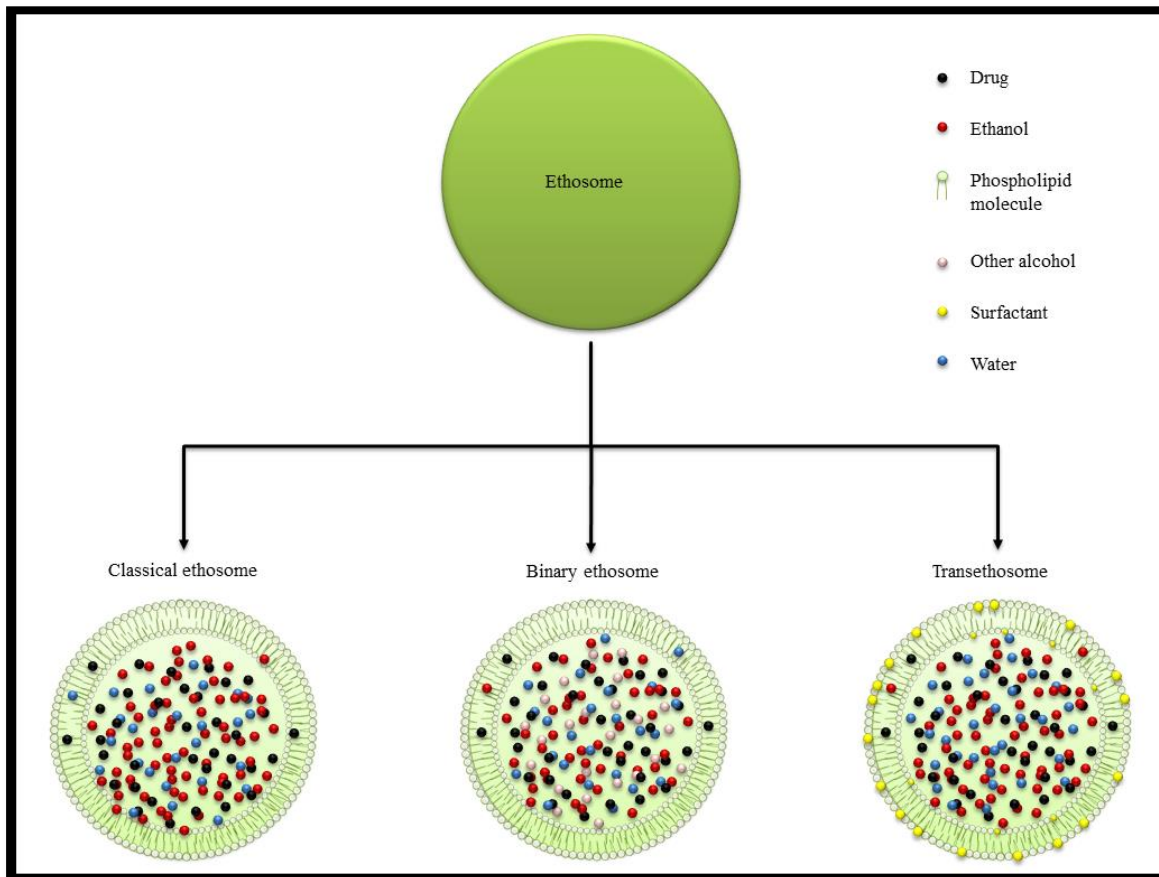
Adapted from ^{1,92}

Figure 3.4-1: A schematic showing the different types of ethosomes and their components. All ethosomes contain a phospholipid bilayer and a hydro-ethanolic core which may or may not contain an API. Binary ethosomes contain additional alcohol Ethosomal drug delivery is a non-invasive administration route which allows the API to be delivered into the deep skin layers such as the dermis. Also, because of their high ethanol concentration, the phospholipid bilayer is packed less tightly than conventional vesicles but has equivalent stability, The resultant malleable vesicle owe its flexibility to ethanol which acts as a plasticizer.²² Molecular weights of drugs entrapped in classical ethosomes have ranged from 130 - 24 000 kDa.⁹² Researchers have investigated the effects of drug encapsulated vesicles on biological systems.^{91,93-95} The effect of an increase in drug flux is significant when applied to transdermal permeation. The size range of these vesicles, ranging from nm to μm , may be adapted to suit its intended function.

Table 3.4-1: Ethosomes loaded with active pharmaceutical ingredients (APIs) prepared for transdermal drug delivery

Author	API	Molecular weight (g/mol)	Indication	Conclusion
Ainbinder <i>et al</i> (2005) ⁹⁶	Testosterone	288.42	Testosterone replacement therapy	<i>In vitro</i> permeation profiles indicated that ethosomal formulations enhanced transdermal permeation of testosterone by six fold
Manish <i>et al</i> (2011) ⁹⁵	Ketoprofen	254.28	Anti-inflammatory	<i>In vitro</i> release study through adult female human skin revealed higher transdermal flux with ethosomal formulation compared to hydroalcoholic drug solution. <i>In vitro</i> data indicated improved
Paolino <i>et al</i> (2012) ⁹⁷	Paclitaxel	855.90	Treatment of squamous cell carcinoma	permeation of paclitaxel in a stratum corneum-epidermis membrane model and increased its anti-proliferative activity in a squamous cell carcinoma model as compared to the free drug. <i>In-vivo</i> study using rat paw oedema
Pathan <i>et al</i> (2018) ⁹⁸	Curcumin	368.38	Pain management	revealed a significant increase in oedema inhibition using curcumin loaded ethosomes compared to oral curcumin administration
Xie <i>et al</i> (2018) ⁹⁹	Hyaluronic acid	846.80	Transdermal delivery carrier	<i>In vitro</i> permeation through rat dorsal skin indicated hyaluronic acid enhanced the penetration efficiency of the model drug rhodamine B.
Yan <i>et al</i> (2016) ⁹⁰	Sinomenine hydrochloride	365.80	Anti-inflammatory	<i>In vivo</i> study using xylene-induced ear edema indicated that sinomenine loaded ethosomes presented strong anti-inflammatory activity.

3.5. Phospholipids

Phospholipids are biocompatible polymers which form the phospholipid bilayer of ethosomes.¹⁰⁰ To formulate ethosomes, a variety of phospholipids from different sources have been used. Although these phospholipids have different chemical structures, (e.g. phosphatidylcholine (PC) (**Figure 3.5-1**), hydrogenated PC, phosphatidic acid (PA), phosphatidylserine (PS), phosphatidylethanolamine (PE), phosphatidylglycerol (PPG) and phosphatidylinositol (PI) as formulation excipients, they serve the same function – to form the outer shell of the nano-vesicle and encapsulate the drug within.⁶⁵

The selection of phospholipid type and concentration for the formulation are important factors during the development of an ethosomal system because they will influence the size, encapsulation efficacy, zeta potential (ζ_p), stability, and penetration properties of the vesicles. The most significant parameters include: the effect on vesicle size and the effect on encapsulation efficiency.¹⁰¹

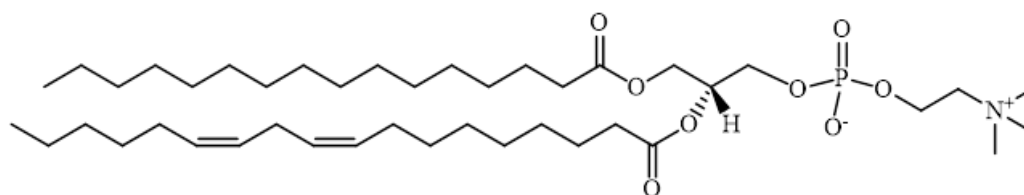


Figure 3.5-1: Chemical structure of phosphatidylcholine

The effect on vesicle size is directly proportional to a certain concentration, with an increase in phospholipid concentration resulting in an increase in ethosomal size.⁵⁷ It has been reported that vesicles with higher phosphatidylcholine content lead to the production of more stable vesicles. The surface charge of the phospholipid used also influences the ζ -potential of ethosomes.⁹¹ Incorporation of anionic lipids, e.g. 1,2-dipalmitoyl-sn-glycero-3-phosphatidylglycerol, produces highly negatively charged vesicles whereas cationic lipids e.g. 1,2- dioleoyl-3-trimethylammonium-propane [chloride salt] produce positively charged vesicles.¹⁰²

Increasing phospholipid concentration will increase entrapment efficiency significantly.¹⁰³ However, the relationship is true only until a certain concentration, where further increment in phospholipid concentration will have no effect on entrapment efficiency.²⁰ As a supplementary function, phospholipids may serve as a protective layer by preventing endogenous degradation.

3.6. Ethanol

Ethanol is known as an efficient permeation enhancer that is believed to act by affecting the intercellular region of the stratum corneum. Its inclusion in liposomes to form ethosomes has already been investigated.¹

Ethanol influences a variety of ethosomal characteristics in terms of size, ζ_p , stability, encapsulation efficacy, and enhanced skin permeability. The concentration of ethanol in ethosomal systems varies from 10-50 %. These concentrations vary depending on the drug incorporated into the vesicular system. Researchers have found that, up to a certain concentration, the relationship between ethanol concentration and vesicle size is inversely proportional, with an increase in ethanol concentration resulting in a decrease in vesicle size.⁶⁴ In comparison to liposomes (lipid vesicular systems not containing ethanol) it has been proven that there is a vast difference between vesicular sizes.^{1,20} The mean diameter of ethosomes is approximately 40 % smaller than classical liposomes. However, even though ethanol has shown to decrease vesicle size up to a certain concentration, there is a fine balance between reducing vesicle size and maintaining vesicle stability. Increasing ethanol concentration beyond the optimum level would cause the bilayer to be leaky and lead to a slight increase in vesicular size and severe decrease in entrapment efficacy, and by further increasing in ethanol concentration it would solubilize the vesicles.^{22,55,57}

There are a number of proposed mechanisms by which ethanol reduces vesicle size. A few studies involving the ethosomal synthesis have shown that high ethanolic concentrations causes interpenetration of the ethanol hydrocarbon chain which leads to a decreased membrane thickness, therefore resulting in a decreased vesicular size.^{23,55,104,105} Other studies have shown that ethanol influences the surface charge of the ethosomes as well as the surrounding boundary layer resulting in enhanced steric stabilization and a decreased mean vesicle size.¹⁰⁶ Research has shown that the high ethanolic concentration leads to a negative vesicle charge. This is important in maintaining the stability of the systems by electrostatic repulsion whilst in suspension. Up to a certain concentration, there is a directly proportional relationship between the concentration and the entrapment efficiency. Generally, increasing ethanol concentration will increase entrapment efficiency. This effect applies to molecules of varying lipophilicities, whereby ethanol increases the solubility of the lipophilic and amphiphilic drugs and hence increases drug loading. This relationship was found to be linear, with ethanol concentrations between 20% and 40%. For this reason, ethanol concentration

should be optimized during the formulation process, as at low concentrations entrapment efficacy will be minimal, and at very high concentrations ethosomal membrane will be more permeable because phospholipids can easily be dissolved in ethanol, leading to a significant reduction in encapsulation efficacy (EE).⁹³

3.7. Cholesterol

Cholesterol is a C₂₇ rigid steroid molecule which has a structure that facilitates lipid based vesicle structure integrity. This characteristic of cholesterol is influential in the structural parameters of the drug, such as the vesicle stability, as well as the ability of the vesicle to encapsulate the loaded drug and liberate it from its core. Thus, EE as well as vesicle stability, are influenced by the concentration of cholesterol within the system.⁹⁸

Research has shown that concentrations ranging from 3-70 % have been included in ethosomal formulations.¹⁰⁶⁻¹⁰⁸ The varying concentrations are dependent on the ideal properties of the intended formulation to suit its function. These concentrations are also dependent on the type of drug that was encapsulated within the ethosome as well as the excipients of the ethosomal formulation which, collectively, influence the overall vesicle properties.

Amongst the aforementioned characteristics, cholesterol has also shown to prevent vesicular leakage, i.e. ensuring that encapsulated drug is not liberated prematurely. If the polymer is to be considered as the cement of the structure, then it is the cholesterol which acts as stones within the cement to form concrete which is much more rigid and stable once set.

An important factor to consider when determining the optimum cholesterol concentration for nanoparticles is to consider its influence on vesicle size. This is critical when taking the disease, the intended formulation and the intended route of administration into account as vesicle size will influence drug delivery. The influence of cholesterol on the vesicle size may be managed by comminution which is dependent on the method employed in ethosomal synthesis.¹⁰⁹

The inclusion of cholesterol has also shown to influence the elasticity of ethosomes which are, apart from being relatively smaller than other lipid based nano-systems, generally able to transverse biological membranes because they are flexible. This is an ideal property for transdermal formulations. However, increasing the cholesterol concentration and thus

increasing the rigidity, has shown to decrease this elastic property. *In vitro* studies using Franz diffusion cells and confocal laser-scanning microscopy showed that these multilamellar vesicles (MLVs) were not able to pass across the stratum corneum due to the higher rigidity, making it more difficult for the drug to permeate the skin.^{11,18,23}

The inclusion of cholesterol in ethosomal vesicles has both advantages and disadvantages which must be managed during formulation development. Ethosomal parameters are easily influenced by any addition of any excipient and thus care must be taken during formulation to ensure that the ideal properties for its intended use are maintained.

3.8. Ethosome mechanism of permeation

During this non-invasive method of drug delivery, the vesicle encapsulating the drug is able to move by passive diffusion where it moves from a higher concentration at the stratum corneum to the deeper layers of the dermis. Although this is a generic model of transdermal drug delivery, it is well known, there are characteristics which are specific to ethosomes that enhance efficiency of the process. It is noteworthy that the mechanism by which the ethosomal system enhances drug delivery into and across the skin differs from the mode of action of other lipid vesicles.^{1,89,108}

There are 5 recognised mechanisms (**Figure 3.8-1 A-E**) of transdermal permeation for lipid based drug delivery systems, each with its own distinct feature which allows APIs to transverse the SC. All pathways are described by either or both of the following principles:

- Increase in thermodynamic activity due to evaporation of ethanol known as “push effect”.
- “Pull effect” in which penetration of drug molecule is increased due to reduction in barrier property of subcutaneous tissue by ethanol.¹⁰¹

As an individual component, it is well known that ethanol is a permeation enhancer.¹¹⁰ Ethosomes contain ethanol which is pertinent in transdermal drug flux. These nano-vesicles are propelled by ethanol which is liberated from a higher concentration gradient within the ethosomes to the interstitial fluid surrounding corneocytes. The liberation of ethanol has also shown to disrupt the layers of the SC, essentially creating an avenue which allows the ethosomes to move easily. In addition, ethanol also adds flexibility to ethosomes as it is located within the phospholipid bilayers. This generates a soft structured vesicle with a

fluidised bilayer.⁹² This elastic property of ethosomes allows them to transverse biological membranes both trans-appendeagally and trans-cellularly. Ethanol penetrates into intercellular lipids and increases the fluidity of cell membrane lipids and decrease the density of the lipid multilayer of cell membrane. Ethosomes are able to fuse with skin lipids and release the drug into the viable epidermal and dermis layers of the skin.²²

Adapted from ^{23,55}

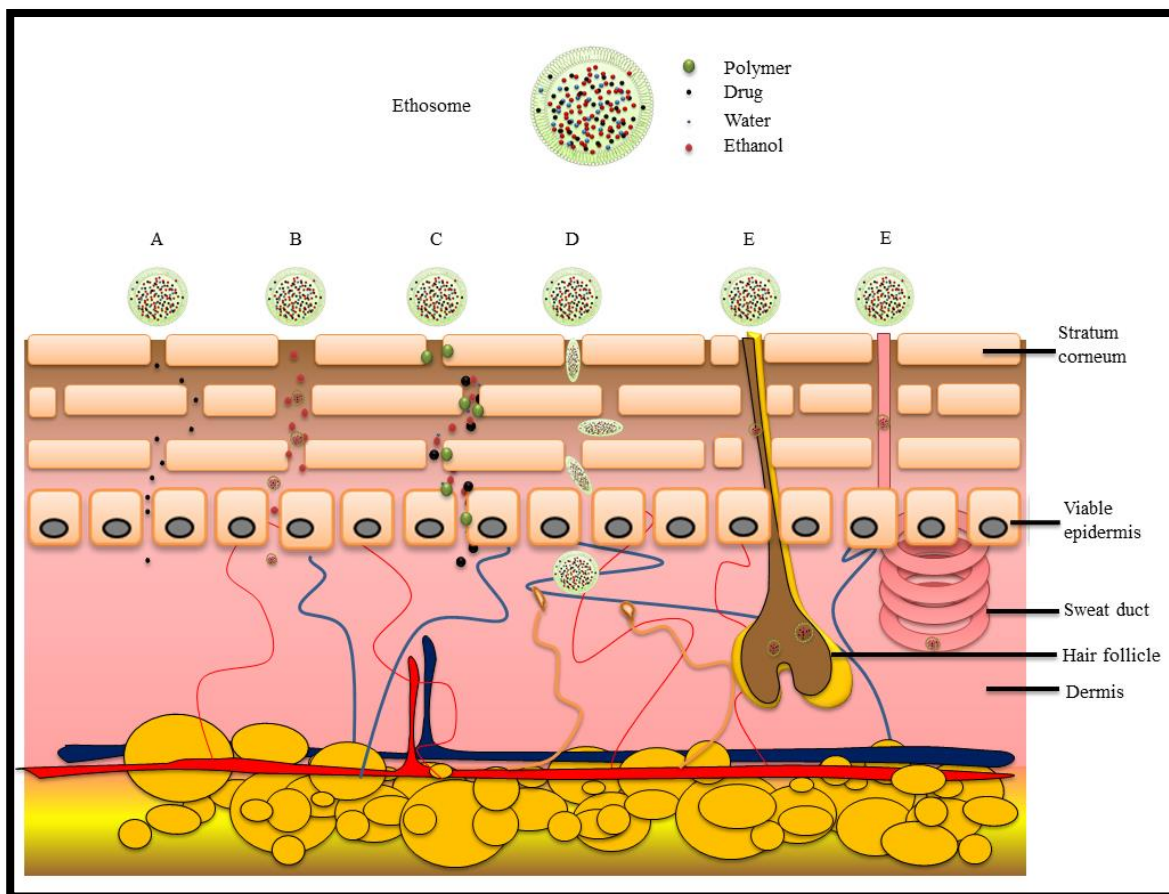


Figure 3.8-1: Proposed mechanisms of action for lipid based drug delivery systems:

- A. Free drug, released from ethosomes, is able to move intercellularly
- B. The concentration gradient created by ethanol release into its surroundings may disrupt the SC and allow the drug to transverse biological membranes with less restriction caused by the phospholipid bilayer of cell membranes.
- C. Intact vesicles may permeate the stratum corneum and the fusion of the respective ethosomal and cellular phospholipid bilayers results in the release of encapsulated drug to target dermal tissue.

- D. Intact vesicles may penetrate the SC and be absorbed into the deep tissue layers of the skin.
- E. The vesicles may penetrate the epidermis via the transappendageal route. Hair follicles are the more plausible route of permeation as it is a passive process. Although sweat ducts are a possible route, it is unlikely to be effective. Sweat ducts are constantly active in maintaining homeostasis, therefore, permeation would require active transport against the flow of sweat.

A model representing the mode of ethosomal system action was proposed based on system characteristics and numerous skin penetration and permeation studies which revealed that ethosomes perform significantly better than each of their individual system components or combinations.^{1,15} Using confocal laser scanning microscopy (CLSM) it was shown that a drug delivered *in vivo* from ethosomes, penetrated rat skin through the inter-corneocyte pathways, which typically exist along the lipid domain of the SC. (**Figure 3.8-1 route D**). In contrast, significantly lower fluorescence staining of the intercellular penetration pathway and no inter- or intra-corneocyte fluorescence were observed with drug hydro-ethanolic solution and liposomes, respectively.^{17,57,95} Confirmed by both *in vitro* and *in vivo* skin delivery studies, it was shown that the individual components included in ethosomal systems work synergistically to enhance penetration through the stratum corneum.

3.9. Advantages and disadvantages of ethosomes as novel drug delivery systems in transdermal permeation

In comparison to other transdermal delivery systems, ethosomes show essential advantages which make them an ideal candidate for drug delivery.^{21,22,25,54,66,82,107,131,132}

Advantages

- Enhanced permeation of drug through skin for transdermal drug delivery.
- It contains biocompatible raw material in formulation which increases its safety profile.
- The ethosomal system is passive and non-invasive
- Ethosomal drug delivery system can be applied widely in Pharmaceutical, Veterinary, Cosmetic fields.

- Simple method for drug delivery in comparison to Iontophoresis and Phonophoresis and other complicated methods.
- May increase efficacy and therapeutic index.
- Ethosomes improve skin delivery of drugs both under occlusive and non-occlusive conditions.
- Suitable for a variety of APIs, differing in aqueous solubility and polarity.
- Ethosomes are relatively smaller than other conventional lipid nano-vesicles.

Disadvantages

- A low yield may not be economical.
- Percutaneous absorption depends on the molecular size of the drug, thus restricting possible APIs in formulation of nanovesicles.
- Ethosomal drug delivery system is limited to potent drugs and not for drugs that require high blood levels.
- Skin irritation or dermatitis may occur in some patients due to permeation enhancer or the excipients used.
- Ethosomal administration is not a means to achieve rapid bolus type drug input, rather it is usually designed to offer slow, sustained drug delivery.
- Adequate solubility of the drug in both lipophilic and aqueous environments to reach dermal microcirculation and gain access to the systemic circulation.



UNIVERSITY *of the*
WESTERN CAPE

CHAPTER 4:

NANOPARTICLE

SYNTHESIS



School of
PHARMACY

4. Introduction

In this chapter, the general principles for nanoparticle synthesis are reviewed. Additionally, the reason for each step in the methodology was researched to get a comprehensive understanding of the variables influencing ethosomal characteristics. Characterisation methods and their limitations are also reviewed.

4.1. Nanoparticle synthesis

Nanoparticles can be synthesised from 2 general methods - each with their own advantages and limitations.⁷¹

The top-down method involves the physical comminution of the drug crystals into nano-sized particles by wet or dry milling techniques.⁷¹ These particle size reduction processes are utilised to decrease the particle size of larger materials to within the nano-range. The recent development in size reduction technologies, such as media milling, micro-fluidization and high pressure homogenization, has resulted in a variety of methods available for different types of materials.¹¹² Although useful in reducing the particle size, these approaches demonstrate a number of limitations and drawbacks. The high energy forces and mechanical stresses applied to materials have the potential to degrade thermolabile compounds.¹¹³ Compounds may also be subjected to conditions which facilitate polymorphism which might alter the physicochemical properties of such materials.¹¹⁴ Depending on the comminution process used, impurities may also be introduced.

The bottom-up method is based upon controlled precipitation of nanoparticles which occurs as a result of the addition of an anti-solvent, containing stabilizers from dissolution, in a suitable solvent.¹¹⁵ The approach avoids difficulties resulting from high pressure milling or homogenization techniques. To-date, there are four main bottom-up approaches which are employed to prepare nanoparticles. Such approaches include: the solvent-anti-solvent method, supercritical fluid technology, spray drying and emulsion-solvent evaporation.¹¹⁶ However, some of the drawbacks for this kind of approach are low drug loading and process scale-up.¹⁰⁹

4.2. Comminution of nanoparticles in suspension

During the synthesis of nanoparticles, it may be necessary to reduce the particle size to ensure that they are suited to their function. Comminution techniques such as sonication, extrusion and homogenization, have been devised to reduce the mean size of lipid based particles for nano drug delivery systems.¹¹² These particles may be classified based on their size and lamellarity as shown in **Table 4.2-1**

Table 4.2-1: The size classification of lipid based drug delivery vesicles

TYPES OF VESICLES	ABBR	DIAMETER	NUMBER OF LIPID BILAYERS
Small unilamellar vesicles	SUVs	Around 100 nm	Single bilayers
Oligolamellar vesicles	OLVs	0.1 – 1 μm	Approximately 5 lipid bilayers
Multilamellar vesicles	MLVs	500 – 5,000 nm	Concentric bilayers
Large unilamellar vesicles	LUVs	200 – 800 nm	Single bilayers
Multivesicular vesicles	MVVs	>1 μm	Multi-compartmental structure

- SUVs - due to their homogeneity in size, are more suitable for parenteral administration than MLVs. However, their small size results in lower encapsulation of hydrophilic drugs.
- OLVs - due to their lamellarity, may have sustained release of encapsulated material
- LUVs - due to their larger aqueous core, can entrap a higher amount of hydrophilic drugs relative to SUVs
- MLVs - due to their large lamellarity, are more suited to incorporate lipophilic molecules compared to hydrophilic substances.⁵⁷
- MVVs - due to their large aqueous phase to lipid ratio; are very efficient at entrapping large volumes of hydrophilic material and providing sustained release¹¹⁷

Apart from reducing the particle size, these methods may also be used to decrease the size distribution to be within a certain range. This distribution of homogeneity, commonly referred to as the poly dispersity index (PDI) is a measurement of the frequency of the average size of the nanoparticles measured by dynamic light scattering.

4.2.1. Sonication

Sonication refers to the application of sonic energy, typically 20 - 40 kHz, to reduce the size of suspended particles to micro and nano size ranges. The disruption of polymeric particle shells occurs by a phenomenon referred to as cavitation, shown in **Figure 4.2.1-1**.¹¹⁸ During cavitation, acoustic waves generate a pressure gradient where bubbles form spontaneously in the bulk medium. These cavitation bubbles can be characterized by the dynamics of oscillations and the maximum temperatures (approx. 5,000 K) and pressures (approx. 2,000 atm) reached when they collapse.¹¹⁹

Adapted from ^{118,119,126}

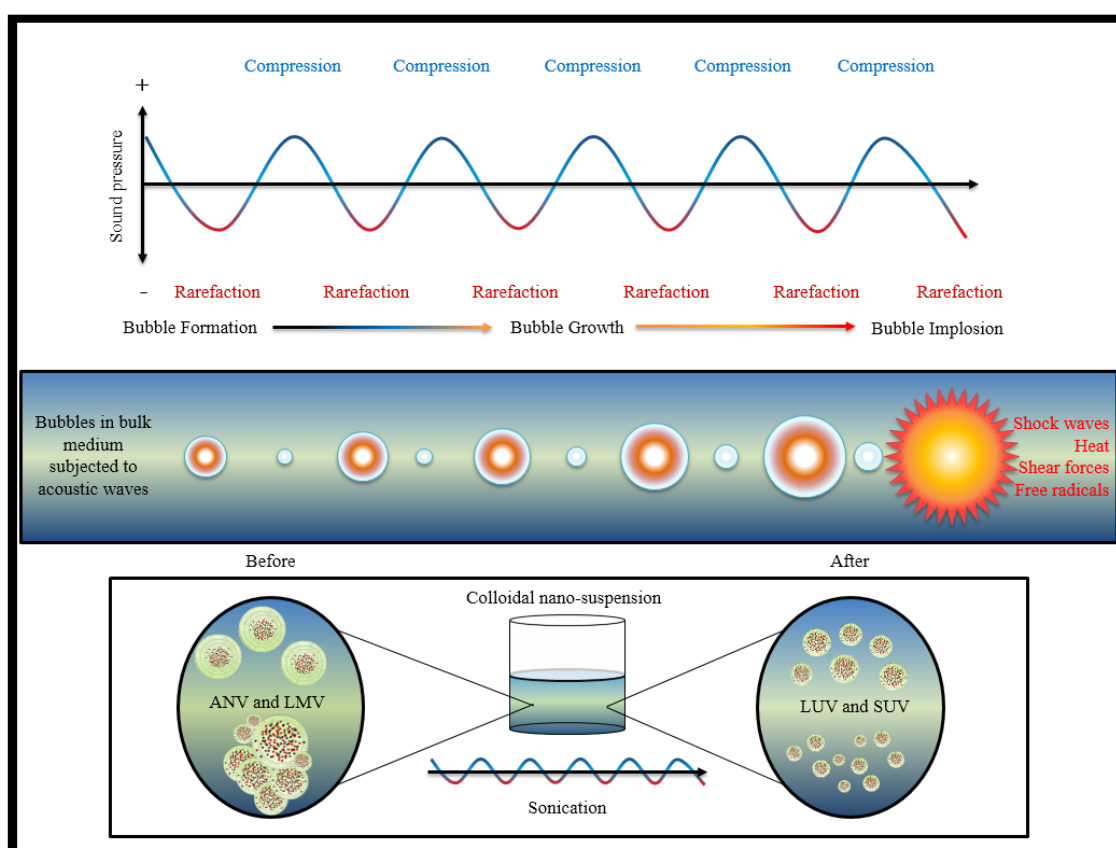


Figure 4.2.1-1: A schematic representation showing the mechanism in which comminution is achieved by sonication.

In a sonication cycle, there is a compression and an expansion event where these bubbles shrink and grow in size. The size of the bubble is directly proportional to the acoustic power and inversely proportional to the ultrasound frequency.¹²⁰ Since the rate of expansion is greater than the rate of compression, the bubble increases in size until it implodes. The

implosion results in the liberation of shock waves, heat, shear forces and free radicals resulting in comminution.¹²¹

To reduce the particle sizes of lipid based nanosystems, ultrasonic bath sonicators and probe sonicators are typically used. In this method, macro and micro sized vesicles in suspension are subjected to cycles of high and low pressure. During the low-pressure cycle, high-intensity ultrasonic waves create microscopic vacuum bubbles or voids in the liquid which attain a maximum volume at which they can no longer absorb energy. During the high pressure cycle they collapse violently and generate a localized shock wave that releases tremendous mechanical and thermal energy. This entropic exchange is what drives comminution of lipid based nanoparticles in suspension.¹²² Although both systems generate sonic waves by a similar mechanism, it is ultimately the mechanism of sonic wave delivery that differs. Each one has its respective set of advantages and disadvantages.

Probe sonicators act by direct sonication where the probe is immersed in the lipid suspension. The probe makes direct contact with the lipid suspension and a subsequent high energy is transferred. Unfortunately, the high energy imparted onto the system may generate a lot of heat and may degrade the polymer. Sonication tips may release titanium particles into the lipid suspension which must be removed by centrifugation prior to use.¹²³

Ultrasonic bath sonicators act by indirect sonication where a vessel (beaker, volumetric flask etc.) containing a lipid suspension is immersed into a liquid (typically water) propagating ultrasonic waves. The sound waves must travel through both the bath or cup liquid (typically water) and the wall of the sample container before reaching the suspension. In direct sonication, the probe is in contact with the suspension, reducing the physical barriers to wave propagation and therefore delivering a higher effective energy output into the suspension.¹²⁴

Sonication results in the clarification of a suspension which becomes more transparent as the size of the particles decrease in mean size and distribution are influenced by composition, concentration, temperature, sonication time and power, volume, and sonicator tuning.^{125,126} Since it is nearly impossible to reproduce the conditions of sonication, size variation between batches produced at different times is not uncommon. Although useful in particle size reduction of LMVs, when applied to LUVs, vesicles may lyse resulting in the leaking of nano-vesicles and a reduction in the encapsulation efficiency.

4.2.2. Extrusion

Extrusion is a method used to reduce the particle size of lipid based drug delivery systems.^{17,63,105,127} In this process, the prepared lipid suspension is passed through a membrane filter of a defined pore size for a predetermined number of cycles. Compared to sonication, extrusion is much more reproducible at producing nanoparticles with a decreased polydispersity index (PDI). Relative to sonication, the technique requires less energy to reduce particle size from larger to smaller size ranges.¹²⁸

Adapted from¹²⁸

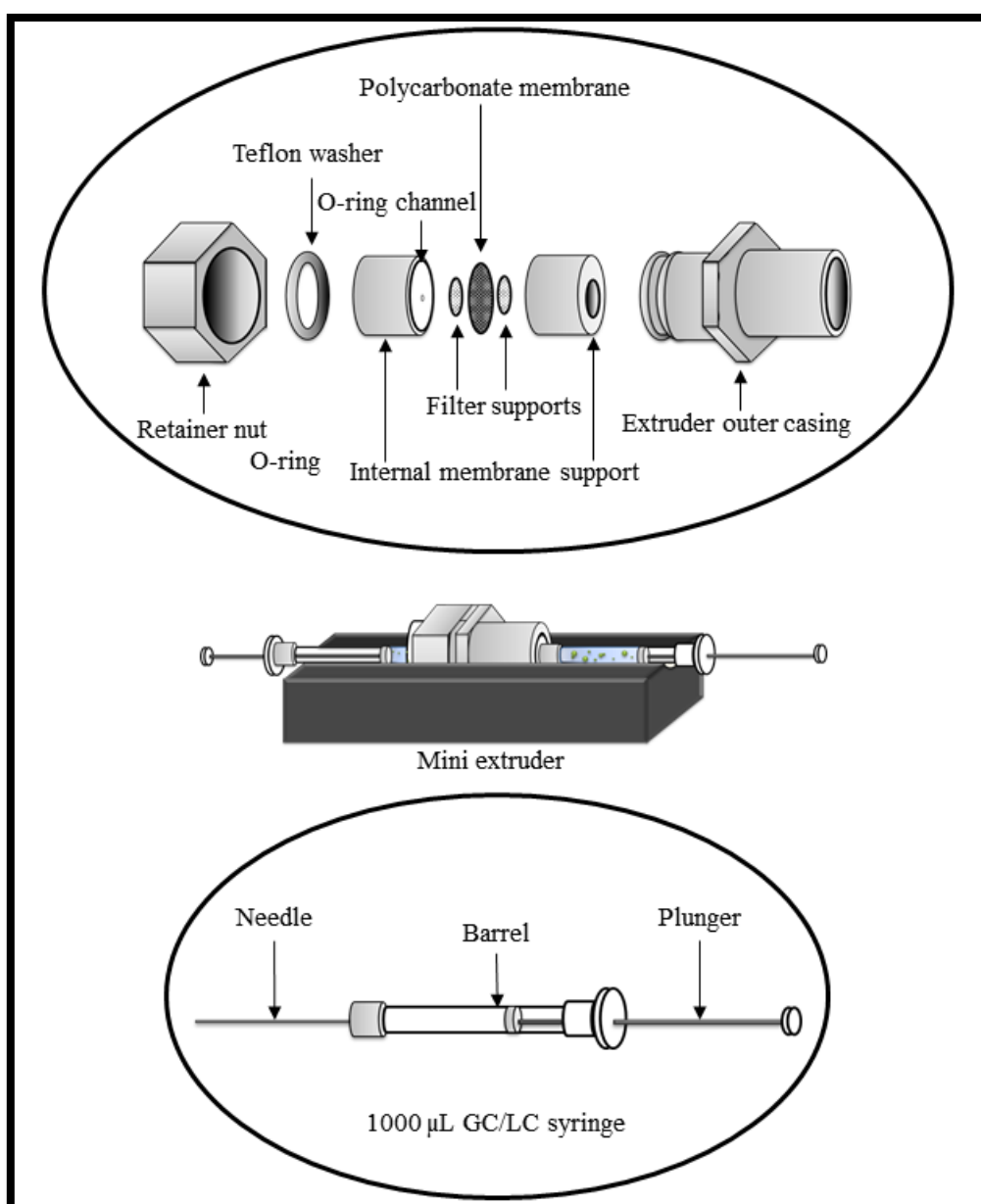


Figure 4.2.2-1: A mini extruder and its components.

In a desktop mini-extruder (**Figure 4.2.2-1**)¹²⁸, the amount of sample extruded per cycle is limited to the volume of the syringe. Typically, syringes are up to 1000 μml in volume and the technique is thus conducive for small samples but larger samples can be quite time consuming.¹²⁹

It is important to control the parameters which influence particle size and the size distribution of lipid based drug delivery vesicles in suspension. The number of extrusion cycles, pore size, temperature and applied pressure are variables which need to be considered, as they influence the average particle size and the PDI.¹¹² The number of extrusion cycles may influence both the PDI and particle size. Fewer cycles result in a bimodal particle size distribution with large and small nanoparticles whereas an increased number of cycles results in a unimodal distribution with the size of the particles directly related to the membrane pore size. Since the pressure is manually controlled by the force applied by the operator, it is important to keep the pressure consistent. The applied pressure will influence the flow rate of the suspension passing through the membrane. Membranes varying in pore size are interchangeable and influence mean particle size and PDI, with a smaller pore size resulting in a decreased mean diameter and decreased PDI. The influence of temperature on the sample is directly related to the flow rate and its rheological properties. The subsequent increase of the flow rate makes extrusion easier for the operator.

4.3. Centrifugation

Centrifugation is a tool that is useful to separate particles within a preparation or sample based on their respective molecular weights. Centrifugation causes separations of matter on the basis of differences in molecular weight, polydispersity with respect to density, and therefore with regard to chemical composition, is amenable to direct analysis.¹³⁰ Separation is achieved through rapid spinning which imposes high centrifugal forces on suspended particles. The force generated by the centrifuge can be expressed as revolutions per minute (RPM) or relative centrifugal force (RCF). RPM is used to quantify how fast the rotor is rotating.¹³¹ This rotation speed is an independent variable relative to the rotor size. The RCF is a more valuable parameter regarding purification or isolation of nanoparticles in a colloidal suspension as it expresses the force exerted on the sample. RCF is measured in g-force and may be calculated using the equation:

$$RCF = 1.1118 \times 10^{-5} \times r \times rpm^2$$

Equation 1: Relative centrifugal force

Where:

- r is the rotor radius in centimetres

Regarding lipid nano drug delivery systems containing thermolabile polymers, the centrifuge can be modified to contain a cooling system for operation at lower temperatures. This is important in maintaining the synthesised vesicles with little risk of denaturation of phospholipid bilayers.

4.4. Lyophilisation

Freeze drying, also known as lyophilisation is a technique employed to remove solvents, typically water, within a hydrated/solvated preparation sample by sublimation and desorption under vacuum. Sublimation, as defined by the IUPAC, is “the direct transition of a solid to a vapour without passing through a liquid phase.”

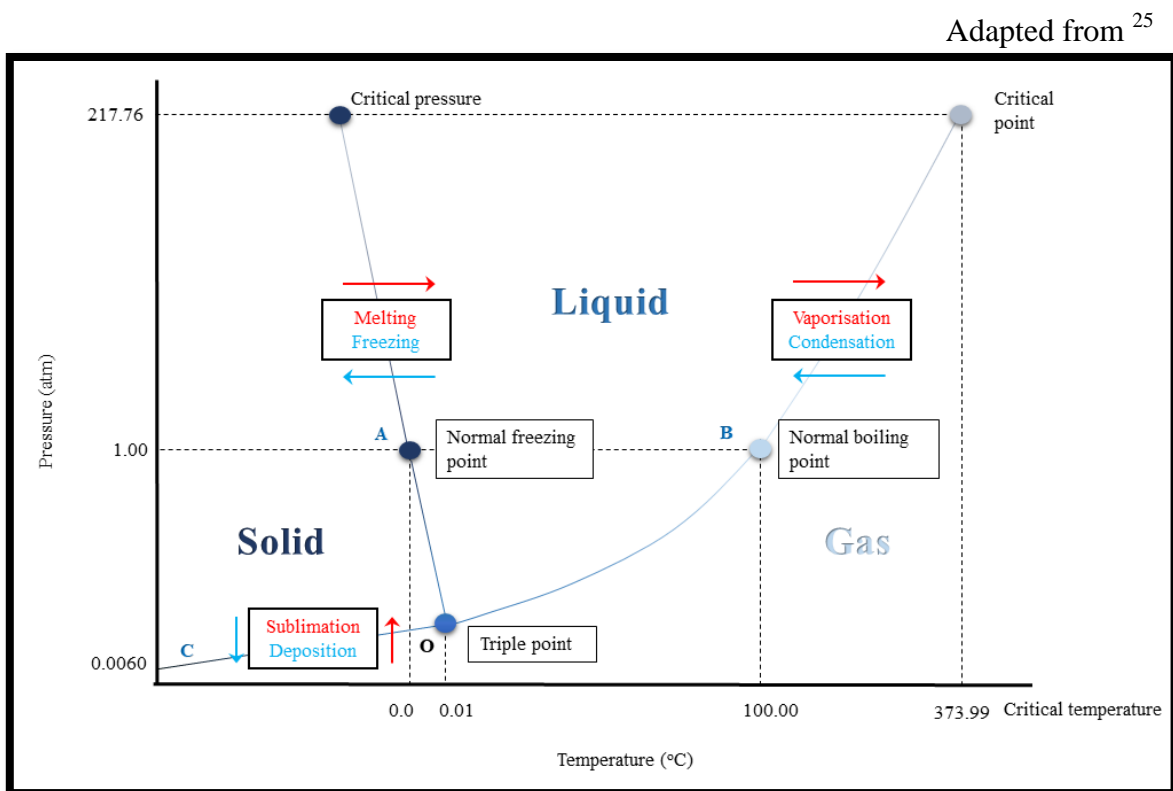


Figure 4.4-1: Phase diagram of water

This phenomenon occurs when a solvent is within specific temperature and pressure conditions. An example of a common macroscopic view of this phenomenon can be seen when “dry ice” vaporises at standard temperature and pressure.

The relationship of a solvent’s phase transitions under different standard temperature and pressure is represented as a phase diagram. As shown in the phase diagram of water (**Figure 4.4-1**), sublimation conditions are met across line O-C, when water transitions from solid to vapour without a characteristic melt. These conditions can be met by lyophilisation.

When it comes to formulation components, the solid state is the most stable form. Whether as pure drugs, excipients or medicines, materials stored in solid state have a longer shelf-life and are less susceptible to microbial contamination. One of the major challenges in nanoparticle synthesis is in preserving the compound for future use in formulations or for analytical purposes. When stored as aqueous suspensions for extended periods, nanoparticles in suspension are prone to aggregation/particle fusion and/or chemical instability such as hydrolysis and leaking of encapsulated drug into the bulk medium. One way to overcome this physical/chemical instability is to freeze dry the samples and remove the solvent to obtain a cake with: short reconstitution time, low residual moisture content and good long-term stability.

A well freeze dried sample should meet the following criteria:¹³²⁻¹³⁴

- The lyophilizate should be easily reconstituted with a quick reconstitution rate
- The physicochemical characteristics (e.g. vesicle size, drug entrapment) of the lyophilizate should be retained
- The residual moisture content of the sample should be low
- The stability of the freeze dried product should be maintained.

4.5. Characterisation of Nanoparticles

Nanoparticles may be characterised by a number of parameters which influence its functionality, for example in this study we look at transdermal drug delivery. Their behaviour in biological systems is influenced by parameters such as: size, membrane permeability, encapsulation efficiency, chemical and physical stability, as well as the quantity and purity of the starting materials.^{23,55} It is essential to consider these parameters when developing a method for ethosomal synthesis used in transdermal drug delivery and to take care when

selecting excipients due to their influence on vesicle characteristics. These parameters will influence the pharmacokinetics of the encapsulated API. In order to characterise ethosomes, various parameters are analysed. Selected parameters are represented in **Table 4.5-1**

Table 4.5-1: Parameters which influence ethosomes and the analytical techniques used for analysis

PARAMETER	SIGNIFICANCE	ANALYTICAL TOOL/TECHNIQUE
Morphology and/or polydispersity index	To determine ethosomal skin permeability and predict transdermal route of absorption	Scanning electron microscopy, transmission electron microscopy, dynamic light scattering, photon correlation spectroscopy, size exclusion chromatography, field-flow fractionation
Zeta potential (ζ_p)	To determine the stability of ethosomes as a colloidal dispersion	Dynamic light scattering, Zeta Meter,
Entrapment efficiency	To determine the efficiency of the synthesis method	Ultracentrifugation, High performance liquid chromatography, UV spectrophotometry
Drug content	To determine the amount of ethosomes to be included in a transdermal formulation for pharmacotherapeutic application	High performance liquid chromatography, UV spectrophotometry
Stability studies	To determine the shelf life of the ethosomal formulation in suspension and/or solid state	Scanning electron microscopy, transmission electron microscopy, dynamic light scattering, High performance liquid chromatography
In vitro dissolution	To determine the rate at which the encapsulated drug is released from ethosomes	Franz diffusion cells, High performance liquid chromatography, UV spectrophotometry
Skin permeation	To determine the rate of drug transport through skin	Confocal laser scanning microscopy
Transition temperature	To determine encapsulation, purity	Hot stage microscopy, Differential scanning calorimetry, thermogravimetric analysis.
Chemical interactions	To determine possible chemical interactions between functional groups formulation components	Fourier-transform infrared spectroscopy

All of the parameters listed are important in the qualitative and quantitative analysis of ethosomes.

4.6. Dynamic light scattering

Dynamic light scattering (DLS), also referred to as photon correlation spectroscopy (PCS), is an analytical tool used to characterise the particle size and size distribution of nanoparticles in suspension. The technique is based on the principle of Brownian motion and the tendency of nanoparticles, of varying sizes, in suspension to refract light.¹³⁵ Brownian motion is the random movement of particles due to the bombardment by the solvent molecules that surround them. The particle size is inversely proportional to the speed of its movement, with larger particles displaying a decreased displacement. Smaller particles are “kicked” further by the solvent molecules and move more rapidly.¹³⁶ When a focused light beam is directed at these particles, constructive and destructive interference of the photons commences. This is measured as a time dependent intensity fluctuation which can be detected and correlated to particle size.

DLS is affected by parameters such as viscosity and temperature which are directly related. The viscosity of a liquid is a known input into the DLS system, thus it important to maintain the temperature to provide accurate results as convection currents in the sample will cause non-random movements that will ruin the correct interpretation of size.¹³⁷

4.6.1. Particle size

The hydrodynamic diameter (HdD) is a measurement of the particle size of nanoparticles in suspension. This size correlates to how a particle diffuses within a fluid. The size of a particle is calculated from the translational diffusion coefficient¹³⁸ by using the Stokes- Einstein equation:

$$d(H) = kT / 3\pi\eta D$$

Equation 2: Stokes- Einstein equation

Where:

- $d(H)$ = hydrodynamic diameter
- D = translational diffusion coefficient (velocity of Brownian motion)
- k = Boltzmann’s constant
- T = absolute temperature
- η = viscosity

The diameter that is obtained by this technique is the diameter of a sphere that has the same translational diffusion coefficient as the particle. The translational diffusion coefficient will depend not only on the size of the particle “core”, but also on any surface structure, as well as the concentration and type of ions in the medium. There are multiple factors that affect the diffusion speed of particles such as, the ionic concentration of the medium and, the surface structure of the particle.¹³⁹ The ions in the medium and the total ionic concentration can affect the particle diffusion speed by changing the thickness of the electric double layer called the Debye length (κ^{-1}). Thus a low conductivity medium will produce an extended double layer of ions around the particle, reducing the diffusion speed and resulting in a larger, apparent hydrodynamic diameter. Conversely, higher conductivity media will suppress the electrical double layer and the measured hydrodynamic diameter. Additionally, any change to the surface of a particle that affects the diffusion speed will correspondingly change the apparent size of the particle. An adsorbed polymer layer projecting out into the medium will reduce the diffusion speed more if the polymer is lying flat on the surface. The aforementioned factors may affect the polymer conformation, which in turn can change the apparent size by several nanometres.

4.6.2. Polydispersity Index

The polydispersity index (PDI) of nanoparticles is an important parameter used to describe the uniformity of the sample. To characterise nanoparticles accurately as the mean particle size, it is important to have a normal particle size distribution - the narrower the distribution, the better the representation of the actual particle size.^{103,137} In general, samples with PDI below 0.1 are considered monodisperse, whereas samples with PDI above 0.1 are referred to as polydisperse. The higher the PDI value, the less uniform the sample is. A sample size distribution which is less than <0.5 is considered acceptable as it indicates that the size distribution of the particles is close to the mean size.

It is important to note that, when using DLS to obtain a PDI value, the particle size is measured in terms of a spherical particle. A similar scatter plot as non-spherical particles will be obtained, hence the need to confirm the physical characteristics of the sample in conjunction with another analytical technique is required. Apart from the non-discrimination involved in particle shape, this technique may include the solvation layer of solvent molecules around suspended colloidal particles to be a part of them. The resultant measurement may be an overcompensation for the particle size and thus not the true size.¹⁴⁰

4.6.3. Zeta potential

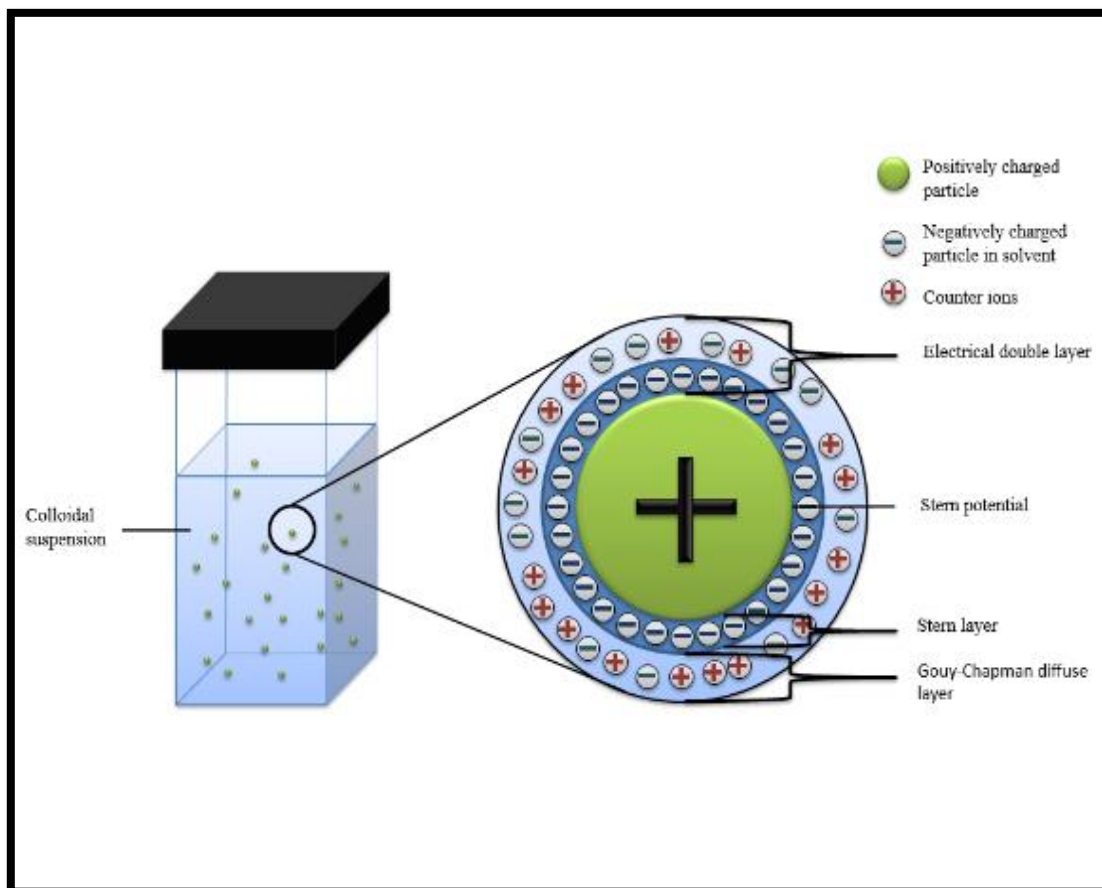
Adapted from ¹⁷⁶

Figure 4.6.2-1: A diagrammatical representation of the electrical double layer of a nanoparticle dispersed within a colloidal suspension.

Zeta potential (ζ_p) is measured using a zeta meter and indicates the overall charge a particle acquired in a specific medium. The overall charge occurs as a result of the attractive Van der Waal's forces and repulsive forces created by the electrical double layer.¹⁴¹ The net charge density on a microfluidic substrate in contact with an aqueous solution gives rise to an electrical double layer (**Figure 4.6.2-1**). This potential (mV) exists at the solid-liquid interface which varies according to the distance of the liquid molecule from the particle surface.¹⁴²

The stability of a nano-suspension as a lipid based drug delivery system and its subsequent shelf-life can be predicted by the ζ_p . Nano-suspensions, such as ethosomes, remain stable because of the degree of repulsion between the suspended vesicles with one another and with the solvent in which they are suspended. In order for ethosomes to remain suspended (i.e.

with a net force greater than gravity) the charge should be great enough to prevent aggregation to keep these particles within the suspension. Generally, high ζ_p (negative or positive) prevents aggregation of the particles due to electric repulsion and electrically stabilizes the nanoparticle dispersion. On the other hand, in the case of low ζ_p , attraction exceeds repulsion and the dispersion coagulates or flocculates.¹⁴³

Table 4.6.3-1: The standard zeta potential values and their related stability behaviour.

ZETA POTENTIAL (mV)	STABILITY BEHAVIOUR
0 to ± 5	Swift flocculation
± 10 to ± 30	Initial instability
± 30 to ± 40	Modest stability
± 40 to ± 60	Fine stability
More than ± 61	Tremendous stability

As shown in **Table 4.6.3-1**, nanoparticles with a ζ_p above (+/-) 30 mV indicate that the nanoparticles should remain in a deflocculated state.

4.7. High performance liquid chromatography

High performance liquid chromatography (HPLC) is a sensitive, versatile and reproducible analytical technique with many pharmaceutical research applications accounting for both qualitative and quantitative analysis.¹⁴⁴ Commonly utilised in pharmaceutical chemistry, preparative HPLC refers to the process of isolation and purification of compounds. However, when used in pharmaceuticals, analytical HPLC is preferred. In this instance, HPLC is used to analyse and quantify, the sample containing a (usually known) compound.^{82,87} This can be applied to experiments such as: tablet dissolution studies, shelf life determinations, stability studies, identification of APIs, pharmaceutical quality control, the encapsulation efficiency and entrapment efficiency of nanoparticles.¹³¹

For the accurate analysis of a compound, there are parameters which must be controlled to influence the quality of results (**Table 4.7-1**). Methods need to be validated for known compounds to ensure accuracy and reproducibility. For unknown compounds, HPLC methods need to be developed and then validated.

Table 4.7-1: An overview of the influence of selected parameters on the quality of HPLC analysis

PARAMETER	SIGNIFICANCE	RELATIONSHIP BETWEEN VARIABLE AND ANALYTE	INFLUENCE ON CHROMATOGRAM
Internal diameter of column	Determines quantity of analyte.	The lower the internal diameter of the column, the lower quantity of analyte retrieved from the sample. Lower IDs also reduce sample loading capacity.	Reduced area under the curve (AUC) of retention peaks
Column particle size	Determines quality of analyte separation. (Peak resolution)	The smaller the particle size, the greater the greater surface area, and the better the separation of the analyte.	Reduced peak width and better resolution.
Pore size of packing material	Determines quality of analyte separation. (Peak resolution) Pore size defines an ability of the analyte molecules to penetrate inside the particle and interact with its inner surface.	The smaller the pore size, the greater the surface area.	Reduced peak width and better resolution
Pump Pressure	Determines quality of separation and retention time of the analyte.	The higher the pressure, the quicker the velocity of the mobile phase and the faster the movement of the analyte through the column.	Reduced peak width, shorter retention time of the analyte
Temperature	Determines the viscosity of the mobile phase and the rate of the retention time of the analyte.	The higher the pressure, the lower the viscosity of the mobile phase	Reduced retention time of the analyte
Mobile phase concentration	Influences the partitioning of the analyte.	The greater the affinity of the analyte for the mobile phase, the faster the retention time.	Influences the retention time, quality and quantity of analyte separation.
Injection Volume	Determines the amount of sample to be analysed	An increase in the injection volume results in an increase in the quantity of the analyte	Increased AUC of analyte.
Sample	Determines the	An increase in sample	Increased AUC of

concentration	amount of sample to be analysed	concentration results in an increase in the quantity of the analyte	analyte.
----------------------	---------------------------------	---	----------

When utilised for determination of encapsulation efficiency, entrapment efficiency and vesicle stability of lipid drug delivery systems, the API may be analysed either directly or indirectly. Using the direct method, the vesicle is first lysed using a suitable solvent and/or sonication method. The liberated drug is obtained by ultracentrifugation. Depending on its affinity, it can be obtained as a pellet or a supernatant. The pure API is then qualitatively assayed using any developed method (e.g. HPLC) and then quantitatively analysed using HPLC. In the indirect method, the supernatant of the ultra-centrifuged lipid colloidal suspension is analysed.

4.8. Fourier transform infrared spectroscopy

Fourier transform infrared spectroscopy (FTIR) is a qualitative analytical tool used for the identification of functional groups within a compound. A compound examined using FTIR is subjected to IR radiation within the wavelength range from 2.5 μm to 15 μm (wavenumber range 4000 cm^{-1} to 660 cm^{-1}). Electromagnetic irradiation of the sample triggers molecular vibrations, which are characteristic of the associated 2D and 3D movements of the bonds of atoms corresponding to certain functional groups. These characteristics are influenced by the strength of the bonds, conjugation and polarity of the atoms within the compound. The presence of electron withdrawing groups such as oxygen influences the formation of dipole moments which influences the movement of hydrogens within the magnetic field. This influences the bending, compression and stretching of bonds within the compound observed. The vibrational frequency may be expressed according to an adaptation of Hooke's law using the following equation:¹⁴⁶

$$\tilde{\nu} = \frac{1}{2\pi} \sqrt{\frac{k}{\mu}}$$

Equation 3: Fundamental vibrational frequency

Where:

- $\tilde{\nu}$ = fundamental vibration frequency
- k = force constant

- μ = Reduced mass

$$\text{Reduced mass} = (m_1 m_2) / (m_1 + m_2)$$

Where:

- m_1 and m_2 are the component masses for the chemical bond under consideration

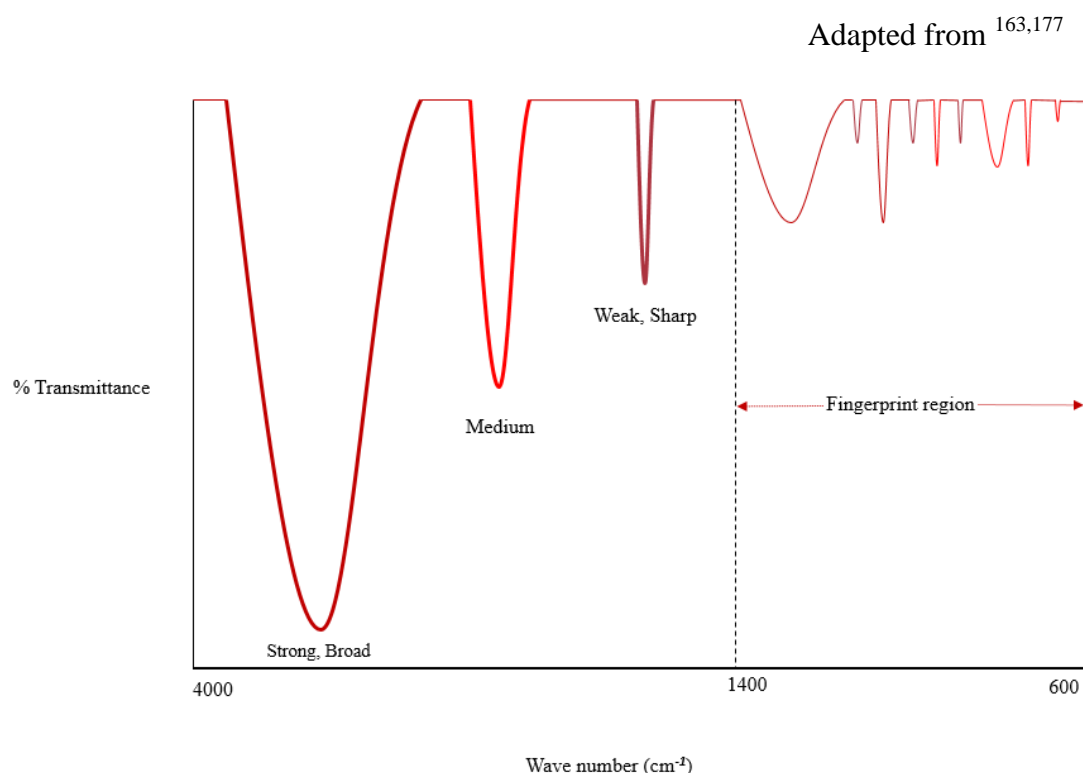


Figure 4.8-1: A simplified FTIR spectrogram showing the different peak sizes.

IR data are represented as bands on a spectrogram which displays the relationship of (absorbance or transmittance) vs wave number. With respect to relative intensity, these bands can be classified as strong, medium or weak; regarding the band width and are classified as broad or narrow (**Figure 4.8-1**). The fingerprint region ($1400 - 600 \text{ cm}^{-1}$), is a series of bands that are specific to any compound. This feature, used in conjunction with other analytical techniques (e.g. nuclear magnetic resonance - NMR), can be used to verify the identity of compounds to provide a comprehensive picture of its morphology and physicochemical properties.

In the determination of encapsulation of drugs within nano-vesicles, the bands of the pure components compared to that of the vesicle are compared. Changes in the properties (e.g. disappearance, broadening, variations in peak intensity, peak shifts) of respective characteristic bands are indicative of interactions and/or nanoparticle formation

4.9. Scanning electron microscopy

Scanning electron microscopy (SEM) is an analytical technique that, apart from elemental and state analysis, typically provides information regarding the morphology of the sample observed. As opposed to traditional optical microscopes, which use a light source to observe the sample, SEM uses a high energy electron beam. Using a raster scan, a high resolution image of the sample surface is provided by a mechanism involving the scattering of electrons. An electron gun is used to bombard the sample with electrons. When electrons enter the sample, they are scattered within it. Some of this energy is absorbed by the sample. Variables such as the electron energy, atomic number of the elements and the density of the atoms influence the scattering range and interaction of these electrons. The scattering of electrons provides signals such as secondary electron emission, back-scattered-electrons, cathode-luminescence and X-rays, which can be detected. The diversity of electron scattering shows differences in origin, energy and source. Collectively, a comprehensive data set is generated which can be displayed as an image. The resolution of the image is dependent on the array of signals detected.¹⁴⁷

4.10. Thermoanalyses

As the name suggests, thermoanalysis involves the introduction of heat into a system to analyses it. Thermoptometry is a term used to describe “a family of thermoanalytical techniques in which an optical property of the sample is monitored versus time or temperature, while the temperature of the sample in a specified atmosphere, is programmed”.¹⁴⁸

When characterising compounds using thermoanalyses, commonly used techniques include: hot stage microscopy (HSM), differential scanning calorimetry (DSC) and thermogravimetric analysis TGA, which work synergistically to categorise physical transitions of compounds. When viewed collectively, the data generated from these analytical techniques provide a comprehensive picture regarding the morphology and physicochemical properties of the compound. When used independently, the data may provide an incomplete picture.²⁰

4.10.1. Hot stage microscopy

Hot stage microscopy (HSM), also referred to as thermo-microscopy, is an analytical technique that combines light microscopy with the introduction of heat provided by a hot stage, to perform solid state characterisation.¹⁴⁸ The addition of thermal events allows for the observation of phase transitions which, in conjunction with other thermoanalytical techniques (such as TGA and DSC), provide a comprehensive profile of the physicochemical properties of the sample observed. Since analyses such as TGA and DSC are in closed systems where the sample is shielded from the naked eye of the researcher, it is beneficial to include this complementary technique as an alternative perspective. HSM is useful in providing information such as

- Solid-solid transformations
- Interaction between different compounds
- Dissolution of one compound in another
- Sublimation and/or evaporation
- Melting or liquefaction upon heating (solid-liquid transformations)
- Solidification upon cooling (liquid-solid transformations)¹⁴⁹

The quality of the data obtained from HSM is influenced by sample preparation, size distribution and the heating rate of the sample observed. As a tool in the analysis of nanoparticles, its use is warranted due to the added benefit of a small quantity required for analysis.¹⁵⁰

Used in isolation, it does not possess the sensitivity or accuracy of TGA or DSC. The marriage of hot-stage microscopy to new technology, such as high-resolution colour cameras and image manipulation software, video-enhanced microscopy offers even greater possibilities for the characterization of materials.¹⁵¹

4.10.2. Differential scanning calorimetry

Differential scanning calorimetry (DSC) is an analytical tool useful in the solid-state characterization of substances. This is because of its ability to provide detailed information about the physical and energetic properties of substances.¹⁵² As an analytical tool, DSC is useful in determining the following physical transitions:^{65,132,133,153}

- Melting, crystallisation, glass transitions and mesophase transitions
- The evaporation of liquid samples
- Drying (desorption of adsorbed moisture or solvents)
- The sublimation of solid samples
- Decomposition of hydrates or solvates with the elimination of the water
- Chemical reactions
- Thermal decomposition
- Polymerisation

Table 4.10.2-1: Characteristics which influence glass transition temperatures of solid state compounds using thermogravimetric analysis

PARAMETER	EFFECT ON GLASS TRANSITION
Crystallinity	Increasing crystallinity results in smaller step height with a subsequent larger and broader glass transition
Crosslinking, Curing, Polymerisation, Molar Mass	Tg shifts to a higher temperature with increasing molar mass or crosslinking
Orientation and Storage Below Tg	Internal stresses and storage shift Tg and increase of the enthalpy relaxation peak
Plasticizers	Plasticisers shift Tg to lower temperatures
Mixtures	Incompatible mixtures give two transitions, compatible mixtures only one
Co-Polymers	Block and graft copolymers of compatible monomers and statistical co-polymers show only one transition, otherwise two transitions
Chemical Modification	Tg step height and the width of the transition can change, several transitions can occur

The glass–liquid transition (T_g), or glass transition, is the gradual and reversible transition in amorphous materials, from a hard and relatively brittle "glassy" state into a viscous or rubbery state as the temperature is increased. As shown in (Table 4.10.2-1), it may be influenced by sample characteristics.

4.10.3. Thermogravimetric analysis

Thermogravimetric analysis (TGA) is an analytical tool used to analyse the change in the mass of a sample with respect to a fluctuation in temperature. It is a thermal balance that provides information regarding the phase transitions that occur as a result of enthalpy changes at a fixed gradient over a specified period.¹⁵⁴ This thermoanalytical technique measures a sample's weight as it is heated and/or cooled in a furnace in a controlled atmosphere with a purged gas that is inert and does not induce combustion. When used in the analyses of nanoparticles, it provides complementary data to validate encapsulation. Changes in the temperature of the phase transitions, relative to the pure components, could be indicative of the formation of a nanovesicle. The temperature of phase transitions can either be attributed to weight gain or weight loss. Weight loss may be attributed to:

- Chemical reactions (decomposition and water loss of crystallisation, combustion, reduction of metals)
- Physical transitions (vaporisations, evaporation, sublimation, desorption, drying)

Whereas weight gain may be attributed to:

- Chemical reactions (reactions with gaseous substances in the purge gas such as O₂)
- Physical transitions (absorption of gaseous substances)

Much like the aforementioned thermoanalyses, TGA is best utilised in conjunction with other types of thermoanalyses to provide comprehensive characterisation of the physicochemical nature of a compound.

4.11. Drug release

Drug release refers to the mechanism describing the conversion of an API into a bioavailable constituent which may be utilised by the body for pharmacotherapeutic effect. The mechanism of release (**Figure 4.11-1**) may be directly involved in the pharmacokinetic properties of the API, affecting its absorption, distribution, metabolism and excretion. As such, it is important to determine the drug release because, apart from describing how the API is released from a drug delivery system such as a nano carrier, the “when” is just as important as it will assist in determining the environment that the API will be subjected to.¹⁴²

The drug release profile may subsequently help with determining the bioavailability, therapeutic dose and toxic levels associated with administration of pharmaceuticals.

Adapted from ^{158,178}

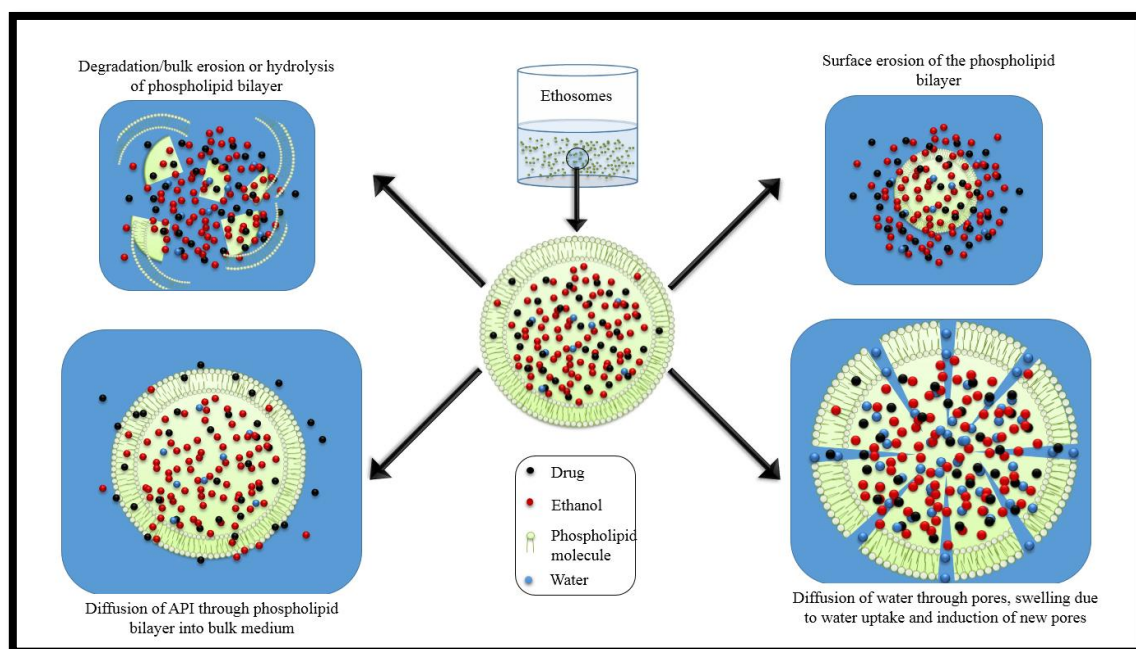


Figure 4.11-1: A diagrammatical representation of the possible mechanisms of drug release of ethosomes.

Factors affecting the drug release may be the result of various phenomena and mechanisms such as dissolution, diffusion, osmotically driven release and erosion.¹⁵⁵ Generally, these mechanisms occur simultaneously with one mechanism being most predominant. When evaluating spherical nano-vesicles, it was found that the release was dependent on the location of the API- either embedded within the polymer matrix, adsorbed onto to the surface, or located within the core.¹¹⁶ For lipid based nanoparticles such as ethosomes, it was found that the behaviour of the polymer system is one of the most influential factors in determining the drug release. The reversible nature of the drug-carrier interaction allows for encapsulated API to be released in a controlled or sustained manner.^{95,156} Other factors may include: physicochemical properties of the API, the properties of the release medium and excipients in the formulation. The impact of these factors may be regulated by altering the drug solubility, excipient composition and nano-structure, all of which influence the drug release profile.¹¹¹

4.12. Mathematical models of drug release

Mathematical models are research tools which predict the release of APIs from a variety of dosage forms and drug delivery systems. These equations can be used to design new systems by selecting the geometry, method of formulation and particle size. Established mathematical models can be applied to drug release data sets where the mechanism of drug release can be determined by comparison of plots.¹⁰⁷ For most models, it is essential that the data is plotted as the cumulative percentage drug release over time. Drug release can be classified into four main categories – each influenced by the magnitude of the initial burst release and the subsequent release kinetics:¹⁰⁷

High initial burst release + Minor additional release	Low initial burst release + Minor additional release	High initial burst release + Steady-state release	Low initial burst release + Steady-state release
---	--	---	--

With knowledge of the core parameters influencing the kinetics, mathematical models may predict the mechanism of drug release from a variety of dosage forms and drug delivery systems. As such, the most common¹⁵⁷ models were identified and tabulated (**Table 4.12-1**).

Table 4.12-1: Mathematical models and their associated release mechanisms

MODEL	MATHEMATICAL EQUATION	RELEASE MECHANISM
Zero order	$C = C_0 - K_0t$	Diffusion Mechanism
First order	$\log C = \log C_0 - Kt/2.303$	Fick's first law, diffusion Mechanism
Higuchi Model	$C = [D(2qt - Cs)Cs t]^{1/2}$	Diffusion medium based Mechanism in Fick's first law
Korsemeyer - Peppas Model	$Ct/C_\infty = Kt^n$	Semi empirical model, diffusion based mechanism
Hixson-Crowell Model	$C_0^{1/3} - Ct^{1/3} = K_{HC}t$	Erosion release mechanism
Weibull Model	$C = C_0 [1 - \exp\{-\frac{(t - T)^b}{a}\}]$	Empirical model, life-time distribution function

Each mathematical model is influenced by a fixed set of assumptions regarding the factors influencing the drug release. Such assumptions may include: The drug release is independent of its concentration (Zero-order), diffusion occurs only in one dimension (Higuchi), Dissolution of the polymer matrix (Korsmeyer-Peppas), drug particles are uniform in size and diminish during dissolution (Hixon-Crowell), and the intrinsic dissolution of the drug is not considered (Weibull).¹⁵⁸ Therefore, consideration of the physiological parameters is important as they influence which models should be applied and, supplemented by scientific literature, reduces the probability of making arbitrary comparisons. The most suitable mathematical model may be selected by comparing the respective adjusted correlation coefficients (R^2 adjusted), the mean square error (MSE), the standard deviation of residuals (Sy.x), Akaike Information Criterion (AIC), and the Model Selection Criterion (MSE) to determine goodness of fit.¹⁵⁹

Ethosomes have a variety of drug release mechanisms, often influenced by the components and their respective concentrations used in their respective formulations.



UNIVERSITY *of the*
WESTERN CAPE

CHAPTER 5

MATERIALS AND

METHODS



School of
PHARMACY

5. Introduction

In this chapter, the materials and methodology used to synthesize the ethosomes as well as the analytical techniques used to study the ethosomes are outlined.

5.1. Identification of betamethasone valerate, hydrocortisone acetate and cholesterol Pure betamethasone valerate (BMV), hydrocortisone acetate (HCA) and cholesterol were identified using the British Pharmacopoeia 2009 (BP) identification assays and were compared with reference standards in their respective monographs.⁷³ The analytical tests chosen to evaluate the compounds were differential scanning calorimetry (DSC) and Fourier transform infrared spectroscopy (FT-IR). Using DSC, a compound was accepted on the condition that the melting point was within ± 1 °C of the assay, with the absence of endothermic peaks, indicating impurities, prior to the characteristic melting point. In order for acceptable identification to be met using FTIR, the relative peak intensities and frequencies within their respective fingerprint regions on the experimental spectrogram had to match those in BP reference standards.⁷³

5.2. Preparation of unloaded ethosomes

The conventional cold method (CM) and hot method (HM) for the preparation of classical ethosomes, as described by Touitou *et al*, 2003 with slight modifications were used.¹

5.2.1. Cold Method

Figure 5.2.1-1 illustrates the CM and HM. For the CM, unloaded ethosomes were prepared at room temperature (25 °C). All compounds were weighed using an analytical balance (Mettler, USA) An organic phase (3 ml) and an aqueous phase (7 ml) were prepared in two separate 20 ml polytop vials. The volumes were measured using 5 ml and 10 ml disposable syringes. The organic phase consisted of 0.05 g L- α Soy phosphatidylcholine (PC) (> 95 % purity) (Avanti ® polar lipids Inc. USA) and 3 ml 99.9 % ethanol (Merck, South Africa). These were mixed using a magnetic stirrer (Labcon, USA) at 1500 rpm for 10 min until a clear solution formed.

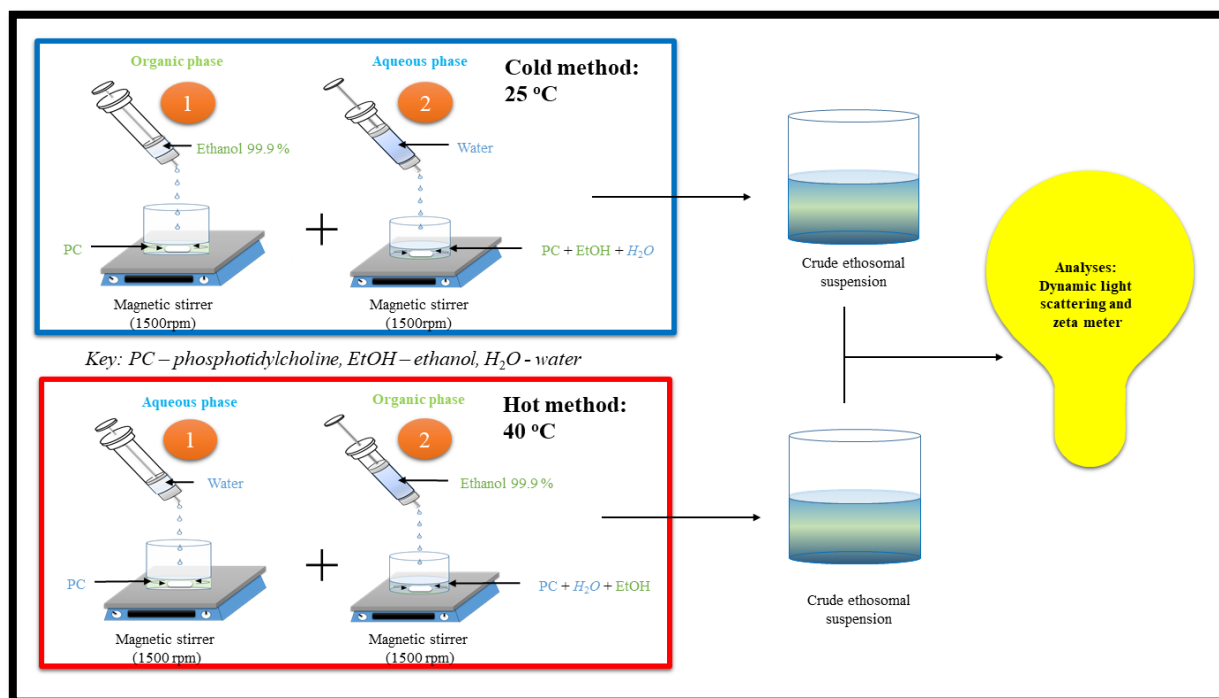


Figure 5.2.1-1: An overview of the hot and cold method used for ethosome synthesis.

The organic phase formed the base of the suspension. The aqueous phase, consisting of 7 ml MilliQ® water (H₂O), was transferred to a 10 ml syringe fitted with a micro-needle. It was then slowly injected (drop-wise) into the organic phase to form a colloidal suspension consisting of 30 % v/v organic phase and 70 % v/v aqueous phase. The duration of mixing upon the addition of the aqueous phase until completion was 15 min.¹

5.2.2. Hot Method

Similar to the CM, the HM (**Figure 5.2.1-1**) involved the preparation of an organic phase and an aqueous phase using the same excipients. The volumes and masses of the components were maintained, with the main difference being the temperature of the system during preparation. Using a magnetic stirrer with a hot plate set at 40 °C, both the organic and the aqueous phases were prepared. The temperature was monitored using a temperature probe and was maintained to ± 5 °C. The organic phase consisted of pure ethanol which was heated in a sealed polytop vial, whereas the aqueous phase consisted of PC dispersed in H₂O heated in a separate sealed polytop vial.

The aqueous phase, consisting of 7 ml H₂O + PC (40 °C), formed the base of the suspension. The organic phase 3 ml Ethanol (40 °C) was transferred to a 5 ml syringe fitted with a micro-needle. The organic phase was slowly injected (drop wise) into the aqueous phase to form a

colloidal suspension consisting of 30 % organic phase v/v and 70 % v/v aqueous phase. The duration of mixing from the addition of ethanol until completion was 15 min using the magnetic stirrer.⁹²

5.2.3. Preparation of corticosteroid loaded ethosomes

Hydrocortisone acetate (HCA) and betamethasone valerate (BMV) were selected for ethosome encapsulation with both having poor aqueous solubility. As such, these compounds were dissolved in the organic phase. 0.01 g of each was dissolved in 3 ml of ethanol. This was achieved for both the aforementioned HM and CM. (Table 5.2.3-1)

Table 5.2.3-1: Ethosome formulations containing BMV and HCA

METHOD	PC (g)	BMV (g)	HCA (g)	Ethanol (mL)	H ₂ O (mL)
HM	50		N/A	3	7
	50	0.01		3	7
	50		0.01	3	7
CM	50		N/A	3	7
	50	0.01		3	7
	50		0.01	3	7

All the ethosomes resulting from the HM and CM, at this stage, are referred to as crude ethosomes as no further processing was done.

5.3. Comminution of ethosomes

To determine the best method for particle size reduction, 2 methods were used and compared: extrusion and sonication (Figure 5.3-1). Ethosomes resulting from Table 5.2.3-1 were sonicated or extruded using the following methods

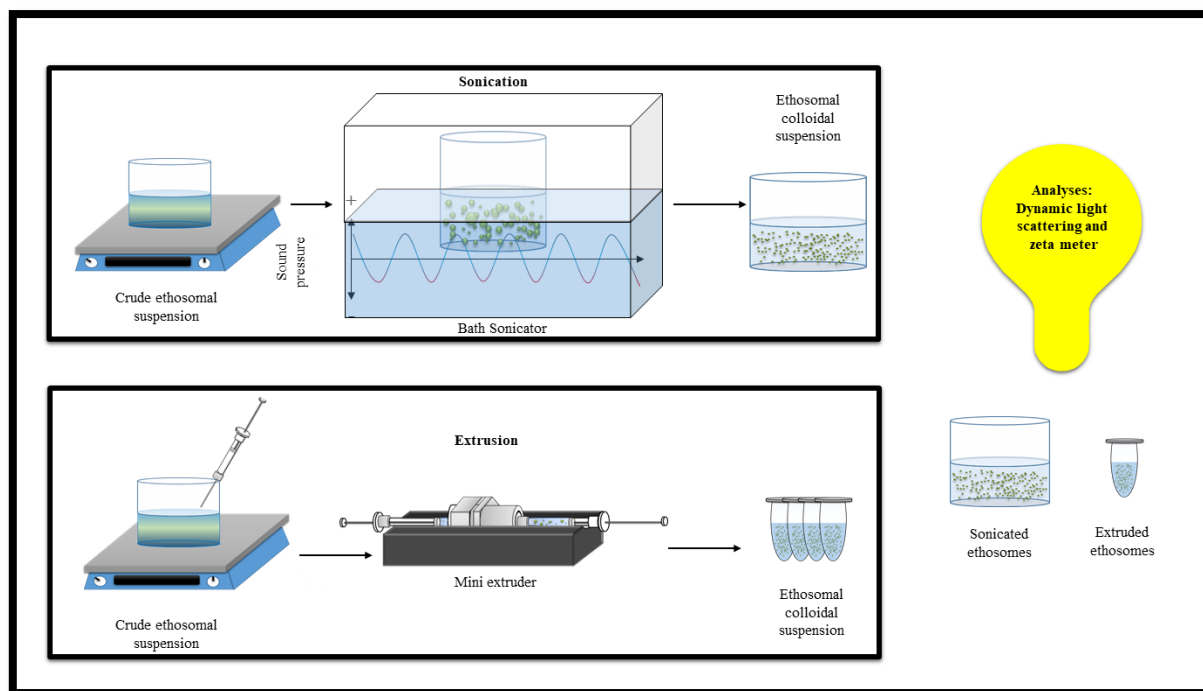


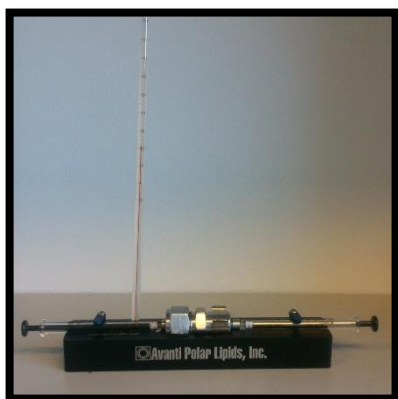
Figure 5.3-1: An overview of the comminution methods utilised in ethosome synthesis

5.3.1. Sonication



For particle size reduction, the crude ethosomal suspension in the 20 ml polytop vial, prepared via CM, was subjected to water bath sonication using an ultra-sonic bath (Labotec, South Africa) at high frequency, 25 °C for 1 cycle of 5 min. The crude ethosomal suspension prepared via the HM method was subjected to the same conditions with the only difference being in the change in temperature which was set at 40 °C.

5.3.2. Extrusion



Smaller vesicles were obtained by extruding crude ethosomes (prepared using HM and CM) using a desktop mini extruder (Avanti Polar Lipids, Inc., USA). For ethosomes generated from the CM, 1 ml of sample was extruded at room temperature using 1 ml Hamilton® glass syringes. The sample was passed through 0.1µm Whatmann polycarbonate membranes 5 times. The

extruded sample was transferred into 1.5 ml Eppendorf® tubes for purification. For ethosomes generated from the HM, the extruder was placed on a hot plate set at 40 °C. The temperature was monitored using a mercury thermometer. Extrusion was done manually and care was taken to keep the pressure in the syringes loaded with crude ethosomal formulations as consistent as humanly possible during the extrusion process.

5.4. Purification

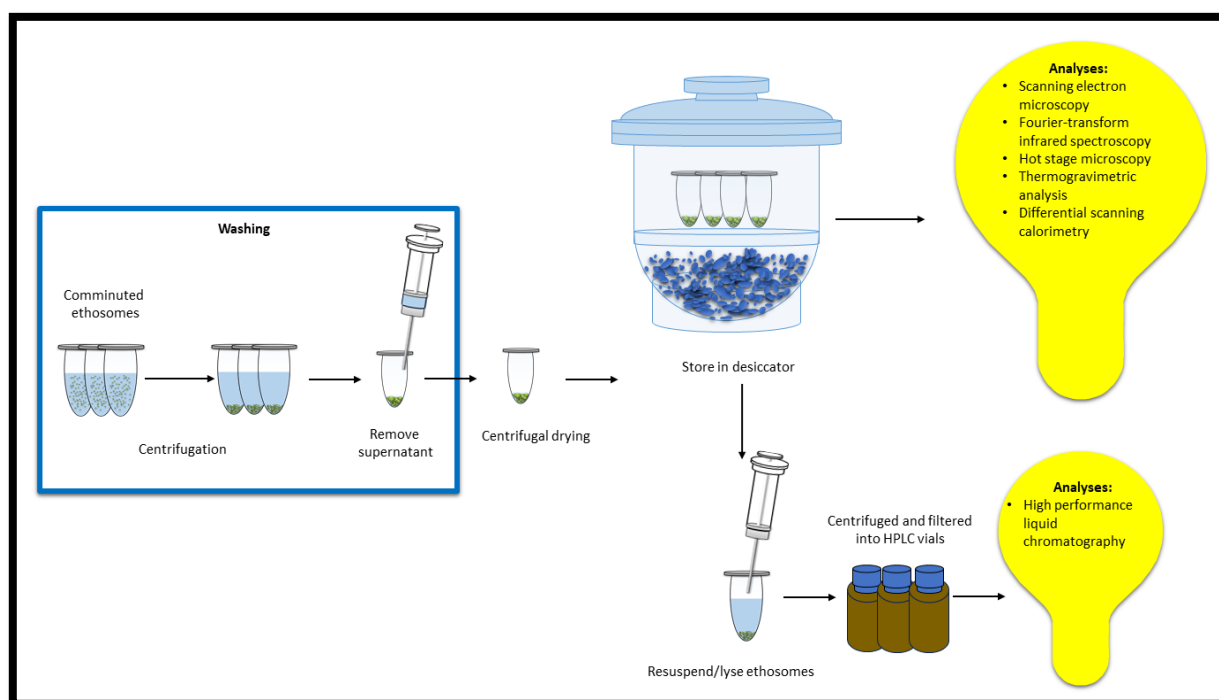


Figure 5.4-1: An overview of the purification and isolation methods used in this study

In order to isolate the ethosomes, 2 methods were employed: centrifugation and centrifugal drying (**Figure 21**). The ethosomes resulting from these methods were resuspended in the same solvent system as used in the preparation, analysed and evaluated according to the following parameters: HdD, PdI and ζ p.

5.4.1. Centrifugation



Centrifugation was used to separate ethosomes from the raw materials. This was an important step to ensure that subsequent analyses regarding ethosomal characterisation were accurate, especially those analyses regarding quantification of the API in loaded ethosomes. The comminuted samples prepared via HM and CM were centrifuged using an Eppendorf® centrifuge (Eppendorf®, USA) at 20817 rcf (14000 rpm) for 2 hours at 4°C. Once the run had completed, the supernatant was removed using disposable syringes fitted with hypodermic needles (Avanti). The pellet was resuspended in the same solvent system used in synthesis and washed again. For loaded ethosomes, the supernatant was refrigerated (6-8 °C) in the Eppendorf® tubes for further analysis using HPLC to quantify the amount of API in the supernatant.

5.4.2. Centrifugal drying



Ethosomes were dried to allow for solid state characterisation where thermal events corresponding to molecular interactions and encapsulation were identified. Ethosomal pellets, stored after centrifugation containing residual moisture, were resuspended to 1.5 ml using the same solvent system as used in the HM and CM synthesis. Samples were dried for 6-8 hours using a MiVac Centrifugal drier (United Scientific) with a vacuum pump (DUP-23050-L00) and speed trap (MST-23050-L00). The MiVac was set to remove H₂O and ethanol at a temperature of 40°C. Dried samples were stored in a desiccator at room temperature, away from direct sunlight.

5.5. Analysis and characterisation

At designated stages, the ethosomes synthesised using the HM and CM methods were analysed and evaluated according to the following parameters: HdD, PdI and ζ p. Apart from the nano-range being essential, the PdI indicated the homogeneity of the particle size distribution. These served as the core parameters regarding this study as particle size

influences topical delivery. The ζ_p provided an indication of the stability of the ethosomes in suspension. However, although useful regarding stability, optimisation of ethosome stability was not an objective for this study. As such, ethosomes were analysed within 72 hours of manufacture.

5.5.1. Hydrodynamic Diameter and Polydispersity Index



The HdD and Pdl was measured to determine if the prepared ethosomes were of suitable size for topical drug delivery. In order to determine the HdD and Pdl, suspended ethosomes were measured using dynamic light scattering (DLS) on a Nano ZS 90 Zetasizer (Malvern Instruments Ltd., U.K.) with the 4 mW He-Ne laser operating at a wavelength of 633 nm. The HdD of the synthesized ethosomes was measured at 25°C (CM) and 40°C (HM) using DLS at an angle of 90° to the laser beam. 1 ml of the prepared ethosomal colloidal suspension was added to a disposable plastic cuvette (ZEN0118). The material analysed was set as polystyrene latex, with a refractive index of 1.590 and an absorbance of 0.010. The dispersant analysed was water, with a viscosity of 0.887 cP and a refractive index of 1.330 at a temperature of 25°C (equilibration time 120 seconds). The measurement angle was 90° with a measurement duration of 5 runs: 60 seconds/run, 3 measurements, 0 delay between measurements. The z-average diameter and the polydispersity index of the ethosomes were automatically generated by the instrument using cumulative analysis with software loaded on to the instrument. All readings were performed in triplicate using independently prepared samples.

5.5.2. Zeta-potential

The ζ_p of ethosomal colloidal suspensions was determined to evaluate the stability of the colloidal ethosomal system by measuring the surface charge of colloidal particles. Suspended ethosomes samples were prepared by resuspension of the ethosome pellet after purification. Samples were measured using a laser Doppler anemometer coupled to the Nano ZS 90 Zetasizer (Malvern Instruments Ltd., U.K.). For ζ_p characterization, a disposable folded capillary cell (DTS1070) was flushed with MilliQ® water using a 1 mL syringe prior to analyses as recommended by the manufacturer and 700 μ L of suspended ethosomes was

added to the cell. The samples were then analysed with a voltage of 4 mV at 25°C at an angle of 173° to the laser beam. The intensity-weighted mean value was measured and the average of three 15 cycle measurements was taken per sample. All readings were performed in triplicate using independently prepared samples.

5.6. High performance liquid chromatography

High Performance Liquid Chromatography (HPLC) was used quantitatively to determine, encapsulation efficiency (EE), drug loading (DL) and drug release (DR) of loaded ethosomes. In order to quantify the encapsulated corticosteroids, it was important to ensure that a reliable method, suitable to the components of the HPLC system was used. Since both BMV and HCA are known compounds, their HPLC methods have been developed and are published in literature. The methods were obtained from the BP 2009 and were modified.⁷³

5.6.1. Preparation of the standard solutions for calibration

The HCA and BMV standard samples were prepared by dissolving 10 mg of each respective API in 10 ml H₂O:ethanol (30:70). This solvent was chosen as it represented the same conditions of the APIs solvent system. Using a magnetic stirrer (Labcon, USA), the standard solution was agitated at 1500 rpm for 30 min forming a clear solution. 3 ml of the standard sample solution was retrieved using a 5 ml Avicare disposable syringe and was filtered using a 0.22 µm filter. After filtering 2 ml of the standard solution, 1 ml was transferred into an HPLC vial. The final concentrations of the standard solutions were 1 mg/ml, which is identical to the concentrations of the prepared ethosomal formulations. The mobile phase was prepared using acetonitrile (ACN) and H₂O. Using isocratic elution, the mobile phase was set at 60:40 % (ACN:H₂O). The ACN was HPLC grade (Sigma-Aldrich) and the H₂O was collected from the water purification system (Purite, USA) available at UWC, School of Pharmacy.

5.6.2. HPLC chromatographic conditions



HPLC analysis was conducted using an (Azura, Germany) HPLC system coupled with ClarityChrom® software. The system consisted of an auto sampler (AS 6.1 L), a quaternary pump (P 6.1 L), a thermostatted column compartment (CT 2.1) and a diode array detector (DAD 2.1 L). A Phenomenex Luna 5 μm C18 (2) 100 Å column was used and the flow rate was set to 1 mL per minute with the column temperature being maintained at 20 °C. The injection volume was set at 1 μL and the wavelength was set to 254 nm. The detection wavelength was changed from 254 nm to 240 nm. PDA detection was used to identify an optimal wavelength for the detection of the APIs. An increased amount of analyte was detected at 240 nm. The optimised method was validated using the International Council on Harmonisation (ICH) guidelines to ensure reliability of results.¹⁶⁰

5.7. HPLC method validation

To ensure that the methods were suitable for BMV and HCA analysis using the HPLC system, the methods were validated using ICH guidelines using the following analytical parameters: specificity, repeatability, linearity, accuracy, precision, limit of detection, limit of quantification and robustness.¹⁶⁰

5.7.1. Specificity

Specificity expresses the extent to which other substances interfere with the determination of a substance according to a given procedure.¹⁶⁰ To determine the specificity of the method for BMV and HCA, HPLC analysis was performed using an aliquot of the prepared stock solutions. An HPLC vial containing 1 ml of the mobile phase ACN:H₂O (60:40) was also prepared and analysed. These analyses were conducted to determine if there are any overlapping peaks, i.e. analytes eluting with an identical retention time as that of the APIs, which may have influenced the amount of API analyte detected using the method.

5.7.2. Repeatability

Repeatability expresses the closeness of the results obtained with the same sample (or subsamples of the same sample) using the same measurement procedure, same operators, same measuring system, same operating conditions and same location over a short period of time.¹⁶⁰ To determine repeatability, BMV and HCA were analysed 6 times at the theoretical 100 % (1 mg/ml) value.

5.7.3. Linearity

Linearity may be defined as the method's ability to obtain test results which are directly proportional to the concentration of analyte in the sample.¹⁶⁰ To determine linearity, standard solutions of the same concentration were injected into the system by changing the injection volume from 0.1, 0.2, 0.5, 1, 2.5 and 5 μL . Each concentration was injected twice, with the theoretical 100 % concentration injected six times. Samples were analysed using the aforementioned HPLC method. The mean area % of the peaks obtained for each concentration was used to construct a calibration curve displaying absorbance vs concentration for BMV and HCA.

5.7.4. Accuracy

The accuracy may be defined as the degree of agreement between the experimental value, obtained by replicate measurements.¹⁶⁰ The accuracy was determined by calculating the percentage recovery of the theoretical 100 % concentration which was injected 6 times. The individual sample and mean % recovery was determined using the following equation:

$$\text{Recovery \%} = \frac{m_{\text{known}}}{m_{\text{calculated}}} \times 100$$

Equation 4: Percentage recovery

Where: m_{known} is the mass of the analyte contained in the sample

$m_{\text{calculated}}$ the amount of analyte calculated using the calibration curve.

The accuracy of the method was determined by the percentage difference of the mean measurements.

5.7.5. Intermediate Precision

Precision is the measure of the degree of repeatability of an analytical method under normal operation.¹⁶⁰ Three concentrations of the API within the calibration range were used, and the precision was determined by inter-day precision over a period of three consecutive days. The average values, standard deviation and % relative standard deviation (RSD) were compared to determine the inter-day precision.

5.7.6. Limit of detection and limit of quantification

The limit of detection (LOD) was used to determine the lowest amount of analyte that could be detected accurately using the method parameters. The limit of quantification (LOQ) was used to determine the lowest amount of analyte that could be quantified accurately using the method parameters. LOD and LOQ were determined using the following equations:

$$3.3 \times \frac{\sigma}{S}$$

Equation 5: Limit of detection

$$10 \times \frac{\sigma}{S}$$

Equation 6: Limit of quantification

Where: σ = Standard deviation of the response

and S = the slope of the calibration curve

BMV and HCA were quantified using the linearity curves constructed for each respective analyte.

5.7.7. Robustness

The robustness of the method was determined by deliberately changing the wavelength of detection of the analyte. The Azura Knauer HPLC system was fitted with a PDA detector which scanned a series of wavelengths ranging from 190 - 700 nm. BMV and HCA were analysed at both 254 and 240 nm and the mean area % and SD of the peaks obtained for each API was determined.

5.8. Percentage yield

The percentage yield is expressed as the % of nanoparticles recovered after formulation. To determine the percentage yield, the mass of the empty Eppendorf® centrifuge tube was weighed: before introduction of the prepared ethosomes, and after drying. The empty vials and the vials containing the dried samples were determined using an electronic balance. The mass of the ethosomes was determined by mass difference using the following formula:

$$\frac{\text{Mass of freeze dried ethosomes} - \text{Mass of empty centrifuge vial}}{\text{Mass of API} + \text{mass of PC} + \text{excipients in formulation}}$$

Equation 7: Percentage yield

5.9. Determination of drug loading

Drug loading (DL) is an expression of the % of API in the formulation relative to the amount of excipients. To determine the DL, the mass of API within the ethosomes was determined. To achieve this, the prepared freeze dried ethosomes were lysed using 1.5 ml of ethanol. The sample was sonicated for 15 min to disrupt the phospholipid bilayer of the ethosomes. The sample was centrifuged for 15 min at 15 000 rpm and filtered using 0.45 µm micro-filters into HPLC vials. HPLC was used to determine the area % of the analyte which was translated into a mass using the correlation curve (determined using linearity). The DL was determined using the following equation:

$$\frac{\text{mass of API used in formulation}}{\text{mass of PC} + \text{excipients used in formulation}} \times 100$$

Equation 8: Drug loading

5.10. Determination of encapsulation efficiency

The encapsulation efficiency (EE) is the expression of the % efficacy of the encapsulation process. This percentage indicates how efficient the method is at encapsulating the API used in the formulation. To determine the EE, the prepared ethosomes in suspension, after comminution, were centrifuged at 4°C for 2 cycles of 1 hour and 1 ml of supernatant was removed for HPLC analysis. After 2 cycles of washing followed by centrifugal drying, the dried ethosomes were lysed using 1.5 ml of ethanol. The sample was sonicated for 15 min to disrupt the phospholipid bilayer of the ethosomes. The sonicated sample was centrifuged for

15 min at 15 000 rpm and filtered using the 0.45 μm micro-filters into HPLC vials. The sample was analysed using HPLC to determine the concentration using the standard linearity curves. The EE was determined using the following equation:

$$\frac{\text{mass of API determined using direct analysis}}{\text{mass of API in lysed ethosomes} + \text{mass of API in supernatant}} \times 100$$

Equation 9: Encapsulation efficiency

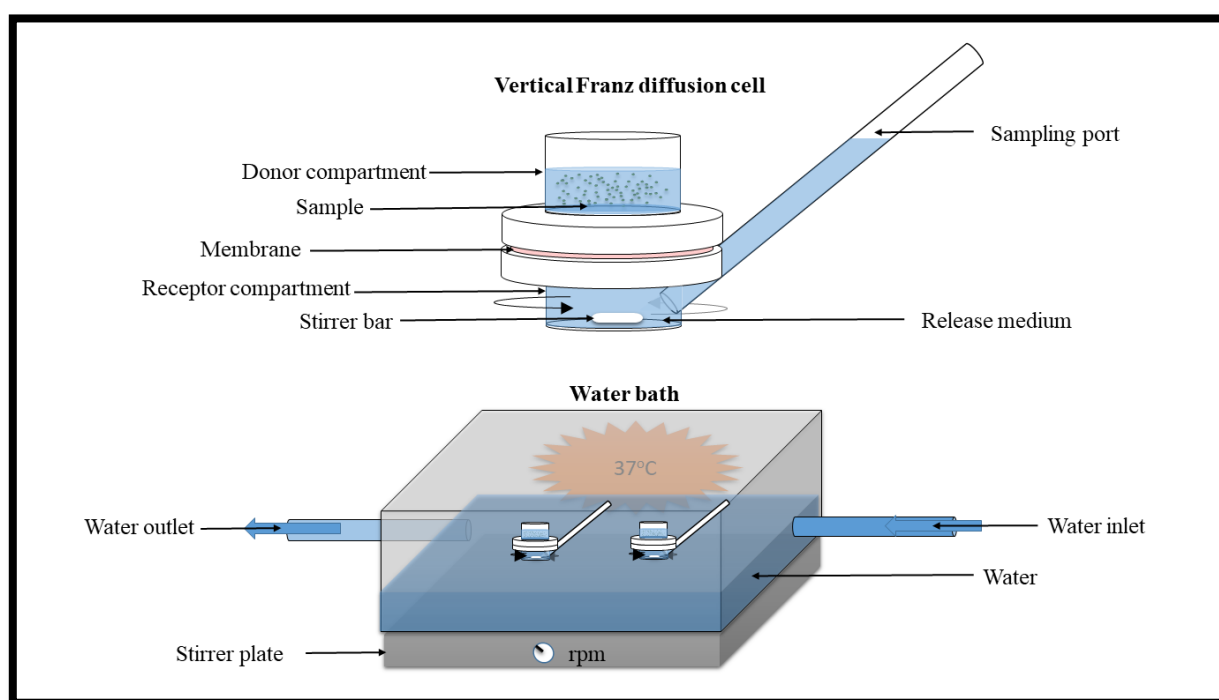


Figure 5.10-1: A summary of the experimental setup for drug release determination from corticosteroid loaded ethosomes using Franz diffusion cells.

5.11. *In-vitro* drug release of ethosomes

Ethosomes loaded with HCA and BMV were subjected to *in vitro* drug release testing to determine the percentage of encapsulated drug that was released over time. Resuspended ethosomes were fractioned into 1.5 ml sets for analysis. For the drug release assay, ethosomes from the same batch used for determining EE and DL were used. 0.2 ml of the 1.5 ml fractioned ethosomal suspension, were placed into the donor compartment of a 2 ml vertical Franz diffusion cell. Phosphate buffered solution (PBS) at a pH of 7.4 served as the receptor medium and was filled to a volume of 1.8 ml in the receptor compartment. Although the skin has a pH of 5.5-6, the drug release of topical drug delivery systems have been investigated at this pH. This is because of the pH of blood, which is at a pH of 7.4. Assuming that

transdermal permeation was achieved, the API would be subjected to this pH environment in the vasculature of the dermis. The Franz diffusion cell containing a 0.45 μm polymer membrane pre-soaked in receptor medium was placed in a multi-stirrer water bath with temperature set to 37 ± 0.5 °C. The stirring rate was set to 200 rpm and the experiment was conducted for 36 hours. At predetermined time intervals (1, 2, 3, 4, 6 hours) 1.8 ml was retrieved from the receptor compartment using a 5 ml graduated syringe and was transferred into an 2 ml Eppendorf® tube (**Figure 5.11-1**). The receptor compartment was replenished with 1.8 ml fresh receptor medium. The Eppendorf® tube was centrifuged at room temperature for 15 min at 14 000 rpm. The supernatant was filtered through a 0.22 μm syringe filter and transferred into an HPLC vial for HPLC analysis. The API was quantified using the validated linearity curves constructed for BMV and HCA.

5.11.1. Mechanism of release

The mechanism of release is important in understanding how the API will be released *in vivo*. Various models have mathematical models have been developed to depict drug release, each with their own specific parameters influencing drug release and limitations. To determine the most probable mechanism of drug release, a cumulative % release curve was plotted after quantifying the API using HPLC. The curve for each respective formulation was plotted against a mathematical model and the highest R^2 value was used to determine the best fit model. DDSolver 1.0 software was used for the linear regression analysis. The best fit model was then analysed using its own set of criteria.

5.12. Scanning electron microscopy

Particle size analysis, vesicle morphology and encapsulation of the APIs in loaded ethosomes were verified using scanning electron microscopy (SEM). Dried ethosomes were placed on carbon adhesive tape applied on an aluminium stub, and thereafter dried completely under a fume hood. The dried sample was coated with gold palladium for 30 sec using an Emitech K550X (England) sputter coater and viewed with the Auriga HR-SEM F50 (Zeiss, South Africa) with a voltage of 5 KV.

5.13. Fourier-transform infrared spectroscopy



Encapsulation of the APIs within loaded ethosomes was verified and possible molecular interactions were identified using FTIR. FTIR spectra were obtained using a Perkin Elmer Spectrum 400 FTIR/NIR (Perkin Elmer, USA) fitted with a diamond attenuated total reflectance (ATR) crystal. The instrument was programmed and spectrograms were collected using Spectrum® software version 6.3.5 for sample analysis. Samples were scanned in the spectral region of 4000 to 650 cm^{-1} . A small amount of dried sample (~1 mg) was placed on the crystal and pressure was applied to 60 %. The sample was scanned at 2 $\text{cm}^{-1}/\text{sec}$ 4 times at a resolution of 4 $\text{cm}^{-1}/\text{sec}$. The average of three scans was plotted as a spectrogram showing percentage transmittance recorded against frequency. The spectrograms were interpreted to determine functional groups associated with characteristic bands. Changes in the characteristic bands of the encapsulated API such as disappearance, broadening, variations in peak intensity or shifts in wave number supported compound identification and nanoparticle formation.

5.14. Hot stage microscopy



Dried CM unloaded and GC loaded ethosomes were analysed using hot stage microscopy (HSM) to observe any changes in the melting profile compared to the pure standards and to identify encapsulation of APIs. HSM cover slips were prepared by placing a drop of silicone oil on a cover slip. A dissecting needle was used to transfer a small amount of sample into the silicone oil on the cover slip which was then covered with a second cover slip. The prepared cover slip was transferred to the hot stage (Linkam® THMS600 temperature control stage) which was connected to a link pad (T95 Linkpad® System Controller). The link pad was used to control the heating rate (10 $^{\circ}\text{C}/\text{min}$) and temperature limit (250 $^{\circ}\text{C}$) for HSM analysis. The hot stage was connected to an Olympus SZX7 stereoscopic microscope connected to an Olympus UC30 video camera, where samples under thermal stress could be viewed by the operator. The sample was focused accordingly. Stream Essential software®

was used to capture and save the images which were taken at 10 min intervals, using the time stack function offered by the software, for the duration of the run. To ensure the accuracy of the analysis, all the measurements were run in triplicate ($n=3$).

5.15. Thermogravimetric analysis



Thermogravimetric analysis (TGA) was used to identify the changes in thermal stability. This analytical tool was used in conjunction with the qualitative data generated from HSM to quantify the thermal events observed in terms of the effect of the % mass of the sample. As with HSM, the pure components were first analysed and were used as a reference for the unloaded ethosome and GC-loaded ethosome comparison. Samples from the same batch used in HSM preparation were analysed using a Perkin Elmer thermogravimetric analyser *TGA 4000* (Waltham USA), with the flow rate of nitrogen gas at 20 ml/min. To prepare the sample for analysis, an empty porcelain crucible was tarred to zero the balance. Once stable, sample was transferred to the crucible and the weight of the sample was recorded. Samples were analysed over a temperature range from 30 – 600 °C at an increasing temperature rate of 10 °C/min. Data were collected and analysed using Pyris™ software. The instrument was calibrated using three different references: alumel (m.p = 154.2 °C), Perk alloy (m.p = 596 °C) and iron (m.p = 780 °C) at 1 and 2 °C/min.

5.16. Differential scanning calorimetry



Encapsulation of the APIs in the ethosomes was verified using differential scanning calorimetry (DSC). To prepare a sample for analysis, an aluminium DSC pan and lid was placed on a zeroed analytical balance and it was tarred. ~1-1.5 mg of sample was transferred to the DSC pan and the exact mass was recorded. The loaded pan was hermetically sealed using a punch and a small hole was punched in the lid using a needle. To conduct the experiment, a Perkin Elmer DSC-7 analyser (Waltham, USA), utilizing the Pyris™ software program, was used. The sample was heated from 40 °C to 250 °C at 10 °C /min. The instrument was calibrated

by measuring the onset temperatures of the melting of zinc (m.p = 419.5 °C) and indium (m.p = 156.6 °C) while the heat flow was calibrated from the enthalpy of melting of indium (28.62 J/g).



UNIVERSITY *of the*
WESTERN CAPE



School of
PHARMACY

6. Introduction

This chapter compares the physical and chemical results of the ethosomes prepared using the hot method (HM) and cold method (CM) with different phosphatidylcholine (PC) concentrations. Prepared ethosomes were exposed to sonication and extrusion particle size reduction methods. The HM and CM ethosomes were analysed using thermal and structural nano characterisation techniques to determine the effect of PC concentrations on the size, polydispersity index, zeta-potential and morphology of unloaded ethosomes.

6.1. Analysis of pure components

Betamethasone valerate (BMV), hydrocortisone acetate (HCA), phosphatidylcholine (PC) and cholesterol (Chol) were identified using British Pharmacopoeia (BP) identification assays and were compared with reference standards in their respective monographs.⁷³ The assays used to evaluate the compounds were Fourier transform infrared spectroscopy (FTIR) where the fingerprint region was compared to the fingerprint region found in literature, and differential scanning calorimetry (DSC), where the melting point and other thermal events obtained were correlated to that found in literature.⁷³

6.1.1. FTIR analysis of pure compounds

FTIR analysis of BMV

The FTIR spectra for comparison is shown in **Figure 6.1.1-1**, with the BMV experimental spectrum in blue and the BMV reference standard¹⁶¹ in black. The table correlating the identified functional groups to their respective wave numbers is provided (**Table 6.1.1-1**), as well as the theoretical chemical structure annotated with the functional groups observed on the FTIR spectrum **Figure 6.1.1-2**.

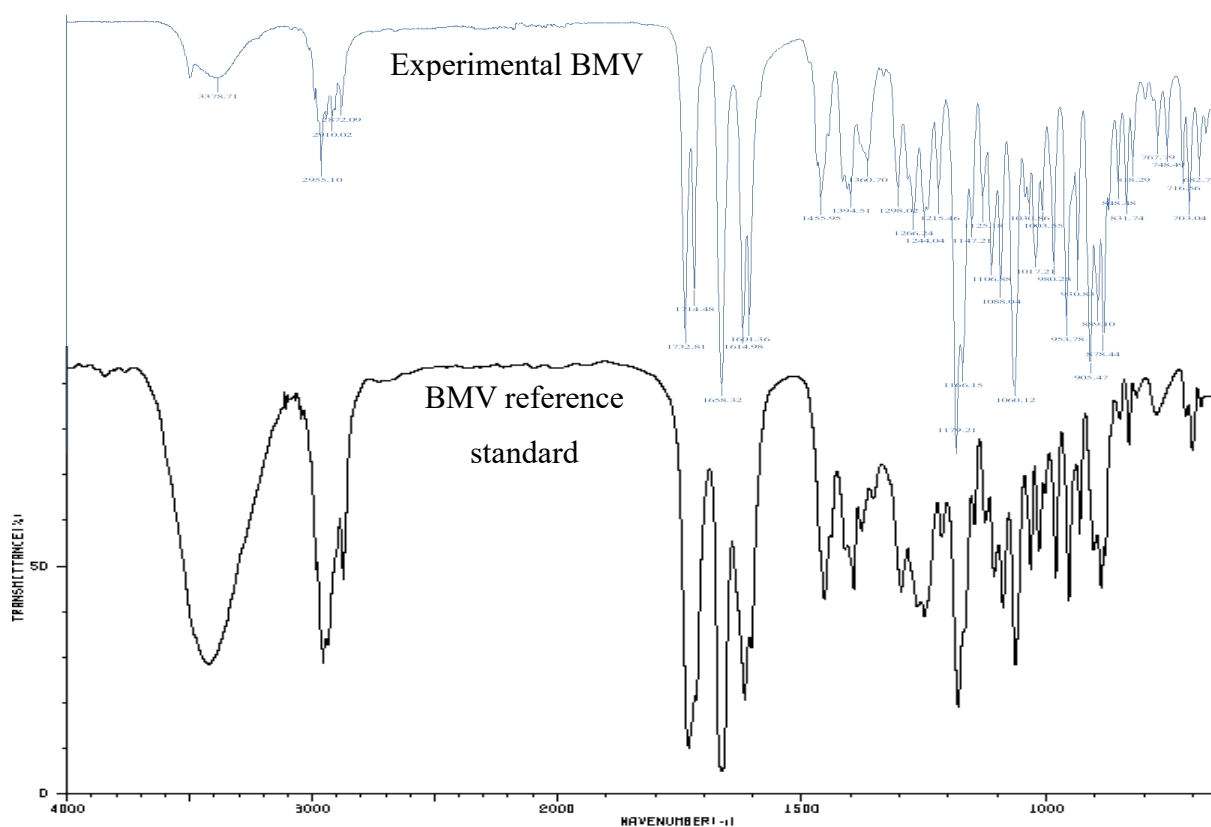


Figure 6.1.1-1: Fourier transform infrared spectroscopy (FTIR) spectra of pure betamethasone valerate (BMV) compared to its reference spectrum.

The fingerprint regions were compared and associated peaks with functional groups were identified and characterised using an interpretation guide.¹⁶² The peaks of interest in the fingerprint region, listed in **Table 6.1.1-1**, showed the characteristic bands of the C-H bends at 1394.51 cm^{-1} . Sp^2 C-O stretches were observed at 1298.02 cm^{-1} , 1266.24 cm^{-1} , 1244.04 cm^{-1} , 1215.46 cm^{-1} , 1179.21 cm^{-1} and 1166.15 cm^{-1} . The frequency of the peaks corresponding to the C-O stretches may be attributed to intermolecular interactions which altered the electromagnetic environment of the C-O bonds. A strong Sp^3 C-O stretch was

observed at 1060.12 cm^{-1} , which may be attributed to the C-O bond at C 17 of BMV at the location of the esterified valeric acid ion.

Table 6.1.1-1: The experimental and theoretical Fourier transform infrared spectroscopy (FTIR) spectrum frequencies analysed for betamethasone valerate (BMV) fingerprint region ($<1400\text{ cm}^{-1}$)

Sample	Experimental frequency (cm^{-1})	Theoretical Frequency ¹⁶³ (cm^{-1})	Functional group	Intensity	Shape
BMV	1394.51	1395.00 – 1365.00	Alkane C-H bend	Medium	
	1298.02			Medium	
	1266.24			Medium	
	1244.04			Medium	Narrow
	1215.46	1350.00 – 1150.00	sp ² C-O stretch	Medium	
	1179.21			Strong	
	1166.15			Strong	
	1060.12	1100.00 – 1000.00	sp ³ C-O stretch	Strong	

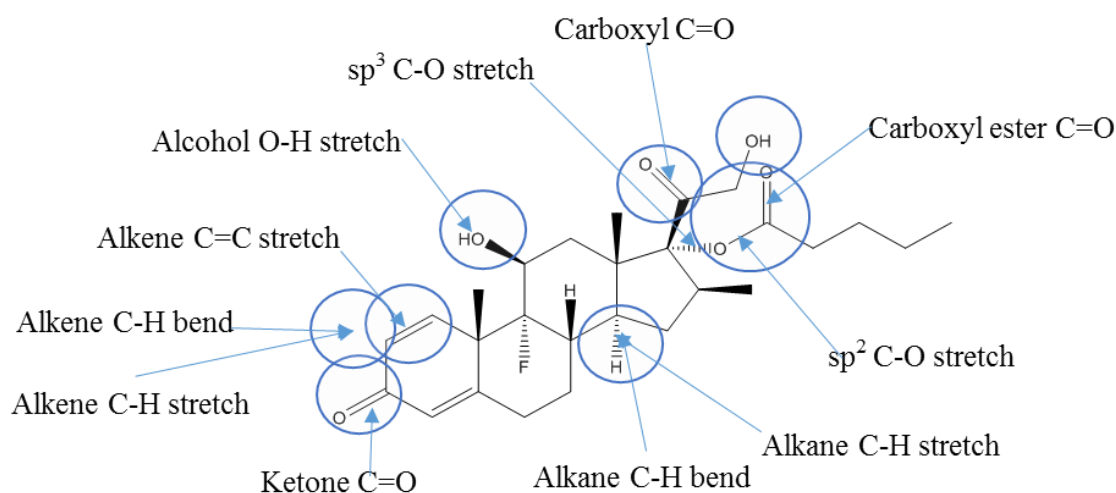


Figure 6.1.1-2: The chemical structure of betamethasone valerate annotated with functional groups observed in the Fourier transform infrared spectroscopy (FTIR) spectrum.

FTIR analysis of HCA

The FTIR spectra for HCA is shown in **Figure 6.1.1-3**, with the experimental spectrum in red and the HCA reference standard¹⁶¹ in black. The identified functional group relative to its respective wave number is seen in **Table 6.1.1-2**, with an annotated chemical structure of HCA observed with **Figure 6.1.1-4**.

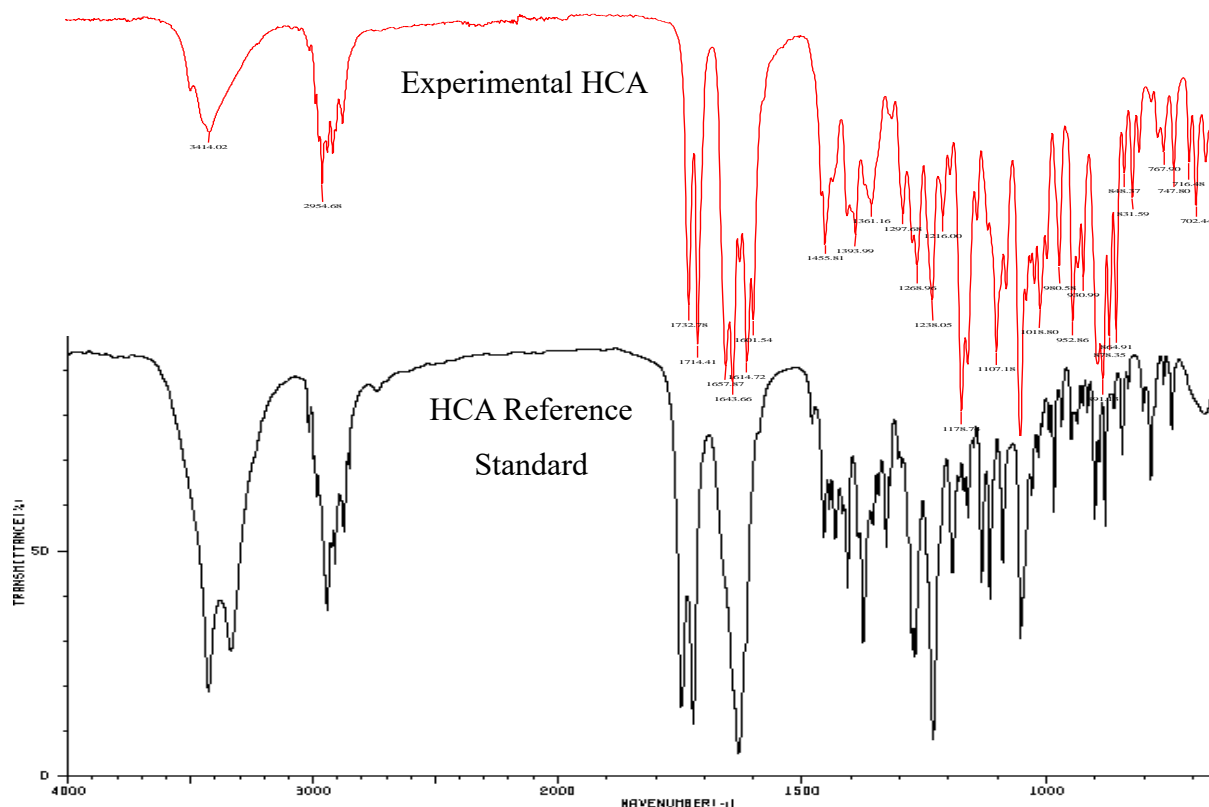


Figure 6.1.1-3: Fourier transform infrared spectroscopy (FTIR) spectra of pure hydrocortisone acetate compared to its reference spectrum.

When analysing the FTIR spectrum of HCA, the peaks of interest in the fingerprint region showed characteristic bands of the C-H bends at 1393.99 and 1361.16 cm^{-1} . Sp^2 C-O stretches were observed at 1297.68 cm^{-1} , 1268.96 cm^{-1} , 1238.05 cm^{-1} , 1216 cm^{-1} , 1178.74 cm^{-1} and 1107.18 cm^{-1} . Similar to the bands observed in BMV, the frequency of the peaks corresponding to the C-O stretches may be attributed to intermolecular and intramolecular interactions which altered the electromagnetic environment of the C-O bonds. This feature was expected as they are similar in structure. A strong narrow Sp^3 C-O stretch was observed at 1087.32 cm^{-1} , which may be attributed to the C-O bond at C 21, of HCA at the location of the esterified acetic acid ion.

Table 6.1.1-2: The experimental and theoretical Fourier transform infrared spectroscopy (FTIR) spectrum frequencies analysed for hydrocortisone acetate (HCA) fingerprint region ($<1400\text{ cm}^{-1}$)

Sample	Experimental frequency (cm^{-1})	Theoretical Frequency ¹⁶³ (cm^{-1})	Functional group	Intensity	Shape
HCA	1393.99	1395.00 – 1365.00.	Alkane C-H bend	Medium	
	1361.16			Medium	
	1297.68			Medium	
	1268.96		Medium		
	1238.05	1350.00 – 1150.00	sp ² C-O stretch	Medium	Narrow
	1216			Medium	
	1178.74		Strong		
	1107.18		Strong		
	1087.32	1100.00 – 1000.00	sp ³ C-O stretch	Strong	

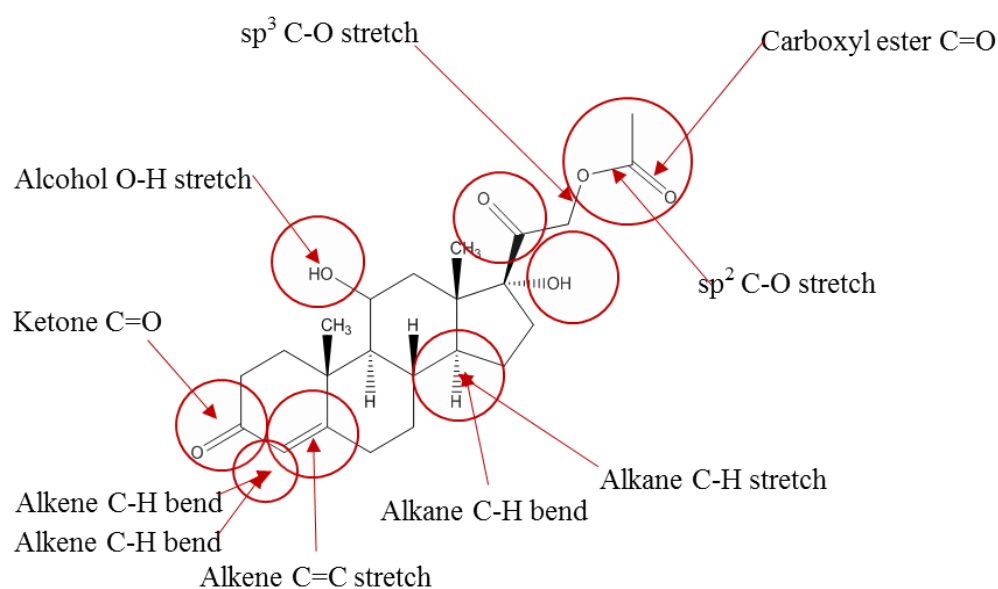


Figure 6.1.1-4: The chemical structure of hydrocortisone acetate (HCA) annotated with functional groups observed on the Fourier transform infrared spectroscopy (FTIR) spectrum.

FTIR analysis of PC

The FTIR spectra for PC is shown in **Figure 6.1.1-5**, with the experimental spectrum in green and the HCA reference standard¹⁶¹ in black. **Table 6.1.1-3** correlates the identified functional groups to their respective wave numbers and the annotated chemical structure is given in **Figure 6.1.1-6**.

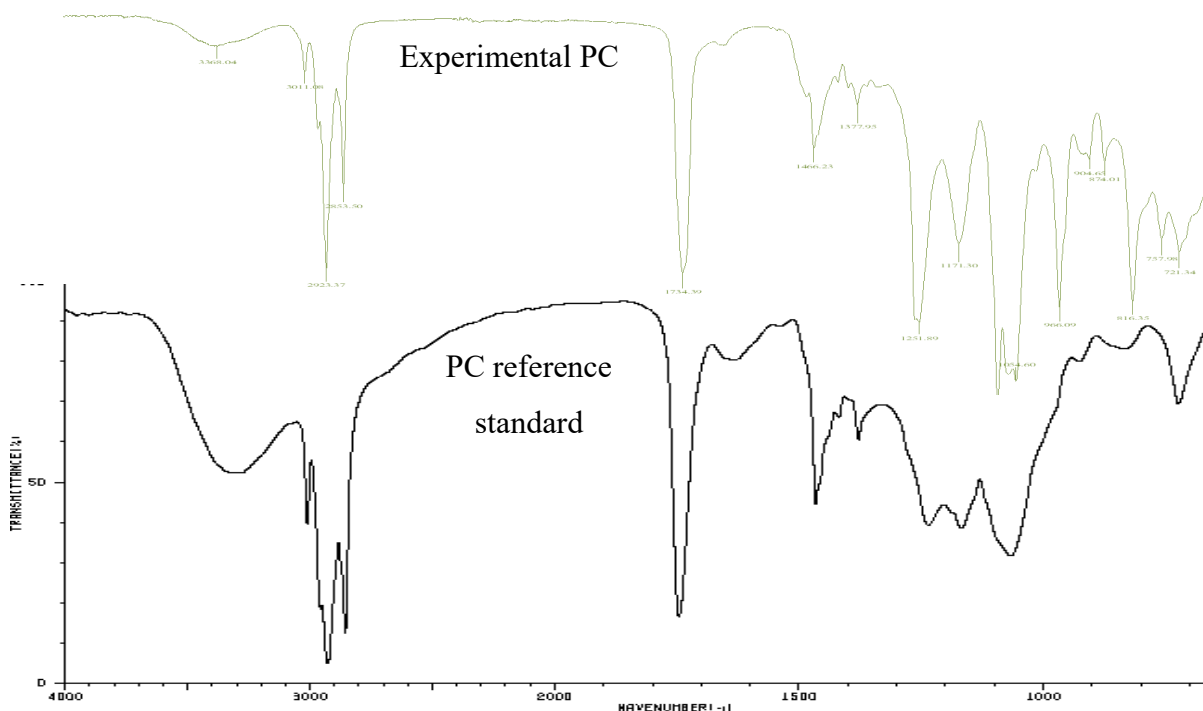


Figure 6.1.1-5: Fourier transform infrared spectroscopy (FTIR) spectra of pure phosphatidylcholine compared to its reference spectrum.

The FTIR spectrum of PC displayed significant peaks of interest in the fingerprint region listed in **Table 6.1.1-3**. The characteristic alkane C-H bends were identified at 1377.95 cm^{-1} . Sp^2 C-O stretches were observed at 1251.89 cm^{-1} and 1171.30 cm^{-1} . Strong narrow stretches were observed at 1090.53 cm^{-1} and 1054.60 cm^{-1} , which may be attributed to the P-O bond of the phosphate group or the Sp^3 C-O bond at the ester. The polar regions of the aforementioned functional groups, displayed in **Figure 6.1.1-6** may be sites of weak molecular interactions within formulated ethosomes.

Table 6.1.1-3: The experimental and theoretical Fourier transform infrared spectroscopy (FTIR) spectrum frequencies analysed for phosphatidylcholine (PC) fingerprint region ($<1400\text{ cm}^{-1}$)

Sample	Experimental frequency (cm^{-1})	Theoretical Frequency ¹⁶³ (cm^{-1})	Functional group	Intensity	Shape
PC	1377.95	1395.00 – 1365.00	Alkane C-H bend	Weak	Sharp
	1251.89	1350.00 – 1150.00	Csp ² -O stretch	Medium	
	1171.30			Medium	
	1090.53	1100.00 – 1000.00	Csp ³ -O stretch	Strong	
	1054.60	1100.00 - 1000.00	Csp ³ -O stretch	Strong	

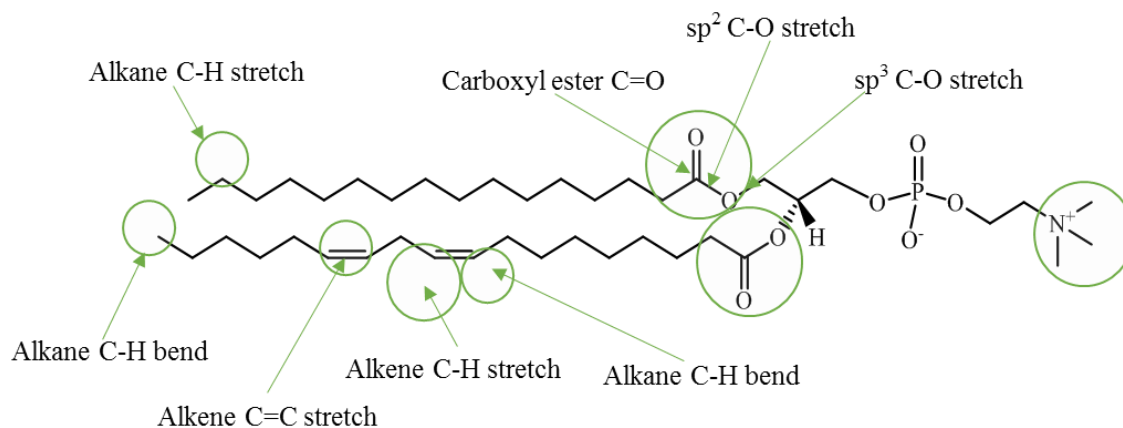


Figure 6.1.1-6: The chemical structure of phosphatidylcholine (PC) annotated with functional groups observed on the Fourier transform infrared spectroscopy (FTIR) spectrum

FTIR analysis of Cholesterol

The FTIR spectra Chol is shown in **Figure 6.1.1-7**. The experimental spectrum in orange and the HCA reference standard¹⁶¹ in black were compared for purity. The table correlating the identified functional groups to their respective wave numbers is provided in **Table 6.1.1-4**, as well as the chemical structure annotated with the functional groups observed on the FTIR spectrum **Figure 6.1.1-8**.

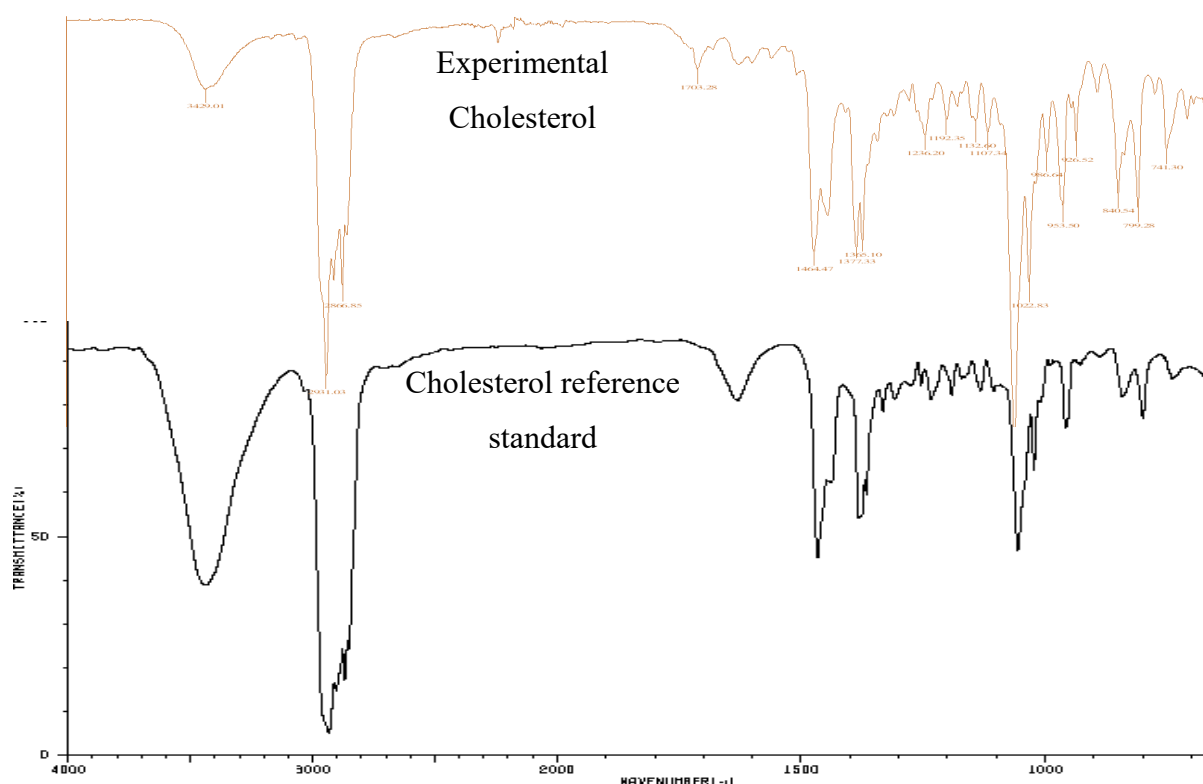


Figure 6.1.1-7: Fourier transform infrared spectroscopy (FTIR) spectra of pure cholesterol compared to its reference spectrum.

The FTIR spectrum of cholesterol displayed a characteristic alkane C-H bend identified at 1377.33 cm^{-1} and an Sp^2 C-O stretch was observed at 1236.20 cm^{-1} . Although cholesterol contains a similar carbon scaffold to the corticosteroids, it was noted that the fingerprint region of the spectrum displayed less FTIR activity. This may be due to the absence of esters and the presence of fewer oxygen containing functional groups oxygen, resulting in fewer intermolecular dipole interactions within the cholesterol molecules, as well as the abundant C-C interactions which are not diagnostically relevant in FTIR spectra. A strong narrow C-O stretch, which may be attributed to the primary alcohol, was observed at 1050.30 cm^{-1} .

Table 6.1.1-4: The experimental and theoretical Fourier transform infrared spectroscopy (FTIR) spectrum frequencies analysed for cholesterol's fingerprint region ($< 1400 \text{ cm}^{-1}$)

Sample	Experimental frequency (cm^{-1})	Theoretical Frequency ¹⁶³ (cm^{-1})	Functional group	Intensity	Shape
	1377.33	1395 - 1365	Alkane C-H bend	medium	
Cholesterol	1236.20	1350 - 1150	sp ² C-O stretch	Strong	Narrow
	1050.30	1100 - 1000	sp ³ C-O stretch	Strong	

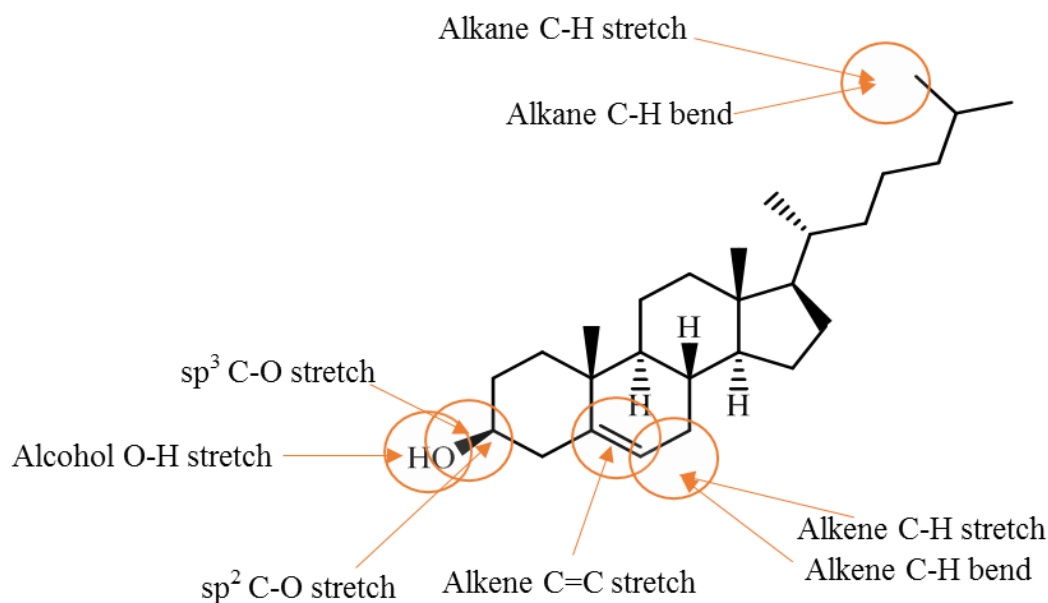


Figure 6.1.1-8: The chemical structure of cholesterol annotated with functional groups observed on the Fourier transform infrared spectroscopy (FTIR) spectrum

6.1.2. DSC Analysis of pure components

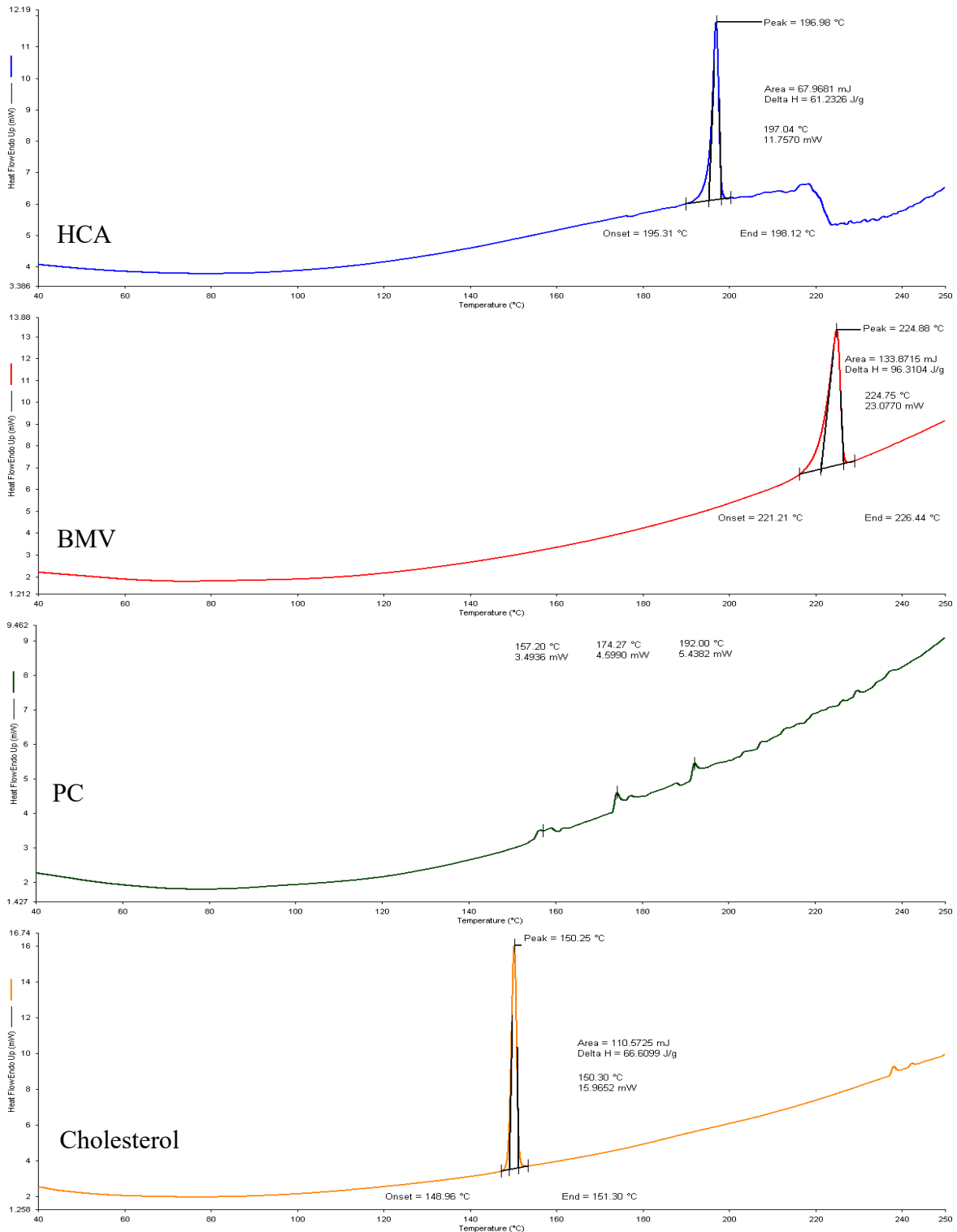


Figure 6.1.1-1: Differential scanning calorimetry (DSC) thermograms of hydrocortisone acetate (HCA), betamethasone valerate (BMV), phosphatidylcholine (PC) and cholesterol.

According to the respective BP monographs⁷³, the theoretical melting points of BMV, HCA and cholesterol is about 196 °C, 222 - 225 °C and 148 °C respectively.⁷³ PC is an amorphous semi-solid which does not have a theoretical melting point. The DSC thermograms, (**Figure 6.1.2-1**) show that there are no impurities at temperatures lower than the theoretical melting points. BMV, HCA and Chol displayed endothermic peaks at and 195.31 - 198.12 °C, 221.21 – 226.44 °C and 148.96 - 151.30 °C respectively. The experimental endothermic peaks corresponded to the theoretical melting points identified in literature.

Using the fingerprint region of the FTIR spectra, the pure components showed a fingerprint match with differences in intensity. The difference in intensity was attributed to the difference in the techniques used as the references in literature were performed using a KBr plate, whereas the pure components were analysed using a FTIR coupled with an ATR crystal. The pressure in the force gauges of the respective techniques may have differed. The reference also did not quantify the amount of sample analysed. DSC, a complementary technique, was used to identify the compounds based on the characteristic melting point of the sample. Compounds were accepted on the condition the experimental melting point was within ± 1 °C. The theoretical values were within the onset-end range of temperatures as determined using Pyris™ Software. Based on these results, it was concluded that the samples were validated from the suppliers.

6.2. The effect of PC concentration on ethosomes

Ethosomes were prepared using the HM and CM described in *Chapters 5.2.1* and *5.2.2*. Unloaded ethosomes synthesised using HM and CM were analysed to determine the effect of the PC concentration on ethosomal hydrodynamic diameter (HdD), polydispersity index (PDI) and zeta-potential (ζ_p) (**Table 6.2-1**). To test these parameters, prepared samples were analysed using dynamic light scattering (DLS) as described in *Chapters 5.6.1* and *5.6.2*. Ideally, the particle size for transdermal permeation is ~200 nm and a PDI < 0.5 indicates an acceptable particle size distribution. A $\zeta_p = \pm 30$ mV is an indication of good stability of an ethosomal colloidal suspension.

Table 6.2-1: The hydrodynamic diameter (HdD), polydispersity index (PdI) and zeta-potential (ζ_p) of unloaded ethosomes prepared using the HM and CM with varying phosphatidylcholine concentrations ($n=3$)

Formulation	PC (mg/ml)	HdD (d.nm)	PdI	ζ_p (mV)
HM ₁₀ C	10	623.5±22.8	0.713	+1.09
CM ₁₀ C	10	351.5±22.6	0.147	-1.99
HM ₂₅ C	25	645.4±18.5	0.695	+1.09
CM ₂₅ C	25	352.5±30.0	0.227	-1.75
HM ₅₀ C	50	777.4±13.1	0.866	+1.00
CM ₅₀ C	50	355.0±26.0	0.137	-1.26

HM = Hot Method, CM = Cold Method, _c= Crude, Crude = no comminution

The effect of phosphatidylcholine concentrations on the particle size of unloaded ethosomes

Crude ethosomes had a unimodal size distribution (**Figure 6.2-1**). The unloaded ethosomes showed an increase in HdD with an increase in PC concentration. As confirmed by similar studies, the formation of these multilamellar vesicles in the crude preparation have shown to increase with an increase in PC concentration.^{23,101} The mean HdD of the ethosomes (**Table 6.2-1**) was 623.5 d.nm (HM₁₀) and 351.5 d.nm (CM₁₀), 645.4 d.nm (HM₂₅) and 352.5 d.nm (CM₂₅), 777.4 d.nm (HM₅₀) and 355 d.nm (CM₅₀) for formulations containing 10, 25 and 50

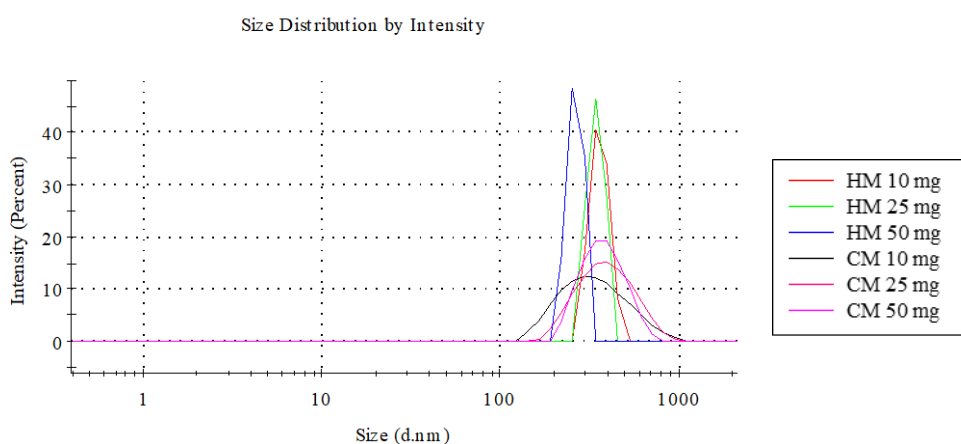


Figure 6.2-1: The size distribution of ethosomes synthesised using the hot and cold methods at PC concentrations of 10 mg/ml, 25 mg/ml and 50 mg/ml.

mg PC, respectively. The results of the CM ethosomes indicate that PC concentration had no significant effect on the particle size.

This may have been due to the solubility of the PC in ethanol. Upon addition of the aqueous phase, the concentration of PC in the organic phase may have been too dilute to influence the agglomeration to form ethosomes. Perhaps increasing the concentration could have produced ethosomes of a similar size range. Another contributing factor to the CM size similarity may have been the controlled temperature relative to the HM. CM ethosomes remained at room temperature throughout the process, from synthesis and during analysis. This may have assisted in maintaining the stability of the system so that ethosomes remained in suspension.

Overall, the size difference of the ethosomes, when comparing HM is significant. In the HM, the formation of the ethosomes is dependent on an increased temperature (40 °C) to suspend the phospholipid in water. The free energy of the colloidal particles in suspension may allow for the ethosomes to be dispersed at a smaller size when maintained at 40 °C. When returning to room temperature (25 °C), and then analysed using DLS, the ethosomes may have agglomerated and increased in size. The implications of the temperature fluctuation complicated the synthetic process and, when analysed, produced ethosomes of a larger mean HdD compared to their respective CM counterparts. When analysed using DLS and 40 °C, the ethosomes have a larger (almost double) mean size. From the ethosomes generated using HM and CM, the CM produced smaller vesicles.

Regarding the effect of PC concentration on the ethosomes prepared, it was noted that the particle size was variable for ethosomes prepared via the HM at the tested PC concentration ranges.

The effect of phosphatidylcholine concentrations on the polydispersity index of unloaded ethosomes

The unloaded ethosomes showed an increase in PdI with an increase in concentration of PC. The size distribution was greater for the ethosomes synthesised using HM than using the CM. Generally, samples with a PdI < 0.1 are considered monodisperse, whereas those with a PDI > 0.1 are considered polydispersed.¹⁰³ For nanoparticles to be accepted according to their size distribution, the PdI may have an acceptable polydispersity of < 0.5.¹³⁷ The unloaded ethosomes had a PdI of 0.713 (HM₁₀) and 0.147 (CM₁₀), 0.695 (HM₂₅) and 0.227 (CM₂₅),

0.866 (HM₅₀), and 0.137 (CM₅₀) for formulations containing 10, 25 and 50 mg PC respectively (Table 6.2-1).

Based on these results, it was evident that the concentration of the PC had no appreciable effect on the PDI as the size distribution remained within the 0.1 - 0.5 limit for those prepared using CM. However, HM ethosomes were polydisperse and did not meet the acceptance criteria.

The effect of PC concentrations on the zeta potential of unloaded ethosomes

Ethosomes synthesised using HM and CM were analysed directly after synthesis. The unloaded ethosomes had a zeta-potential (ζ_p) of +1.09 mV (HM) and -1.99 mV (CM), +1.09 mV (HM) and -1.75 mV (CM), +1.00 mV (HM), and -1.26 mV (CM) for formulations containing 10, 25 and 50 mg PC, respectively. The ζ_p of the unloaded ethosomes was positively and negatively charged for HM and CM ethosomes respectively. Regardless of the positive or negative charge, the stability of the ethosomes corresponding to their ζ_p ranged 0 to ± 5 mV (Figure 6.2-2) suggested swift flocculation. Although research has shown that increasing the ethanolic concentration could improve the ζ_p , the ethanol was a fixed variable and had therefore not changed.⁹² The concentration of the PC had no appreciable effect on the ζ_p . All of the experimental concentrations indicated swift flocculation ($< \pm 5$ mV) regardless of the ethosome preparation method used.

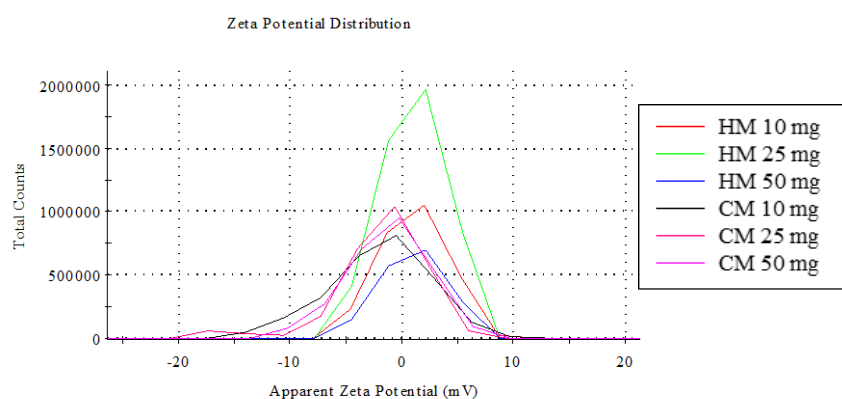


Figure 6.2-2: The zeta-potential of crude ethosomes synthesised using the hot and cold methods at phosphatidylcholine (PC) concentrations of 10 mg/ml, 25 mg/ml and 50 mg/ml.

6.3. The effect of sonication and extrusion on unloaded ethosomes

To test the effect of sonication and extrusion on the HdD, PdI and ζ_p of ethosomes, 50 mg/ml PC was taken as the standard concentration. Although it showed an increase in particle size for the HM ethosomes, PC concentration did not affect the ethosomal properties analysed at this stage under the evaluated criteria. Unloaded ethosomes were prepared via the HM and CM methods described in *Chapter 5 (5.2.1 and 5.2.2)* and 10 ml samples were subjected to either sonication or extrusion as described in *Chapter 5 (5.3.1 and 5.3.2)*. Unloaded ethosomes were analysed to determine the effect of comminution on ethosomal HdD, PdI and ζ_p (**Table 15**). Prepared samples were analysed using DLS as described in *Chapter 5 (5.5.1 and 5.5.2)*.

Table 6.3-1: The hydrodynamic diameter (HdD), polydispersity index (PdI) and zeta-potential (ζ_p) of crude, sonicated and extruded ethosomes prepared using the hot and cold methods ($n=3$)

FORMULATION	COMMINUTION METHOD	HdD (d.nm)	PdI	ζ_p (mV)
HM _C	N/A	852.40±39.38	1.00	+1.29
CM _C	N/A	379.60±92.45	0.26	-0.06
HM	Sonication	769.30±55.90	1.00	-10.60
CM	Sonication	283.10±111.50	0.16	-1.99
HM	Extrusion	156.60±31.97	0.13	-3.89
CM	Extrusion	155.90±32.98	0.08	-12.80

HM: Hot Method, CM: Cold Method, _C: Crude

Sonicated and extruded ethosomes had a unimodal size distribution (**Figure 6.3-1**).

The effect of sonication on the hydrodynamic diameter of unloaded ethosomes

The HM and CM crude ethosomes had mean sizes of 852.40 d.nm and 379.60 d.nm, respectively. This was consistent with the standards produced in the previous experiment. To reduce the particle size, sonication was conducted at 40 °C for the HM samples, which resulted in the application of an operational temperature change (from room temperature at 25°C) to the sample. After a sonication cycle of 5 min, the ethosomes reduced in size by approximately 10 % to 769.30 d.nm for HM ethosomes and by approximately 25 % to 283.10 d.nm for CM ethosomes.¹⁶⁴

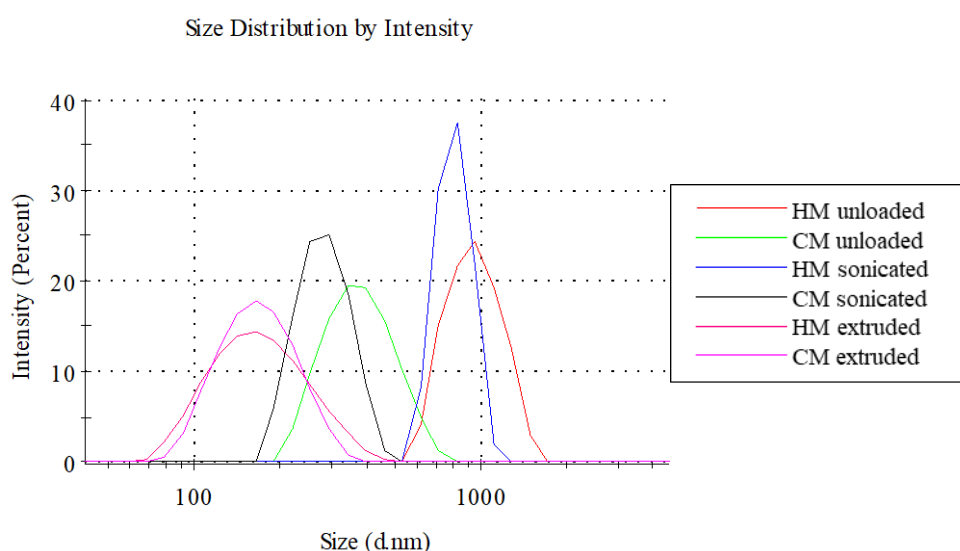


Figure 6.3-1: The size distribution of unloaded, sonicated and extruded crude ethosomes synthesised using the hot and cold methods at a PC concentration of 50 mg/ml.

Sonication, as a comminution technique, served ineffective at reducing the particle size to acceptable transdermal permeation ranges (**Table 6.3-1**). This may be attributed to the parameters of the instrument which affected the particle size such as the duration, frequency, temperature and number of cycles. These variables are not standardised and vary according to the ethosomal formulation and the sonicator used. In this experiment, the parameters of the sonicator bath may have been optimised to achieve favourable particle size reduction. Literature has supported the use of sonicators to achieve nanoparticles of a desirable size range.^{65,106,165} However, for this study, these size ranges were not met. Sonication was not an effective tool for reducing particle size of the unloaded ethosomes to the desired HdD.

The effect of extrusion on the hydrodynamic diameter of unloaded ethosomes

HM ethosomes were extruded on a hot plate with temperatures ranging from 35-45 °C which were monitored using a digital thermometer. The temperature change affected the rheological properties of the colloidal suspension, making the sample easier to extrude by reducing its viscosity. CM ethosomes were extruded at room temperature and did not undergo the same thermal stress imparted on the HM ethosomes.



Figure 6.3-2: A macroscopic view of the ethosomal colloidal suspensions showing a change in turbidity before and after extrusion. (Extruding from right syringe to left syringe.)

On a macroscopic level, an immediate change in turbidity was observed upon extrusion (**Figure 6.3-2**). Extrusion was effective at reducing the particle size of the ethosomes to within acceptable ranges (< 0.5). This may have been due to the membrane which allowed ethosomes of a certain size range ($0.1\mu\text{m}$) to pass through under pressure. The particle size was within the targeted range of < 200 nm with extruded ethosomes at 156.6 d.nm and 155.9 d.nm for the HM and CM respectively.

The effect of sonication on the polydispersity index of unloaded ethosomes

The size distribution of crude HM ethosomes was poor (1.00). According to the PDI classification, a PDI > 0.5 is unacceptable.¹⁴⁰ This served as the control and sonication was conducted to improve the polydispersity of the ethosomes i.e. make the ethosomes more monodisperse. The sonicated HM ethosomes maintained an undesirable PDI of 1.00 which indicated that the ethosome size distribution was polydisperse. However, the CM ethosomes had a PDI of 0.26 and 0.16 before and after sonication, respectively. When the HM was

utilised, sonication did not serve as an effective technique to homogenise the size distribution ($PdI > 0.5$), whereas the PdI for CM ethosomes improved. This result is in accordance with the effect of sonication on particle size reduction of the ethosomes prepared using both the HM and CM.

The effect of extrusion on the polydispersity index of unloaded ethosomes

The HM ethosomes had a PdI of 1.00 and 0.13 before and after extrusion respectively. CM ethosomes had a PdI of 0.26 and 0.08 before and after extrusion respectively. While both methods resulted in nanoparticles of an accepted PdI , extruded CM ethosomes had a PdI of < 0.1 which suggest monodispersity. The narrow particle size distribution of extruded CM ethosomes showed that extrusion was more effective at producing ethosomes of an acceptable PdI , compared to the HM ethosomes. This may be attributed to the difference in the respective crude particle sizes. The HM ethosomes were > 2 times larger than the CM ethosomes in crude form. Considering the difference in particle size distribution and that the ethosomes were extruded the same number of times, it is possible that it was easier improve the PdI at a quicker rate for CM ethosomes.

After evaluating the effects of sonication and extrusion, extrusion was a more favourable comminution method. The resultant ethosomes had a relatively narrower PdI compared to sonicated ethosomes and supported literature that the PdI of polymeric nanoparticles has shown to be more readily controlled when using extrusion.¹¹² This property may be directly attributed to the pore size of the polymeric membrane. Research has shown that the membrane is more effective at regulating the size and the homogeneity of the nanoparticles, in comparison to the cavitation mechanism employed in the sonication method.

The effect of sonication on the zeta-potential of unloaded ethosomes

Comminution of crude HM ethosomes shifted the ζ_p from a positive to negative charge (**Table 6.3-1**). HM ethosomes had a ζ_p of +1.29 mV and -10.60 mV for crude and sonicated HM ethosomes, respectively. The negative charge may be attributed to the ethanol which may have been ionised via hydrogen bonding within the colloidal suspension, resulting in electrostatic repulsion. Therefore, it is possible that sonication influenced more ethanol to be saturated at the stern plane, thus increasing the stability. According to the relationship between ζ_p values and their related stability behaviour, this showed that the ethosomes stability shifted from swift flocculation (0 to ± 5 mV) to an initial instability (± 10 to ± 30

mV).¹³⁷ This might have been due to the thermal stress on the vesicles used during analysis as HM ethosomes were analysed at 40 °C to maintain the environment during synthesis. However, CM ethosomes had a ζ_p of -0.06 mV and -2.30 mV for crude and sonicated samples respectively. As shown in **Figure 6.3-3**, the effect on the stability was relatively insignificant as the ethosomes remained within the swift flocculation range.

The effect of extrusion on the zeta-potential of unloaded ethosomes

Extrusion of HM ethosomes did not have any significantly appreciable effect on the ζ_p , as indicated by the shift in charge from +1.29 to -3.89 mV. Although the ζ_p changed from positive to negative, the colloidal suspension demonstrated swift flocculation (0 to ± 5 mV). In contrast, the CM ethosomes displayed an increase in stability as the surface charge changed from -0.06 to -12.80 mV after extrusion.

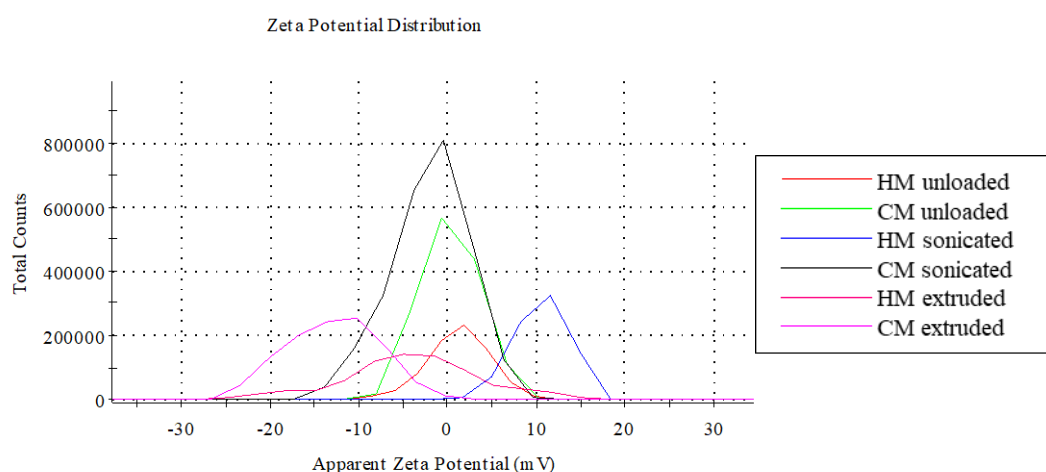


Figure 6.3-3: The zeta-potential of unloaded crude ethosomes synthesised using the hot and cold methods at a phosphatidylcholine concentration of 50 mg/ml.

According to literature, the negative charge of the ethosomes in the colloidal suspension is attributed to the interdigitation of the ethanol within the phospholipid bilayer. These interlocking bonds may result in a greater saturation of ethanol aggregating at the stern layer and hence an increase in the ζ_p . This phenomenon may be evident in the CM ethosomes. However, it is important to note that the surface charge at the slipping plane may be influenced by the turbidity of the colloidal suspensions. Extruded ethosomes are macroscopically less turbid than the crude formulations. This may have influenced the ζ_p of the ethosomes. It has been documented that, in order to circumvent this dilemma, samples

may be diluted “appropriately”. However, the samples were analysed directly after synthesis and were not diluted at this development stage.

6.4. Conclusion

The objective of this experiment was to characterise the nanoparticles according to their physical and chemical stability and to compare the results of the different methods based on the HdD, PdI and ζ_p . Objectives were achieved as seen by the experimental determination of a suitable initial concentration of PC for ethosome synthesis. Ethosomes containing varying concentrations of PC were prepared using the HM and CM and evaluated using DLS according to the following criteria: HdD < 200 nm, PdI < 0.5, $\zeta_p = \pm 30$ to ± 40 mV. Based on the analyses it was determined that 50 mg PC would be the most suitable mass for ethosome synthesis for all continuing experiments. The highest PC concentration (50 mg/ml) was selected as research has shown that increased PC concentrations may result in increased encapsulation efficiency.^{100,101} Since APIs were to be added next, this was a critical consideration at this stage to ensure increase the potential for API encapsulation.



UNIVERSITY *of the*
WESTERN CAPE



School of
PHARMACY

7. Introduction

After determining the effect of PC concentration and comminution on the DLS properties of unloaded ethosomes, BMV and HCA were each incorporated as active pharmaceutical ingredients (APIs) into both hot method (HM) and cold method (CM) formulations. The ethosomes were characterised to determine the effect of corticosteroid loaded ethosomes using the mean H_{dd}, P_{dI} and ZP relative to the unloaded ethosomes. Additionally, drug loading (DL) and encapsulation efficiency (EE) were determined using high performance liquid chromatography (HPLC).

7.1. The preparation of hydrocortisone acetate and betamethasone valerate loaded ethosomes

Guided by the results of the ethosomes synthesised in the previous experiment **Chapter 6**, a series of new experimental formulations were prepared using the HM and CM described in **Chapter 5.2.3**, Corticosteroid loaded ethosomes were analysed using DLS to determine the effect of the PC concentration on ethosomal H_{dd}, P_{dI} and Zeta potential (**Table 7.2-1**). A macroscopic view of the crude ethosomes is displayed in **Figure 7.1-1**.



1. Blank ethosomes HM
2. Blank ethosomes CM
3. BMV loaded ethosomes HM
4. BMV loaded ethosomes CM
5. HCA loaded ethosomes HM
6. HCA loaded ethosomes CM

Figure 7.1-1: Vials containing ethosomal colloidal suspensions showing the difference in turbidity and sedimentation. Image captured 24 hours after synthesis.

7.2. The effect of corticosteroids on crude ethosomes

Table 7.2-1: The hydrodynamic diameter (HdD), polydispersity index (PdI) and zeta-potential (ζ_p) of unloaded and corticoid loaded ethosomes ($n=3$)

FORMULATION		HdD (d.nm)	PdI	ζ_p (mV)
Unloaded ethosomes	HM	852.40±239.38	1.00	1.29
	CM	299.60±92.45	0.26	0.07
Loaded ethosomes	HM _{BMV}	753.50±21.26	1.00	-24.20
	CM _{BMV}	362.50±95.35	0.28	-12.60
	HM _{HCA}	858.00±81.70	1.00	-3.36
	CM _{HCA}	265.40±55.90	0.16	-4.27

HM = Hot Method, CM = Cold Method, BMV = betamethasone valerate, HCA = hydrocortisone acetate.

The effect of corticosteroids on the particle size of crude ethosomes

Ethosomes had a unimodal size distribution (**Figure 7.2-1**). Similar results were observed as that of the previous experiment (**Table 6.2-1 and Table 6.3-1**), where the unloaded CM crude ethosomes had a lower mean particle size compared to the HM crude ethosomes. The addition of HCA and BMV resulted in loaded crude ethosomes with differences in HdD relative to the unloaded crude ethosomes. The results (**Table 7.2-1**) suggest that HM HCA loaded ethosomes had a similar size to their respective unloaded ethosomes, whereas the CM HCA loaded ethosomes had an 11.3 % reduction in HdD. Conversely, BMV loaded ethosomes had an HdD decrease of 11.6 % and an increase of 21.1 % for the HM and CM respectively. Overall, HCA loaded ethosomes had a smaller HdD when compared to BMV loaded ethosomes when using the CM and a larger HdD when using the HM. This contrast may have been due to the difference in their respective solubility and lipophilicity. Research has shown that the addition of an API may result in the increase of the particle size.¹⁶⁶ A decrease in particle size may be due to instability in the phospholipid bilayer resulting in leaking of API.

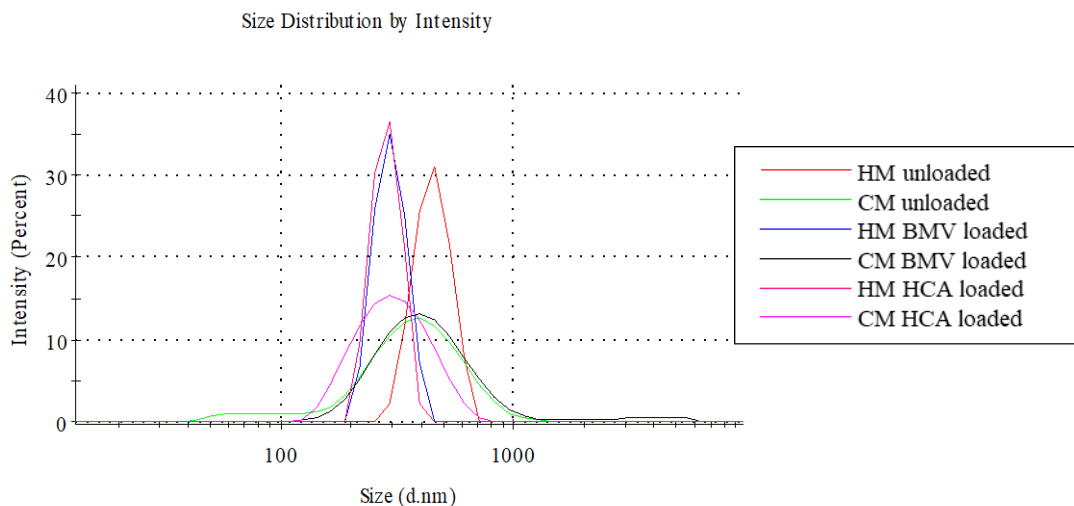


Figure 7.2-1: The size distribution of unloaded, betamethasone valerate (BMV) loaded and hydrocortisone acetate (HCA) loaded crude ethosomes synthesised using the hot and cold method

Although both glucocorticoids (GCs) have a greater affinity for the organic phase, HCA is more soluble than BMV in ethanol. This is significant considering the implications on ethosome HdD. Since HCA has a relatively greater ethanolic solubility, it may be in higher concentrations in the core, HCA loaded ethosomes were smaller in size. Since BMV is less soluble in ethanol, it may have had a greater affinity for the PC and added to the lamellarity. Additionally, BMV has a long valeric acid chain making the compound more lipophilic. It was anticipated that this may result in it having a propensity for the phospholipid bilayer. Regardless of the magnitude of increase or decrease, it was evident that the addition of GCs affected the HdD of ethosomes.

The effect of corticosteroids on the polydispersity of crude ethosomes

As shown with the unloaded ethosomes, ethosomes prepared via the HM had an unacceptable PdI of more than > 0.5 , indicating that the ethosomes varied in size distribution. Ethosomes prepared using the CM had an acceptable PdI of 0.26. When loaded with GCs, it was shown that the results were similar regarding the effect on PdI when comparing the HM and CM. Regardless of the loaded API, the PdI of GC loaded ethosomes prepared using the HM remained poor (PdI = 1). The difference in PdI was more evident when comparing the loaded ethosomes prepared using the CM. It was shown that, although both BMV and HCA had acceptable PdIs of < 0.5 , HCA loaded ethosomes had a more favourable PdI. This showed that the HCA had a better homogeneity of size distribution. It is important to note that the HCA

loaded ethosomes also had a smaller mean particle size and standard deviation when compared to BMV loaded ethosomes. As discussed previously, this difference may be attributed to their respective affinities for the lipophilic and hydroethanolic phases.

The effect of corticosteroids on the zeta-potential of crude ethosomes

Both the unloaded CM and HM ethosomes had a ζ_p indicating swift flocculation. When loaded with the GCs, the result remained unfavourable as it was not within the targeted range of ± 30 mV. However, it was noted that there was a difference when comparing the ζ_p of the different APIs. (Figure 7.2-2)

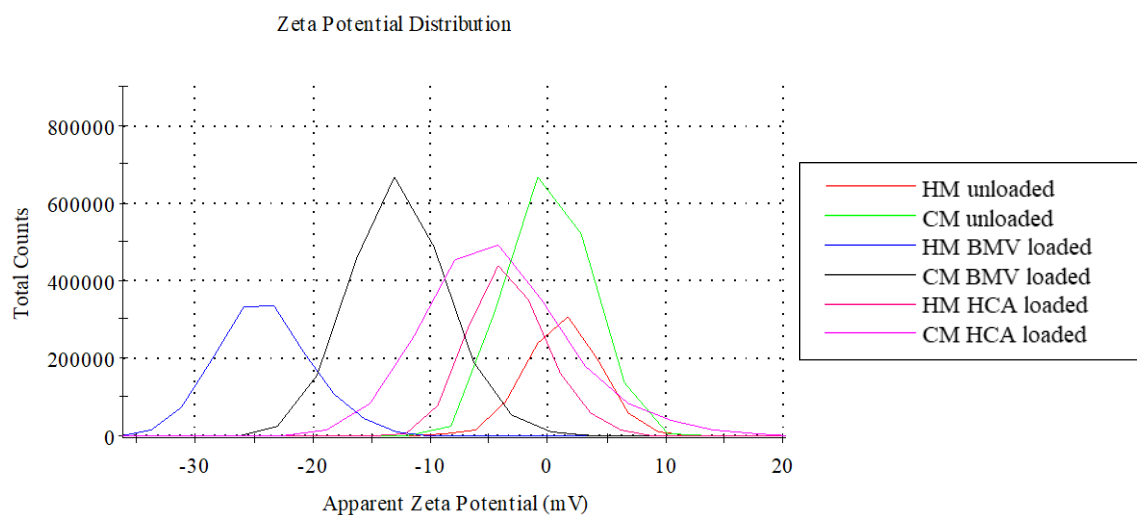


Figure 7.2-2: The zeta-potential of unloaded, betamethasone valerate (BMV) loaded and hydrocortisone acetate (HCA) loaded crude ethosomes synthesised using the hot and cold methods.

It was evident that the effect on the ζ_p was more influenced by the drug than the method, with BMV loaded ethosomes being more stable than their HCA loaded counterparts. HCA loaded ethosomes had a ζ_p of -3.36 mV and -4.27 mV for the HM and CM respectively. Although the ζ_p increased, it remained within the swift flocculation range. BMV loaded ethosomes, had a ζ_p of -24.20 mV and -12.60 mV for HM and CM respectively, showing an initial instability ($(\pm 10$ to ± 30 mV).).

Based on the results, it was evident that, when ethosomes were loaded with BMV, there was a greater concentration of anions at the stern plane. Apart from indicating the stability of the ethosomes within the colloidal system, the ζ_p may also be an indication of the ability of the

ethosomes to be retained within the epidermis. The interaction between the negative charge of the ethosomes and the positive charge of the human skin (+23 mV) may increase the retention time in the target tissue. When comparing the difference in the effect of the GCs it was noted that BMV loaded ethosomes generated appeared to be more stable. This could have been due to the location (hydroethanolic core or the phospholipid bilayer) of the API within the ethosome. Literature suggests that the negative ζ_p is influenced by the interdigitation of the ethanol within the phospholipid bilayer.¹⁷ Since PC is a zwitterion, this may also have affected the surface charge of the ethosomes with the exposure of polar functional groups.¹⁰⁸ PC may have interacted with BMV more than HCA which may be attributed to the location of the API within prepared ethosomes.

Overall, it was evident that GCs influenced the variables under scrutiny, and thus, would influence the subsequent ethosome analyses.

7.3. The effect of corticosteroid loading on sonicated and extruded ethosomes

Ethosomes were prepared using the HM and CM described in *Chapters 5.2.3* were sonicated and extruded (*Chapters 5.3.1 and 5.3.2*). Unloaded, BMV loaded and HCA loaded ethosomes were analysed to determine the effect of corticosteroid loading on sonicated and extruded samples. Using DLS as described in *Chapters 5.5.1 and 5.5.2*, the ethosomes were analysed and the results were tabulated, as shown in **Tables 7.3-1 and 7.3-2**. The evaluation criteria was maintained as in previous experiments where: HdD = ~200 nm, PdI < 0.5 and $\zeta_p = \pm 30$ mV

Table 7.3-1: The hydrodynamic diameter (HdD), polydispersity index (PdI) and zeta-potential (ζ_p) of sonicated (S) unloaded and corticosteroid loaded ethosomes ($n=3$)

FORMULATION		HdD (d.nm)	PdI	Z.P (mV)
Unloaded ethosomes	HM _S	1751.00±381.70	1.00	-6.37
	CM _S	283.10±116.50	0.16	-5.08
Loaded ethosomes	HM _{HCA S}	969.50±207.25	0.04	-5.94
	CM _{HCA S}	227.50±21.71	0.42	-6.05
	HM _{BMV S}	1035.00±45.04	1.00	-3.57
	CM _{BMV S}	326.30±40.38	0.05	-4.21

HM = Hot Method, CM = Cold Method, BMV = betamethasone valerate, HCA = hydrocortisone acetate

The effect of corticosteroid loading on the hydrodynamic diameter of sonicated ethosomes

Sonicated ethosomes had a unimodal size distribution (**Figure 7.3-1**). After sonication, the HM unloaded ethosomes showed a 100 % increase in mean HdD. The HdD measured 1751.00 d.nm, which was above the targeted size of ~ 200 nm. The standard deviation (± 381.7 d.nm) of the ethosome size indicated that the sonication technique for comminution created challenges in producing ethosomes of a reproducible size range. The increase in size from 852.40 d.nm may have been due to the parameters used when setting up the experiment. Although research has shown that sonication has proved effective at reducing particle size of ethosomes, those results were not reflected in this experiment.^{89,123} A possible reason for the increase in particle size may have been attributed to the fact that the analysis was conducted at a higher temperature (40 °C) compared to that at which they were stored (25 °C). Cavitation, the mechanism for particle size reduction when using sonication, had a negative effect on particle size which may have resulted in the lysis of ethosomes and agglomeration of the fragments. The fluctuation in temperature in between synthesis, comminution and analysis may have impacted the stability of the ethosomes and subsequently may have affected the size. For the aforementioned reasons, the HM, coupled with sonication did not seem as a viable particle size reduction method.

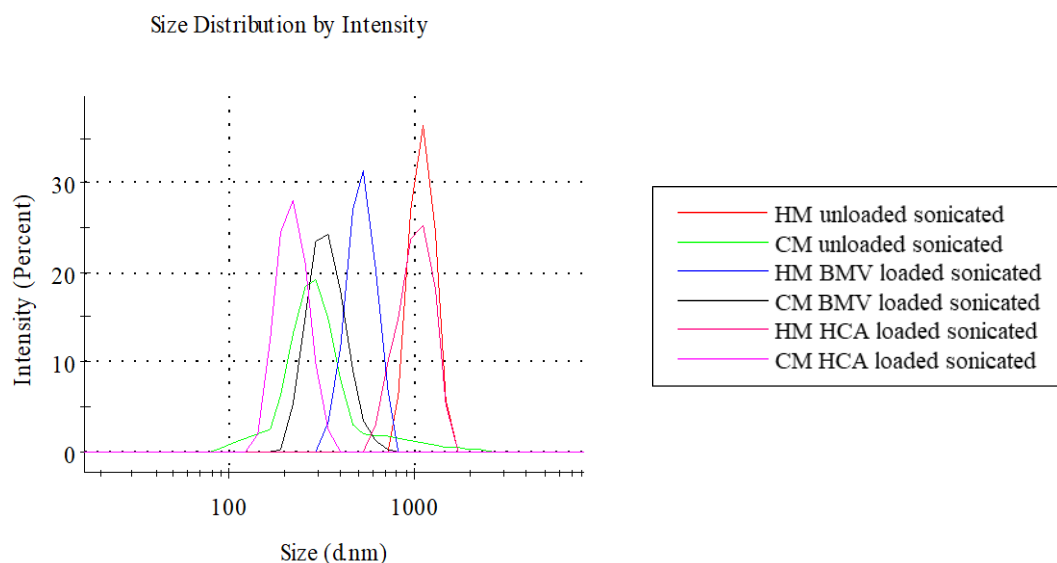


Figure 7.3-1: The size distribution of unloaded, BMV loaded and HCA loaded sonicated ethosomes synthesised using the hot and cold method

Sonicated CM ethosomes (283.10 d.nm) had a slight reduction in the mean HdD, when compared to the unloaded ethosomes (299.60 d.nm). The main difference in the parameters, relative to the HM, was that sonication of the CM ethosomes was conducted at 25 °C. Therefore, since the HdD was measured using DLS at room temperature, there was not much difference in the temperature of the ethosome environment as compared to the HM ethosomes. Since less energy was imparted into the system (i.e. sonication vs increased temperature + sonication), the vesicles did not undergo the same amount of thermal stress resulting from the aforementioned enthalpy change.

When encapsulated with HCA, the size of the HM ethosomes increased by 12.5% after sonication, whereas the CM ethosomes decreased by 15%. HM ethosomes encapsulated with BMV showed a 40 % decrease in mean HdD after sonication whereas the CM equivalents showed a mean HdD increase by 15 %. The APIs showed differences in their influence on particle size before and after sonication using the different methods. These size range differences could be attributed to their relative solubility in ethanol which causes partitioning between the “free drug” in the bulk medium relative to that within the ethosome. Regardless of the synthesis method or the loaded GC, the particle size was not within the targeted size range of ~ 200 nm.

The effect of corticosteroid loading on the polydispersity index of sonicated ethosomes

The PDI of the unloaded HM ethosomes, both crude and sonicated, had a polydispersity above the acceptable PDI. Sonication of the HM ethosomes was not effective at reducing the size nor was it effective at homogenising their size distribution. Conversely, the PDI of unloaded CM ethosomes both crude and sonicated had an acceptable PDI of < 0.5 (0.26 and 0.16 respectively). Although the particle size was not within the targeted range as previously discussed, the distribution of the size improved after sonication, thus imparting homogenisation.

The analysis of the GC loaded ethosomes showed that HCA loaded HM ethosomes had an improved PDI of 0.04 which is indicative of monodispersity. This result indicated that the uniformity of the ethosome size improved substantially. Similar to the unloaded ethosome, API loaded ethosomes displayed similar characteristics regardless of the specific properties of the API included. A possible solution to improve the PDI using sonication may have been to sonicate at room temperature, regardless of the ethosome preparation method used (CM or HM). When sonicating the ethosomal colloidal dispersion, it was apparent that the increased temperature (40 °C) impacted the PDI.

Unlike HM ethosomes, the respective CM ethosomes had a PDI within the acceptable range of <0.5. When comparing the different APIs, it was interesting to note that HCA loaded ethosomes have a narrower size distribution relative to BMV loaded ethosomes. BMV loaded ethosomes had a greater size range and were less homogenous regarding their size distribution in suspension. Considering that HM ethosomes do not display a similar trend, it is clear that temperature regulation is an important component, not just in synthesis, but also in particle size reduction.

The effect of corticosteroid loading on the zeta-potential of sonicated ethosomes

As shown in **Table 7.3-1**, all of the sonicated samples showed no difference in the ζ_p and maintained stability associated with swift flocculation (0 to ± 5 mV).

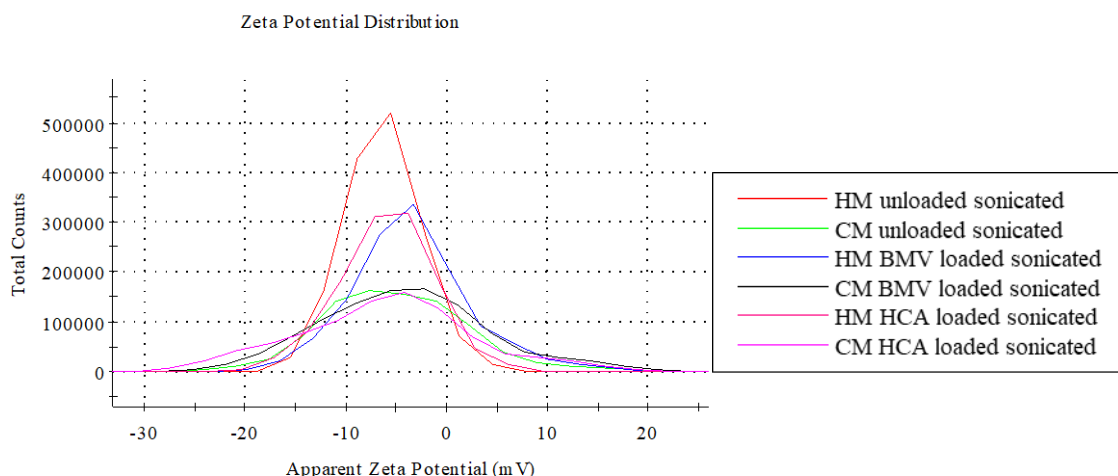


Figure 7.3-2: The ζ_p of unloaded, BMV loaded and HCA loaded sonicated ethosomes synthesised using the hot and cold methods.

The main difference observed in Figure 7.3-2 was observed in the total count where HM ethosomes had a greater count relative to CM ethosomes. This may have been a direct consequence of the increased temperature utilised during HM ethosome analyses which decreased the viscosity and turbidity of the colloidal system thus improving detection.

The effect of corticosteroid loading on the hydrodynamic diameter of extruded ethosomes

Table 7.3-2: The hydrodynamic diameter (HdD), polydispersity index (PdI) and zeta-potential (ζ_p) of unloaded and corticosteroid loaded extruded (E) ethosomes ($n=3$)

Formulation		HdD (d.nm)	PdI	Z.P (mV)
Unloaded ethosomes	HM _E	147.2±25.05	0.17	-5.74
	CM _E	153.1±32.28	0.14	-4.34
Loaded ethosomes	HM _{HCA E}	168.3±28.27	0.06	-4.93
	CM _{HCA E}	147.7±19.91	0.0	-3.31
	HM _{BMV E}	151.4±32.35	0.15	-3.21
	CM _{BMV E}	163.8±31.99	0.11	-3.82

Formulation: HM: Hot Method, CM: Cold Method, BMV: betamethasone valerate, HCA: hydrocortisone acetate.

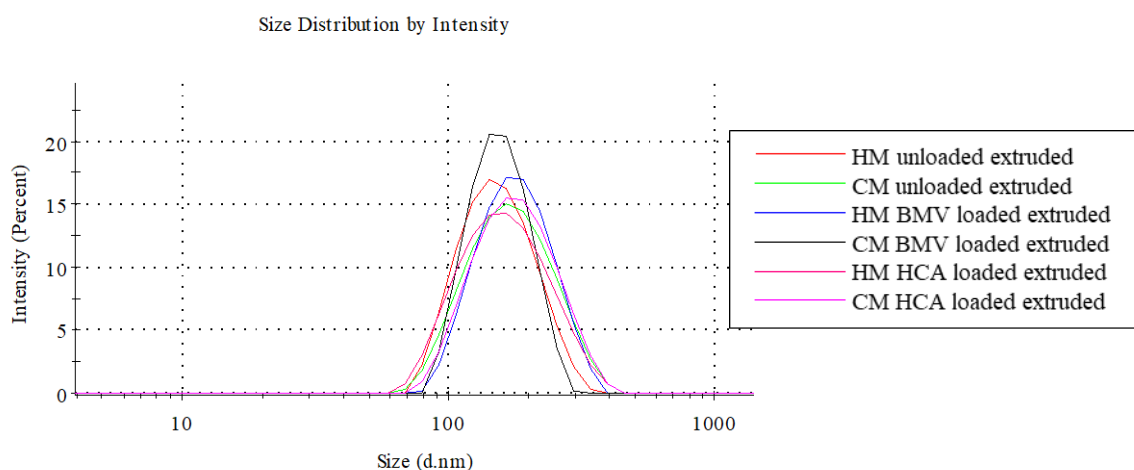


Figure 7.3-3: The size distribution of unloaded, BMV loaded and HCA loaded extruded ethosomes synthesised using the hot and cold method

Extruded ethosomes had a unimodal size distribution (**Figure 7.3-3**). Unloaded extruded ethosomes had a particle size range within the targeted range of ~ 200 nm, with HM ethosomes showing a 4 % reduction in HdD (**Figure 7.3-3**). HM ethosomes were extruded at a higher temperature (40 °C) than CM ethosomes (25 °C). Apart from reducing the viscosity of the colloidal system, the increased extrusion temperature may have directly influenced the flexibility of the phospholipid bilayer. Although the rate of extrusion relative to CM ethosomes was quicker, the increased temperature may have resulted in a decrease in vesicle stability. Multilamellar vesicles (MLVs) may have lysed into large unilamellar vesicles (LUVs) and smaller fragments which were detected as spherical ethosomes via DLS.

GC loaded ethosomes prepared using HM and CM showed a similar result regarding the mean HdD. As with sonication, HM ethosomes loaded with HCA showed an increase in particle size (168.3 ± 28.27) after extrusion relative to their respective unloaded ethosomes, whereas CM ethosomes showed a decrease in particle size (147.7 ± 19.91). This may be indicative of reduced vesicle flexibility for HCA when using CM and an increased flexibility when using HM. Compared to unloaded ethosomes, BMV loaded ethosomes showed a similar size range (151.4 ± 32.35) and an increased HdD (163.8 ± 31.99) for the HM and CM respectively. An increase in HdD has been confirmed in literature regarding encapsulation of APIs relative to unloaded ethosomes.^{61,101} The similar size range identified with the HM may have been attributed to poor encapsulation efficiency for that particular set of experiments.

Both of the steroidal compounds are polycyclic, rigid, pregnane derived structures which add stability to the ethosomal structure. Because of this characteristic, it was expected that these APIs would make the vesicles more compact. The results show that, after extrusion, HCA loaded ethosomes have a higher mean HdD than BMV loaded ethosomes for the HM, whereas HCA loaded ethosomes have a lower mean HdD than BMV loaded ethosomes for the CM. Ethosomes are flexible lipid based nanoparticles.⁹¹ This property was corroborated by the extrusion analyses, as particles had a higher mean HdD than the aperture size of the membrane utilised for extrusion.

The effect of corticosteroid loading on the polydispersity index of extruded ethosomes

Upon extrusion evaluation, it was immediately discovered that the PDI had improved, relative to the crude samples. This was attributed to the size of the membrane which directly impacts the PDI. Once extruded, only ethosomes of a certain size range, influenced by the aperture size of the membrane, were able to pass through. Thus, the size ranges of those particles were narrow. The polydispersity of the ethosomes comminuted by means of extrusion may have been influenced by the flexibility of the vesicle prepared. Research has shown that, more flexible vesicles will have a larger size range and a larger polydispersity.^{91,104} An interesting observation was that, although all of the extruded ethosomes were within the targeted PDI of < 0.5, the HCA loaded ethosomes prepared via HM and CM were monodisperse with PDIs of 0.06 and 0.05 respectively. It was deduced that these ethosomes may have been more compact, with a less flexible phospholipid bilayer.

The effect of corticosteroid loading on the zeta-potential of extruded ethosomes

As shown in **Figure 7.3-4**, all of the extruded samples showed no difference in the ζ_p and maintained stability associated with swift flocculation.

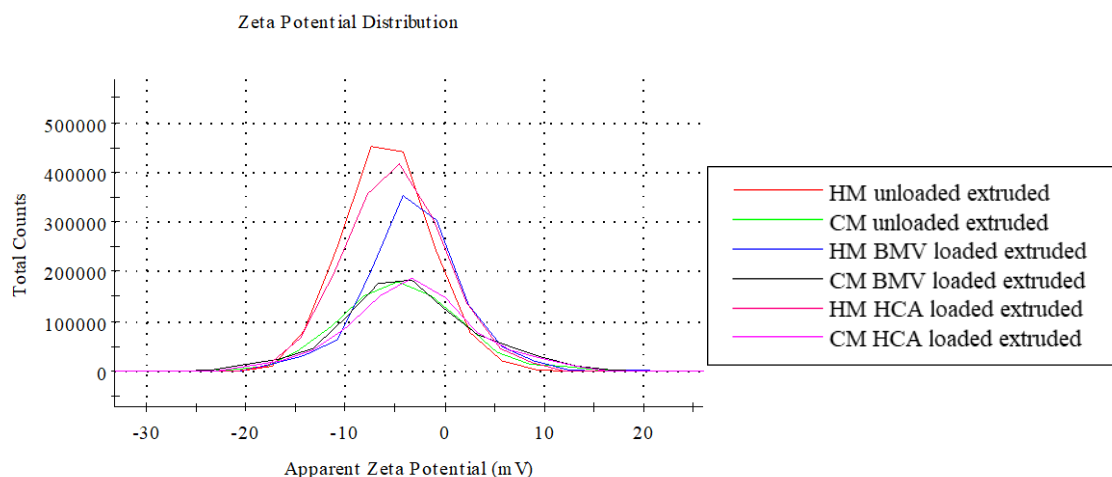


Figure 7.3-4: The zeta-potential of unloaded, BMV loaded and HCA loaded extruded ethosomes synthesised using the hot and cold methods.

Overall, it was found that the loading of corticosteroids influenced the particle size, PdI and ζ_p . Additionally, a significant variability of results was established when sonication was utilised for comminution, whereas extrusion resulted in ethosomes which better fit the criteria ($HdD < 200$ nm, $PdI < 0.5$, $\zeta_p = \pm 30$ to ± 40 mV) with an improved reproducibility. As such, extrusion was selected as the standard method of particle size reduction for all subsequent formulations.

7.4. Preparation of ethosomes for solid state analyses

After HdD, PdI and ζ_p analysis, HM and CM ethosomes were centrifuged and washed twice using ethanol and H₂O to maintain the same solvent environment in which the ethosomes were synthesised. This was done to prevent agglomeration of ethosomes and to maintain the ethosomal characteristics. To minimise possible passive diffusion of encapsulated API, the resuspension time was low (~5 min). Resuspended ethosomes were dried using centrifugal evaporation as described in *Chapter 5.4.2*. All subsequent solid state analyses (FTIR, HSM, DSC and TGA) were conducted using these dried samples.

7.5. Scanning electron microscopy

SEM was used to characterise the morphology of: pure BMV, pure HCA, PC, unloaded and GC loaded ethosomes synthesised using the HM and CM. Samples were analysed using the SEM method as described in *Chapter 5.12*.

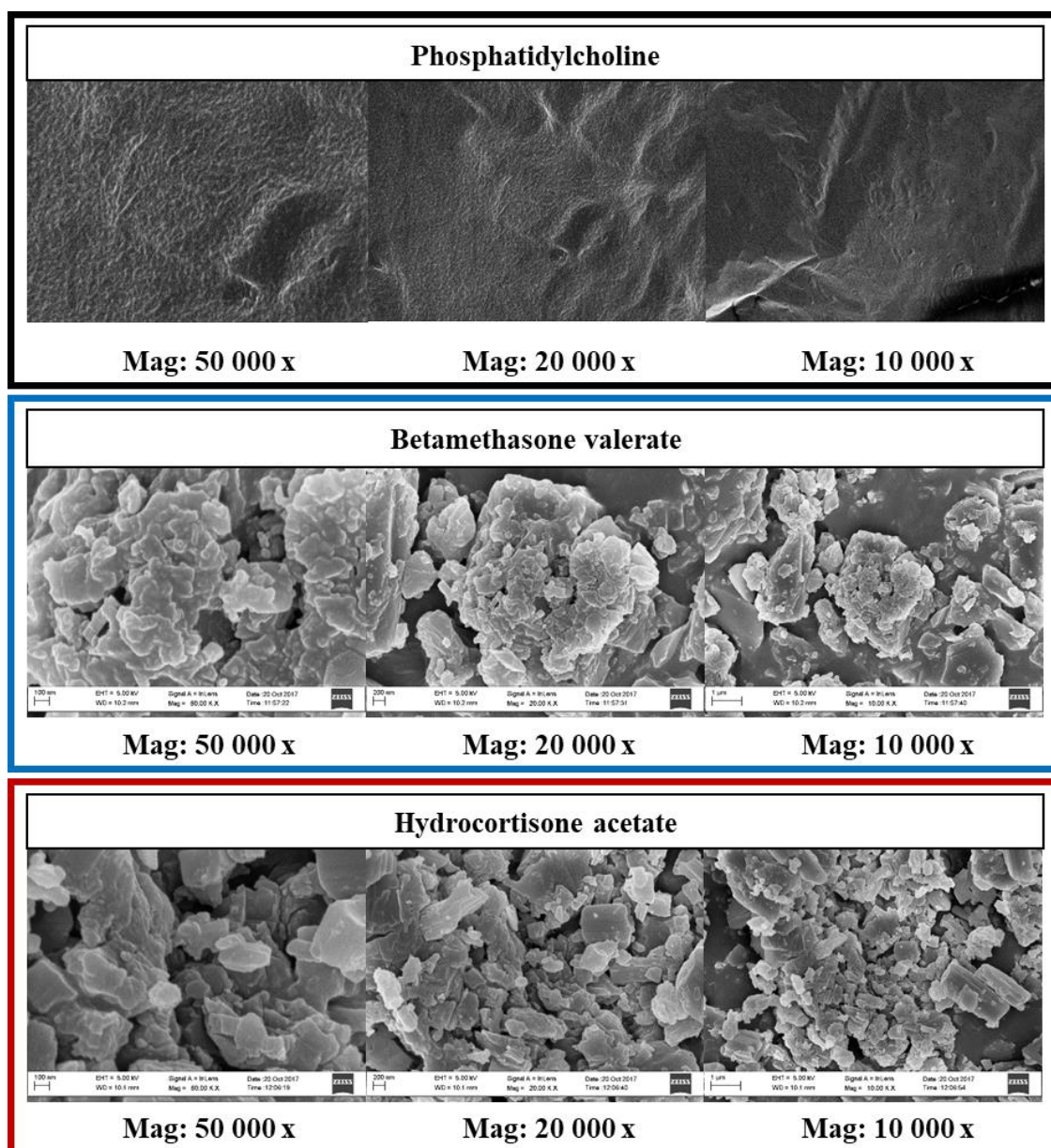


Figure 7.5-1: SEM analyses of phosphatidylcholine, betamethasone valerate and hydrocortisone acetate at different magnifications (Mag).

PC is characterised as an amorphous semisolid with no distinct shape.⁷³ This description was corroborated by the SEM images shown in **Figure 7.5-1**. The SEM image of PC served as a comparative reference to the ethosomes prepared using the HM and the CM. As shown by

Touitou *et al*, 2007, both of these methods are viable for synthesising ethosomes with a spherical morphology.¹ The British Pharmacopoeia (BP) characterises both GCs as white crystalline powders.⁷³ The morphology can be corroborated by the SEM images shown in **Figure 7.5-1**, where it is evident that the GCs had an irregular crystalline shape. The SEM images of the pure components served as a comparative reference for GC loaded ethosomes that were prepared using the HM and the CM.

7.5.1. The morphology of HM and CM ethosomes

Figure 7.5.1-1 shows that spherical ethosomes were synthesised using the HM and CM. These vesicles are different in shape when compared to the pure PC which was amorphous and had no distinct shape. Comparatively, it was evident that vesicles had formed.

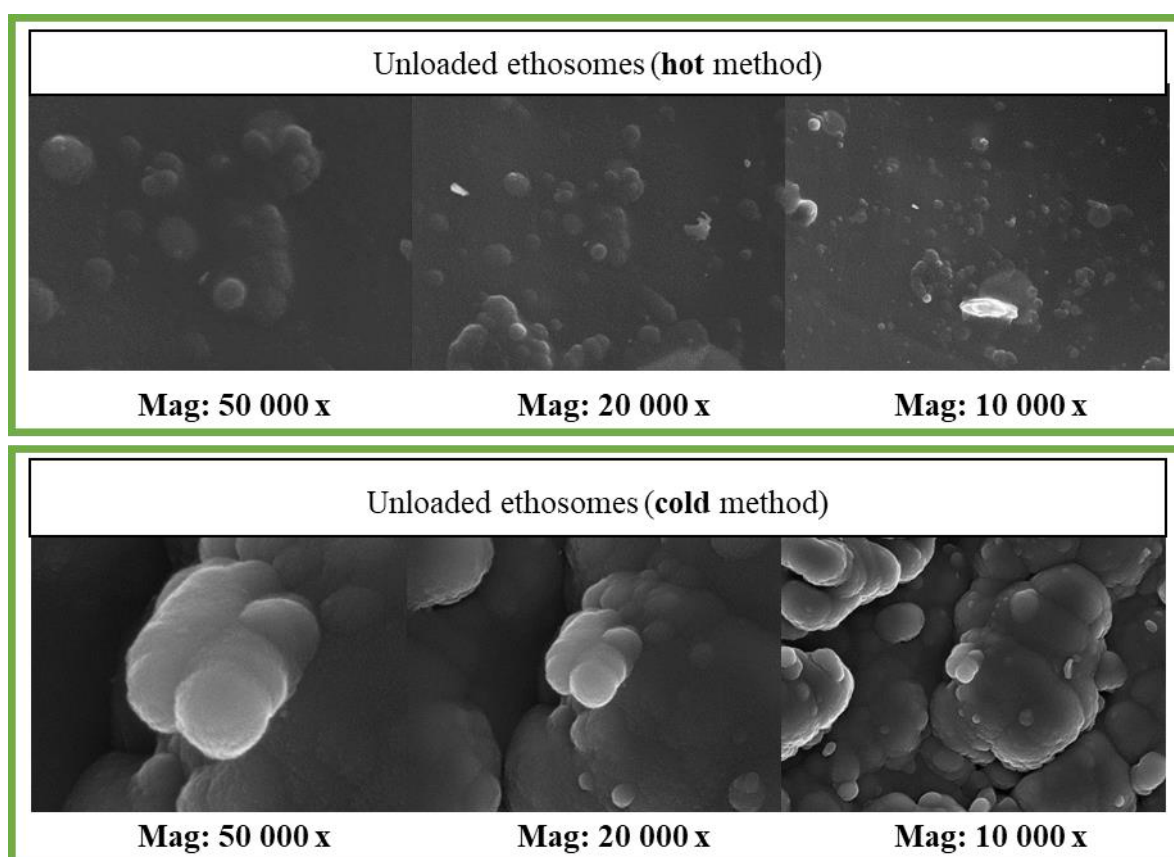


Figure 7.5.1-1: SEM analyses of unloaded extruded ethosomes prepared using the hot and cold methods, at different magnification (Mag)

When the ethosomes synthesised using the HM and CM were compared at the same magnification, it was evident that ethosomes generated from the HM had a relatively smaller diameter than the ethosomes prepared via the CM. SEM images indicated a difference in the

size relative to the DLS because of the manner in which the size measured. However, SEM images were used qualitatively. The particle size using DLS is not a measurement of the true size but rather of a sphere.¹³⁶ Regardless of the shape of a nanoparticle, the reported dimension is reported as spherical. Thus, it was important to corroborate the DLS measurement by observing the morphology.¹⁶⁷ DLS also measures the solvation layer i.e. the shell around a suspended particle, consisting of the molecules of the solvent, as part of the nanoparticle. Due to this process, DLS measured particles often appear larger than their actual size.¹⁶⁷ This was not a concern as a higher HdD relative to the actual SEM image would not have negative implications for transdermal permeation. DLS was advantageous because it was relatively cheaper to run, quick and the sample preparation was simple.

Dried GC loaded ethosomes were analysed using SEM to determine the difference in the morphology of the ethosomes once loaded.

This was important because, for nanovesicles to be viable API carriers for transdermal permeation, a spherical shape is favourable. BMV loaded ethosomes HM (**Figure 7.5.1-2**) indicate that, in comparison to the unloaded HM ethosomes, the morphology changed from

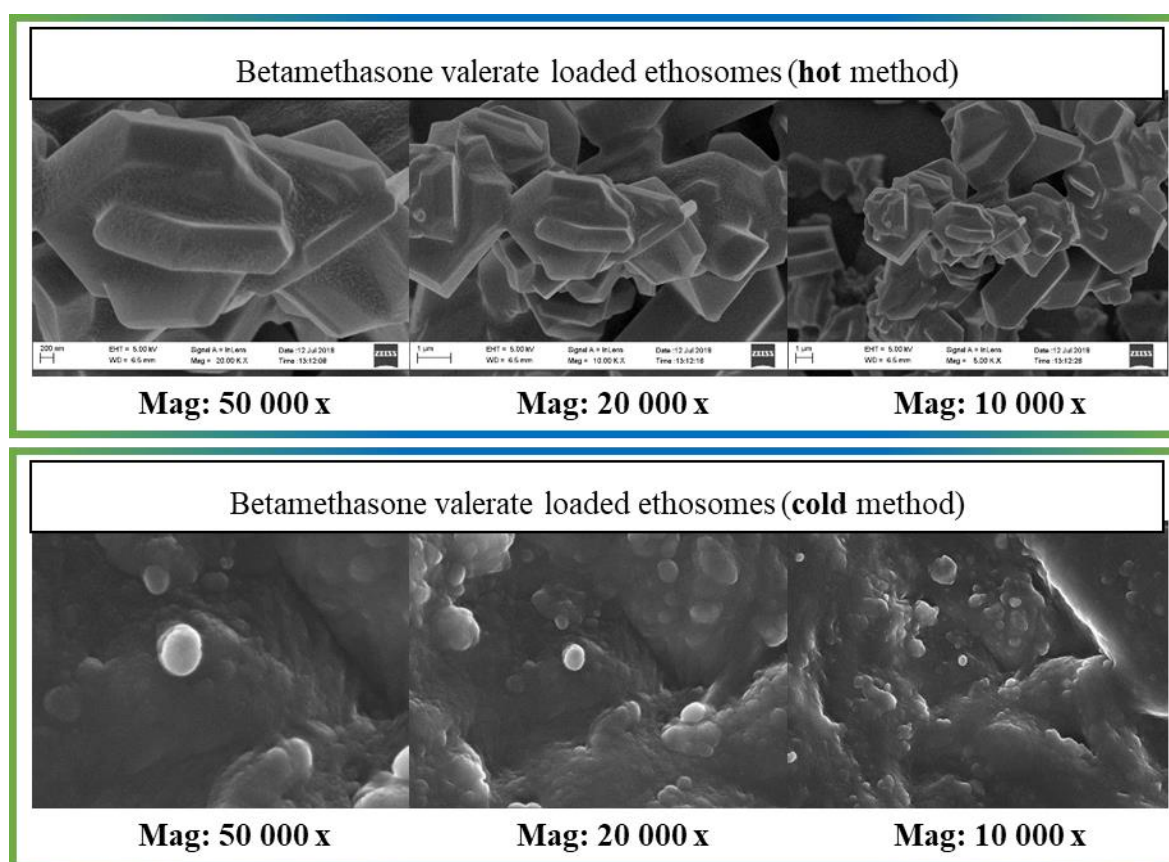


Figure 7.5.1-2: SEM analyses of BMV loaded extruded ethosomes prepared using the hot and cold methods, at different magnification (Mag)

being spherical to being irregular. The irregular shape could be as a direct result of the HM. When synthesising ethosomes using the hot method it is important to note that the PC is added to the aqueous phase. In contrast, BMV loaded CM ethosomes have a spherical shape. However, as with BMV loaded HM ethosomes, there is evidence of agglomeration, as can be seen at Mag 50 000 x. The agglomeration could be attributed to the zeta-potential which indicated an initial instability. Upon drying of the ethosomes to prepare them for solid state analysis, the liberation of the solvent rendered the electrostatic forces and Brownian motion negligible which may have influenced their stability.

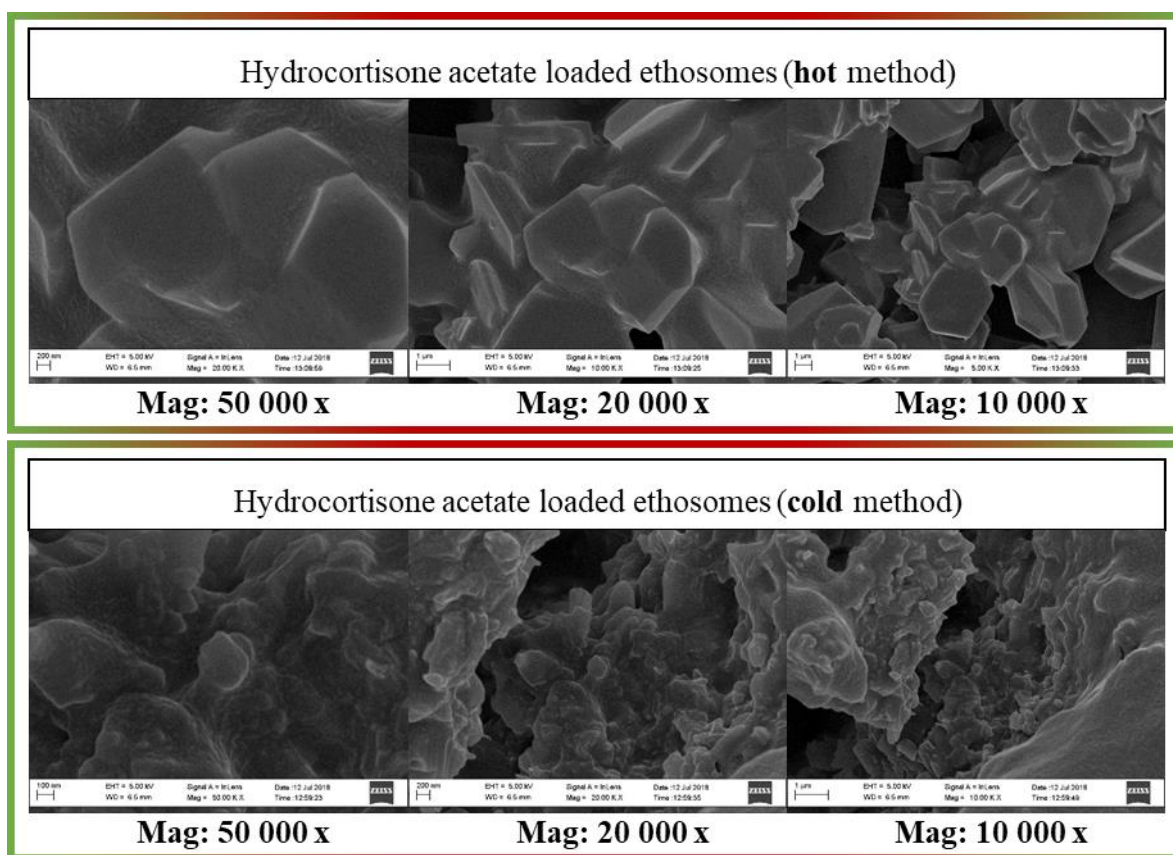


Figure 7.5.1-3: SEM analyses of HCA loaded extruded ethosomes prepared using the hot and cold methods, at different magnification (Mag)

Similarly, HCA loaded ethosomes HM (**Figure 7.5.1-3**) appeared irregular in shape. These ethosomes also appeared to be HCA coated with PC as the crystalline HCA seemed as an apparent scaffold. Agglomeration was also observed.

Overall, it was evident that there was a change in the appearance of the ethosomes relative to the pure components. Due to the irregular ethosome shape, the large particle size (> 200 nm), the variability of the particle size and the polydispersity of the particle size, the

HM seemed less favourable as a method for ethosome preparation. For these reasons, the HM was rejected as a suitable method to synthesise ethosomes as a candidate for topical drug delivery. All subsequent analyses were conducted using the CM for synthesis and extrusion for comminution.

7.6. FTIR analysis of BMV loaded and HCA loaded ethosomes

Using the FTIR analysis method as described in *Chapter 5.13*, FTIR spectroscopy was conducted to identify the functional groups within the diagnostic region attributed to the pure components: PC, BMV and HCA. These spectrograms (**Figure 7.6-1**) would serve as references for: unloaded, BMV loaded and HCA loaded ethosomes. The samples analysed were from the same batch as the ethosomes prepared for SEM analyses. Unloaded ethosomes were then analysed to determine if any interactions occurred between PC and the hydroethanolic environment in which the ethosomes were formed. Once loaded with BMV and HCA, respective ethosomes were analysed to determine if any interactions occurred which may indicate encapsulation. Interactions were identified by peak shifts in wave number, increase/decrease in peak intensities and the appearance /disappearance of characteristic bands.

Upon analysis of BMV using FTIR spectroscopy, a weak OH stretch was identified at 3378.71 cm^{-1} . This site is susceptible to hydrogen bonding due to the presence of the oxygen which serves as an electron withdrawing group. Alkane C-H stretches were identified at, 2955.10 cm^{-1} , 2910.02 cm^{-1} and 2872.09 cm^{-1} . Strong sharp carbonyl stretches were identified at 1732.81 and 1714.48 cm^{-1} , which may be attributed to the esterified valeric acid at C17 or the conjugated ketone at C3. Alkene C=C stretches were identified at 1658.32 cm^{-1} , 1614.98 cm^{-1} and 1601.36 cm^{-1} with C-H bending at 1455.95 cm^{-1} .

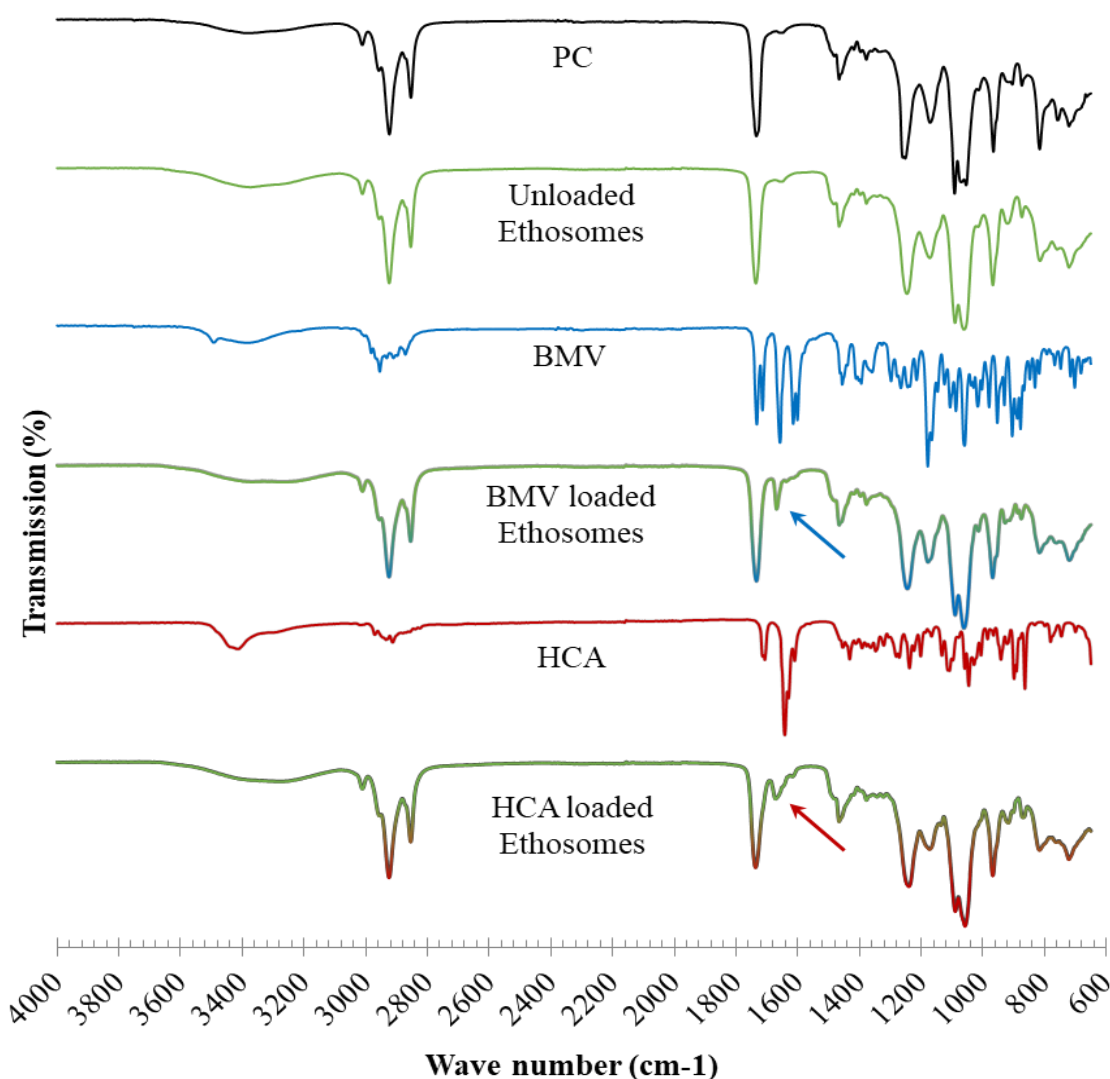


Figure 7.6-1: FTIR spectrograms showing the interactions between the ethosome components. The arrows indicate the peaks at which chemical shifts in wave number or intensity occurred.

PC displayed weak broad bands at 3368.04 cm^{-1} , indicating the presence of O-H/N-H stretches. These bands may correspond to the N-H stretch on the conjugated ammonium phosphate ion or intermolecular hydrogen bonding. Literature suggests that N-H stretches present as medium or weak sharp bands occurring between $3400 - 3300$ and $3330 - 3250\text{ cm}^{-1}$, whereas alcohol stretches appear as a strong broad band present at $3550 - 3200\text{ cm}^{-1}$.¹⁶³ It was difficult to assign the exact functional group because of the similar/overlapping ranges of interpretation. A weak alkene C-H stretch was identified at 3011.08 cm^{-1} which can be attributed to the unsaturated carbon chain with subsequent alkane stretches present at 2923.37 and 2853.5 cm^{-1} . The C=O stretch, identified at 1734.39 cm^{-1} , was attributed to the carbonyl of the ester and the sharp medium peak at 1466.07 cm^{-1} corresponded to alkane C-H bending.

When analysing the unloaded ethosomes, it was found that the O-H/ N-H stretches at 3368.04 cm^{-1} had shifted to 3373.13 cm^{-1} , which may have been due to a weak chemical interaction such as hydrogen bonding. It is possible that the protonated amine may have acted as an acid and donated its proton. Since the wave number is inversely proportional to mass, a mass loss by proton donation will increase the wave number.⁶⁹ This may have also resulted in a decrease in N-H stretching bond length, since bond length is inversely proportional to wave number.¹⁶³

BMV loaded ethosomes displayed a large negative shift in wave number as the O-H/ N-H stretches at 3368.04 cm^{-1} had decreased to 3276.09 cm^{-1} . This large shift in wave number may have been due to a stronger chemical interaction between the BMV and the PC as they both possess polar electron withdrawing group regions. The large decrease in wavenumber may have been due to interactions between electronegative atoms resulting in hydrogen bonds. This may have resulted in reduced bond length resulting in a higher vibration of the N-H/O-H stretch and a subsequent lower wave number. Another notable finding occurred at 1668.51 cm^{-1} where a weak C=C stretch appeared, indicating an intermolecular interaction between BMV and PC. Considering that PC exists at a higher % m/m concentration relative to BMV in the formulation, this was a notable finding because C=C stretches were not evident in PC.⁶⁹ This is an indication of BMV encapsulation.

HCA analysis showed that, the alcohol O-H stretches, were located at C 11 and C 17 of the pregnane backbone, at 3414.02 cm^{-1} . Alkane C-H stretching was observed at 2954.68 cm^{-1} . Carbonyl stretching from the esterified ester and the conjugated ketone at C3 were identified at 1732.78 cm^{-1} and 1714.41 cm^{-1} respectively. Alkene C-H stretches from the pregnane backbone were identified at 1657.87 cm^{-1} , 1643.66 cm^{-1} , 1614.72 cm^{-1} and 1601.54 cm^{-1} with C-H bending at 1455.81 cm^{-1} . These bands serve as characteristic features for comparison with loaded ethosomes.

HCA loaded ethosomes had a FTIR profile similar to that of unloaded ethosomes with a 2 distinct differences in the characteristic bands. Firstly, the band identified at 3285.8 cm^{-1} appeared as a weak broad doublet with a shift from 3373.13 cm^{-1} to 3285.80 cm^{-1} . This may have indicated an interaction between N-H and O-H as these bands are located within the 32550 - 3200 cm^{-1} wave numbers. Typically, primary amines display two distinct weak-medium bands at 3400 - 3300 cm^{-1} and 3330-3250 cm^{-1} . However an O-H stretch occurring between 3550 - 3200 cm^{-1} may also be identified within this region. Thus, exact the

functional group interaction remains unclear but is apparent. Secondly, an alkene C=C stretch is evident at 1671.77. The appearance of a new peak may be evident of a molecular interaction. It is also notable that aforementioned C=C stretches occurred at lower wave numbers. The resultant increase wave number may be indicative of a loss in mass or a decrease in bond length, possibly due to a neighbouring electronegative atom. The absence of characteristic HCA bands is evidence of encapsulation of HCA within the phospholipid.¹⁰

7.7. Hot stage microscopy analysis of BMV loaded and HCA loaded ethosomes

HSM was used as a qualitative tool to observe phase transitions and other thermal events useful in characterising ethosomes. First the pure components (PC, BMV and HCA) were analysed, followed by the unloaded ethosomes and finally the loaded ethosomes. The results of each were compared to determine how the materials were interacting with one another and to determine the thermal profile of the synthesised ethosomes. The HSM data was used in conjunction with other quantitative thermoanalytical tools to identify the thermal events that were quantified using TGA and DSC.

PC had a visually eventful HSM profile. It is important to note that PC was stored in a freezer (-4 °C) to maintain its granulated form in which it was provided. On commencement of the run, an immediate change in turbidity was observed from room temperature until 90 °C. The PC became more transparent and decreased in viscosity. At 90 °C, bubbles gradually started to appear, indicating the presence of a solvent. No change in rate of bubbling was observed between 90 – 140 °C. This may have indicated the absence of or negligible concentration of moisture. At 140 °C, vigorous bubbling occurred indicating a phase transition from liquid to gaseous phase. Although bubbling continued for the entire duration of the run (250 °C), degradation was observed from 230 °C.

The unloaded ethosomes contained PC, H₂O and ethanol. By their classification, ethosomes contain a hydroethanolic core and, subsequently, it was expected that the solvent solution would be liberated as the structural integrity of the ethosomes decreased with the increased temperature. The boiling point of ethanol is approximately 78 °C and water boils at 100 °C. However, no structural changes were observed between room temperature and 150°C. At 150°C there was liberation of a gas which appeared as a faint glow which increased in intensity with increased temperature.

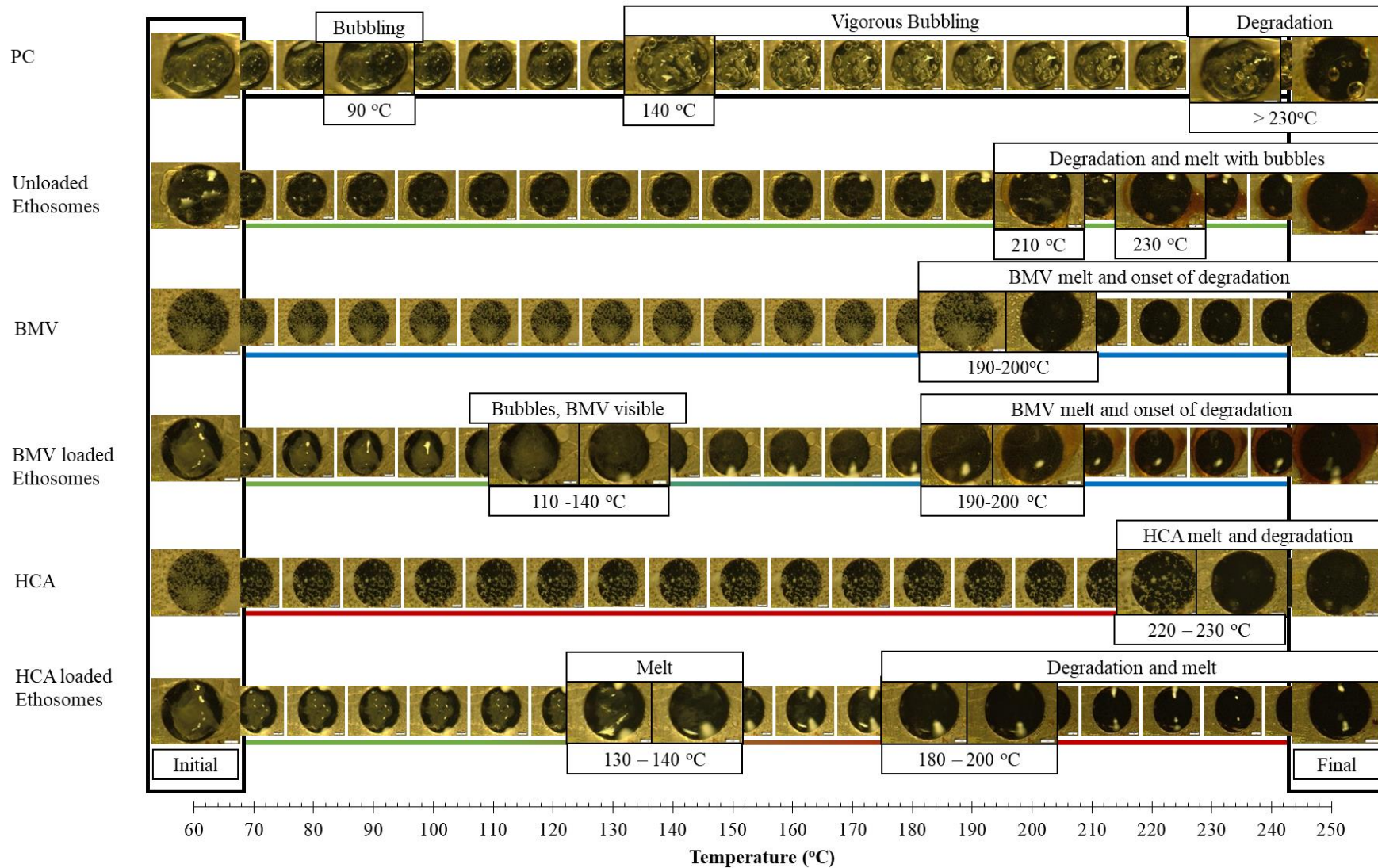


Figure 7.7-1: HSM analyses displaying observed thermal events and the corresponding temperatures for betamethasone valerate (BMV), hydrocortisone acetate (HCA), phosphatidylcholine (PC), unloaded ethosomes, BMV loaded and HCA loaded ethosomes.

Onset of melting occurred at 210 °C where a phase transition from solid to liquid occurred. Degradation of the ethosomes commenced at 230 °C where a colour change from opaque to brown was observed.

According to literature, BMV melts at about 192 °C, with decomposition.⁷³ As shown in **Figure 7.7-1**, no physical change was observed between the starting temperature and 190°C. There are no bubbles present, indicating the absence of moisture. This was expected as BMV is a hydrophobic compound with poor aqueous solubility. An onset of melting of BMV was then observed between 190 – 200 °C with a colour change to dark brown. This indicated that the BMV had degraded. The results observed in this experiment complied with literature.⁷³

BMV loaded ethosomes had an opaque macroscopic appearance, relative to the unloaded ethosomes. No physical change was observed from room temperature to 110 °C. As the temperature increased from 110-140 °C, bubbling occurred. The bubbles suggest the liberation of the hydroethanolic phase. The increased boiling point temperature relative to the pure sample occurred as a result of encapsulation of the solvent. Accompanied by the liberation of a gas, BMV also became visible within this temperature range which agglomerated with increased temperature. The liberation of the gas continued until completion of the run. BMV melted at 190 - 200 °C with an immediate colour change observed, indicating concomitant degradation. The thermal behaviour of BMV within the loaded ethosomes corresponded well with the pure BMV. This indicates that the integrity of the BMV had not been compromised.

According to literature, HCA has a melting point of about 220 °C with decomposition.⁷³ As shown in **Figure 7.7-1**, no physical changes were observed from room temperature until 220 °C. The absence of bubbling indicated that no moisture was extruded from the sample. An onset of melting occurred at 220 °C until completion at 230 °C. The onset of melting corresponded with literature. However, degradation was not observed as there was neither colour change nor a spontaneous bubbling of the sample.

HCA loaded ethosomes presented an opaque semi solid at room temperature. Once the temperature increased, the sample decreased in volume and became more transparent. This indicated that a glass transition occurred resulting in an onset of melting at 130 °C. Compared to the thermal profile of unloaded ethosomes, which exhibits liberation of a solvent at 150 °C, HCA loaded ethosomes exhibits a thermal event at a lower temperature. However, vigorous

bubbling was not observed with HCA loaded ethosomes. Instead, a melt occurred from 130 - 140 °C. On completion of the melt, the sample exhibited a gas which was identified as a yellow glow on the microscopic image. The PC within the ethosome continued to melt with the appearance of bubbles until 180 °C, suggesting degradation of the PC. At 180 °C, the HCA, which appeared as a white powder suspended within the melted PC, commenced with melting. This temperature was much lower than the reported melting point (about 220 °C) in literature.⁷³ The onset of degradation occurred simultaneously, with a distinct colour change from transparent to a dark brown. At 220 °C, the HCA had completely melted with gas being emitted suggesting sublimation of the sample and completion of analysis.

7.8. Differential scanning calorimetry

Dried CM unloaded and GC loaded ethosomes were analysed using differential scanning calorimetry (DSC) to characterise ethosomes and the respective pure components in solid state. Used in conjunction with HSM, DSC provided detailed information regarding the physical and energetic properties of these components (**Figure 7.8-1**).

PC exhibited no physical change before 150 °C. Due to its polymeric complexity, the melting point of PC is unknown. However, prior analysis using HSM indicated the presence of vigorous bubbling at 140 °C. The thermographic profile using DSC did not indicate the presence of a characteristic melting point. Instead, 3 endothermic peak were identified at 157.20 °C, 174.27 °C and 192.00 °C with corresponding heat flows of 3.4936 mW, 4.5990 mW 5.4382 mW respectively.

Similar to PC, unloaded ethosomes displayed no physical change before 150 °C. At 166.40 °C a small peak was identified. However, it was too small to be quantified w.r.t heat flow. Supported by HSM events identified from 150 °C, this small peak was most likely associated with an onset of degradation.

Upon analysis of BMV, the absence of thermal events prior to 190 °C validated its purity. An endothermic peak (196.98 °C - 11.7570 mW), indicative of a melt, appeared with its onset at 195.31 °C and ended 198.12 °C. The peak had an area of 67.9681 mJ with a Delta H of 61.2326 J/g. Degradation was identified at ~ 218 °C. This corresponded to the melting point of BMV (~192 °C) with reported degradation in literature.⁷³ These results can be

corroborated by the HSM results which showed degradation with a colour change from white to dark brown at 220 °C.

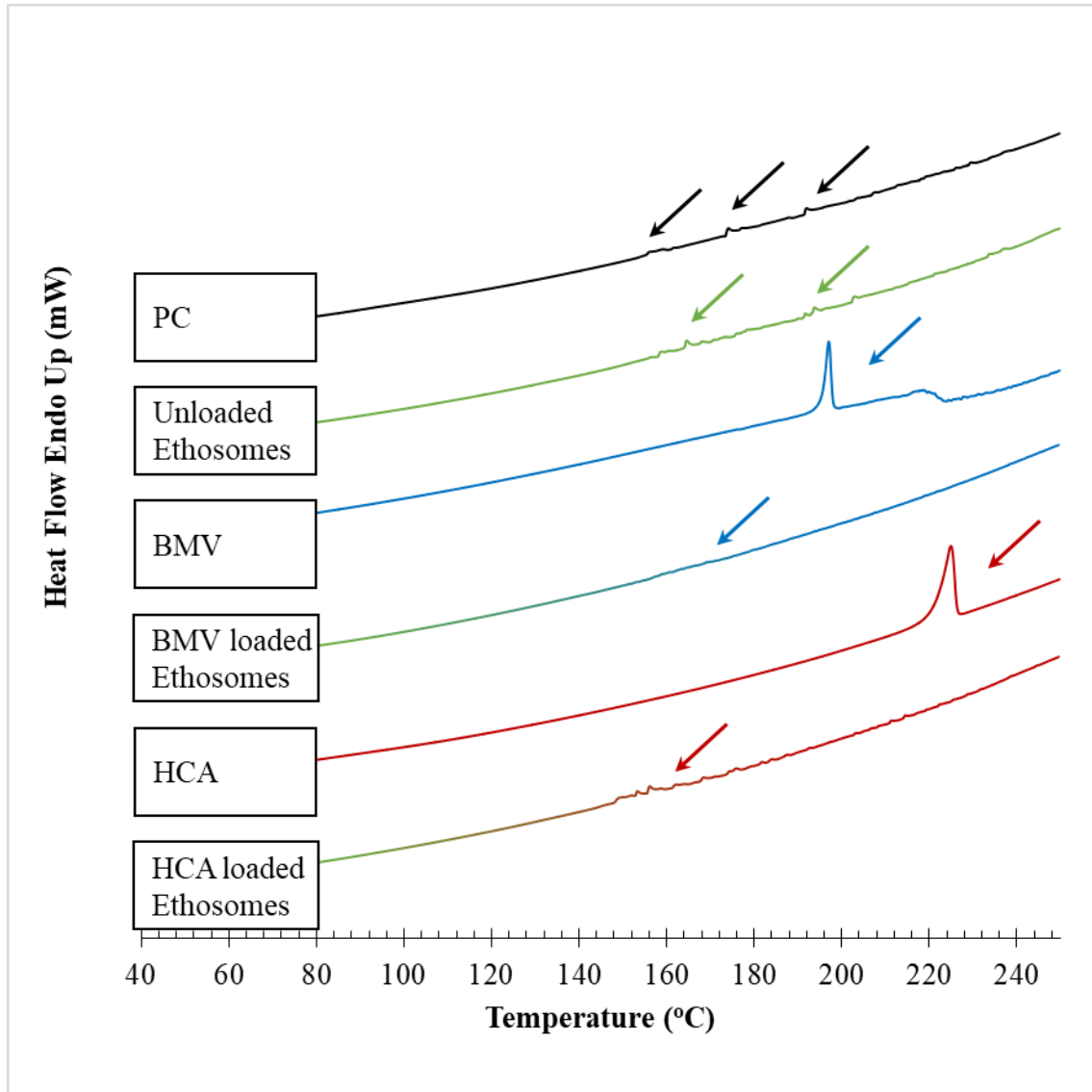


Figure 7.8-1: DSC analyses of betamethasone valerate (BMV), hydrocortisone acetate (HCA), phosphatidylcholine (PC), unloaded ethosomes, BMV loaded and HCA loaded ethosomes. The arrows correspond to the thermal events that were identified in the samples.

BMV loaded ethosomes were uneventful. HSM analysis indicated the liberation of moisture at 110 °C. However, DSC analyses did not show this. The absence of this may have been unquantifiable due to the low moisture concentration. A notable finding was the absence of the characteristic BMV endothermic peak. This is indicative of BMV encapsulation.

HCA had no physical change before 220 °C. HCA has a melting point of ~ 220 °C.⁷³ An endothermic peak, characteristic of a melt was identified at 224.88 °C (23.0770 mW) with an onset of 221.21 °C and ending at 226.44 °C. The peak had an area of 133.8715 mJ and of Delta H 96.3104 J/g

HCA loaded ethosomes showed the presence of thermal excitation at 145 – 175 °C which appeared as small peaks within that temperature range. Although too small to be quantified, the peaks corresponded with the vigorous bubbling identified using HSM analysis. The absence of the characteristic HCA endothermic peak suggests the encapsulation of HCA

7.9. Thermogravimetric analysis

Thermogravimetric analysis (TGA) was used to identify the changes in thermal stability. This analytical tool was used in conjunction with the qualitative data generated from HSM to quantify the thermal events observed in terms of the effect of the percentage mass loss of the sample. As with HSM, the pure components were first analysed and were used as a reference for unloaded ethosome and GC-loaded ethosome comparison. To determine the percentage mass loss over time, the 1st derivative was calculated using Pyris™ Software (**see Appendix A**). Using this data in conjunction with the thermograms, the thermal profile of the unloaded ethosomes, GC loaded ethosomes and their respective pure components were characterised.

The PC is made up the bulk of a phospholipid bilayer serving as a control for comparison. PC exhibited 3 thermal events accounting for 86.00 % weight loss. First, a minor mass loss (13.126 %) occurred between 250-320 °C. The second event (64.02 % mass loss) occurred at 344.27 °C and third event, accounting for 8.86 % mass loss, occurred at 360.69 °C. The respective % weight loss rates of the three events were 2.972, 22.072 and 2.037 weight/min suggesting that PC degraded rapidly between 320-380 °C. The final residue of the sample was 7.015 % weight.

Unloaded ethosomes exhibited 4 thermal events at 289.49, 351.38, 374.86 and 451.16 °C, accounting for a total 87.62 % weight loss. A significant % weight loss of 53.35 % weight was lost between 320 – 390 °C. Complemented by the 1st derivative data, 2 distinct % weight loss steps were identified at 350.94 °C and 374.86 °C with % weight loss rates of 22.017 and 14.913 % weight/min respectively. A residue of 12.755 % remained at the end of the experiment at 600 °C.

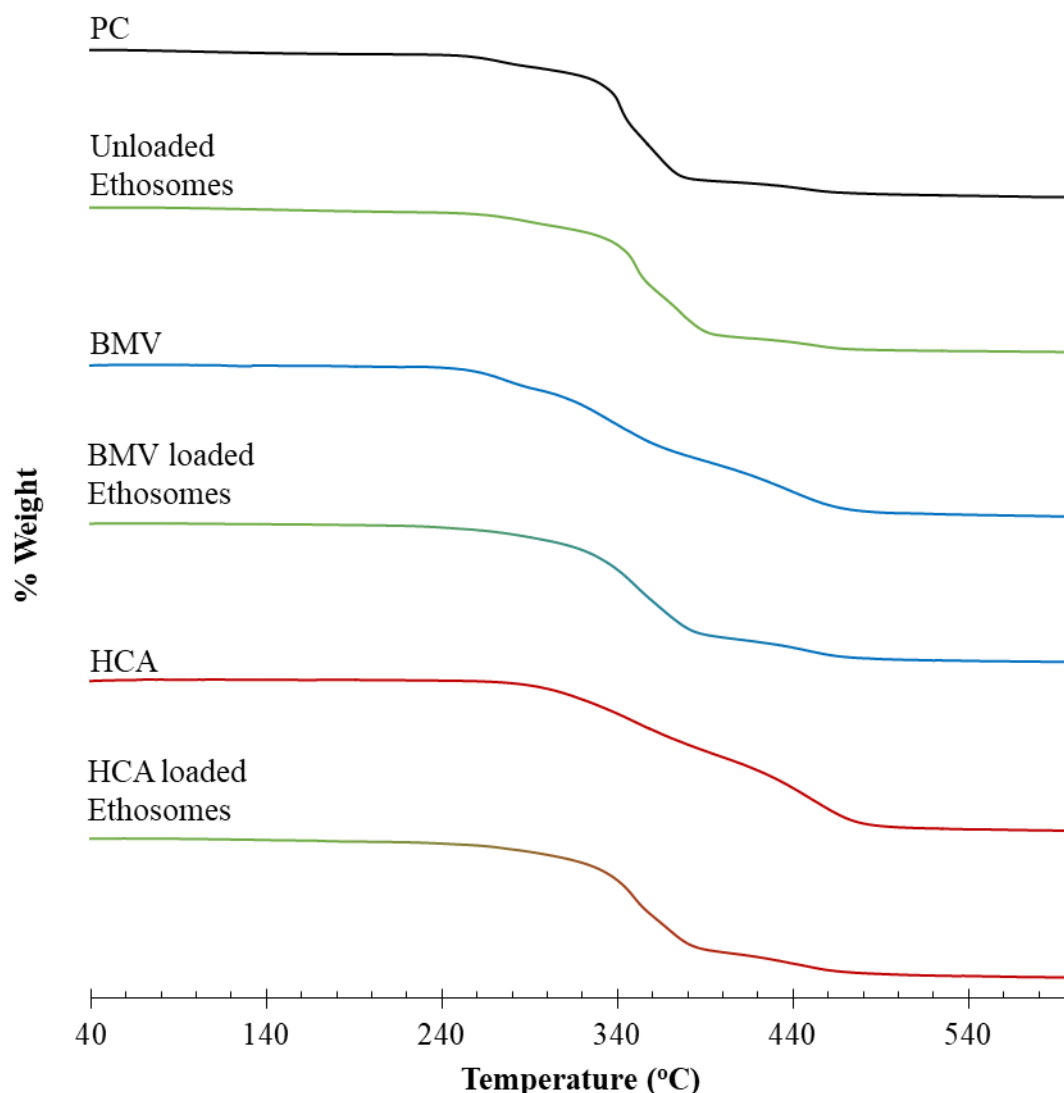


Figure 7.9-1: TGA analyses of betamethasone valerate (BMV), hydrocortisone acetate (HCA), phosphatidylcholine (PC), unloaded ethosomes, BMV loaded and HCA loaded ethosomes.

According to literature, the vesicles are comprised of a hydroethanolic core encompassed by a phospholipid bilayer.¹ **Figure 7.9-1** suggests that PC and the unloaded ethosomes have a TGA profile. The difference in their respective profiles lies in their rates of decomposition as well as the % weight of the residue remaining after completion of the experiment. PC analysis showed that the bulk of the weight was lost between 320 - 380 °C, whereas the unloaded ethosomes bulk weight loss appears 10 °C further between 320 and 390 °C. It was also noted that 64.10 % and 53.35 % were lost over these respective temperature ranges. Notably, the components of the hydroethanolic core i.e. H₂O and ethanol, were not detected

as indicated by the absence of significant weight losses at their respective boiling points of 76 °C and 100 °C. This may have been due to their relative concentrations present after drying.

BMV was characterised by 3 events where a change in the slope of the curve was identified between the temperature range of 250 °C – 480 °C. The temperatures at which these events occurred were at 288.42, 337.51, 436.58 °C with respective rates of mass loss of 6.027, 20.011 and 2.267 % weight/min. The fastest rate of mass loss occurred between 310 and 370 °C. At completion of the experiment, 4.950 % mass of residue remained.

BMV loaded ethosomes had 2 thermal events occurring between 250 – 460 °C accounting for 79.90 % weight loss. The first weight loss, occurring at a rate of 14.621 % weight/min, accounted for 65.784 % weight loss. The second event occurred between 390 – 470 °C and accounted for 14.12 % weight loss. A total residue of 13.309 % remained at 600 °C. Compared to the thermal profile of the pure components (PC and BMV), it was evident that weak molecular interactions had occurred. The number of events had reduced to 2, with the greatest significance being the absence of the third peak evident when comparing PC and the unloaded ethosomes. Compared to the profile of pure BMV, it was noted that the initial mass loss occurred a higher temperature.

HCA was characterised by 2 events where a change in the slope of the curve was identified between 250 °C – 480 °C. The temperatures of these 2 events occurred at 350.31 and 449.56 °C with respective rates of mass loss of -7.590 and -9.746 % weight/min. The fastest rate of mass loss occurred between 410 and 480 °C, with 6.048 % residue left at completion of analysis.

HCA loaded ethosomes had 2 thermal events occurring between 260 – 460 °C accounting for 86.876 % weight loss. The first weight loss, occurred at 15.869 % weight/min, accounted for 78.224 % weight loss. The second % weight loss between 380 – 460 °C accounted for 8.652 % weight. A total residue of 6.716 % remained at 600 °C. Compared to the thermal profile of the pure components (PC and HCA), the temperature range for degradation had decreased. This may have been indicative of intermolecular interactions which increased the ionic strength of the interactions resulting in an increase in degradation onset. Although the number of thermal events did not change, the temperature range at which these events occurred had shifted. Compared to the profile of pure BMV, it was noted that the initial mass loss occurred at a similar temperature. This may have been due to the presence of HCA which had been

liberated from the ethosomes, either as a result of instability during storage or due to reduced membrane integrity after lyophilisation.

According to literature, the vesicles are comprised of a hydroethanolic core encompassed by a phospholipid bilayer.¹ **Figure 7.9-1** suggests that PC and the unloaded ethosomes have a TGA profile. The difference in their respective profiles lies in their rates of decomposition as well as the % weight of the residue remaining after completion of the experiment. PC analysis showed that the bulk of the weight was lost between 320 - 380 °C, whereas the unloaded ethosomes bulk weight loss appears 10 °C further between 320 - 390 °C. It was also noted that 64.10 % and 53.35 % were lost over these respective temperature ranges. Notably, the components of the hydroethanolic core i.e. H₂O and ethanol, were not detected as indicated by the absence of significant weight losses at their respective boiling points of 76 °C and 100 °C. This may have been due to their relative concentrations present after drying.

BMV was characterised by 3 events where a change in the slope of the curve was identified between the temperature range of 250 °C – 480 °C. The temperatures at which these events occurred were at 288.42, 337.51, 436.58 °C with respective rates of mass loss of 6.027, 20.011 and 2.267 % weight/min. The fastest rate of mass loss occurred between 310 and 370 °C. At completion of the experiment, 4.950 % mass of residue remained.

BMV loaded ethosomes had 2 thermal events occurring between 250 – 460 °C accounting for 79.90 % weight loss. The first weight loss, occurring at a rate of 14.621 % weight/min, accounted for 65.784 % weight loss. The second event occurred between 390 – 470 °C and accounted for 14.120 % weight loss. A total residue of 13.309 % remained at 600 °C. Compared to the thermal profile of the pure components (PC and BMV), it was evident that weak molecular interactions had occurred. The number of events had reduced to 2, with the greatest significance being the absence of the third peak evident when comparing PC and the unloaded ethosomes. Compared to the profile of pure BMV, it was noted that the initial mass loss occurred a higher temperature.

HCA was characterised by 2 events where a change in the slope of the curve was identified between 250 °C – 480 °C. The temperatures of these 2 events occurred at 350.31 °C and 449.56 °C with respective rates of mass loss of -7.590 and -9.746 % weight/min. The fastest rate of mass loss occurred between 410 °C and 480 °C, with 6.048 % residue left at completion of analysis.

HCA loaded ethosomes had 2 thermal events occurring between 260 – 460 °C accounting for 86.876 % weight loss. The first weight loss, occurred at 15.869 % weight/min, accounted for 78.224 % weight loss. The second % weight loss between 380 – 460 °C accounted for 8.652 % weight. A total residue of 6.716 % remained at 600 °C. Compared to the thermal profile of the pure components (PC and HCA), the temperature range for degradation had decreased. This may have been indicative of intermolecular interactions which increased the ionic strength of the interactions resulting in an increase in degradation onset. Although the number of thermal events did not change, the temperature range at which these events occurred had shifted. Compared to the profile of pure BMV, it was noted that the initial mass loss occurred at a similar temperature. This may have been due to the presence of HCA which had been liberated from the ethosomes, either as a result of instability during storage or due to reduced membrane integrity after lyophilisation.

7.10. HPLC analyses

HPLC was used for quantification of the GC loaded ethosomal formulations. To ensure validity of the methods sourced from literature, the methods were validated using ICH guidelines.¹⁶⁰ HPLC stock solutions for BMV and HCA were prepared and analysed using the HPLC method described in *Chapter 5*.

7.10.1. BMV chromatogram analysis

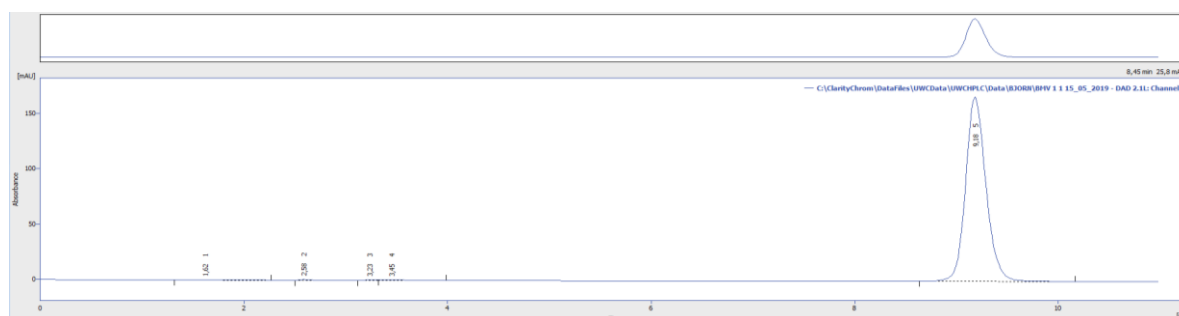


Figure 7.10-1: The HPLC chromatogram of BMV showing the betamethasone valerate (BMV) analyte peak at a retention time of approximately ~9.1 min.

BMV (**Figure 7.10-1**) had a retention time of 9.067 ± 0.01 min with 98.9 ± 0.02 % AUC. The relative area of BMV is indicative of the purity of the sample. As shown in **Table 7.10-1**, the peak resolution was >2 which indicated that it was well separated from other detectable peaks. Tailing factor was <2 which indicated that the sample was well retained on the

stationary phase and that the column was not overloaded with sample. All runs were performed in triplicate (n=3)

Table 7.10.1-1: The chromatographic profile data of betamethasone valerate (BMV) (n=3)

# Peak	Retention Time (min)	Area (mAu)	Area (%)	Asymmetry	Resolution	Symmetry/Tailing
1	1.617	7.530	0.3	2.133	0	1.559
2	2.583	3.956	0.2	1.750	3.111	1.750
3	3.233	3.712	0.2	1.000	3.540	0.857
4	3.450	11.149	0.5	2.375	0.667	2.250
BMV	9.183	2381.022	98.9	1.273	14.497	1.154

7.10.2. HCA Chromatogram

HCA (**Figure 7.17**) displayed a retention time of 3.22 ± 0.012 min with 95.9 ± 0.05 % AUC. The AUC of HCA showed purity of the sample. In **Table 7.5**, the peak resolution was >2 and tailing factor was <2 suggesting well separated peaks, good retention on column and no sample overloading. All runs were performed in triplicate (n=3)

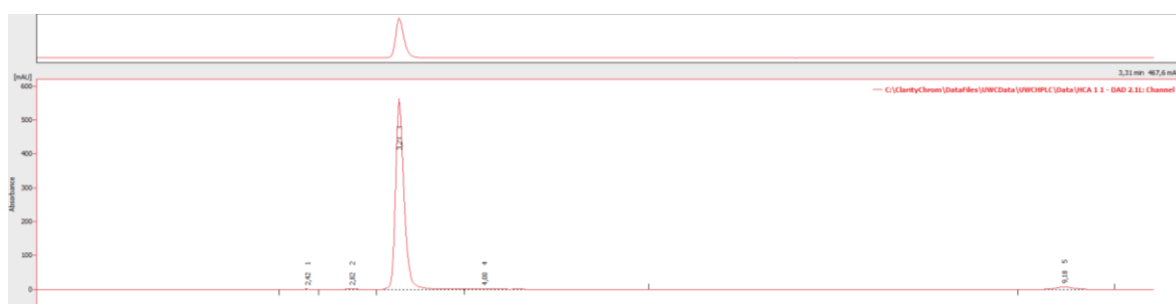


Figure 7.10.2-1: HPLC chromatogram of hydrocortisone acetate (HCA) showing an HCA analyte peak at a retention time of approximately-3.2 min.

Table 7.10.2-1: The chromatographic profile data of hydrocortisone acetate (HCA) (n=3)

# Peak	Retention Time (min)	Area (mAu)	Area (%)	Assymetry	Resolution	Symmetry/Tailing
1	2.41	3.87	0.1	1500		1.100
2	2.81	12.89	0.4	1.333	2.23	0.861
HCA	3.23	3549.33	95.6	1.500	2.26	1.300
4	4.00	37.42	1.2	4.909	1.87	3.591
5	9.18	82.68	2.7	1.200	10.19	1.083

7.10.3. Linearity

Linearity data was obtained by changing the injection volume to: 2.5 µL, 1 µL, 0.5 µL, 0.2 µL, with 1 µL taken as the theoretical 100 % value. All runs were performed in triplicate (n=3). The standard curve equations obtained were:

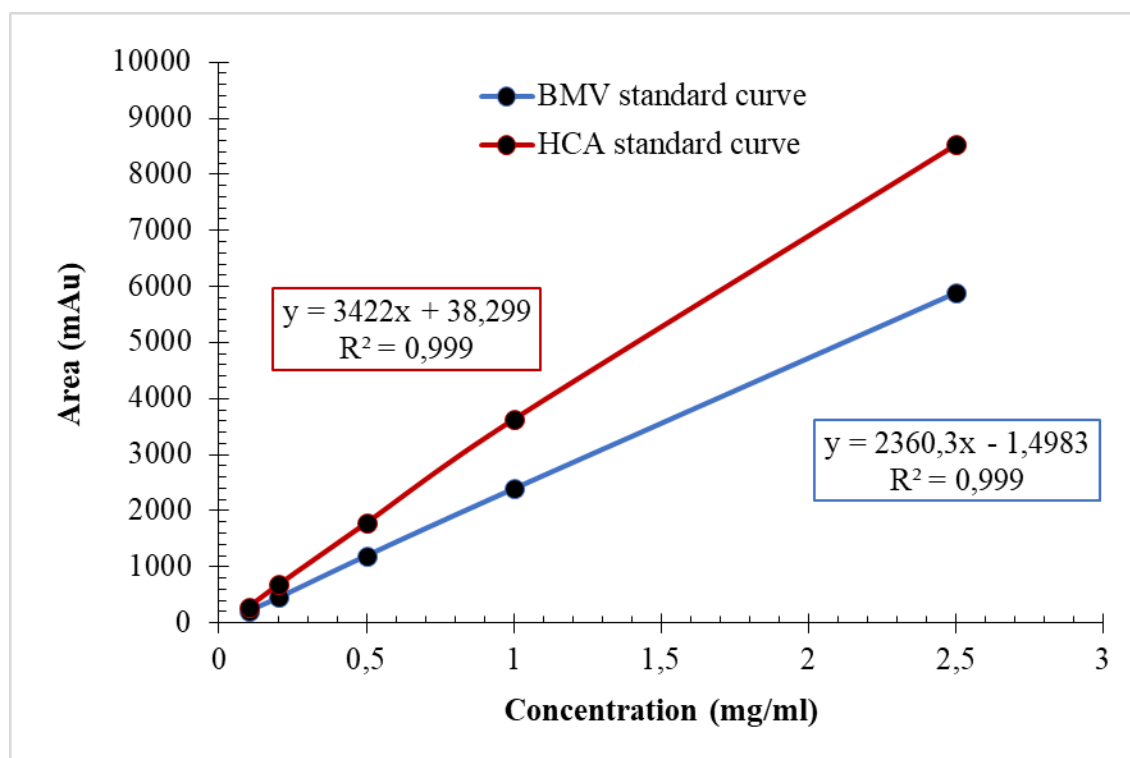


Figure 7.10.3-1: Linearity curves of betamethasone valerate (BMV) and hydrocortisone (HCA).

$$y = 2.360.3x - 1.50$$

Equation 10: Standard curve of BMV

$$y = 3422.0x - 38.30$$

Equation 11: Standard curve of HCA

Where:

y = area (mAu)

x = concentration (mg/ml)

The slope, y-intercept, and correlation co-efficient were obtained by using the “trendline” option in *Microsoft Excel* coupled with the regression analysis function. **Figure 7.10.3-1** shows that both BMV and HCA had a correlation co-efficient of 0.999. This indicated that a correlation of 0.1% could be made using the constructed curve to quantify the concentrations of GCs in unknown samples using their respective standard curves. Between the specified concentration ranges, an acceptable linearity was obtained according to ICH guidelines.¹⁶⁰

7.10.4. Specificity

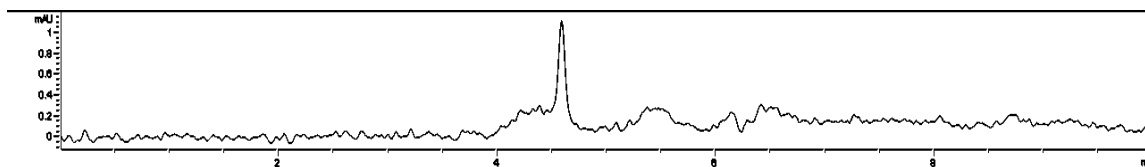


Figure 7.10.4-1: Chromatogram of mobile phase (acetonitrile: H₂O = 60:40)

The elution of the mobile phase (acetonitrile:H₂O = 60:40) indicated that there was no significant overlapping of peaks at the retention times of the GCs. A peak was identified at 4.5 min (**Figure 7.10.4-1**). However, it did not correspond to the elution times of neither BMV (9.1 min) nor HCA (3.2 min). This indicated that the mobile phase was suitable for the analytes eluted using the specified HPLC method and that it did not interfere with their quantification.

7.10.5. Intraday precision (Repeatability) and accuracy

Table 7.10.5-1: Repeatability and accuracy of betamethasone valerate (BMV) and hydrocortisone acetate (HCA) at a concentration of 1 mg/ml

BMV sample	Peak area (mAu)	Calculated recovery (mg)	% recovery	HCA sample	Peak area (mAu)	Calculated recovery (mg)	% recovery
1	2393,41	1,00	99,81	1	3630,77	0,99	98,81
2	2368,86	0,99	98,79	2	3637,37	0,99	98,99
3	2378,74	0,99	99,20	3	3660,61	1,00	99,61
4	2390,59	1,00	99,69	4	3650,93	0,99	99,35
5	2396,94	1,00	99,95	5	3642,92	0,99	99,14
6	2358,31	0,98	98,36	6	3649,64	0,99	99,31
Average	2381,14	0,99	99,30	Average	3645,37	0,99	99,20
SD	15,28	0,01	0,63	SD	10,62	0,00	0,28
% RSD	0,64	0,63	0,63	% RSD	0,29	0,28	0,28

$$\%RSD = (SD/average) \times 100$$

BMV and HCA were each analysed (n = 6) at the theoretical 100% (1mg/ml) value. Each GC sample was injected at the theoretical 100% value (1mg/ml). Using the linearity curves constructed in (7.10.3-1), the mean, standard deviation, % relative standard deviation (%RSD) and % recovery were calculated (Table 7.10.5-1). According to ICH guidelines, the limits of recovery should be within 98 – 102 %.¹⁶⁰ The % recovery was 99.20 % and 99.30 % for BMV and HCA respectively. The results were acceptable as they fell within the acceptable range. This indicated that the results obtained were reproducible over a short period of time using the specified HPLC method.

Accuracy was based on ratio of the measured quantity (1mg/ml) to the calculated quantity. The % RSD, which should not be more than 2%¹⁶⁰, was compared to evaluate the accuracy of the method. The % RSD was 0.64 % and 0.28 % for BMV and HCA respectively, indicating that both GCs passed the accuracy test.

7.10.6. Inter-day precision

Table 7.10.6-1: Inter-day precision of betamethasone valerate (BMV) and hydrocortisone acetate (HCA) (n=3)

		CONCENTRATION (MG/ML)		
		0,1	0,5	1
BMV	Day 1	186,59	1188,34	2393,40
	Day 2	188,16	1166,50	2368,85
	Day 3	191,37	1150,62	2378,73
	Average	188,70	1168,49	2380,33
	SD	2,43	18,94	12,35
	% RSD	1,29	1,62	0,51
	HCA	Day 1	287,27	1785,18
Day 2		281,58	1768,96	3537,37
Day 3		288,14	1787,37	3560,61
Average		285,66	1780,503	3542,91
SD		3,56	10,05824	15,67
% RSD		1,24	0,56	0,44

$$\%RSD = (SD/average) \times 100$$

The inter-day precision was validated using the method discussed in **Chapter 5**. The % RSD was calculated and the results of the study are shown in **Table 7.7**. The results show that BMV had %RSDs of 1.29, 1.62 and 0.51 % for concentrations of 0.1, 0.5 and 1 mg/ml, respectively. HCA had % RSDs of 1.24, 0.56 and 0.44 % for concentrations of 0.1 0.5 and 1 mg/ml, respectively. All % RSDs were within the acceptable limits of < 2 %, indicating that the results were reproducible over 3 days.

7.10.7. Limit of detection and Limit of quantification

For both BMV and HCA, the limit of detection (LOD) and limit of quantification (LOQ) was calculated using **Equation 5** and **Equation 6**, respectively. The results, determined using the standard curve equations generated for linearity, are displayed in **Table 7.8**. Both GCs had a lower limit of detection and quantification of 0.002 mg. This suggested that any values obtained that were < 0.2 % of the 1 mg/ml samples would be unquantifiable using the obtained standard curves.

Table 7.10.7-1: Limits of detection and quantification of betamethasone valerate (BMV) and hydrocortisone acetate (HCA) (n=3)

BMV			HCA	
	Peak area (mAU)	Mass (mg)	Peak area (mAU)	Mass (mg)
LOD	0.055	0.002	0.0951	0.002
LOQ	0.168	0.002	0.288	0.002

LOD = limit of detection, LOQ = limit of quantification

7.10.8. Robustness

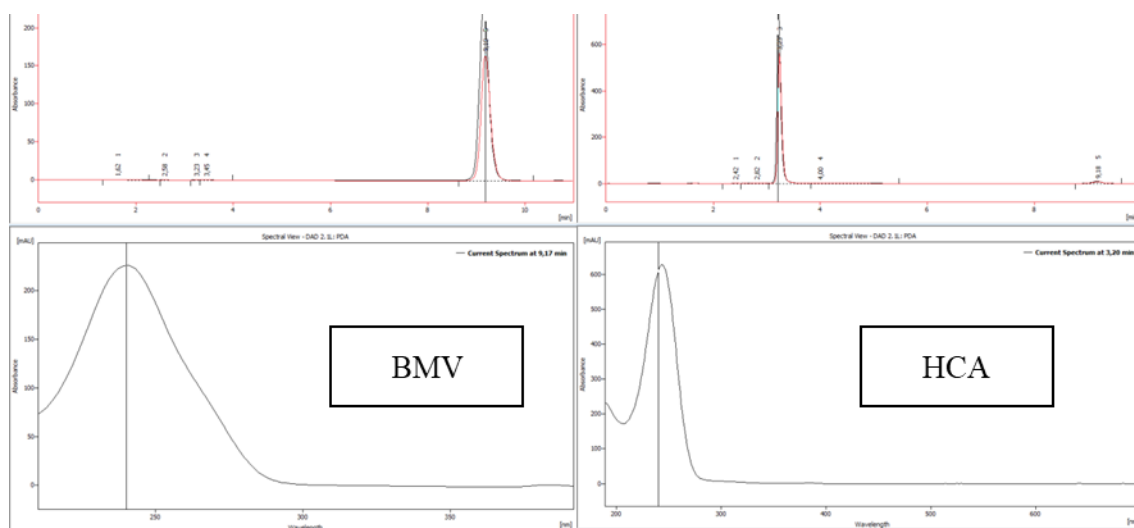


Figure 7.10.7-1: Chromatograms of betamethasone valerate (BMV) and hydrocortisone acetate (HCA) showing the effect of change in wavelength on detection of the analyte. The initial wavelength (254 nm) is shown as a red chromatogram; the altered wavelength (240 nm) is shown as a black chromatogram.

Due to the presence of a PDA detector all samples were scanned from 190 – 700 nm on the *Knauer Azura* HPLC system. In the process of determining robustness, it was identified that the change in wavelength from 254 to 240 nm whilst maintaining the other chromatographic conditions, increased the area under the curve of the chromatograms at the retention times of the analyte of interest. This discovery allowed for the detection of greater amounts of analyte, and subsequent improved quantification limits for lower concentrations. As such, the HPLC methods were optimised to use 240 nm instead of 254 nm as stated in the BP.⁷³

7.11. Drug loading and Encapsulation efficiency

Table 7.11-1: The encapsulation efficiency (EE) and drug loading (DL) of betamethasone valerate (BMV) and hydrocortisone acetate (HCA) loaded ethosomes (n=2)

Formulation	Ethosome mass (g)	API direct (mg/2 ml)	API in Supernatant (mg/ 1.5 ml)	API in 2 ml (mg)	EE (%)	DL (%)	% API recovered
Unloaded ethosomes crude	1,93	N/A	N/A	N/A	N/A	N/A	N/A
Unloaded ethosomes extruded	1,92	N/A	N/A	N/A	N/A	N/A	N/A
BMV loaded ethosomes crude	1,94	1,37	0,61	1,97	69,25	13,85	98,67
BMV loaded ethosomes extruded	1,91	1,56	0,53	2,10	74,57	14,91	104,86
HCA loaded ethosomes crude	1,94	0,59	1,08	1,67	35,22	7,04	83,59
HCA loaded ethosomes extruded	1,95	0,70	1,18	1,88	37,30	7,46	94,21

HCA and BMV were quantified using calibration curves generated using the validated HPLC method. Samples were prepared as described in *Chapters 5*. Using the data generated from the standard curves to determine the mass of the APIs, the encapsulation efficiency (EE) and drug loading (DL) were calculated using **Equations 8 and 9** respectively.

As seen in **Table 7.11-1**, BMV had an encapsulation efficiency of 69.25 % and 74.57 % for crude BMV loaded ethosomes and extruded BMV loaded ethosomes respectively. This indicated that extrusion increased the % EE for BMV loaded ethosomes relative to the crude formulation. The increase in % EE may have been due to the increase in surface area associated with the decrease in particle size, thus increasing the capacity for BMV within loaded ethosomes. A DL of 13.85 % and 14.81 % was achieved for crude BMV loaded ethosomes and extruded BMV loaded ethosomes respectively. However, crude HCA loaded ethosomes and extruded HCA loaded ethosomes had EEs of 35.22 % and 37.30 % respectively. Although these results, apart from reducing particle size, also support the

rationale for extrusion, the EE was poor relative to BMV loaded ethosomes. This may have been due to the polarity of the compounds. HCA is more polar and is relatively more soluble in ethanol than BMV. HCA had a greater affinity for the hydroethanolic phase, whereas BMV had a greater affinity for the non-polar environment associated with the PC. These differences in the dispersion of the GCs within the ethosomal solvent system influenced the respective EEs.^{166,168}

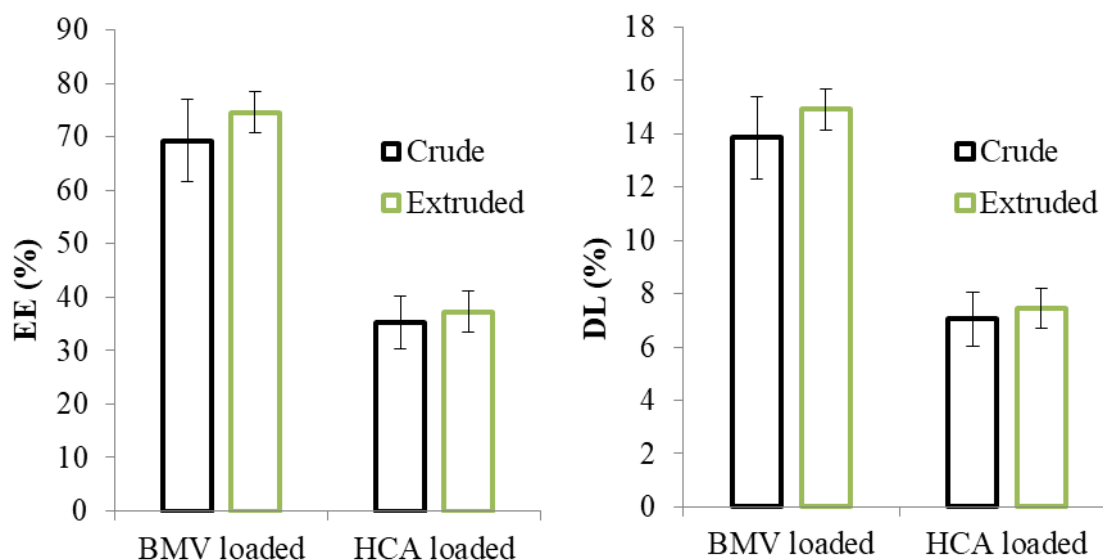


Figure 7.11-1: The encapsulation efficiency (EE) and drug loading (DL) of crude and extruded ethosomes loaded with betamethasone valerate (BMV) and hydrocortisone acetate (HCA).

The drug loading (DL) is an expression of the % of API in the formulation relative to the amount of excipients. Crude BMV loaded ethosomes, extruded BMV loaded ethosomes, crude HCA loaded ethosomes and extruded HCA loaded ethosomes had DLs of 69.25 %, 74.57 %, 35.22 % and 37.30 % respectively (**Figure 7.11-1**). Based on these results, it is evident that extruded ethosomes had a higher DL than their crude counterparts and that BMV had a higher DL compared to HCA. The DL is a parameter that has very little value when used in isolation when characterising a nanoparticle. Used in conjunction with other variables such as the EE, drug release and drug flux it may have more value. It is important to note that, the mass of the solvents were not considered in this expression as their mass is influenced by the drying efficacy and is difficult to quantify. Considering that ethosomes are nano-vesicles with a hydroethanolic core, the mechanism by which the solvent system is removed will influence the mass of the residual moisture. A high DL is favourable when

looking at the cost of production of the ethosomes. Ethosomes were prepared using PC, which is an expensive polymer that constitutes the phospholipid bilayer. Although an increased DL may be favourable economically, it is important consider its effect on other vesicle properties such as membrane flexibility and integrity as well as drug release. A higher DL is also more advantageous when considering the side effect profile of the polymer, as a low DL may lead to an increased risk of polymer toxicity. However, in this scenario, that is not of concern as PC is a biocompatible polymer and establishing its potential risk of toxicity is not in the scope of this study.¹⁰⁰

The percentage of API recovered was tracked to determine the amount of waste during synthesis. These results were obtained by adding the mass of BMV recovered in direct analysis after lysis and induced with the mass of BMV in the supernatant after purification. This is another variable with economic value. The percentage recovery is useful in tracing events of API mass loss or gain which directly influence the % EE. A BMV recovery of 98.67 % and 104.86 % was achieved for crude BMV loaded ethosomes and extruded BMV loaded ethosomes, respectively. BMV mass loss may have occurred upon transfer of the sample, and a gain in mass may have occurred upon reconstitution of the pellet after centrifugation with a lower volume of solvent or an error with dilution. Ethanol, a volatile solvent, may have evaporated, thus rendering samples more concentrated. For this reason, it was important to keep all vials containing ethosomes in suspension tightly sealed. A percentage HCA recovery of 83.59 % and 94.21 % was achieved for crude HCA loaded ethosomes and extruded HCA loaded ethosomes respectively. Less HCA was recovered relative to BMV. Surprisingly, less API was recovered from crude ethosomes relative to extruded ethosomes. It is possible that the formation of smaller, more compact ethosomes may have increased the stability of the encapsulated APIs. It is also possible that extrusion, as a comminution technique, has a direct impact on the DL.

7.12. Conclusion

The objective of the experiments conducted in this chapter was to characterise the ethosomes according to their physical and chemical stability and to determine the influence of corticosteroid loading on the particle size, polydispersity index and zeta-potential. The objective was met by loading ethosomes with BMV and HCA and analysing the loaded samples. DLS results indicated that the size of the loaded ethosomes met the HdD and PdI criteria for topical drug delivery after extrusion. Conversely, sonicated samples did not. As a result, extrusion was employed for the comminution of all subsequent ethosomal formulations. SEM analysis indicated a spherical morphology for CM ethosomes. However, ethosomes prepared using the HM had an irregular shape. The CM was then accepted as a suitable method for the formulation of ethosomes for topical delivery. Encapsulation was confirmed using FTIR and thermoanalyses. The EE and DL was determined for the HCA and BMV loaded samples using a validated HPLC method. HCA loaded samples had a poor EE and DL relative to the BMV loaded samples.



UNIVERSITY *of the*
WESTERN CAPE



School of
PHARMACY

8. Introduction

After determining the effect of corticosteroid loaded ethosomes on mean HdD, PdI and ZP relative to the unloaded ethosomes it was established that their encapsulation maintained the ideal properties for topical drug delivery. A desirable drug loading (DL) and encapsulation efficiency (EE) was achieved for BMV loaded ethosomes but HCA loaded ethosomes required improvement. As such, Cholesterol (Chol) was included into the ethosomal formulations to increase the EE whilst maintaining the ideal properties for topical drug delivery. The unloaded, BMV loaded and HCA loaded Chol ethosomes were characterised to determine the effect of cholesterol on the mean HdD, PdI and ZP relative to the ethosomes without Chol. Additionally, the drug release and release kinetics using mathematical modelling were determined using high performance liquid chromatography (HPLC).

8.1. The effect of cholesterol on the size distribution and zetapotential of unloaded, BMV loaded and HCA loaded Chol ethosomes

Guided by the results achieved in *Chapter 7*, a series of new experimental formulations were prepared using the CM with slight modifications. Relative to the HM, the CM results were more reproducible and reliable. To test the parameters, prepared samples were analysed using dynamic light scattering (DLS) and the results are shown in **Figure 8.1-1** and **Table 8.1-1**. Ideally, the particle size for topical drug delivery is ~200 nm and a PdI < 0.5 indicates an acceptable particle size distribution. A $\zeta_p = \pm 30$ mV is an indication of good stability of an ethosomal colloidal suspension. Crude formulations refer to ethosomes which were analysed directly after synthesis without comminution. Based on the results achieved in *Chapter 7*, extrusion was utilised exclusively for comminution as the results were reliable and reproducible.

Table 8.1-1: The size distribution and zeta potential of unloaded, betamethasone valerate (BMV) loaded and hydrocortisone acetate (HCA) loaded cholesterol (Chol) ethosomes at cholesterol concentrations of 7.5 mg/ml, 10 mg/ml and 15 mg/ml.

FORMULATION	HdD (d.nm)	PdI	Z.P (mV)
Chol _{7.5} crude	521.74±45.95	0.08	-2.71
Chol _{7.5} E	223.21±60.33	0.21	-0.99
Chol _{7.5} HCA E	210.42±55.05	0.21	-1.08
Chol _{7.5} BMV E	167.58±52.55	0.19	-3.29
Chol ₁₀ crude	537.74±40.11	0.66	-2.22
Chol ₁₀ E	224.04±48.18	0.23	-6.96
Chol ₁₀ HCA E	252.91±47.36	0.15	-1.64
Chol ₁₀ BMV E	183.79±37.39	0.11	-1.68
Chol ₁₅ crude	548.12±50.60	0.34	-0.99
Chol ₁₅ E	367.38±74.05	0.25	-1.83
Chol ₁₅ HCA E	247.26±72.10	0.187	-1.87
Chol ₁₅ BMV E	205.68±43.50	0.159	-1.88

BMV = betamethasone valerate, HCA = Hydrocortisone acetate, E = extruded, Crude = no comminution.

Ethosomes had a unimodal size distribution (**Figure 8.1-1**). According to literature, the addition of cholesterol to unloaded formulations results in an increased ethosomal mean HdD.¹⁰¹ The size range (500 - 550 d.nm) of unloaded Chol ethosomes, relative to the size range of ethosomes without cholesterol discussed previously (~300 d.nm), was considerably larger. The size of the unloaded extruded ethosomes reduced by more than 50 %, relative to the crude samples in both formulations containing 7.5 mg/ml and 10 mg/ml. Extruded ethosomes prepared using a higher cholesterol concentration (15 mg/ml), were larger in size relative to the aforementioned formulations. When extruding these ethosomes, the back pressure in the syringe was notable and increased the difficulty of extrusion. This back pressure resulted in slower extrusion, a complete halt of the extrusion process or the rupturing of the extrusion membrane, due to the sheer force.

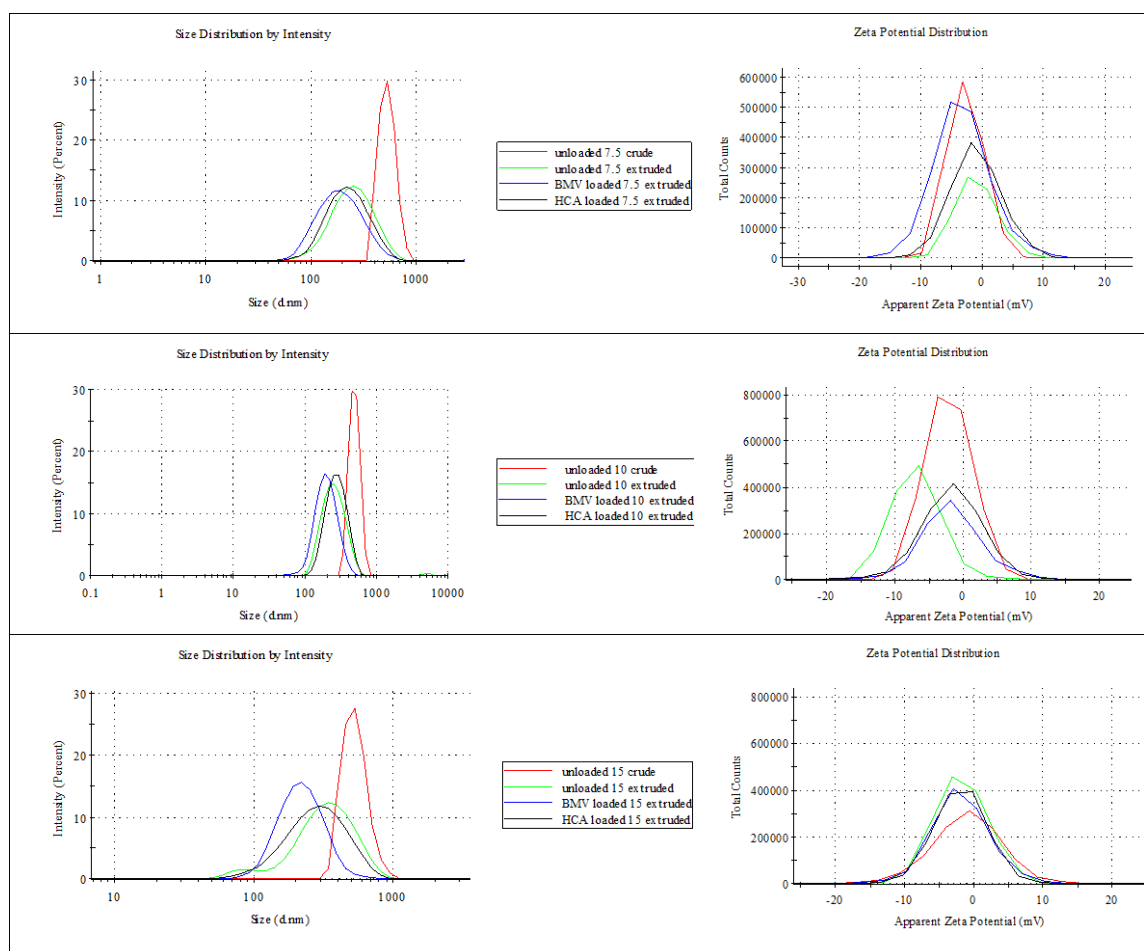


Figure 8.1-1: The size distribution and zeta potential of unloaded, betamethasone valerate (BMV) loaded and hydrocortisone acetate (HCA) loaded cholesterol (Chol) ethosomes at cholesterol concentrations of 7.5 mg/ml, 10 mg/ml and 15 mg/ml.

From a mechanical perspective, this may have indicated that these ethosomes were more rigid in structure and lacked the elasticity of the ethosomes synthesised using the 7.5 mg/ml and 10 mg/ml cholesterol concentration. Possibly owing to the preservation of vesicle flexibility, the results of the mean HdD of ethosomes synthesised using 7.5 and 10 mg/ml cholesterol are similar.

The size of crude ethosomes increased once loaded with either BMV or HCA. However, analysis of extruded ethosomes showed that the inclusion of GCs resulted in a decrease in mean HdD. This trend occurs for all formulations except HCA loaded ethosomes with a cholesterol concentration of 10 mg/ml, where ethosome size increased. It is possible that, due to its relatively greater ethanolic solubility, the HCA may have been present in the bulk medium and that the increased HdD may have been attributed to a greater composition of cholesterol within the ethosome.

8.2. The effect of cholesterol on the PdI of ethosomes

Apart from ethosomes prepared with a cholesterol concentration of 10 mg/ml, the PdI was within the acceptable range of <0.5 , with only the crude 7.5 mg/ml cholesterol formulation possessing a mono-dispersion of <0.1 . With a PdI of approximately 0.67, the crude ethosomes with a cholesterol concentration of 10 mg/ml had an increased size distribution relative to the other concentrations (**Table 8.1-1**). Although extrusion improved the PdI for 10 mg/ml and 15 mg/ml concentrations, the PdI of the ethosomes containing 7.5 mg/ml of cholesterol did not show a size distribution trend similar to the aforementioned concentrations. After extrusion of these ethosomes, the PdI changed from being in an ideal monodisperse state to an acceptable polydispersity. Conversely, the trend of the 10 mg/ml and 15 mg/ml cholesterol formulations were similar. The ethosomes had respective improvement in the PdI after extrusion, after the BMV and HCA loading, respectively. The loading of the APIs influenced the size distribution of ethosomes which may have been due to the fact that they are derivatives of cholesterol and could have influenced the ethosomal morphology by a similar mechanism.

8.3. The effect of cholesterol on the zeta potential of ethosomes

As shown in **Figure 8.1-1**, all of the cholesterol containing ethosomes showed no difference in the ζ_p and maintained stability associated with swift flocculation. (± 5 mV). The

concentrations of cholesterol did not influence the stability of the ethosomes within the colloidal system and agglomeration was apparent. The selection criteria for further analyses were based on ethosomes with the following properties: particle size < 200 nm, PDI < 0.5, $\zeta_p = \pm 30$. Based on these results, a cholesterol concentration of 7.5 mg/ml was chosen based on the smallest particle size and acceptable PDI. The ζ_p findings were documented and discussed but still require optimisation in future studies.

8.4. A comparison of the HdD, PDI and ζ_p of unloaded, BMV loaded and HCA loaded ethosomes, with and without cholesterol

Table 8.4-1: A comparison of the HdD, PDI and ζ_p of unloaded, BMV loaded and HCA loaded ethosomes, with and without cholesterol. ($n=3$)

FORMULATION	HdD (d.nm)	PDI	ζ_p (mV)
Unloaded ethosomes	153,1±32,28	0,14	-4.34
Unloaded Chol ethosomes	223,2±30.325	0,21	-0.994
BMV loaded ethosomes	163,8±31,99	0,11	-3.82
BMV loaded Chol ethosomes	167,5±26.55	0,19	-3.29
HCA loaded ethosomes	147,7±19,91	0,049	-3.31
HCA loaded Chol ethosomes	210,4±17.55	0,021	-1.08

In **Table 8.4-1**, the addition of cholesterol significantly increased the HdD of unloaded ethosomes and HCA loaded ethosomes by 45 % and 42%, respectively. As reported in literature, the increase in particle size may be directly attributed to the addition of cholesterol as an excipient. It was interesting to note that, although cholesterol has been reported to increase the rigidity of ethosomes, the ethosomes were extruded through a membrane with a fixed pore size of 0.1 μm . The effect of cholesterol addition was much more apparent in the laboratory where manual extrusion physically became more difficult. It was expected that the size of the ethosomes would decrease. However, the increase in size may have resulted from the low ζ_p , which lead to agglomeration and subsequently influenced the analysis when using DLS. DLS, as a particle size technique, has its limitations where it is assumed that the sample analysed is spherical. It does not discriminate against different geometries and lamellarity. It is possible that Multivesicular vesicles (MVs) fall in the same limitation bracket. In **Figure 8.1-1**, the size distribution indicates that ethosomes sized < 100 nm are present in the samples

analysed. It is possible that the particle size distribution is thus a reflection of the “stable” agglomeration of such vesicles.

8.5. SEM analysis of corticosteroid loaded Chol ethosomes

Ethosomes were dried for solid state analyses and all subsequent solid-state analyses such as FTIR, HSM, DSC and TGA were conducted using these dried samples. Dried GC loaded ethosomes were analysed using the SEM method to determine the difference in the morphology of the corticosteroid loaded ethosomes after the addition of cholesterol. The intended viable nanovesicles as API carriers for transdermal permeation, a spherical morphological shape is favourable. To compare the influence of cholesterol, GC loaded ethosomes were prepared simultaneously and analysed using SEM (**Figure 8.5-1**).

Analysis of the morphology at different magnification showed that BMV loaded ethosomes had a spherical shape. The appearance of the ethosomes as an agglomeration of spherical nanovesicles corroborates the ζ_p (± 5 mV) which indicates swift flocculation. HCA loaded ethosomes had a spherical shape at higher magnification which indicated that specific areas in the sample had effective signs of encapsulation. At lower magnification showing a more diverse spread of the sample, ethosomes of an irregular shape were observed.

In contrast, the ethosomes containing cholesterol depict a different morphology. BMV loaded Chol ethosomes (**Figure 8.5-1**) appear as multivesicular vesicles (MVVs). Agglomeration of spherical nano vesicles is evident, however, the scale at the highest magnification shows that the vesicles are considerable smaller. This may be corroborated by the DLS findings where this analytical technique is not able to discriminate between MVVs and all sample sizes are based on the premise that the particles are sphericle. This may allude to the notion that optimisation of the ζ_p to ± 30 mV may result in ethosomes of an even smaller size range.

HCA loaded ethosomes had a spherical shape at higher magnification which indicated that specific areas in the sample had effective signs of encapsulation. Lower magnification, showing a more diverse spread of the sample, displayed ethosomes of an irregular shape. This may have indicated that the vesicles were instable and that they ruptured during lyophilisation. As such, it is possible that the drying process requires optimisation.

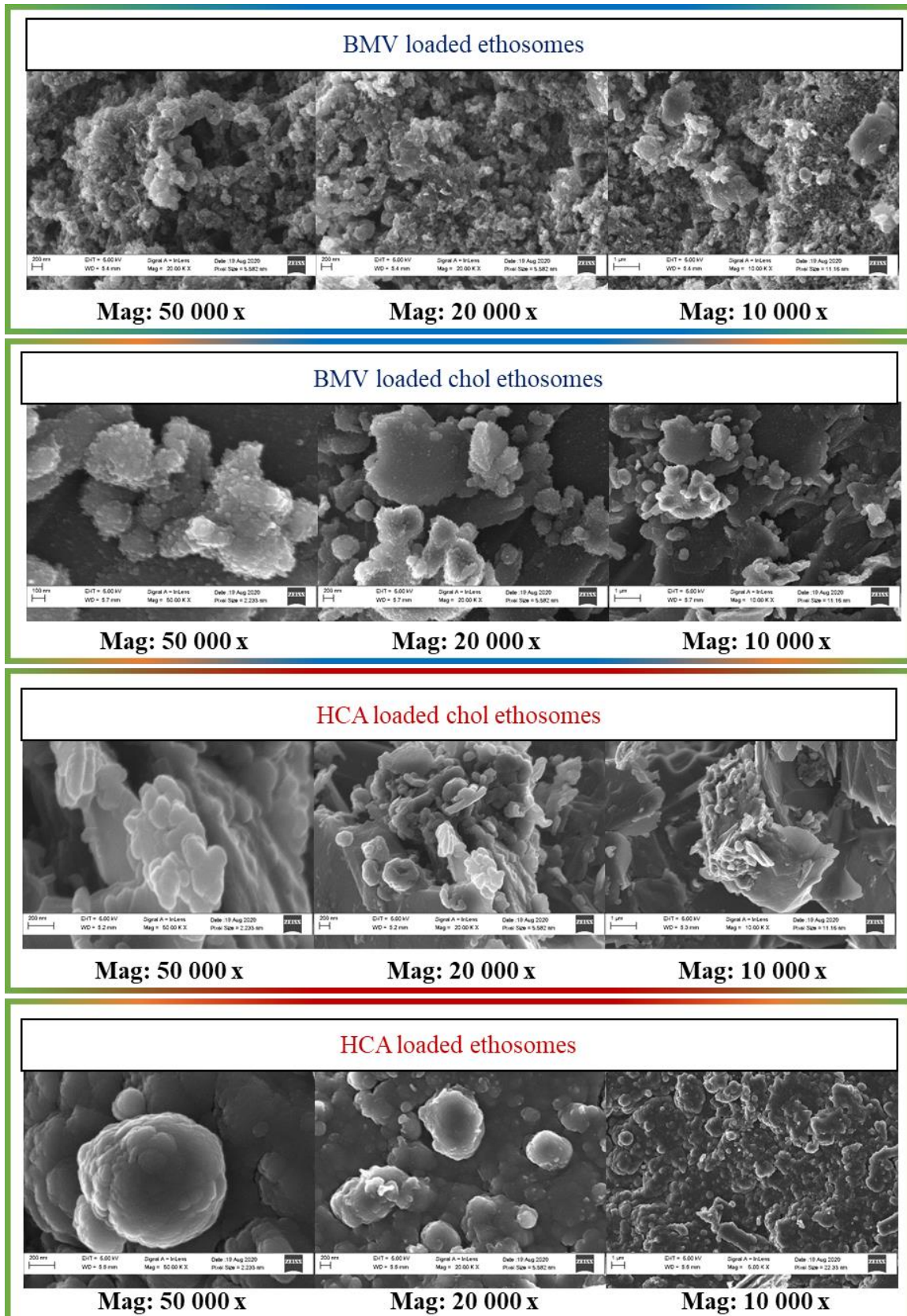


Figure 8.5-1: SEM analyses of betamethasone valerate (BMV) loaded and hydrocortisone acetate (HCA) loaded ethosomes, with and without cholesterol, taken at magnification (Mag).

The addition of cholesterol to produce HCA loaded Chol ethosomes had changed the morphology to produce spherical ethosomes. These ethosomes appeared to be more stable with the absence of recrystallized HCA, as seen in the HCA loaded ethosomes without cholesterol. Overall, it was evident that there was a change in the appearance of the ethosomes after the addition of cholesterol, with BMV loaded ethosomes appearing as BMVs and HCA acquiring a more spherical shape.

8.6. FTIR of analysis of BMV loaded and HCA loaded Chol ethosomes.

FTIR spectroscopy (**Figure 8.6-1**) was conducted to identify the functional groups within the diagnostic region attributed to HCA and BMV loaded Chol ethosomes. The spectrograms were compared with the BMV and HCA loaded ethosomes to identify changes in the intermolecular interactions resulting from the addition of the cholesterol. The samples analysed were from the same batch as the ethosomes prepared for SEM analyses.

Chol ethosomes displayed a weak broad band at 3363.30 cm^{-1} , indicating the presence of O-H/ N-H stretches. Similar to PC findings, these bands corresponded to the N-H stretch on the conjugated ammonium phosphate ion or intermolecular hydrogen bonding. A weak sharp alkene C-H stretch, corresponding to unsaturated carbon chains was identified at 3010.66 cm^{-1} with subsequent strong sharp alkane stretches present at 2924.22 and 2853.77 cm^{-1} . A C=O stretch was identified at 1736.75 cm^{-1} which was attributed to the carbonyl of an ester and the sharp medium peak at 1466.12 cm^{-1} corresponded to alkane C-H bending.

Similar to BMV loaded ethosomes, BMV loaded chol ethosomes displayed a large negative shift in wave number as the O-H/ N-H stretches at 3363.30 cm^{-1} had decreased to 3264.98 cm^{-1} . This large shift in wave number was due to a stronger chemical interaction between the BMV and the PC as they both possess polar electron withdrawing group regions. The large decrease in wavenumber was due to interactions between the electronegative oxygen and fluorine atoms resulting in hydrogen bonds. This resulted in reduced bond length resulting in a higher vibration of the N-H/O-H stretch and a subsequent lower wave number. Similar to BMV loaded ethosomes, a weak C=C stretch appeared at 1669.65 cm^{-1} . This again was indicative of an intermolecular interaction between BMV and PC. Considering that PC was incorporated at a higher % m/m concentration relative to BMV in the ethosomal formulations, this was a notable finding because C=C stretches were not evident in PC.

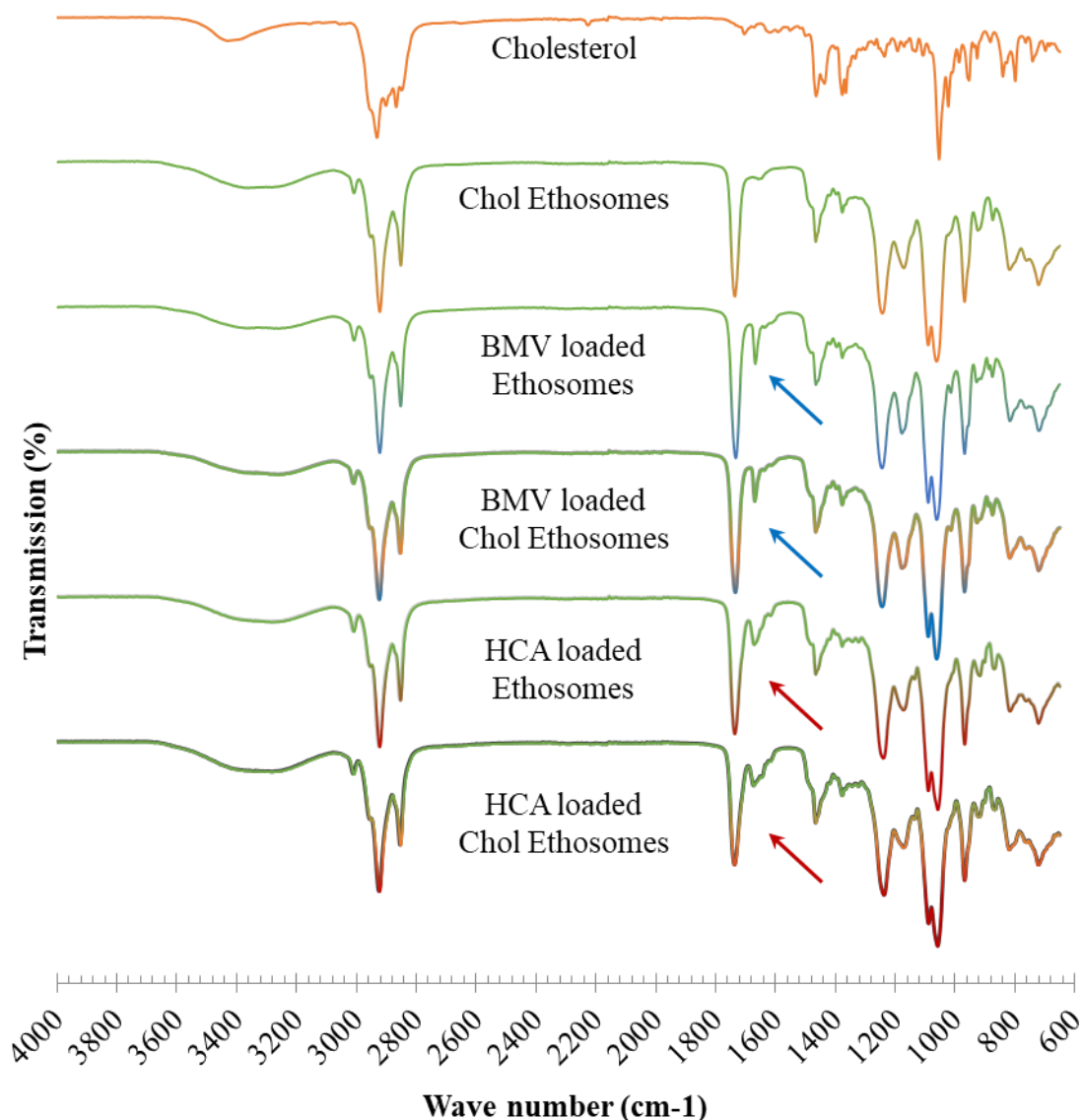


Figure 8.6-1: FTIR spectrograms of betamethasone valerate (BMV) loaded and hydrocortisone acetate (HCA) loaded ethosomes with and without cholesterol. Arrows indicate peaks shifts in wave number and/or intensity occurred and/or absence/appearance of new peaks.

HCA loaded Chol ethosomes had a FTIR profile similar to that of unloaded ethosomes with 2 distinct differences in the characteristic bands. The O-H/ N-H stretches identified in unloaded Chol ethosomes at 3363.30 cm^{-1} shifted to 3285.8 cm^{-1} . This was an indication that an interaction between O-H/ N-H of the PC and the hydroxyl groups of HCA occurred. Typically, primary amines display two distinct weak-medium bands at $3400\text{-}3300\text{ cm}^{-1}$ and $3330\text{-}3250\text{ cm}^{-1}$. However an O-H stretch occurring between $3550\text{-}3200\text{ cm}^{-1}$ was also identified within this region. Therefore, the exact functional group interaction remains unclear but is evident. Secondly, an alkene C=C stretch appeared at 1673.09 cm^{-1} . It was

absent for all of the other components except for HCA. The appearance of a new peak may be evident of a molecular interaction and the encapsulation of HCA. The resultant increase wave number may be indicative of a loss in mass or a decrease in bond length, possibly due to a neighbouring electronegative atom. The absence of characteristic HCA bands may have been evident of encapsulation of HCA within the phospholipid.

8.7. HSM analyses of BMV loaded and HCA loaded ethosomes with and without cholesterol.

Cholesterol melts at 148-150 °C.⁷³ Cholesterol is stored in a freezer at -4 °C to maintain its crystalline form with evidence of moisture present in the sample upon heating. At around 140 °C, cholesterol became more transparent until it eventually melted. Completion of melt was identified at 170 °C. The completion of melt was complemented by the liberation of gas with the sample appearing opaque on the HSM image. The change to opacity of the sample during the melt signals moisture being released just prior to degradation of the sample.

Unloaded Chol ethosomes had no thermal event and seemed to maintain its stability until 200 °C, where a change in turbidity was observed. The change in turbidity coupled with a liquid phase change was indicative of a melt. Following the melt, at 230 °C, degradation was observed as the sample changed in colour from transparent to dark brown.

BMV loaded Chol ethosomes appeared more transparent at 60 °C than BMV loaded ethosomes without cholesterol and maintained its form until 110 °C. Subsequently, bubbles were identified which is an indication of residual moisture after drying. The bubbles may be identified as the liberation of the hydroethanolic phase. The increased boiling point temperature relative to the pure sample occurred as a result of encapsulation of the solvent. Alternatively, the bubbles may have been due to PC which had previously displayed bubbling at 90 °C when analysed. It is important to note that this same event was identified with the HSM analysis of BMV loaded ethosomes (**Figure 8.7-1**). At 210-250°C, an immediate colour change from transparent to brown was observed, suggestive of degradation of the sample.

HCA loaded Chol ethosomes had no thermal activity until 100 °C. Thereafter, the sample became transparent as 2 distinct melting events occurred. The first is a glass transition that occurred as the sample became more transparent. The second, as with HCA loaded ethosomes, a melt occurred, resulting from either cholesterol or PC.

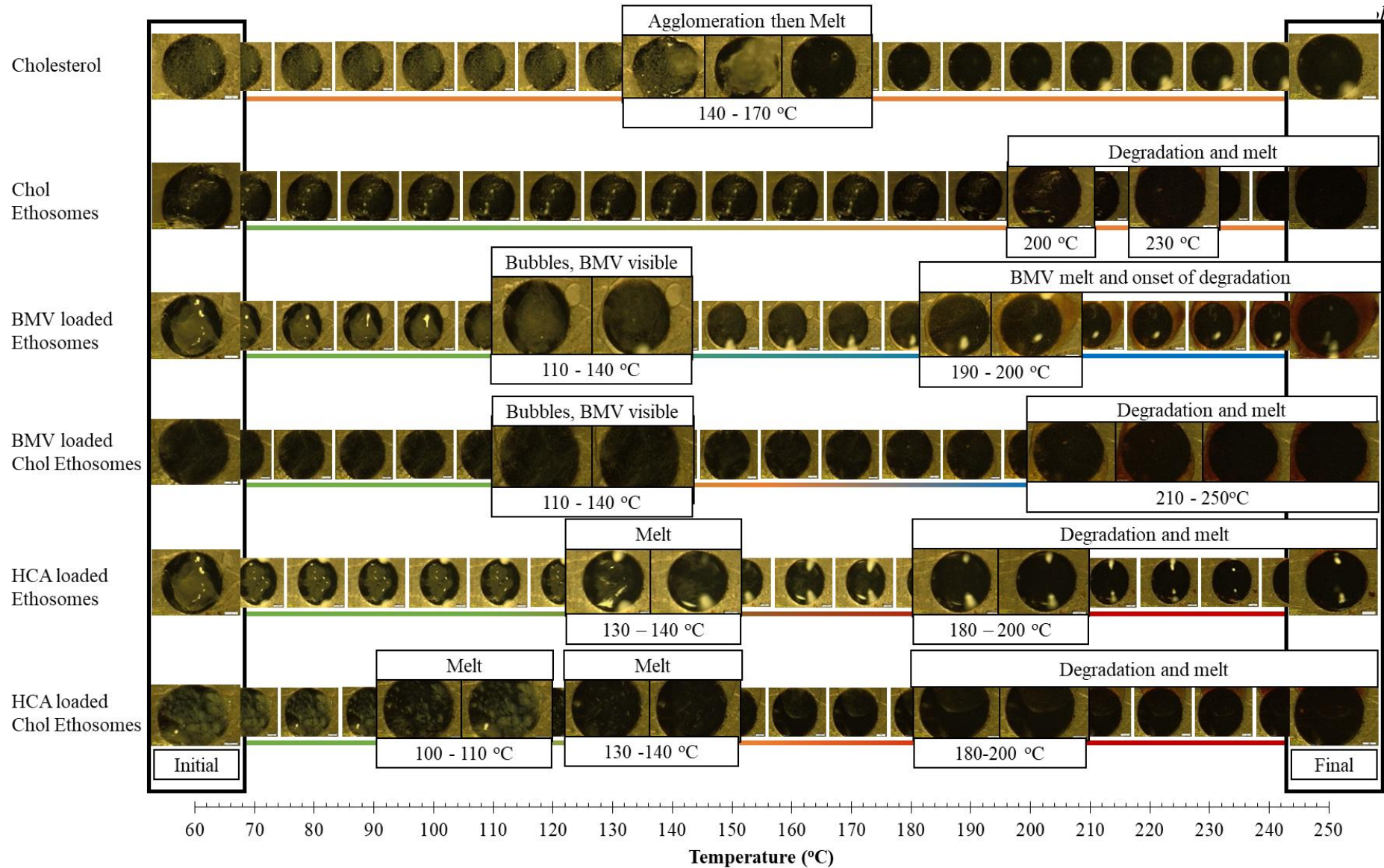


Figure 8.7-1: HSM analyses displaying observed thermal events and their corresponding temperatures for cholesterol, unloaded, betamethasone valerate (BMV) loaded ethosomes with and without cholesterol and hydrocortisone acetate (HCA) loaded ethosomes with and without cholesterol

8.8. Differential scanning calorimetry analyses of corticosteroid loaded Chol ethosomes

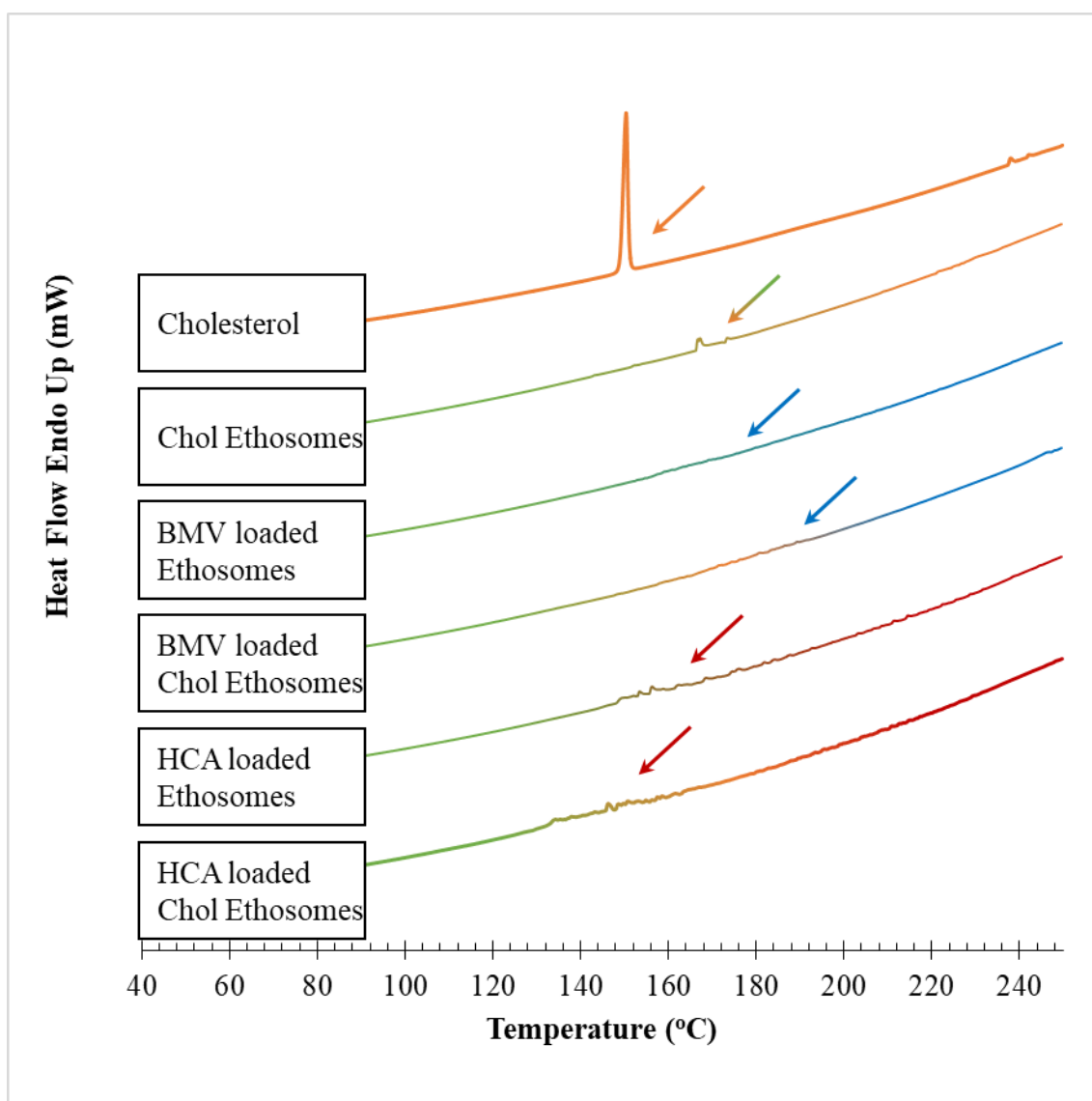


Figure 8.8-1: Differential scanning calorimetry (DSC) thermograms of cholesterol (Chol), Chol ethosomes, betamethasone valerate (BMV) loaded and hydrocortisone acetate (HCA) loaded ethosomes with and without cholesterol.

Cholesterol has an onset of melt at 149.04 °C with a single thermal event. The melt required 111.2790 mJ and completed at 151.08 °C. The thermal event was characterised by a Delta H of 67.67 J/g and a Delta Cp of 150.794 J/g* °C. The Tg half Cp extrapolated is 149.06 °C which corroborates the melting point in literature.⁷³ The single event suggests purity of sample. These findings were supported by the HSM analysis where an onset of melt at 140 °C

with completion at 170 °C was observed. HSM also showed that degradation occurred at 230 °C.

Chol ethosomes had a single thermal event with an onset at 166.40 °C. The melt had an area of 6.6238 mJ and ended at 167.38 °C. The melting point was characterised by Tg half Cp extrapolated at 167.93 °C with a Delta Cp of 411.678 J/g*°C. HSM analysis showed an onset of melt from 140 °C with completion at 170 °C, with degradation observed at 230 °C.

BMV loaded Chol ethosomes were uneventful quantitatively with DSC analysis. A glass transition occurred between 160-180 °C but the peaks were too small to be quantified. In **Figure 8.8-1**, BMV loaded Chol ethosomes confirms the absence of the characteristic BMV and cholesterol thermal events. This suggests that the BMV is encapsulated within the Chol ethosomes.

HCA loaded chol ethosomes had a single thermal event which could be quantified as Tg half Cp extrapolated at 146.36 °C with Delta Cp: 99.508 J/g*°C. The peak had an onset at 145.69 °C with an area of 3.5851 mJ. This could correlated to the melt from 140 °C with completion at 170 °C observed with HSM.

Figure 8.8-1 illustrates the shift in activity at a higher temperature with the BMV loaded samples after the addition of cholesterol. Conversely, a shift in activity was also identified at a lower temperature with HCA loaded ethosomes containing cholesterol. These findings are confirmed with the HSM analyses which correspond to a later onset of degradation and an earlier glass transition for BMV loaded and HCA loaded ethosomes, respectively.

8.9. Thermogravimetric analysis of unloaded, BMV loaded and HCA loaded Chol ethosomes

To determine the percentage mass loss over time, the 1st derivative was calculated (see **Appendix A**). In **Figure 8.9-1**, cholesterol exhibited a single mass loss event accounting for 99% weight loss. At 322.03 °C, the rate of mass loss was 1.069 % weight/min. This corresponds to the purity of the crystalline compound.

Unloaded Chol ethosomes exhibited 3 thermal events when analysed using TGA. These events occurred at 285.75 °C, 344.44 °C and 434.52 °C with % weight loss rates of 5,035, 19,111 and 2,042 % weight/min, respectively.

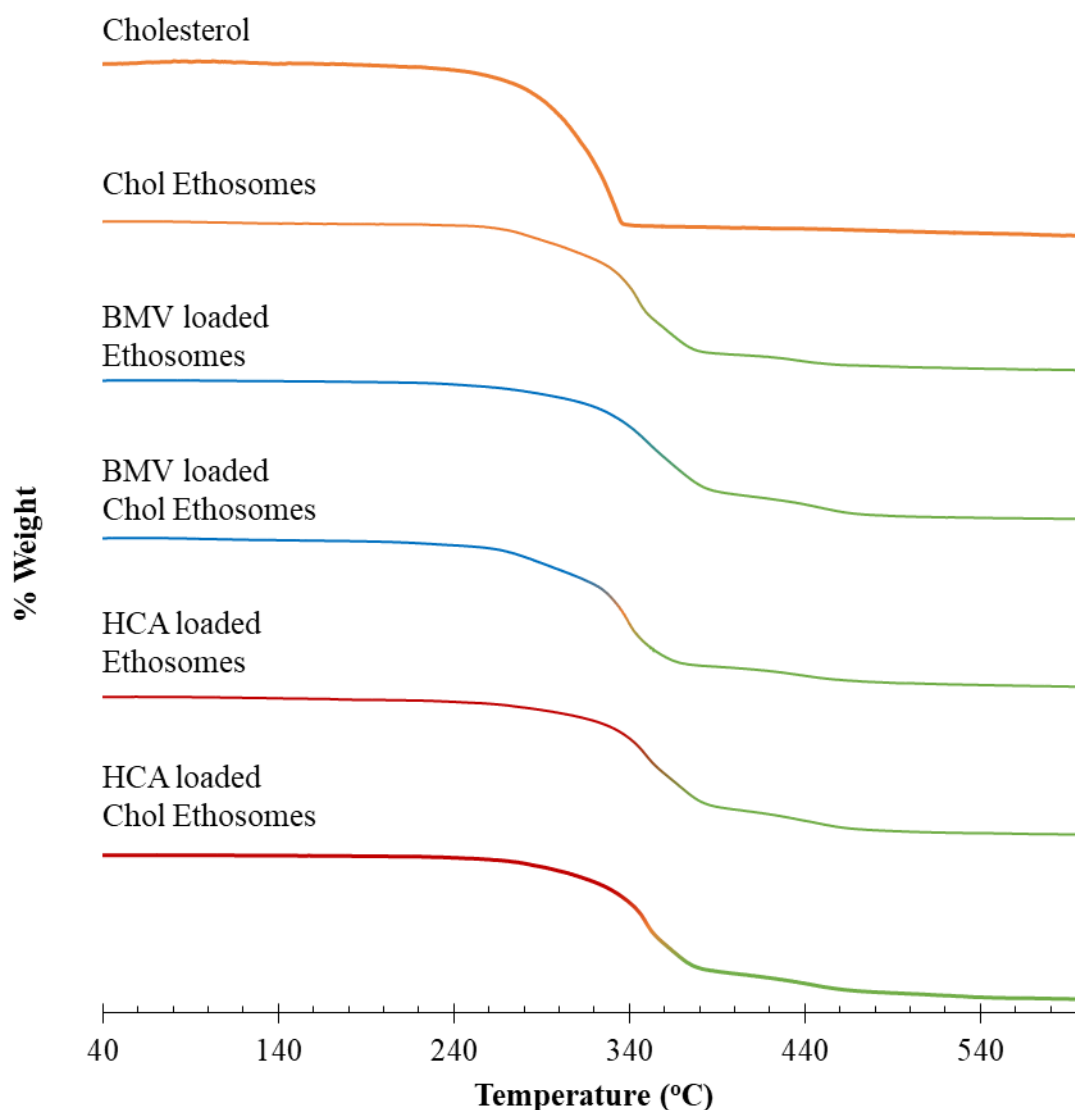


Figure 8.9-2: Thermogravimetric analyses thermograms of cholesterol (Chol), Chol ethosomes, betamethasone valerate (BMV) loaded and hydrocortisone acetate (HCA) loaded ethosomes with and without cholesterol.

BMV loaded Chol ethosomes exhibited 3 thermal events. These events occurred at 276.15 °C, 337.51 °C and 437.82 °C with weight loss rates of 5.157, -9.303 and 6.722 % weight/min, respectively.

HCA loaded Chol ethosomes exhibited 2 thermal events when analysed using TGA. These events occurred at 349.78 °C and 443.75 °C with weight loss rates of 17,906 and 2,798 % weight/min, respectively.

TGA results show that BMV loaded ethosomes exhibited an additional mass loss event once cholesterol had been included whereas HCA loaded ethosomes had similar profiles with 2 thermal events.

8.10. Drug loading and encapsulation efficiency

Table 8.10-1: The encapsulation efficiency (EE) and drug loading (DL) of betamethasone valerate (BMV) and hydrocortisone acetate (HCA) loaded Chol ethosomes (n=2)

FORMULATION	Ethosome mass (g)	API direct (mg/2 ml)	API in Supernatant (mg/ 1.5 ml)	API in 2 ml (mg)	EE (%)	DL (%)	% API recovered
BMV loaded Chol ethosomes crude	1,91	0,99	0,40	1,39	71,10	14,22	69,58
BMV loaded Chol ethosomes extruded	1,92	1,05	0,41	1,45	72,04	14,41	72,63
HCA loaded Chol ethosomes crude	1,92	0,60	1,13	1,74	34,72	6,94	86,82
HCA loaded Chol ethosomes extruded	1,97	0,71	1,18	1,89	37,41	7,48	94,34

HCA and BMV were quantified using calibration curves generated using the validated HPLC method. Using the data generated from the standard curves to determine the mass of the APIs, the encapsulation efficiency (EE) and drug loading (DL) were calculated using **Equations 8 and 9**, respectively. The results have been tabulated in **Table 8.10-1**.

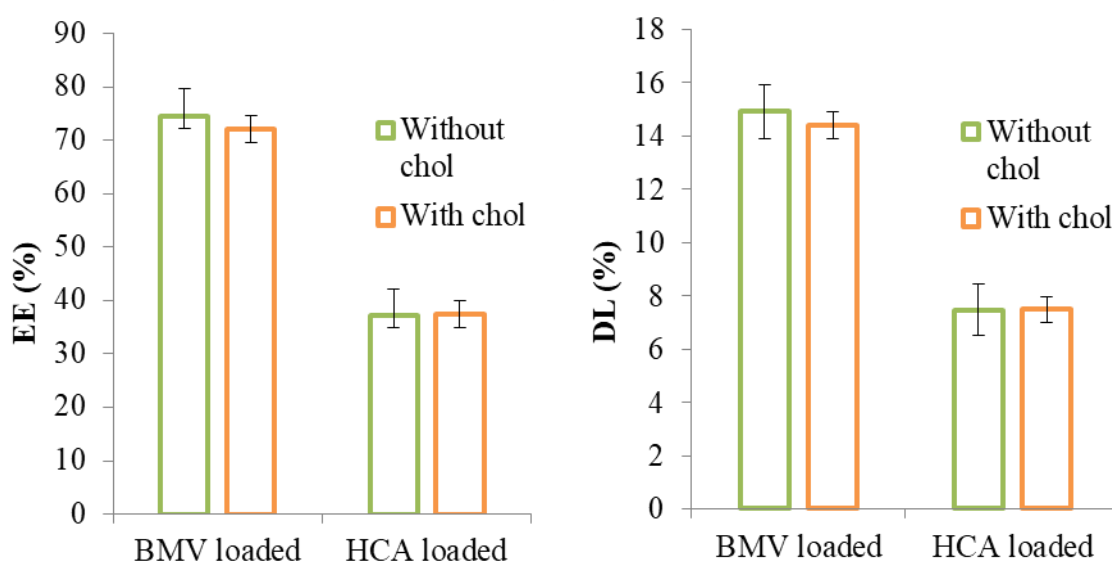


Figure 8.10-1: encapsulation efficiency (EE) and drug loading (DL) of betamethasone valerate (BMV) and hydrocortisone acetate (HCA) loaded Chol ethosomes with and without cholesterol.

The EE of both formulations show no significant change after the inclusion of cholesterol, with EE's of 72.04 % and 37.41 % for BMV and HCA loaded Chol ethosomes, respectively. Similarly, the inclusion of cholesterol did not significantly change the DL of the ethosomes. In **Figure 8.10-1**, the DLs are 14.41 % and 7.48 % for BMV and HCA loaded ethosomes, respectively. The addition of cholesterol did not change the EE and DL. Supplementary ethosomal properties such as the shelf-life and transdermal permeability may have changed, however these characteristics were not part of the scope of this study.

8.11. Drug release

Drug release was determined using the *in vitro* drug release method described in **Chapter 5.11**. Using Franz diffusion cells, the solution in the donor compartment was analysed to quantify the amount of API using the validated HPLC method. The percentage drug release was calculated and plotted against time for 200 μ L samples of 1 mg/ml GC formulations as observed in **Figure 8.11-1**.

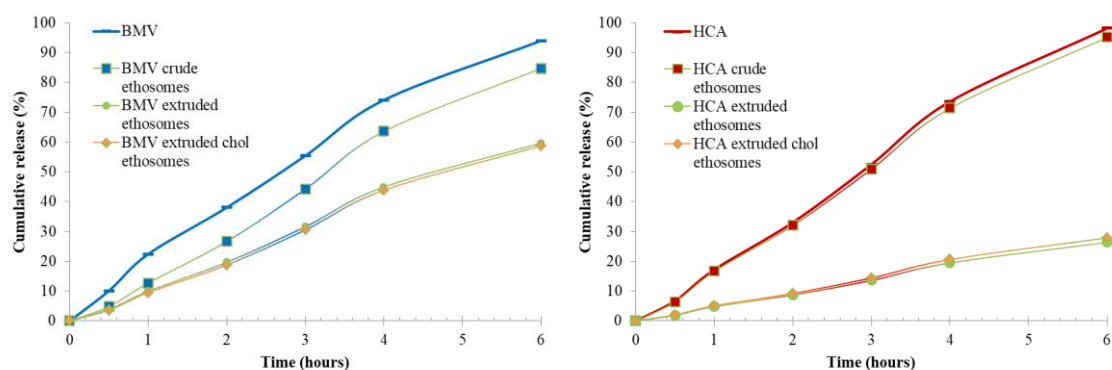


Figure 8.11-1: The percentage drug release of different ethosomal formulations and the respective standards over a period of 6 hours. Crude = ethosomes without comminution.

BMV had the highest quantity of drug released (93 %) over a 6 hour period. Crude BMV loaded ethosomes had the second highest quantity, with 84% drug release. A significant reduction in release was observed for the extruded formulations when compared to the crude samples at similar time intervals. The addition of cholesterol did not seem to influence the rate of BMV release as both curves had an identical shape with 59 % and 60 % of BMV released for the loaded extruded samples with and without cholesterol, respectively. A 33 % decrease in the amount of drug released over the 6 hour period was observed relative to the control. The HCA control and the crude HCA loaded ethosomes had similar rates of release with a percentage release of 99 % and 96 % release over the 6 hour period. Extruded HCA samples had a much slower release rate compared to the control and crude samples with 27 % and 28 % release for extruded HCA loaded samples without and with cholesterol, respectively.

When comparing the results of the % release across all formulations, it is noted that extrusion significantly influenced the quantity of drug released. Particle size had a direct influence on the amount of drug released from the ethosomes, with smaller ethosomes retaining the API for a longer duration. The reduced rate of GC liberation is due to the compact nature of the smaller ethosomes. Extrusion affects the arrangement of the phospholipid bilayer by increasing its integrity. The inclusion of cholesterol as an excipient did not have any appreciable effect on the release of the ethosomes *in vitro*, regardless of the characteristics of loaded API.

8.12. Release kinetics and mathematical modelling of GC loaded ethosomes

Table 8.12-1: Mathematical modelling of betamethasone valerate (BMV) loaded and hydrocortisone acetate (HCA) loaded ethosomal release kinetics.

Mathematical Model	BMV control	BMV crude	BMV loaded ethosomes	BMV loaded Chol ethosomes	HCA control	HCA crude	HCA loaded ethosomes	HCA loaded Chol ethosomes
Zero Order (adj R²)	0,9915	0,9761	0,9927	0,9931	0,9934	0,9932	0,9949	0,9949
(k0)	14,542	17,057	10,311	10,082	17,013	16,500	4,534	4,779
First Order (adj R²)	0,9451	0,9690	0,9802	0,9776	0,9337	0,9394	0,9950	0,9949
(k1)	0,221	0,298	0,138	0,133	0,282	0,269	0,051	0,054
Higuchi (adj R²)	0,8417	0,9168	0,8559	0,8480	0,8630	0,8624	0,8614	0,8615
(kH)	28,178	33,804	20,058	19,567	33,158	32,153	8,831	9,309
Korsmeyer-Peppas (adj R²)	0,9899	0,9936	0,9915	0,9917	0,9929	0,9927	0,9943	0,9943
(kKP)	14,327	22,472	10,695	10,112	18,068	17,508	4,739	5,000
(n)	1,010	0,814	0,976	0,998	0,960	0,960	0,970	0,970
Peppas-Sahlin (adj R²)	0,9926	0,9952	0,9936	0,9935	0,9948	0,9948	0,9945	0,9945
k1	-23,121	-30,470	-15,418	-13,788	-24,212	-24,671	-4,042	-4,267
k2	35,910	52,073	25,197	22,998	40,917	40,800	8,529	9,000
m	0,360	0,289	0,354	0,370	0,354	0,349	0,393	0,393

To determine the mechanism of release from ethosomes, mathematical models were applied to the release data shown in **Figure 8.12-1**. Using *DDsolver*, an add-in program used in *Microsoft Excel*, the following models were applied: Zero-order, first order, Higuchi, Korsmeyer Peppas and Peppas-Sahlin. The best model was selected based on the adjusted R², as shown in the green highlighted cells in **Table 8.12-1**.

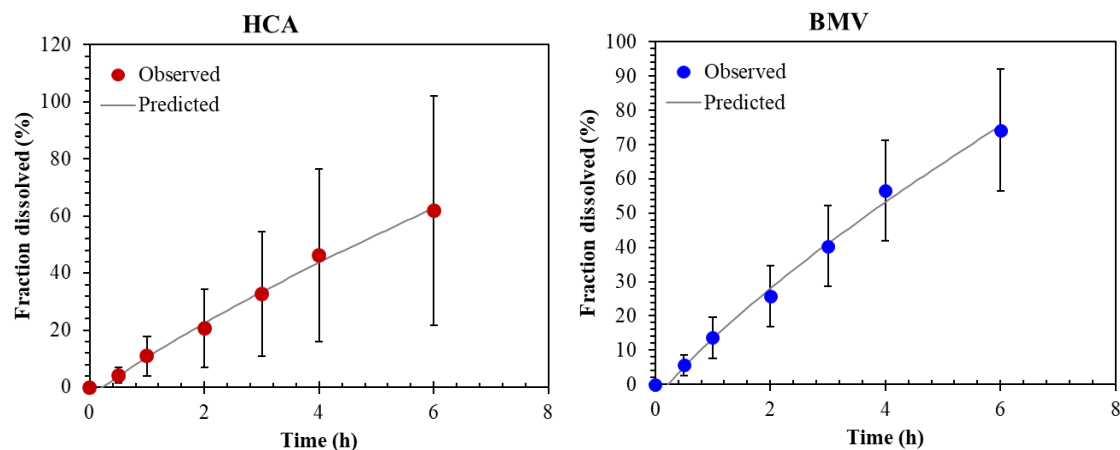


Figure 8.12-1: The release of betamethasone valerate (BMV) and hydrocortisone acetate (HCA) loaded formulations plotted against the Peppas-Sahlin model.

Evaluation of the mathematical models showed that the data fit best in the following descending order: Peppas-Sahlin, Zero-order, Korsmeyer-Peppas. Peppas-Sahlin had the best fit accounting for the highest r^2 values for all of the formulations containing BMV. To determine the mechanism of release, the k_1 and k_2 values were compared, where: k_1 is the constant related to the Fickian kinetics, k_2 is the constant related to Case-II relaxation kinetics and m is the diffusional exponent for a device of any geometric shape which inhibits controlled release.

All of the BMV formulations had a high k_2 associated with Case II relaxation kinetics. Case II relaxation is indicative of relaxation of the polymer.¹⁶⁹ In this instance, the relaxation of the phospholipid bilayer facilitates the release of the API into the bulk medium. This is different from Fickian kinetics where the movement of the API is passively driven by a concentration gradient.¹⁷⁰ The high negative k_1 value indicates that Fickian diffusion is negligible. The HCA control and crude HCA loaded ethosomes shared a similar mechanism to BMV loaded ethosomes. However, the extruded HCA loaded ethosomes had identical R^2 values (0.9949) correlating to zero-order release. In this mechanism, the release rate is independent of the concentration of API.⁹³

The quicker drug release of BMV, relative to HCA, may be attributed to higher drug loading of BMV. Since the BMV loaded ethosomes were similar in size, and BMV has a higher drug loading than HCA, it was deduced that the ethosomes are more saturated with BMV. Therefore, BMV may have had a shorter path than HCA. With more BMV saturated at the perimeter, it may be released quickly by erosion or swelling of the polymer. Although BMV

is released at a quicker rate and in higher concentrations, the mechanism accounting for this is the same for both GCs. These findings can be corroborated by the Korsmeyer-Peppas equation where $n > 0.87$ is indicative of super case II transport which is also associated with polymer relaxation or erosion of the polymer chains and zero order drug release. The polymer relaxation may be influenced by the increase in temperature, as the drug release experiment was conducted in a hot water bath at $37 \text{ }^\circ\text{C} \pm 0.5 \text{ }^\circ\text{C}$ to simulate body temperature.

8.13. Conclusion

The objective of this experiment was to formulate cholesterol containing ethosomes using the CM and extrusion as a comminution technique. Cholesterol was included as an excipient in an attempt to optimise the DL and EE based on the results of *Chapter 7*. The objective was met by the successful synthesis of cholesterol containing ethosomes which met the acceptance criteria for topical drug delivery regarding HdD and PdI. Although the ζ_p was not appreciable, a few positives can be taken from the outcome of this study. Firstly, the addition of cholesterol resulted in the formation of multivesicular vesicles (MVs) for BMV loaded ethosomes and greater spherical morphology for HCA loaded ethosomes. Encapsulation was confirmed using FTIR, thermoanalyses and HPLC. The EE and DL were determined for the HCA and BMV loaded samples containing cholesterol using the validated HPLC method. Although HCA loaded samples did not improve the EE and DL relative to the BMV loaded samples, a number of research avenues have been created as a result to determine how cholesterol affects ethosomal characteristics which were out of the scope of this study, such as stability and drug flux. Drug release was determined by the use of vertical Franz diffusion cells where the bulk medium was extracted and replenished at predetermined time intervals. The drug release and release kinetics were determined by plotting % cumulative drug release curves and fitting drug release models. It was found that the release kinetics best fit the Peppas-Sahlin model indicative of an anomalous non-Fickian diffusion coupled with polymer relaxation and zero order release.



UNIVERSITY *of the*
WESTERN CAPE

CHAPTER 9:

CONCLUSION AND

RECOMMENDATION



School of
PHARMACY

9. Conclusion

The aim of this study was to formulate and characterise corticosteroid loaded ethosomes for topical delivery. In this chapter, a summary of the objectives and achievements with limitations will be reviewed. This leads us to concluding remarks and recommendations for future studies.

A comprehensive literature search was conducted to determine the obstacles surrounding transdermal drug delivery regarding atopic dermatitis (AD). AD was characterised as a complex disease with a multifactorial pathophysiology influenced by hereditary and environmental factors. Although no generic cure was identified, betamethasone valerate (BMV) and hydrocortisone acetate (HCA) were identified as mild and moderately potent glucocorticoids (GCs) utilised in the management of inflammation associated with AD. The skin, in itself, is a rate limiting barrier for topical formulations.²⁸ Exacerbated by lichenified skin, an increase in the thickness of the epidermis, topical formulations may not be suitable to deliver active pharmaceutical ingredients (APIs) through a reinforced epidermal barrier. As such, mechanisms to enhance permeation by the use of nanoparticles were researched.^{15,17,55}

An array of nanoparticles was identified including: dendrimer nano-carriers (DNCs), silica nanoparticles (SNPs), carbon nanoparticles (CNPs) and magnetic nanoparticles (MNPs).^{60,79} Ethosomes were chosen as suitable nanoparticles which could enhance the topical delivery of hydrophobic APIs such as BMV and HCA. The selection of ethosomes for topical delivery was motivated by the biocompatibility of the raw material, the passive and non-invasive means of drug delivery and the small size relative to conventional lipid nano-drug delivery systems.

Methods regarding the synthesis of ethosomes were studied and formulations incorporating the GCs were developed. Using the hot method (HM) and the cold method (CM), by *Touitou et al, 2007* ethosomes were synthesised.¹ These methods used the preparation of a double emulsion (o/w/o), centrifugation and solvent evaporation method.

Using the HM and CM, unloaded ethosomes were synthesised using different concentrations of phosphatidylcholine (PC). HM and CM ethosomes were characterised using dynamic light scattering (DLS) according to their hydrodynamic diameter (HdD), polydispersity index (PdI) and zeta potential (ζ p) to determine the influence of PC on the ethosomes. Based on the DLS results, a PC concentration of 50 mg/ml was selected as the resultant ethosome which met the

acceptance criteria. The effect of comminution on ethosomes was determined by sonicating and extruding all of the HM and CM formulations. These samples were once again characterised according to their HdD, PdI and ζ_p to determine the influence of sonication and extrusion on the aforementioned parameters.

Both HM and CM ethosomes were then each loaded with BMV and HCA. The loaded samples were characterised according to their HdD, PdI and ζ_p to determine the influence of BMV and HCA. The most suitable comminution method was determined by sonicating and extruding the GC loaded HM and CM formulations and characterised. The mini-extruder results, regarding particle size and distribution, were reproducible. Although sonication has been used in other studies to reduce the particle size^{93,171,172}, the reproducibility of the results did not meet the acceptance criteria of this study. Consequently, sonication was rejected due to the poor HdD and PdI of the ethosomes relative to the extruded samples.

SEM analyses of unloaded HM and CM ethosomes showed spherical ethosomes after extrusion; however, once loaded with GCs, HM ethosomes no longer yielded a spherical shape. Since the spherical shape of the ethosomes was a characteristic feature which promoted topical delivery, the CM was utilised for subsequent analyses and development.

CM ethosomes were purified, isolated and dried using centrifugation and centrifugal drying to achieve a solid state for further analyses. Using FTIR, possible interactions were identified between the PC and the encapsulated GCs. Both BMV and HCA had weak intermolecular interactions which appeared as a peak indicative of a weak C=C stretch. The exact location of the interaction between the components was unknown due to the presence of many possibilities. The absence of the characteristic bands in the fingerprint region of the GCs was indicative of encapsulation. These findings were supported by the thermoanalyses. Using HSM, the ethosomes were observed microscopically under thermal stress and the characteristic melts of the encapsulated APIs had either shifted or were absent. When utilising DSC, it was noted that the characteristic endothermic peak associated with the melting point of the pure component had either shifted or disappeared. The TGA analyses showed that the characteristic thermal events corresponding to the mass loss of these shifts or disappearance of peaks, which suggested encapsulation of the GCs.

Encapsulation was further supported by the application of validated HPLC methods where the loaded API was quantified and the samples were analysed to determine the encapsulation efficiency (EE) and drug loading (DL).

In an attempt to optimise the ethosomal characteristics under investigation, cholesterol was then added to the formulations. Research supports the use of cholesterol to improve ethosomal characteristics such as DL and EE, with the risk of an increase in ethosome size and rigidity.^{88,98,173} Different concentrations of cholesterol were tested and the most acceptable concentration (7.5 mg/ml) was selected based on the resultant ethosomes which met the acceptance criteria regarding HdD and PdI. Similar to the ethosomes without cholesterol, the analytical techniques employed showed that the GCs had been encapsulated once loaded. However, no significant differences in the HdD, PdI, ζ_p , DL and EE were established.

The drug release from the ethosomes was determined using Franz diffusion cells where a difference in the release rate of the loaded GCs was established. BMV loaded ethosomes released the loaded BMV at a quicker rate than the HCA loaded ethosomes.

Mathematical models were applied using DDSolver to determine the release kinetics of the loaded formulations. The best fit of the BMV loaded samples corresponded to the Peppas-Sahlin model.¹⁷⁰ This indicated that the relaxation of the polymer resulted in the liberation of BMV, however HCA loaded samples were released according to Zero-order kinetics where the release of HCA was independent of its concentration.

9.1. Recommendation

The promising results from this study present an array of avenues for further investigation, particularly in the field of optimisation.

- Although the HM was not as useful as the CM in producing ethosomes suitable for the parameters of this study, SEM analyses did indicate the presence of spherical unloaded vesicles. With the main difference in the CM and HM being the introduction of temperature as a variable, thus better control of the temperature during synthesis may result in acceptable loaded ethosomes.
- The ζ_p was a parameter that indicated swift flocculation of ethosomes. It may be of interest to increase the ζ_p to > 30 mV by including a surfactant or a secondary alcohol to the formulation which has been shown to inhibit aggregation and increase vesicle stability.^{65,111}
- When formulating the ethosomes in this study, the API concentrations, water and ethanol ratio were maintained to limit the influence of the variables under scrutiny.

The ethosomal formulations may be optimised using Response Surface Methodology (RSM) software to alter concentrations of the API and the excipients.

- Sonication, as a tool for comminution, may be optimised to produce greater reproducibility. The parameters in this study were not changed. The number of cycles, frequency, temperature and duration could be optimised to produce more reliable results. Alternatively, since a bath sonicator was used in this study, the application of probe sonication may achieve further desirable results.
- The stability of the ethosomes is an important characteristic in determining the shelf-life and feasibility of mass production. Therefore, stability studies, such as accelerated stability studies or water sorption studies, can be done to determine the effect of storage on the characteristics of the ethosomes.
- Permeation studies are pivotal to determining the viability of ethosomes for topical drug delivery. The premise of the study was to set the foundation for *in vivo* studies as to establish the influence of GC encapsulation on drug flux. Permeation studies could be achieved using synthetic membranes or animal models.

Finally, based on the results achieved, it is evident that ethosomes have potential as novel drug delivery systems regarding topical drug delivery for AD. This study has shed light on the influence of different preparation methods, comminution techniques and a variety of factors influencing the successful preparation and evaluation of ethosomes. Based on the small particle size (~ 200 nm), acceptable polydispersity (< 0.5), ease of preparation, high EE and DL, the encapsulation of GCs shows promise and studies are needed further evaluation and development. A variety of research avenues have been created for further exploration. Supported by prospective data generated from comprehensive research, GC loaded ethosomes may move out of the pre-formulation stage and in to topical formulations

9.2. References

1. Touitou E, Godin B. Ethosomes for skin delivery. *J Drug Deliv Sci Technol* [Internet]. 2007;17(5):303–8. Available from: [http://dx.doi.org/10.1016/S1773-2247\(07\)50046-8](http://dx.doi.org/10.1016/S1773-2247(07)50046-8)
2. Intercollegiate Guidelines Network S. Management of atopic eczema in primary care Scottish Intercollegiate Guidelines Network. 2011;(March).
3. Bunikowski R, Staab D, Kussebi F, Brautigam M, Weidinger G, Renz H, et al. Low-dose cyclosporin A microemulsion in children with severe atopic dermatitis: clinical and immunological effects. *Pediatr Allergy Immunol*. 2001;12(4):216–23.
4. Halim TYF, Steer CA, Mathä L, Gold MJ, Martinez-Gonzalez I, McNagny KM, et al. Group 2 innate lymphoid cells are critical for the initiation of adaptive T helper 2 cell-mediated allergic lung inflammation. *Immunity*. 2014;40(3):425–35.
5. Davies E, Rogers NK, Lloyd-Lavery A, Grindlay DJC, Thomas KS. What's new in atopic eczema? An analysis of systematic reviews published in 2015. Part 1: epidemiology and methodology. *Clin Exp Dermatol* [Internet]. 2018;1–5. Available from: <http://doi.wiley.com/10.1111/ced.13377>
6. Sinclair W, Aboobaker J, Green R, Jordaan F, Levin M, Lewis H, et al. Guidelines on the management of atopic dermatitis in South Africa. *South African Med J*. 2008;98(4):303–20.
7. Angelova-Fischer I, Bauer A, Hipler UC, Petrov I, Kazandjieva J, Bruckner T, et al. The Objective Severity Assessment of Atopic Dermatitis (OSAAD) score: Validity, reliability and sensitivity in adult patients with atopic dermatitis. *Br J Dermatol*. 2005;153(4):767–73.
8. Hengge UR, Ruzicka T, Schwartz RA, Cork MJ. Adverse effects of topical glucocorticosteroids. *J Am Acad Dermatol*. 2006;54(1):1–18.
9. Shao M, Hussain Z, Thu HE, Khan S, Katas H, Ahmed TA, et al. Drug nanocarrier, the future of atopic diseases: Advanced drug delivery systems and smart management of disease. *Colloids Surfaces B Biointerfaces* [Internet]. 2016;147:475–91. Available from: <http://dx.doi.org/10.1016/j.colsurfb.2016.08.027>
10. Rosado C, Silva C, Reis CP. Hydrocortisone-loaded poly(ϵ -caprolactone) nanoparticles for atopic dermatitis treatment. *Pharm Dev Technol*. 2013;18(3):710–8.
11. Senyigit T, Ozer O. Corticosteroids for Skin Delivery: Challenges and New Formulation Opportunities. *Glucocorticoids - New Recognit Our Fam Friend*. 2012;595–612.
12. Mooney E, Rademaker M, Dailey R, Daniel BS, Drummond C, Fischer G, et al. Adverse effects of topical corticosteroids in paediatric eczema: Australasian consensus statement. *Australas J Dermatol*. 2015;56(4):241–51.
13. Fisher D a. Adverse effects of topical corticosteroid use. *West J Med*. 1995;162(2):123–6.
14. Siddique MI, Katas H, Iqbal Mohd Amin MC, Ng SF, Zulfakar MH, Buang F, et al.

- Minimization of Local and Systemic Adverse Effects of Topical Glucocorticoids by Nanoencapsulation: In Vivo Safety of Hydrocortisone-Hydroxytyrosol Loaded Chitosan Nanoparticles. *J Pharm Sci*. 2015;104(12):4276–86.
15. Honeywell-Nguyen PL, Bouwstra JA. Vesicles as a tool for transdermal and dermal delivery. *Drug Discov Today Technol*. 2005;2(1):67–74.
 16. Tanner T, Marks R. Delivering drugs by the transdermal route: Review and comment. *Ski Res Technol*. 2008;14(3):249–60.
 17. El Maghraby GM, Barry BW, Williams AC. Liposomes and skin: From drug delivery to model membranes. *Eur J Pharm Sci*. 2008;34(4–5):203–22.
 18. Uchechi O, Ogbonna JDN, Attama AA. Nanoparticles for Dermal and Transdermal Drug Delivery. *Appl Nanotechnol Drug Deliv* [Internet]. 2014; Available from: <http://www.intechopen.com/books/application-of-nanotechnology-in-drug-delivery/nanoparticles-for-dermal-and-transdermal-drug-delivery>
 19. Bhatia A, Shard P, Chopra D, Mishra T. Chitosan nanoparticles as Carrier of Immunorestoratory plant extract: Synthesis, characterization and Immunorestoratory efficacy. *Int J Drug Deliv*. 2011;1(2):381–5.
 20. Mishra DK, Shandilya R, Mishra PK. Lipid based nanocarriers: a translational perspective. *Nanomedicine Nanotechnology, Biol Med* [Internet]. 2018;14(7):2023–50. Available from: <https://doi.org/10.1016/j.nano.2018.05.021>
 21. Zorec B, Zupančič Š, Kristl J, Pavšelj N. Combinations of nanovesicles and physical methods for enhanced transdermal delivery of a model hydrophilic drug. *Eur J Pharm Biopharm*. 2018;127(March):387–97.
 22. Akiladevi D, Basak S. Ethosomes -- a Noninvasive Approach for Transdermal Drug Delivery. *Int J Curr Pharm Res*. 2010;2(4):2–5.
 23. Patrekar P V, Mali Lecturer SS, Mujib MT, Hosmani AH, Patrekar Shri Jagdishprasad Jhabarmal P V, Inamdar SJ, et al. Ethosomes as novel drug delivery system: A review. *Pharma Innov J TPI* [Internet]. 2015;4(49):10–21. Available from: www.thepharmajournal.com
 24. Monograph P. Product monograph. Packag (Boston, Mass). 2007;(100479):1–27.
 25. Aulton ME, Taylor KMG. Aulton's *Pharmaceutics - The Design and Manufacture of Medicines*, 4th Ed. Harcourt Publishers Limited, London. 2013. 12, 13, 93,135, 758, 759 p.
 26. Landriscina A, Rosen J, Friedman A. Nanotechnology, Inflammation and the Skin Barrier: Innovative Approaches for Skin Health and Cosmesis. *Cosmetics* [Internet]. 2015;2(2):177–86. Available from: <http://www.mdpi.com/2079-9284/2/2/177/>
 27. Gomes M. Lipid nanoparticles for topical and transdermal application for alopecia treatment. 2012;(July).
 28. Trommer H, Neubert RHH. Overcoming the stratum corneum: The modulation of skin penetration. A review. In: *Skin Pharmacology and Physiology*. 2006. p. 106–21.

29. Tončić RJ, Kezić S, Hadžavdić SL, Marinović B. Skin barrier and dry skin in the mature patient. *Clin Dermatol*. 2018;36(2):109–15.
30. Cartlidge P. The epidermal barrier. *Semin Neonatol*. 2000;5(4):273–80.
31. Upton E, Schellack N, Motswaledi MH. A review of the risk factors and clinical presentation of childhood atopic eczema at the primary healthcare level. *Curr Allergy Clin Immunol*. 2016;29(1).
32. H Mitchell BH, Hamilton TS, Steggerda R, Bean HW, Husbandry A. THE CHEMICAL COMPOSITION OF THE ADULT HUMAN BODY AND ITS BEARING ON THE BIOCHEMISTRY OF GROWTH* the Division of Animal Nutrition, and the Departments of. Available from: <http://www.jbc.org/>
33. Thomsen SF, Xiwei Zheng, Cong Bi, Marissa Brooks and DSH, Khan SJ, Dharmage SC, Matheson MC, Gurrin LC, et al. HHS Public Access. *Anal Chem* [Internet]. 2018;28(4):377–83. Available from: <http://dx.doi.org/10.1016/j.jaci.2018.03.002>
34. Thomsen SF. Epidemiology and natural history of atopic diseases. *Eur Clin Respir J* [Internet]. 2015;2(1):24642. Available from: <https://www.tandfonline.com/doi/full/10.3402/ecrj.v2.24642>
35. Thomsen SF. Epidemiology and natural history of atopic diseases. 2015;1:1–6.
36. Hammer-Helmich L, Linneberg A, Obel C, Thomsen SF, Møllehave LT, Glümer C. Mental health associations with eczema, asthma and hay fever in children: A cross-sectional survey. *BMJ Open*. 2016;6(10).
37. Eng SS, Defelice ML. The role and immunobiology of eosinophils in the respiratory system: A comprehensive review. *Clin Rev Allergy Immunol*. 2016;50(2):140–58.
38. Lule SA, Mpairwe H, Nampijja M, Akello F, Kabagenyi J, Namara B, et al. Life-course of atopy and allergy-related disease events in tropical sub-Saharan Africa: A birth cohort study. *Pediatr Allergy Immunol*. 2017;28(4):377–83.
39. Khan SJ. Is the atopic march related to confounding by genetics and early-life environment? A systematic review of sibship and twin data. 2017;(June):17–28.
40. Sánchez J, Páez B, Macías A, Olmos C, De Falco A. Atopic dermatitis guideline. Position paper from the Latin American Society of allergy, asthma and immunology. *Rev Alerg Mex*. 2014;61(3):178–211.
41. Beltrani VS. Atopic Dermatitis : The Spectrum of Disease. 1999;3:8–15.
42. Brunner PM, Guttman-Yassky E, Leung DYM. The immunology of atopic dermatitis and its reversibility with broad-spectrum and targeted therapies. *J Allergy Clin Immunol* [Internet]. 2017;139(4):S65–76. Available from: <http://dx.doi.org/10.1016/j.jaci.2017.01.011>
43. Sehra S, Yao Y, Howell MD, Nguyen ET, Kansas GS, Leung DYM, et al. IL-4 Regulates Skin Homeostasis and the Predisposition toward Allergic Skin Inflammation. *J Immunol* [Internet]. 2010;184(6):3186–90. Available from: <http://www.jimmunol.org/cgi/doi/10.4049/jimmunol.0901860>

44. Zinkeviciene A, Kainov D, Lastauskiene E, Kvedariene V, Bychkov D, Byrne M, et al. Serum Biomarkers of Allergic Contact Dermatitis: A Pilot Study. *Int Arch Allergy Immunol* [Internet]. 2016;168(3):161–4. Available from: <http://www.karger.com/?doi=10.1159/000442749>
45. Paller AS, Kabashima K, Bieber T. Therapeutic pipeline for atopic dermatitis: End of the drought? *J Allergy Clin Immunol* [Internet]. 2017;140(3):633–43. Available from: <http://dx.doi.org/10.1016/j.jaci.2017.07.006>
46. Schellack N, Upton E, Schellack G. The allergic scholar. *SA Pharm J* [Internet]. 2015;82(7):9–16. Available from: <http://www.embase.com/search/results?subaction=viewrecord&from=export&id=L606002769>
47. Gomez-Sanchez E, Gomez-Sanchez CE. The multifaceted mineralocorticoid receptor. *Compr Physiol*. 2014;
48. Salter BM, Oliveria JP, Nusca G, Smith SG, Watson RM, Comeau M, et al. Thymic stromal lymphopoietin activation of basophils in patients with allergic asthma is IL-3 dependent. *J Allergy Clin Immunol* [Internet]. 2015;136(6):1636–44. Available from: <http://dx.doi.org/10.1016/j.jaci.2015.03.039>
49. He A, Feldman SR, Fleischer AB. An assessment of the use of antihistamines in the management of atopic dermatitis. *J Am Acad Dermatol* [Internet]. 2018; Available from: <https://doi.org/10.1016/j.jaad.2017.12.077>
50. Löffler H, Steffes A, Happle R, Effendy I. 1. Löffler H, Steffes A, Happle R, Effendy I. Allergy and Irritation: An Adverse Association in Patients with Atopic Eczema. *Acta Derm Venereol*. 2003;83(5):328–31. Allergy and Irritation: An Adverse Association in Patients with Atopic Eczema. *Acta Derm Venereol*. 2003;83(5):328–31.
51. Ericson-Neilsen W, Kaye AD. Steroids: pharmacology, complications, and practice delivery issues. *Ochsner J* [Internet]. 2014;14(2):203–7. Available from: <http://www.pubmedcentral.nih.gov/articlerender.fcgi?artid=4052587&tool=pmcentrez&rendertype=abstract>
52. Roberts MS, Mohammed Y, Pastore MN, Namjoshi S, Yousef S, Alinaghi A, et al. Topical and cutaneous delivery using nanosystems. *J Control Release* [Internet]. 2017;247:86–105. Available from: <http://dx.doi.org/10.1016/j.jconrel.2016.12.022>
53. Riessman C. University of Huddersfield Repository University of Huddersfield Repository. *Narrat Mem everyday life*. 2010;1–7.
54. Alsharea AY. Formulation and characterization of ciprofloxacin hydrochloride emulgel with the attempt to synthesis new derivatives of ciprofloxacin. *MSC thesis* [Internet]. 2015;P 2, 71. Available from: P 2, 71
55. Prasanthi D, Lakshmi PK. Vesicles - mechanism of transdermal permeation: A review. *Asian J Pharm Clin Res*. 2012;5(1):18–25.
56. Arora N, Agarwal S, Murthy RSR. Review Article Latest Technology Advances in Cosmeceuticals. *Int J Pharm Sci Drug Res*. 2012;4(May 2007):168–82.
57. Zhou X, Hao Y, Yuan L, Pradhan S, Shrestha K, Pradhan O, et al. Nano-formulations

- for transdermal drug delivery: A review. *Chinese Chem Lett* [Internet]. 2018;29(12):1713–24. Available from: <https://doi.org/10.1016/j.ccllet.2018.10.037>
58. Drug absorption through the skin. 2006;1–3. Available from: file:///Users/a_/Backup/Papers2/Articles/2006/Unknown/2006-5.pdf%5Cpapers2://publication/uuid/6097528B-C325-435E-89DD-6E9FC0BEFAA9
 59. Simões A, Veiga F, Figueiras A, Vitorino C. A practical framework for implementing Quality by Design to the development of topical drug products: Nanosystem-based dosage forms. *Int J Pharm* [Internet]. 2018;548(1):385–99. Available from: <https://doi.org/10.1016/j.ijpharm.2018.06.052>
 60. Pradhan M, Alexander A, Singh MR, Singh D, Saraf S, Saraf S, et al. Understanding the prospective of nano-formulations towards the treatment of psoriasis. *Biomed Pharmacother* [Internet]. 2018;107(February):447–63. Available from: <https://doi.org/10.1016/j.biopha.2018.07.156>
 61. Natsheh H, Touitou E. Phospholipid Vesicles for Dermal/Transdermal and Nasal Administration of Active Molecules: The Effect of Surfactants and Alcohols on the Fluidity of Their Lipid Bilayers and Penetration Enhancement Properties. *Molecules*. 2020;25(13).
 62. Naderkhani E. Investigation and optimization of liposome formulation for use as drug carrier for the anticancer agent camptothecin. 2011;9.
 63. Gogoll K. Imiquimod based transcutaneous immunization – insights and novel concepts. 2014;
 64. Hua S. Lipid-based nano-delivery systems for skin delivery of drugs and bioactives. *Front Pharmacol*. 2015;6(SEP):2011–5.
 65. Kapoor B, Gupta R, Singh SK, Gulati M, Singh S. Prodrugs, phospholipids and vesicular delivery - An effective triumvirate of pharmacosomes. *Adv Colloid Interface Sci* [Internet]. 2018;253:35–65. Available from: <https://doi.org/10.1016/j.cis.2018.01.003>
 66. Sultan A. Steroids: A Diverse Class of Secondary Metabolites. *Med Chem (Los Angeles)*. 2015;5(7):310–7.
 67. Sultan A. Steroids: A Diverse Class of Secondary Metabolites. *Med Chem (Los Angeles)* [Internet]. 2015;5(7):310–7. Available from: <https://www.omicsonline.org/open-access/steroids-a-diverse-class-of-secondary-metabolites-2161-0444-1000279.php?aid=56565>
 68. Dr. Brandt. Steroid Chemistry and Steroid Hormone Action. *Endocr Notes Suppl*. 1999;1–18.
 69. Kasal A, Budesinsky M, Griffiths WJ. Spectroscopic Methods of Steroid Analysis. *Steroid Anal*. 2010;27–161.
 70. Becker DE. Basic and Clinical Pharmacology of Glucocorticosteroids. *Anesth Prog*. 2013;60(1):25–32.
 71. Nikalje AP. Nanotechnology and its Applications in Medicine. *Med Chem (Los*

- Angeles) [Internet]. 2015;5(2):81–9. Available from:
<https://www.omicsonline.org/open-access/nanotechnology-and-its-applications-in-medicine-2161-0444-1000247.php?aid=41535>
72. Bakker P. for the Tropics.
 73. Prichard JE. The British Pharmacopoeia 2009. British Medical Journal. 2009.
 74. Ahmed I, Marrium H, Wahid Z. Efficacy of potent topical corticosteroid (betamethasone valerate 0.1%) compared with mild topical corticosteroid (hydrocortisone 1%) in the management of acute radiodermatitis. *J Pakistan Assoc Dermatologists*. 2006;16(3):151–5.
 75. Sultan A. Steroids: A Diverse Class of Secondary Metabolites. *Med Chem (Los Angeles)*. 2015;5(7):310–7.
 76. Rhen T, Cidlowski JA. Antiinflammatory Action of Glucocorticoids — New Mechanisms for Old Drugs. *N Engl J Med*. 2005;353(16):1711–23.
 77. Blauvelt A, de Bruin-Weller M, Gooderham M, Cather JC, Weisman J, Pariser D, et al. Long-term management of moderate-to-severe atopic dermatitis with dupilumab and concomitant topical corticosteroids (LIBERTY AD CHRONOS): a 1-year, randomised, double-blinded, placebo-controlled, phase 3 trial. *Lancet*. 2017;389(10086):2287–303.
 78. Ingenieurwissenschaften D Der, Ramazani A. This thesis is dedicated to my parents for their love, endless support and encouragement. 2013;(411):1–318.
 79. Wilczewska AZ, Niemirowicz K, Markiewicz KH, Car H. Nanoparticles as drug delivery systems. *Pharmacol Reports [Internet]*. 2012;64(5):1020–37. Available from: [http://dx.doi.org/10.1016/S1734-1140\(12\)70901-5](http://dx.doi.org/10.1016/S1734-1140(12)70901-5)
 80. Buzea C, Pacheco II, Robbie K. Nanomaterials and nanoparticles: Sources and toxicity. *Biointerphases*. 2007;2(4):MR17–71.
 81. Akhtar N, Verma A, Pathak K. Exploring preclinical and clinical effectiveness of nanoformulations in the treatment of atopic dermatitis: Safety aspects and patent reviews. *Bull Fac Pharmacy, Cairo Univ [Internet]*. 2017;55(1):1–10. Available from: <http://linkinghub.elsevier.com/retrieve/pii/S1110093116300539>
 82. Carter P, Narasimhan B, Wang Q. Biocompatible nanoparticles and vesicular systems in transdermal drug delivery for various skin diseases. *Int J Pharm*. 2019;
 83. English D, Deshong P. Nanotechnology Medical Applications. :1–2.
 84. Disorders T. Is Nanotechnology the Answer for the Treatment of Cisplatin- Induced Ototoxicity ? 2016;1(Ii):1–5.
 85. Pradhan M, Alexander A, Singh MR, Singh D, Saraf S, Saraf S, et al. Understanding the prospective of nano-formulations towards the treatment of psoriasis. *Biomed Pharmacother [Internet]*. 2018;107(July):447–63. Available from: <https://doi.org/10.1016/j.biopha.2018.07.156>
 86. Duangjit S, Pamornpathomkul B, Opanasopit P, Rojanarata T, Obata Y, Takayama K,

- et al. Role of the charge, carbon chain length, and content of surfactant on the skin penetration of meloxicam-loaded liposomes. *Int J Nanomedicine*. 2014;9(1):2005–17.
87. Buzea C, Pacheco II, Robbie K. Nanomaterials and nanoparticles: Sources and toxicity. *Biointerphases* [Internet]. 2007;2(4):MR17–71. Available from: <http://avs.scitation.org/doi/10.1116/1.2815690>
 88. Li G, Fan Y, Fan C, Li X, Wang X, Li M, et al. Tacrolimus-loaded ethosomes: Physicochemical characterization and in vivo evaluation. *Eur J Pharm Biopharm* [Internet]. 2012;82(1):49–57. Available from: <http://dx.doi.org/10.1016/j.ejpb.2012.05.011>
 89. Chen JG, Liu YF, Gao TW. Preparation and anti-inflammatory activity of triptolide ethosomes in an erythema model. *J Liposome Res*. 2010;20(4):297–303.
 90. Yan Y, Zhang H, Sun J, Wang P, Dong K, Dong Y, et al. Enhanced transdermal delivery of sinomenine hydrochloride by ethosomes for anti-inflammatory treatment. *J Drug Deliv Sci Technol* [Internet]. 2016;36:201–7. Available from: <http://dx.doi.org/10.1016/j.jddst.2016.10.013>
 91. Zhang YT, Shen LN, Wu ZH, Zhao JH, Feng NP. Comparison of ethosomes and liposomes for skin delivery of psoralen for psoriasis therapy. *Int J Pharm* [Internet]. 2014;471(1–2):449–52. Available from: <http://dx.doi.org/10.1016/j.ijpharm.2014.06.001>
 92. Abdulbaqi IM, Darwis Y, Khan NAK, Assi RA, Khan AA. Ethosomal nanocarriers: The impact of constituents and formulation techniques on ethosomal properties, in vivo studies, and clinical trials. *Int J Nanomedicine*. 2016;11:2279–304.
 93. Iizhar SA, Syed IA, Satar R, Ansari SA. In vitro assessment of pharmaceutical potential of ethosomes entrapped with terbinafine hydrochloride. *J Adv Res* [Internet]. 2016;7(3):453–61. Available from: <http://dx.doi.org/10.1016/j.jare.2016.03.003>
 94. Oliveira CA, Gouvêa MM, Antunes GR, Freitas ZMF de, Marques FF de C, Ricci-Junior E. Nanoemulsion containing 8-methoxypsoralen for topical treatment of dermatoses: Development, characterization and ex vivo permeation in porcine skin. *Int J Pharm* [Internet]. 2018;547(1–2):1–9. Available from: <https://doi.org/10.1016/j.ijpharm.2018.05.053>
 95. Chourasia MK, Kang L, Chan SY. Nanosized ethosomes bearing ketoprofen for improved transdermal delivery. *Results Pharma Sci* [Internet]. 2011;1(1):60–7. Available from: <http://dx.doi.org/10.1016/j.rinphs.2011.10.002>
 96. Ainbinder D, Touitou E. Testosterone ethosomes for enhanced transdermal delivery. *Drug Deliv J Deliv Target Ther Agents*. 2005;
 97. Paolino D, Celia C, Trapasso E, Cilurzo F, Fresta M. Paclitaxel-loaded ethosomes®: Potential treatment of squamous cell carcinoma, a malignant transformation of actinic keratoses. *Eur J Pharm Biopharm*. 2012;
 98. Pathan IB, Jaware BP, Shelke S, Ambekar W. Curcumin loaded ethosomes for transdermal application: Formulation, optimization, in-vitro and in-vivo study. *J Drug Deliv Sci Technol* [Internet]. 2018;44(November 2017):49–57. Available from:

<https://doi.org/10.1016/j.jddst.2017.11.005>

99. Xie J, Ji Y, Xue W, Ma D, Hu Y. Hyaluronic acid-containing ethosomes as a potential carrier for transdermal drug delivery. *Colloids Surfaces B Biointerfaces* [Internet]. 2018;172(May):323–9. Available from: <https://doi.org/10.1016/j.colsurfb.2018.08.061>
100. Singh RP, Gangadharappa H V., Mruthunjaya K. Phospholipids: Unique carriers for drug delivery systems. *J Drug Deliv Sci Technol* [Internet]. 2017;39:166–79. Available from: <http://dx.doi.org/10.1016/j.jddst.2017.03.027>
101. Pandey V, Golhani D, Shukla R. Ethosomes: Versatile vesicular carriers for efficient transdermal delivery of therapeutic agents. *Drug Deliv*. 2015;22(8):988–1002.
102. N’Guessan A, Fattal E, Chapron D, Gueutin C, Koffi A, Tsapis N. Dexamethasone palmitate large porous particles: A controlled release formulation for lung delivery of corticosteroids. *Eur J Pharm Sci*. 2018;113(August 2017):185–92.
103. Danaei M, Dehghankhold M, Ataei S, Hasanzadeh Davarani F, Javanmard R, Dokhani A, et al. Impact of particle size and polydispersity index on the clinical applications of lipidic nanocarrier systems. *Pharmaceutics*. 2018;10(2):1–17.
104. Naik US, Sciences B. The synthesis and characterisation of novel ultra- flexible lipidic vesicles using propanol. 2013;
105. Venkatesh DN, Kalyani K, Tulasi K, Priyanka VS, Ali SKA, Kiran HC. Transferosomes: A novel technique for transdermal drug delivery. *Int J Res Pharm Nano Sci*. 2014;3(4):266–76.
106. Tosato MG, Maya Girón J V., Martin AA, Krishna Tippavajhala V, Fernández Lorenzo de Mele M, Dicelio L. Comparative study of transdermal drug delivery systems of resveratrol: High efficiency of deformable liposomes. *Mater Sci Eng C* [Internet]. 2018;90(April):356–64. Available from: <https://doi.org/10.1016/j.msec.2018.04.073>
107. Mircioiu C, Voicu V, Anuta V, Tudose A, Celia C, Paolino D, et al. Mathematical modeling of release kinetics from supramolecular drug delivery systems. *Pharmaceutics*. 2019;11(3).
108. Behtash Oskuie A, Nasrollahi SA, Nafisi S. Design, synthesis of novel vesicular systems using turpentine as a skin permeation enhancer. *J Drug Deliv Sci Technol*. 2018;43(October 2017):327–32.
109. Verma S, Utreja P. Vesicular nanocarrier based treatment of skin fungal infections: Potential and emerging trends in nanoscale pharmacotherapy. *Asian J Pharm Sci* [Internet]. 2019;14(2):117–29. Available from: <https://doi.org/10.1016/j.ajps.2018.05.007>
110. Yang L, Wu L, Wu D, Shi D, Wang T, Zhu X. Mechanism of transdermal permeation promotion of lipophilic drugs by ethosomes. *Int J Nanomedicine*. 2017;12:3357–64.
111. Sala M, Diab R, Elaissari A, Fessi H. Lipid nanocarriers as skin drug delivery systems: Properties, mechanisms of skin interactions and medical applications. *Int J Pharm* [Internet]. 2018;535(1–2):1–17. Available from: <https://doi.org/10.1016/j.ijpharm.2017.10.046>

112. Ong SGM, Chitneni M, Lee KS, Ming LC, Yuen KH. Evaluation of extrusion technique for nanosizing liposomes. *Pharmaceutics*. 2016;8(4):1–12.
113. Matteucci ME, Hotze MA, Johnston KP, Williams RO. Drug nanoparticles by antisolvent precipitation: Mixing energy versus surfactant stabilization. *Langmuir*. 2006;
114. Verma S, Gokhale R, Burgess DJ. A comparative study of top-down and bottom-up approaches for the preparation of micro/nanosuspensions. *Int J Pharm*. 2009;
115. Ahmadi Tehrani A, Omranpoor MM, Vatanara A, Seyedabadi M, Ramezani V. Formation of nanosuspensions in bottom-up approach: theories and optimization. *DARU, J Pharm Sci*. 2019;27(1):451–73.
116. Lee YS, Johnson PJ, Robbins PT, Bridson RH. Production of nanoparticles-in-microparticles by a double emulsion method: A comprehensive study. *Eur J Pharm Biopharm* [Internet]. 2013;83(2):168–73. Available from: <http://dx.doi.org/10.1016/j.ejpb.2012.10.016>
117. Emami S, Azadmard-Damirchi S, Peighambaroust SH, Valizadeh H, Hesari J. Liposomes as carrier vehicles for functional compounds in food sector. *J Exp Nanosci* [Internet]. 2016;11(9):737–59. Available from: <https://doi.org/10.1080/17458080.2016.1148273>
118. Taurozzi JS, Hackley VA, Wiesner MR. Ultrasonic dispersion of nanoparticles for environmental, health and safety assessment issues and recommendations. *Nanotoxicology*. 2011;5(4):711–29.
119. Canavese G, Ancona A, Racca L, Canta M, Dumontel B, Barbaresco F, et al. Nanoparticle-assisted ultrasound: A special focus on sonodynamic therapy against cancer. *Chem Eng J* [Internet]. 2018;340(January):155–72. Available from: <https://doi.org/10.1016/j.cej.2018.01.060>
120. Brotchie A, Grieser F, Ashokkumar M. Effect of power and frequency on bubble-size distributions in acoustic cavitation. *Phys Rev Lett*. 2009;
121. Birkin PR, Offen DG, Joseph PF, Leighton TG. Cavitation, shock waves and the invasive nature of sonoelectrochemistry. *J Phys Chem B*. 2005;
122. Cohen JM, Beltran-Huarac J, Pyrgiotakis G, Demokritou P. Effective delivery of sonication energy to fast settling and agglomerating nanomaterial suspensions for cellular studies: Implications for stability, particle kinetics, dosimetry and toxicity. *NanoImpact* [Internet]. 2018;10(November 2017):81–6. Available from: <https://doi.org/10.1016/j.impact.2017.12.002>
123. Pradhan S, Hedberg J, Blomberg E, Wold S, Odnevall Wallinder I. Effect of sonication on particle dispersion, administered dose and metal release of non-functionalized, non-inert metal nanoparticles. *J Nanoparticle Res*. 2016;18(9):1–14.
124. Zupanc M, Pandur Ž, Stepišnik Perdih T, Stopar D, Petkovšek M, Dular M. Effects of cavitation on different microorganisms: The current understanding of the mechanisms taking place behind the phenomenon. A review and proposals for further research. *Ultrason Sonochem*. 2019;57(April):147–65.

125. Paris JL, Mannaris C, Cabañas MV, Carlisle R, Manzano M, Vallet-Regí M, et al. Ultrasound-mediated cavitation-enhanced extravasation of mesoporous silica nanoparticles for controlled-release drug delivery. *Chem Eng J*. 2018;340:2–8.
126. Askari S, Halladj R. Effects of ultrasound-related variables on sonochemically synthesized SAPO-34 nanoparticles. *J Solid State Chem*. 2013;201:85–92.
127. Amnuakit T, Limsuwan T, Khongkow P, Boonme P. Vesicular carriers containing phenylethyl resorcinol for topical delivery system; liposomes, transfersomes and invasomes. *Asian J Pharm Sci [Internet]*. 2018;13(5):472–84. Available from: <https://doi.org/10.1016/j.ajps.2018.02.004>
128. Burgess S. Liposome Preparation - Avanti® Polar Lipids. Avanti Polar Lipids [Internet]. 1998;1–4. Available from: <https://www.sigmaaldrich.com/technical-documents/articles/biology/liposome-preparation.html>
129. Drive IP. The Mini -Extruder The Mini -Extruder. PoLAR.
130. Shore PA, Schachman HK. Ultracentrifugation in Biochemistry. *AIBS Bull*. 1960;10(1):35.
131. Spanner SG. An introduction to ultracentrifugation. *Neuropharmacology*. 1974;13(5):399.
132. Otori R, Akita T, Yamashita C. Effect of temperature ramp rate during the primary drying process on the properties of amorphous-based lyophilized cake, Part 2: Successful lyophilization by adopting a fast ramp rate during primary drying in protein formulations. *Eur J Pharm Biopharm [Internet]*. 2018;130(March):83–95. Available from: <https://doi.org/10.1016/j.ejpb.2018.06.010>
133. Kasper JC, Winter G, Friess W. Recent advances and further challenges in lyophilization. *Eur J Pharm Biopharm [Internet]*. 2013;85(2):162–9. Available from: <http://dx.doi.org/10.1016/j.ejpb.2013.05.019>
134. Fonte P, Reis S, Sarmiento B. Facts and evidences on the lyophilization of polymeric nanoparticles for drug delivery. *J Control Release [Internet]*. 2016;225:75–86. Available from: <http://dx.doi.org/10.1016/j.jconrel.2016.01.034>
135. Chang M. Dynamic Light Scattering Marisol Chang. 2010;(eq 2):1–9.
136. Babick F. Dynamic light scattering (DLS). In: *Characterization of Nanoparticles: Measurement Processes for Nanoparticles*. 2019. p. 137–72.
137. Bhattacharjee S. DLS and zeta potential - What they are and what they are not? *J Control Release [Internet]*. 2016;235:337–51. Available from: <http://dx.doi.org/10.1016/j.jconrel.2016.06.017>
138. Meller A, Bar-Ziv R, Tlusty T, Moses E, Stavans J, Safran SA. Localized dynamic light scattering: A new approach to dynamic measurements in optical microscopy. *Biophys J*. 1998;74(3):1541–8.
139. Freud PJ, Plantz PE. Sizing nanoparticles with dynamic light scattering. *Powder Bulk Eng*. 2005;19(2):35–41.

140. Rane SS, Choi P. Polydispersity Index: How Accurately Does It Measure the Breadth of the Molecular Weight Distribution? *Chem Mater*. 2005;17(4):926–926.
141. Kirby BJ, Hasselbrink EF. Zeta potential of microfluidic substrates: 1. Theory, experimental techniques, and effects on separations. *Electrophoresis*. 2004;25(2):187–202.
142. Kaszuba M, Corbett J, Watson FMN, Jones A. High-concentration zeta potential measurements using light-scattering techniques. *Philos Trans R Soc A Math Phys Eng Sci*. 2010;368(1927):4439–51.
143. Medrzycka KB. The effect of particle concentration on zeta potential in extremely dilute solutions. *Colloid Polym Sci*. 1991;269(1):85–90.
144. Instituto de Química. Basic principles of HPLC. Introduction to the theory of HPLC. 2019;174–82.
145. Siddique MI, Katas H, Amin MCIM, Ng SF, Zulfakar MH, Jamil A. In-vivo dermal pharmacokinetics, efficacy, and safety of skin targeting nanoparticles for corticosteroid treatment of atopic dermatitis. *Int J Pharm* [Internet]. 2016;507(1–2):72–82. Available from: <http://dx.doi.org/10.1016/j.ijpharm.2016.05.005>
146. Ghoraishi MS, Hawk JE, Phani A, Khan MF, Thundat T. Clustering mechanism of ethanol-water mixtures investigated with photothermal microfluidic cantilever deflection spectroscopy. *Sci Rep* [Internet]. 2016;6(April):1–7. Available from: <http://dx.doi.org/10.1038/srep23966>
147. Zhou W, Apkarian R, Wang ZL, Joy D. Fundamentals of scanning electron microscopy (SEM). *Scanning Microsc Nanotechnol Tech Appl*. 2007;1–40.
148. Vitez IM, Newman AW, Davidovich M, Kiesnowski C. The evolution of hot-stage microscopy to aid solid-state characterizations of pharmaceutical solids. *Thermochim Acta*. 1998;324(1–2):187–96.
149. Panna W, Wyszomirski P, Kohut P. Application of hot-stage microscopy to evaluating sample morphology changes on heating. *J Therm Anal Calorim*. 2016;125(3):1053–9.
150. Dorado JMG, Blanco MJA, Rabasco-Alvarez AM, Gonzalez-Rodriguez ML, Cozar-Bernal MJ, P.J. Sanchez-Soto. Application of Hot Stage Microscopy (HSM) to the thermal study of two binary systems of pharmaceutical interest: Triamterene-Polyethyleneglycol (PEG) 6000 and Triamterene-Beta-Cyclodextrin. *Microsc Adv Sci Res Educ* [Internet]. 2014;(December):1015–9. Available from: <http://www.formatex.info/microscopy6/book/>
151. Lin SY. Molecular perspectives on solid-state phase transformation and chemical reactivity of drugs: Metoclopramide as an example. *Drug Discov Today* [Internet]. 2015;20(2):209–22. Available from: <http://dx.doi.org/10.1016/j.drudis.2014.10.001>
152. Lin SY, Wang SL. Advances in simultaneous DSC-FTIR microspectroscopy for rapid solid-state chemical stability studies: Some dipeptide drugs as examples. *Adv Drug Deliv Rev* [Internet]. 2012;64(5):461–78. Available from: <http://dx.doi.org/10.1016/j.addr.2012.01.009>
153. Rask MB, Knopp MM, Olesen NE, Holm R, Rades T. Comparison of two DSC-based

- methods to predict drug-polymer solubility. *Int J Pharm* [Internet]. 2018;540(1–2):98–105. Available from: <https://doi.org/10.1016/j.ijpharm.2018.02.002>
154. Thermogravimetric T, Family I. *Thermogravimetric Analysis (TGA) A Beginner ’ s Guide*. 1960;
 155. Siepmann J, Siepmann F. Mathematical modeling of drug delivery. *International Journal of Pharmaceutics*. 2008.
 156. Zandi G, Lotfipour F, Ghanbarzadeh S, Medghalchi M, Hamishehkar H. A comparative study on the potentials of nanoliposomes and nanoethosomes for Fluconazole delivery. *J Drug Deliv Sci Technol*. 2018;44(December 2017):264–9.
 157. Yang Z, Li X, Li J, Ding L. Design on key parts of cable-driven hanging transportation system for orchard. *Nongye Gongcheng Xuebao/Transactions Chinese Soc Agric Eng*. 2014;30(7):18–24.
 158. Arifin DY, Lee LY, Wang CH. Mathematical modeling and simulation of drug release from microspheres: Implications to drug delivery systems. *Advanced Drug Delivery Reviews*. 2006.
 159. Siepmann J, Peppas NA. Mathematical modeling of controlled drug delivery. *Advanced Drug Delivery Reviews*. 2001.
 160. Procedures A. *Guidance for Industry Q2B Validation of Analytical Procedures: Methodology*. 1996;20857(November):301–827. Available from: <http://www.fda.gov/cder/guidance/index.htm%5Cnhttp://www.fda.gov/cber/guidelines.htm>
 161. Japanese Pharmacopoeia. *Japanese Pharmacopoeia Sixteenth Edition XVI. Powder Diffraction*. 2011;2011(65):1–2319.
 162. John C. *Interpretation of Infrared Spectra, A Practical Approach*. *Encycl Anal Chem* [Internet]. 2000;10815–37. Available from: <http://www.spectroscopynow.com/details/education/sepspec10120education/Interpretation-of-Infrared-Spectra-A-Practical-Approach.html?&tzcheck=1>
 163. Coates J. *Interpretation of IR Spectra*. *Encycl Anal Chem*. 2000;10815–10837.
 164. Browning R, Stride E. Microbubble-Mediated Delivery for Cancer Therapy. *Fluids*. 2018;3(4):74.
 165. Mainardes RM, Evangelista RC. PLGA nanoparticles containing praziquantel: Effect of formulation variables on size distribution. *Int J Pharm*. 2005;290(1–2):137–44.
 166. Reis CP, Jerónimo AR, Pinto P, Silva CO, Candeias S. Hydrocortisone acetate-loaded PCL nanoparticles as an innovative dermatological therapy for atopic dermatitis. *Biomed Biopharm Res*. 2013;10(1):73–82.
 167. Of F, Engineering B. *CZECH TECHNICAL UNIVERSITY IN PRAGUE Characterization of size of polydisperse nanoparticles of various shape: Comparative study of AFM and DLS methods* Bc. Andrea Mineva. 2017;
 168. Rizi K, Green RJ, Khutoryanskaya O, Donaldson M, Williams AC. Mechanisms of

- burst release from pH-responsive polymeric microparticles. *J Pharm Pharmacol*. 2011;63(9):1141–55.
169. Barakat NS, Elbagory IM, Almurshedi AS. Controlled-release carbamazepine granules and tablets comprising lipophilic and hydrophilic matrix Components. *AAPS PharmSciTech*. 2008;9(4):1054–62.
 170. Ciro Y, Rojas J, Salamanca CH, Alhaji MJ, Carabali GA. Production and characterization of chitosan–polyanion nanoparticles by polyelectrolyte complexation assisted by high-intensity sonication for the modified release of methotrexate. *Pharmaceuticals*. 2020;13(1).
 171. Shankar G, Agrawal YK. Formulation and evaluation of polymeric micelles for a poorly absorbed drug. *Res J Pharm Biol Chem Sci*. 2015;6(3):1314–21.
 172. Habib BA, Sayed S, Elsayed GM. Enhanced transdermal delivery of ondansetron using nanovesicular systems: Fabrication, characterization, optimization and ex-vivo permeation study-Box-Cox transformation practical example. *Eur J Pharm Sci* [Internet]. 2018;115(December 2017):352–61. Available from: <https://doi.org/10.1016/j.ejps.2018.01.044>
 173. Zhang Y, Ng W, Feng X, Cao F, Xu H. Lipid vesicular nanocarrier: Quick encapsulation efficiency determination and transcutaneous application. *Int J Pharm*. 2017;
 174. Katayama I, Aihara M, Ohya Y, Saeki H, Shimojo N, Shoji S, et al. Japanese guidelines for atopic dermatitis 2017. *Allergol Int* [Internet]. 2017;66(2):230–47. Available from: <http://dx.doi.org/10.1016/j.alit.2016.12.003>
 175. Custovic A, Sonntag HJ, Buchan IE, Belgrave D, Simpson A, Prospero MCF. Evolution pathways of IgE responses to grass and mite allergens throughout childhood. *J Allergy Clin Immunol* [Internet]. 2015;136(6):1645-1652e8. Available from: <http://dx.doi.org/10.1016/j.jaci.2015.03.041>
 176. Kirby BJ, Hasselbrink EF. Zeta potential of microfluidic substrates: 1. Theory, experimental techniques, and effects on separations. *Electrophoresis* [Internet]. 2004;25(2):187–202. Available from: <http://www.ncbi.nlm.nih.gov/pubmed/14743473>
 177. Wade, Jr. LG. (IR) Theory and Interpretation of IR spectra presentation for additional examples of How do we know. *Org Chem*. 2003;5th:853–66.
 178. Zeng L, An L, Wu X. Modeling Drug-Carrier Interaction in the Drug Release from Nanocarriers. *J Drug Deliv*. 2011;2011:1–15.

APPENDIX

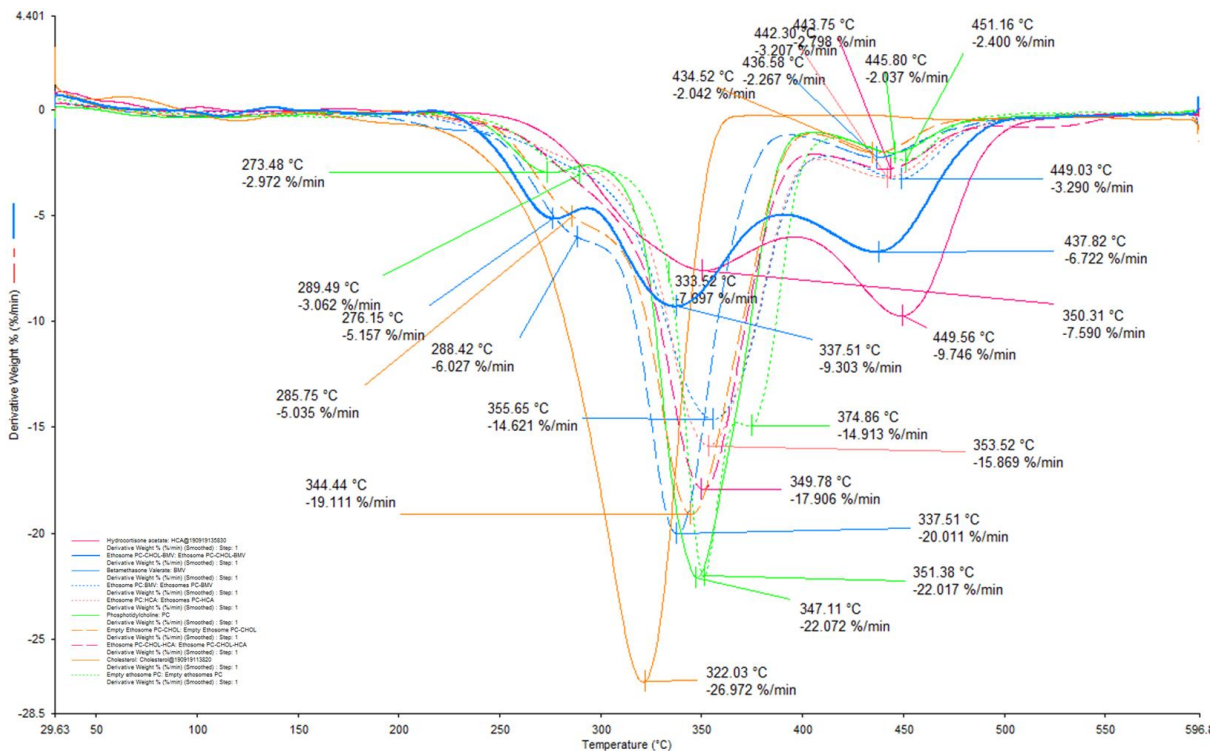


Figure A-1: Thermogravimetric analyses 1st derivative data of pure components and ethosomes, showing thermal events generated using Pyris™ Software

Table A-1: FTIR analyses of Chol ethosomes with assigned functional groups.

Sample analysed	Experimental frequency bands (cm ⁻¹)	Theoretical Group Frequency (cm ⁻¹)	Functional group assignment	Intensity	Shape
Unloaded Chol ethosomes	3363,3	3400-3300 and 3330-3250	Primary amine	Weak	Broad doublet
	3010,66	3100-3000	Alkene C-H stretch	Weak	Sharp
	2924,22	3000-2840	Alkane C-H	Strong	Sharp
	2853,77	3000-2840	Alkane C-H	Medium	Sharp
	1736,75	1735	Ester	Strong	Sharp
	1466,12	1465	Alkane C-H bend	Medium	Sharp
BMV loaded ethosomes	3276,09	3400-3300 and 3330-3250	Primary amine	Weak	Broad doublet

	3010,31	3100-3000	Alkene C-H stretch	Weak	Sharp
	2924,69	3000-2840	Alkane C-H	Strong	Sharp
	2854,29	3000-2840	Alkane C-H	Medium	Sharp
	1733,62	1735	Ester	Strong	Sharp
	1668,51	1668-1678	C=C stretch	Weak	Sharp
	1465,75	1465	Alkane C-H bend	Medium	Sharp
BMV loaded Chol ethosomes	3264,98	3400-3300 and 3330-3250	Primary amine	Weak	Broad doublet
	3010,34	3100-3000	Alkene C-H stretch	Weak	Sharp
	2924,58	3000-2840	Alkane C-H	Strong	Sharp
	2854,09	3000-2840	Alkane C-H	Medium	Sharp
	1734,41	1735	Ester	Strong	Sharp
	1669,65	1668-1678	C=C stretch	Weak	Sharp
	1465,84	1465	Alkane C-H bend	Medium	Sharp
HCA loaded ethosomes	3285,8	3400-3300 and 3330-3250	Primary amine	Weak	Broad doublet
	3010,36	3100-3000	Alkene C-H stretch	Weak	Sharp
	2924,15	3000-2840	Alkane C-H	Strong	Sharp
	2854,11	3000-2840	Alkane C-H	Medium	Sharp
	1736,52	1735	Ester	Strong	Sharp
	1671,77	1668-1678	C=C stretch	Weak	Sharp
	1465,89	1465	Alkane C-H bend	Medium	Sharp
Unloaded ethosomes	3284,83	3400-3300 and 3330-3250	Primary amine	Weak	Broad doublet
	3010,4	3100-3000	Alkene C-H stretch	Weak	Sharp
	2924,6	3000-2840	Alkane C-H	Strong	Sharp
	2853,89	3000-2840	Alkane C-H	Medium	Sharp
	1737,02	1735	Ester	Strong	Sharp
	1673,09	1668-1678	C=C stretch	Weak	Sharp
	1465,97	1465	Alkane C-H bend	Medium	Sharp